Critical State Soil Mechanics

Andrew Schofield and Peter Wroth
Lecturers in Engineering at Cambridge University

Preface

This book is about the mechanical properties of saturated remoulded soil. It is written at the level of understanding of a final-year undergraduate student of civil engineering; it should also be of direct interest to post-graduate students and to practising civil engineers who are concerned with testing soil specimens or designing works that involve soil.

Our purpose is to focus attention on the critical state concept and demonstrate what we believe to be its importance in a proper understanding of the mechanical behaviour of soils. We have tried to achieve this by means of various simple mechanical models that represent (with varying degrees of accuracy) the laboratory behaviour of remoulded soils. We have not written a standard text on soil mechanics, and, as a consequence, we have purposely not considered partly saturated, structured, anisotropic, sensitive, or stabilized soil. We have not discussed dynamic, seismic, or damping properties of soils; we have deliberately omitted such topics as the prediction of settlement based on Boussinesq's functions for elastic stress distributions as they are not directly relevant to our purpose.

The material presented in this book is largely drawn from the courses of lectures and associated laboratory classes that we offered to our final year civil engineering undergraduates and advanced students in *1965/6* and 1966/7. Their courses also included material covered by standard textbooks such as *Soil Mechanics in Engineering Practice* by K. Terzaghi and R. B. Peck (Wiley 1948), *Fundamentals of Soil Mechanics* by D. W. Taylor (Wiley 1948) or *Principles of Soil Mechanics* by R. F. Scott (Addison-Wesley 1963).

In order to create a proper background for the critical state concept we have felt it necessary to emphasize certain aspects of continuum mechanics related to stress and strain in chapter 2 and to develop the well-established theories of seepage and one-dimensional consolidation in chapters 3 and 4. We have discussed the theoretical treatment of these two topics only in relation to the routine experiments conducted in the laboratory by our students, where they obtained close experimental confirmation of the relevance of these theories to saturated remoulded soil samples. Modifications of these theories, application to field problems, three-dimensional consolidation, and consideration of secondary effects, etc., are beyond the scope of this book.

In chapters *5* and 6, we develop two models for the yielding of soil as isotropic plastic materials. These models were given the names Granta-gravel and Cam-clay from that river that runs past our laboratory, which is called the Granta in its upper reaches and the Cam in its lower reaches. These names have the advantage that each relates to one specific artificial material with a certain distinct stress – strain character. Granta-gravel is an ideal rigid/plastic material leading directly to Cam-clay which is an ideal elastic/plastic material. It was not intended that Granta-gravel should be a model for the yielding of dense sand at some early stage of stressing before failure: at that stage, where Rowe's concept of stress dilatancy offers a better interpretation of actual test data, the simple Granta-gravel model remains quite rigid. However, at peak stress, when Granta-gravel does yield, the model fits our purpose and it serves to introduce Taylor's dilatancy calculation towards the end of chapter *5*.

Chapter 6 ends with a radical interpretation of the index tests that are widely used for soil classification, and chapter 7 includes a suggested computation of 'triaxial' test data that allows students to interpret much significant data which are neglected in normal methods of analysis. The remainder of chapter 7 and chapter 8 are devoted to testing the

relevance of the two models, and to suggesting criteria based on the critical state concept for choice of strength parameters in design problems.

Chapter 9 begins by drawing attention to the actual work of Coulomb – which is often inaccurately reported – and its development at Gothenberg; and then introduces Sokolovski's calculations of two-dimensional fields of limiting stress into which we consider it appropriate to introduce critical state strength parameters. We conclude in chapter 10 by demonstrating the place that the critical state concept has in our understanding of the mechanical behaviour of soils.

We wish to acknowledge the continual encouragement and very necessary support given by Professor Sir John Baker, O.B.E., Sc.D., F.R.S., of all the work in the soil mechanics group within his Department. We are very conscious that this book represents only part of the output of the research group that our teacher, colleague, and friend, Ken Roscoe, has built up over the past twenty years, and we owe him our unbounded gratitude. We are indebted to E. C. Hambly who kindly read the manuscript and made many valuable comments and criticisms, and we thank Mrs Holt-Smith for typing the manuscript and helping us in the final effort of completing this text.

A. N. Schofield and C. P. Wroth

To K. H. Roscoe

Table of contents

Contents

Glossary of symbols

The list given below is not exhaustive, but includes all the most important symbols used in this book. The number after each brief definition refers to the section in the book where the full definition may be found, and the initials (VVS) indicate that a symbol is one used by Sokolovski.

The dot notation is defined in §2.3, whereby $\dot{x}$ denotes a small change in the value of the parameter x. As a result of the sign convention adopted (§2.2) in which compressive stresses and strains are taken as positive, the following parameters only have a *positive* dot notation associated with a *negative* change of value (i.e., $+\dot{x} = -\delta x$):*v,l,r.*

The following letters are used as suffixes: *f* failure, *r* radial, *l* longitudinal; and as superfixes: *r* recoverable, *p* plastic (irrecoverable).

a	Height of Coulomb's wedge of soil	9.1
a	Cross-sectional area of sample in axial-test	5.2
c_u	Half unconfined compression strength	6.10
c_{vc}	Coefficient of consolidation	4.3
d	Diameter, displacement, depth	1.2, 2.5, 3.7
e	Voids ratio	1.5
f, f'	General function and its derivative	3.7
h, h_w	Height, and height of water in standpipe	3.1
i	Hydraulic gradient	3.2
k	Maximum shear stress (Tresca)	2.9
k	Coefficient of permeability	3.3
$\boldsymbol{k}$	Cohesion in eq. (8.1)	(VVS) 8.1
l	Length of sample in axial-test	5.2
l	Constant in eq. (8.3) cf. λ in eq. (5.23)	8.2
m_{vc}, m_{vs}	Coefficients of volume compressibility	4.3
n	Porosity	1.5
n	Normal stress	(VVS) 9.5
p	Effective spherical pressure	5.5
p_e	Equivalent pressure cf. σ'_e	5.10
p_u	Undrained critical state pressure	5.10
p_x	Critical state pressure on yield curve	6.5
p_{LL}	Pressure corresponding to liquid limit	6.9
p_{PL}	Pressure corresponding to plastic limit	6.9
p_Ω	Pressure corresponding to Ω point	6.9
p^*, q^*	Generalized stress parameters	8.2
p, q	Uniformly distributed loading pressures	(VVS) 9.4
p'	Equivalent stress	(VVS) 9.5
q	Axial-deviator stress	5.5
q_u	Undrained critical state value of q	5.10
q_x	Critical state value of q on yield curve	6.5
r	Radial coordinate	3.8
r_1, r_2	Directions of planes of limiting stress ratio	(VVS) 9.5
s	Distance along a flowline	3.2
s_+, s_-	Parameters locating centres of Mohr's circles	(VVS) 9.5
s, t	Stresses in plane strain	App. C

t	Tangential stress (VVS)	9.5
t	Time	1.2
$t_{1/2}$	Half-settlement time	4.6
u	Excess pore-pressure	3.1
u_w	Total pore-pressure	1.6
u	Velocity of stream	1.7
v	Velocity	1.2
v_a	Artificial velocity	3.3
v_s	Seepage velocity	3.3
v	Specific volume	1.5
v_x	Critical state value of v on yield curve	6.5
v_κ, v_λ	Ordinates of κ-line and λ-line	6.1
v_{LL}	Specific volume at liquid limit	6.9
v_{PL}	Specific volume at plastic limit	6.9
Δv_{PI}	Change of specific volume corresponding to plasticity index	6.9
v_Ω	Specific volume corresponding to Ω point	6.9
w	Water content	1.5
w	Weight	1.2
x, y, z	Cartesian coordinate axes	1.7
x_t	Transformed coordinate	3.5
A, A_t	Cross-sectional areas	3.3, 4.1
A, A_m	Fourier coefficients	4.5
$A, B, \overline{B}$	Pore-pressure coefficients	7.10
C_c, C'_c	Compression indices	4.2, 6.9
D	Diameter	1.2
D_0	A total change of specific volume	5.13
E	Young's modulus	2.7
$\dot{E}$	Loading power	5.6
F, F', F^*	Potential functions (Mises)	2.9, 2.11, app. C
F	Frictional force	9.1
G	Shear modulus	2.7
G_s	Specific gravity	1.2
H	Maximum drainage path	4.4
H	Abscissa of Mohr-Coulomb lines (VVS)	8.3
K	Bulk modulus	2.7
K, K_0	Coefficients of earth pressure	6.6
L	Lateral earth pressure force	9.1
M	Mach number	1.7
N	Overcompression ratio	7.10
N	Normal force	9.1
P, P_w, P_s	Vertical loads in consolidometer	4.1
P_A, P_P	Active and passive pressure forces	9.1, 9.2
$\dot{P}$	Probing power	5.6
Q	Quantity of flow	3.3
R	Force of resistance	1.2
T	Tangential force	9.1
T_v	Time factor	4.4

$T_{½}$	Half-settlement time factor		4.6
U	Proportion of consolidation		4.4
$\dot{U}$	Recoverable power		5.6
V, V_t, V_v	Volumes		1.2, 3.3
W	Weight		1.2
$\dot{W}$	Dissipated power		5.7
X_1, X_2, X_3	Loads in simple test system		5.2
Y	Yield stress in tension (Mises)		2.9
LL	Liquid limit		1.3
PL	Plastic limit		1.3
PI	Plasticity index		1.3
α, β	Pair of characteristics		9.9
α, β	Angles		2.4
γ	Engineering shear strain		2.4
γ	Saturated bulk density	(by weight not mass)	1.5
γ_d	Dry bulk density	(by weight not mass)	1.5
γ'	Submerged bulk density	(by weight not mass)	3.3
γ_w	density of water	(by weight not mass)	1.2
δ	Inclination of equivalent stress	(VVS)	9.5
δ	Displacement in simple test system		5.3
ε	Half angle between characteristics	(VVS)	9.1
$\dot{\varepsilon}$	Increment of shear strain		5.5
ε	Cumulative shear strain		6.7
$\dot{\varepsilon}_{ij}$	Components of strain increment		2.10
$\dot{\varepsilon}*$	Generalized shear strain increment		App. C
η	Ratio of stresses q/p		5.8
η	Special parameter	(VVS)	9.9
θ	Angle		9.1
$\boldsymbol{\kappa}$	Special parameter	(VVS)	9.5
κ	Gradient of swelling line		4.2
λ	Gradient of compression line		4.2
λ_+, λ_-	Inclinations of principal stress to a stress discontinuity	(VVS)	9.5
μ	Viscosity		1.2
ν	Poisson's ratio		2.7
$\nu, \nu*$	Scalar factors		2.10, app. C
ξ	Special parameter	(VVS)	9.9
ρ	Settlement		4.1
$\boldsymbol{\rho}$	Angle of friction in eq. (8.1)	(VVS)	8.1
σ	Total stress		1.6
σ'	Effective stress		1.6
σ'_{ij}	Components of effective stress		2.2
σ'_e	Hvorslev's equivalent stress		8.2
σ'_+, σ'_-	Parameters locating centres of Mohr's circles	(VVS)	9.5
τ, τ_m	Shear stresses in direct shear test		5.14
τ_{yz} etc.	Shear stresses		2.2
ϕ	Potential function		1.7

ϕ, ϕ_m	Angles of friction in Taylor's shear tests		5.14
ϕ_+, ϕ_-	Inclinations of principal stress on either side of discontinuity	(VVS)	9.5
ψ	Streamline function		3.7
Γ	Ordinate of critical state line		5.9
Δ	Caquot's angle	(VVS)	9.5
Λ	Parameter relating swelling with compression		6.6
M	Critical state frictional constant		5.7
$\sum'$	Major principal stress	(VVS)	9.5
Ω	Common point of idealized critical state lines		6.9

1
Basic concepts

1.1 Introduction

This book is about conceptual models that represent the mechanical behaviour of saturated remoulded soil. Each model involves a set of mechanical properties and each can be manipulated by techniques of applied mathematics familiar to engineers. The models represent, more or less accurately, several technically important aspects of the mechanical behaviour of the soil-material. The soil-material is considered to be a homogeneous mechanical mixture of two phases: one phase represents the structure of solid particles in the soil aggregate and the other phase represents the fluid water in the pores or voids of the aggregate. It is more difficult to understand this soil-material than the mechanically simple perfectly elastic or plastic materials, so most of the book is concerned with the mechanical interaction of the phases and the stress − strain properties of the soil-material in bulk. Much of this work is of interest to workers in other fields, but as we are civil engineers we will take particular interest in the standard tests and calculations of soil mechanics and foundation engineering.

It is appropriate at the outset of this book to comment on present standard practice in soil engineering. Most engineers in practice make calculations and base their judgement on the model used two hundred years ago by C. A. Coulomb[1] in his classic analysis of the active and passive pressures of soil against a retaining wall. In that model soil-material (or rock) was considered to remain rigid until there was some surface through the body of soil-material on which the shear stress could overcome *cohesion* and *internal friction,* whereupon the soil-material would become divided into two rigid bodies that could slip relative to each other along that surface. Cohesion and internal friction are properties of that model, and in order to make calculations it is necessary for engineers to attribute specific numerical values to these properties in each specific body of soil. Soil is difficult to sample, it is seldom homogeneous and isotropic in practice, and engineers have to exercise a considerable measure of subjective judgement in attributing properties to soil.

In attempts over the last half-century to make such judgements more objective, many research workers have tested specimens of saturated remoulded soil. To aid practising engineers the successive publications that have resulted from this continuing research effort have reported findings in terms of the standard conceptual model of Coulomb. For example, typical papers have included discussion about the ‘strain to mobilize full friction’ or ‘the effect of drainage conditions on apparent cohesion’. Much of this research is well understood by engineers, who make good the evident inadequacy of their standard conceptual model by recalling from their experience a variety of cases, in each of which a different interpretation has had to be given to the standard properties.

Recently, various research workers have also been developing new conceptual models. In particular, at Cambridge over the past decade, the *critical state* concept (introduced in §1.8 and extensively discussed in and after chapter *5)* has been worked into a variety of models which are now well developed and acceptable in the context of isotropic hardening elastic/plastic media. In our judgement a stage has now been reached at which engineers could benefit from use of the new conceptual models in practice.

We wish to emphasize that much of what we are going to write is already incorporated by engineers in their present judgements. The new conceptual models incorporate both the standard Coulomb model and the variations which are commonly considered in practice: the words cohesion and friction, compressibility and consolidation, drained and undrained will be used here as in practice. What is new is the inter-relation of

concepts, the capacity to create new types of calculation, and the unification of the bases for judgement.

In the next section we begin abruptly with the model for sedimentation, and then in §1.3 we introduce the empirical index tests and promise a fundamental interpretation for them (which appears in chapter 6). Mechanical grading and index properties form a soil classification in §1.4, and in §1.5 we define the water content and specific volume of soil specimens. Then in §1.6 we introduce the concept of effective stress and in §1.7 digress to distinguish between the complex mathematical consequences of a simple concept (which will apply to the solution of limiting stress distributions by the method of characteristics in chapter 9) and the simple mathematical consequences of a complex concept (which will apply to the critical states).

1.2 Sedimentation and Sieving in Determination of Particle Sizes

The first model to be considered is Stokes' sphere, falling steadily under gravity in a viscous fluid. Prandtl[2,3] discusses this as an example of motion at very small Reynolds' number. The total force of resistance to motion is found from reasons of dynamical similarity to be proportional to the product (viscosity μ) × (velocity *v)* × (diameter *d).* Stokes' solution gives a force of resistance *R* which y has a coefficient 3π as follows:

$$R = 3\pi\mu v d \tag{1.1}$$

The force must be in equilibrium with the buoyant weight of the sphere, so that

$$3\pi\mu v d = \frac{\pi}{6}(G_s - 1)\gamma_w d^3 \tag{1.2}$$

where $G_s\gamma_w$ is the weight of unit volume of the solid material of the sphere and γ_w is the weight of unit volume of water. Hence, if a single sphere is observed steadily falling through a distance z in a time t, it can be calculated to have a diameter

$$d = \left\{ \frac{18\mu}{(G_s - 1)\gamma_w} \frac{z}{t} \right\}^{1/2} \tag{1.3}$$

This calculation is only appropriate for small Reynolds' numbers: Krumbein and Pettijohn[4] consider that the calculation gives close estimates of diameters of spherical quartz particles settling in water provided the particle diameters are less than 0.005 mm. They also suggest that the calculation continues to hold until particle diameters become less than 0.1 microns (0.0001 mm), despite the effect of Brownian movement at that diameter. This range of applicability between 0.05 mm and 0.0001 mm makes a technique called *sedimentary analysis* particularly useful in sorting the sizes of particles of silt and clay soils.

Typical particles of silt and clay are not smooth and spherical in shape, nor does each separate particle have the same value of *G,* as may be determined from the aggregated particles in bulk. So the sizes of irregularly shaped small particles are *defined* in terms of their settling velocities and we then use adjectives such as 'hydraulic' or 'equivalent' or 'sedimentation' diameter. This is one example of a conceptual model in that it gives a meaning to words in the language of our subject.

The standard[5] experimental technique for quantitative determination of the small particle size distribution in a soil is sedimentation. The soil is pre-treated to break it up mechanically and to dissolve organic matter and calcium compounds that may cement particles together. Then, to counteract certain surface effects that may tend to make particles flocculate together, a dispersion agent is added. About 10 gm of solid particles are dispersed in half a litre of water, and the suspension is shaken up in a tube that is repeatedly inverted. The test begins with a clock being started at the same instant that the

tube is placed in position in a constant temperature bath. After certain specified periods a pipette is inserted to a depth $z = 100\,\text{mm}$ in the tube, a few millilitres of the suspension are withdrawn at that depth and are transferred into a drying bottle.

Let us suppose that originally a weight W of solid material was dispersed in 500 millilitres of water, and after time t at depth 100 mm a weight w of solid material is found in a volume V of suspension withdrawn by the pipette. If the suspension had been sampled immediately at $t = 0$ then the weight w would have been $WV/500$ but, as time passes, w will have decreased below this initial value. If all particles were of a single size, with effective diameter D, and if we calculate a time

$$t_D = \frac{18\mu z}{(G_s - 1)\gamma_w D^2} \tag{1.4}$$

then *before* time t_D the concentration of sediment at the sampling depth $(z = 100\,\text{mm})$ would remain at its initial value $WV/500$: *at* time t_D the particles initially at the surface of the tube would sink past the depth $z = 100\,\text{mm}$, and *thereafter,* as is shown in Fig. 1.1, there would be clear liquid at the depth z.

It is evident that if any particles of one specified size are present at a depth z they are present in their original concentration; (this is rather like dropping a length of chain on the ground: as the links fall they should preserve their original spacing between centres, and they would only bunch up when they strike the heap of chain on the ground). Therefore, in the general case when we analyse a dispersion of various particle sizes, if we wish to know what fraction by weight of the particles are of diameter less than D, we must arrange to sample at the appropriate time t_D. The ratio between the weight w withdrawn at that time, and the initial value

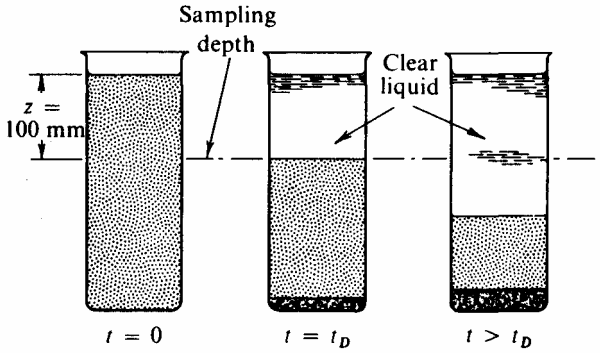

Fig. 1.1 Process of Sedimentation on Dispersed Specimen

$WV/500$, is the required fraction. The fraction is usually expressed as a percentage smaller than a certain size. The sizes are graded on a logarithmic scale. Values are usually found for D = 0.06, 0.02, 0.006, and 0.002 mm, and these data[6-11] are plotted on a curve as shown in Fig. 1.2.

A different technique[5], sieving, is used to sort out the sizes of soil particles of more than 0.2 mm diameter. A sieve is made with wire cloth (a mesh of two sets of wires woven together at right angles to each other). The apertures in this wire cloth will pass particles that have an appropriate intermediate or short diameter, provided that the sieve is shaken sufficiently for the particles to have a chance of approaching the holes in the right way. The finer sieves are specified by numbers, and for each number there is a standard[12] nominal size in the wire cloth. The coarser sieves are specified by nominal apertures. Clearly this technique implies a slightly different definition of diameter from that of sedimentary analysis, but a continuous line must be drawn across the particle size distribution chart of Fig. 1.2: the assumption is that the two definitions are equivalent in

the region about 0.05 mm diameter where sieves are almost too fine and sedimentary settlement almost too fast.

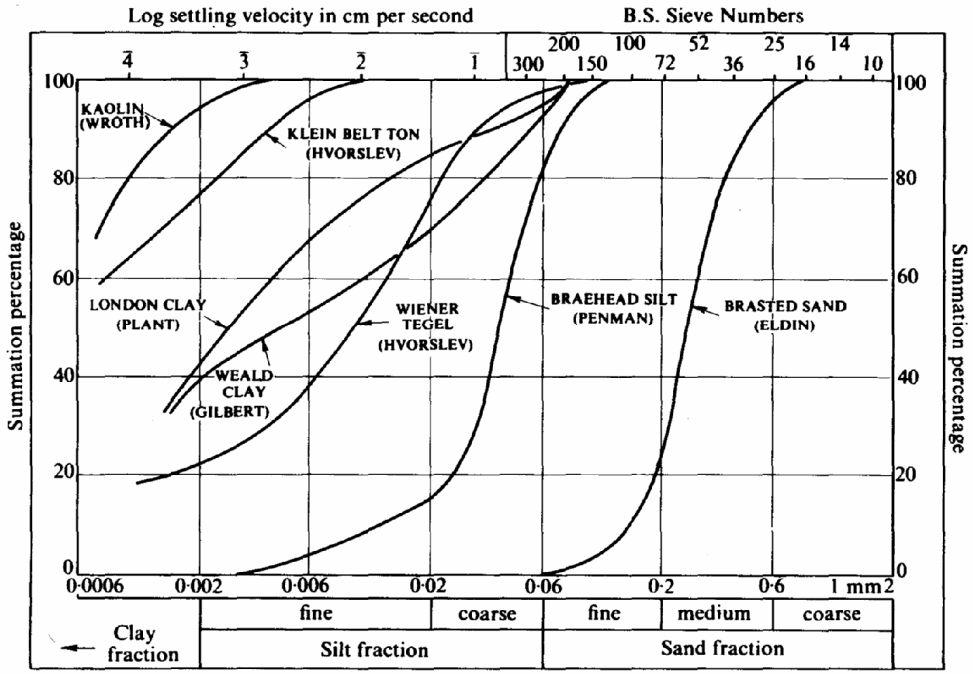

Fig. 1.2 Particle Size Distribution Curves

Civil engineers then use the classification for grain size devised at the Massachusetts Institute of Technology which defines the following names:
Boulders are particles coarser than 6 cm, or 60 mm diameter;
Gravel contains particles between 60 mm and 2 mm diameter;
Sand contains particles between 2 mm and 0.06 mm diameter;
Silt contains particles between 0.06 mm and 0.002 mm diameter;
Clay contains particles finer than 0.002 mm (called two microns, 2μ).

The boundaries between the particle sizes not only give almost equal spacing on the logarithmic scale for equivalent diameter in Fig. 1.2, but also correspond well with major changes in engineering properties. A variety of soils is displayed, including several that have been extensively tested with the results being discussed in detail in this text. For example, London clay has 43 per cent clay size, 51 per cent silt size and 6 per cent sand size.

1.3 Index Tests

The engineer relies chiefly on the mechanical grading of particle sizes in his description of soil but in addition, two index numbers are determined that describe the clayeyness of the finer fraction of soil. The soil is passed through a sieve, B.S. No. 36 or U.S. Standard No. 40, to remove coarse sand and gravel. In the first index test[5] the finer fraction is remoulded into a paste with additional water in a shallow cup. As water is added the structure of fine soil particles is remoulded into looser states and so the paste becomes progressively less stiff. Eventually the soil paste has taken up sufficient water that it has the consistency of a thick cream; and then a groove in the paste (see Fig. 1.3) will close with the sides of the groove flowing together when the bottom of the cup is given a succession of 25 blows on its base. The paste is then at the 'lowest limit' of a continuing

range of liquid states: the water content (defined in §1.5) is determined and this is called the *liquid limit* (LL) of that soil.

The strength of the paste will increase if the paste is compressed either by externally applied pressure, or by the drying pressures that are induced as water evaporates away into the air and the contracting surfaces of water (menisci) make the soil particles shrink into more closely packed states. This hardening phenomenon will be discussed more extensively in later chapters; it will turn out (a) that the strength of the paste increases in direct proportion to the increase of pressure, and (b) that the reduction of water content is proportional to the logarithm of the ratio in which the pressure is increased.

In the second index test[5] the soil paste is continuously remoulded and at the same time allowed to air-dry, until it is so stiff that when an attempt is made to deform the soil plastically into a thin thread of 1/8 in. diameter, the soil thread crumbles. At that state the soil has approximately a hundred times the strength that it had when remoulded at the higher water content that we call the liquid limit: because of the logarithmic relationship between pressure (or strength) and water content it will turn out that this hundred-fold increase in strength corresponds to a characteristic reduction of water content (dependent on the compressibility of the soil). The water content of the crumbled soil thread is determined and is called the *plastic limit* (PL). The reduction of water content from the liquid limit is calculated and is given the name *plasticity index* (PI) = (LL – PL). Soils with a high plasticity index are highly plastic and have a large range of water contents over which they can be remoulded: in English common speech they might be called 'heavy' clay soils.

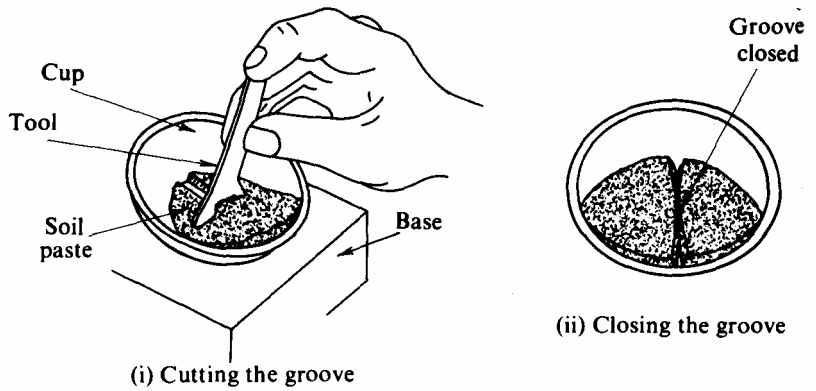

Fig. 1.3 Liquid Limit Test Groove (After Lambe[20])

Skempton[13] found that there is a correlation between the plasticity index of a soil and the proportion of particles of clay size in the soil. If a given specimen of clay soil is mixed with various proportions of silt soil then there is a constant ratio of

$$\text{Activity} = \frac{\text{plasticity index}}{\text{percentage finer than two microns}}$$

The activity of clay soil depends on the clay minerals which form the solid phase and the solute ions in the water (or liquid phase).

1.4 Soil Classification

The engineer's classification of soil by mechanical grading and index tests may seem a little crude: there is a measure of subjective choice in the definition of a mechanical grading, the index tests at first appear rather arbitrary, and we have quite neglected to make any evaluations either of the fabric and origin of the soil, or of the nature of the clay minerals and their state in the clay-water system. However, in this section we will suggest

that the simple engineering classification does consider the most important mechanical attributes of soil.

It is hard to appreciate the significance of the immense diversity of sizes of soil particles. It may be helpful to imagine a city scene in which men are spreading tarred road stone in the pavement in front of a fifteen-story city building. If this scene were reduced in scale by a factor of two hundred thousand then a man of 1.8 metres in height would be nine microns high – the size of a medium silt particle; the building would be a third of a millimetre high – the size of a medium sand grain; the road stones would be a tenth of a micron – the size of what are called 'colloidal' particles; the layer of tar would correspond to a thickness of several water molecules around the colloidal particles. Our eyes could either focus on the tarred stones in a small area of road surface, or view the grouping of adjacent buildings as a whole; we could not see at one glance all the objects in that imaginary scene. The diversity of sizes of soil particles means that a complete survey of their geometry in a soil specimen is not feasible. If we select a volume of 1 m^3 of soil, large enough to contain one of the largest particles (a boulder) then this volume could also contain of the order of 10^8 sand grains and of the order of 10^{16} clay particles. A further problem in attempting such a geometrical or structural survey would be that the surface roughness of the large irregular particles would have to be defined with the same accuracy as the dimensions of the smallest particles.

An undisturbed soil can have a distinctive fabric. The various soil-forming processes may cause an ordering of constituents with concentration in some parts, and the creation of channels or voids in other parts. Evidence of these extensively occurring processes can be obtained by a study of the microstructure of the soil, and this can be useful in site investigation. The engineer does need to know what extent of any soil deposit in the field is represented by each specimen in the laboratory. Studies of the soil-forming processes, of the morphology of land forms, of the geological record of the site will be reflected in the words used in the description of the site investigation, but not in the estimates of mechanical strength of the various soils themselves.

In chapters 5 and 6 we consider macroscopically the mechanical strength of soil as a function of effective pressure and specific volume, without reference to any microscopic fabric. We will suggest that the major engineering attributes of real soils can be explained in terms of the mechanical properties of a homogeneous isotropic aggregate of soil particles and water. We show that the index properties are linked with the critical states of fully disordered soil, and we suggest that the critical state strengths form a proper basis of the stability of works currently designed by practising engineers.

Suppose we have a soil with a measured peak strength which (a) could not be correlated with index properties, (b) was destroyed after mechanical disturbance of the soil fabric, and *(c)* could only be explained in terms of this fabric. If we wished to base a design on this peak strength, special care would be needed to ensure that the whole deposit did have this particular (unstable) property. In contrast, if we can base a design on the macroscopic properties of soil in the critical states, we shall be concerned with more stable properties and we shall be able to make use of the data of a normal soil survey such as the *in situ* water content and index properties.

We gave the name clay to particles of less than 2 micron effective diameter. More properly the name clay should be reserved for clay minerals (kaolinite, montmorillonite, illite, etc.). Any substance when immersed in water will experience surface forces: when the substance is subdivided into small fragments the body forces diminish with the cube of size while surface forces diminish with the square of size, and when the fragments are less than 0.1 micron in size the substance is in 'colloidal' form where surface forces predominate. The hydrous-alumino-silicate clay minerals have a sheet-like molecular

structure with electric charge on the surfaces and edges. As a consequence clay mineral particles have additional capacity for ion-exchange. Clearly, a full description of the clay/water/solute system would require detailed studies of a physical and chemical type described in a standard text, such as that by Grim.[14] However, the composite effects of these physico-chemical properties of remoulded clay are reflected to a large measure in the plasticity index. In §6.9 we show how variation of plasticity corresponds to variation in the critical states, and this approach can be developed as a possible explanation of phenomena such as the al sensitivity of leached post-glacial marine clay, observed by Bjerrum and Rosenqvist.[15]

In effect, when we reaffirm the standard soil engineering practice of regarding the *mechanical grading* and *index properties* as the basis of soil classification, we are asserting that the influence of mineralogy, chemistry and origin of a soil on its mechanical is behaviour is adequately measured by these simple index tests.

1.5 Water Content and Density of Saturated Soil Specimens

If a soil specimen is heated to 105°C most of the water is driven off, although a little will still remain in and around the clay minerals. Heating to a higher temperature would drive off some more water, but we stop at this arbitrary standard temperature. It is then supposed that the remaining volume of soil particles with the small amount of water they still hold is in effect 'solid' material, whereas all the water that has been evaporated is 'liquid'.

This supposition makes a clear simplification of a complicated reality. Water at a greater distance from a clay particle has a higher energy and a lower density than water that has been adsorbed on the clay mineral surface. Water that wets a dry surface of a clay mineral particle emits 'heat of wetting' as the water molecules move in towards the surface; conversely drying requires heat transfer to remove water molecules off a wet surface. The engineering simplification bypasses this complicated problem of adsorption thermodynamics. Whatever remains after the sample has been dried at 105°C is called *solid;* the specific gravity (G_s) of this residue is found by experiment. Whatever evaporates when the sample is dried is called *pore-water* and it is assumed to have the specific gravity of pure water. From the weights of the sample before and after drying the water content is determined as the ratio:

$$\text{water content } w = \frac{\text{weight of pore water}}{\text{weight of solids}}.$$

In this book we will attach particular significance to the volume of space v occupied by unit volume of solids: we will call v the *specific volume* of unit volume of solids. Existing soil mechanics texts use an alternative symbol e called 'voids ratio' which is the ratio between the volume of 'voids' or pore space and the volume of solids: $v = 1 + e.$ A further alternative symbol n called porosity is defined by $n = (v-1)/v = e/v.$ Figure 1.4(a) illustrates diagrammatically the unit volume of solids occupying a space v, and Fig. 1.4(b) shows separately the volumes and weights of the solids and the pore-water. In this book we will only consider *fully saturated soil,* with the space $(v-1)$ full of pore-water.

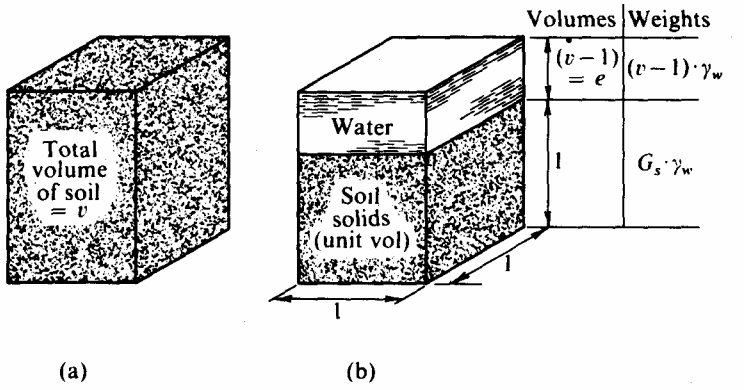

Fig. 1.4 Specific Volume of Saturated Soil

The total weight when saturated is $\{G_s + (v-1)\}\gamma_w$ and dry is $G_s\gamma_w$. These weights within a total volume v lead to the definition of

$$\text{saturated bulk density}, \gamma = \frac{G_s + v - 1}{v}\gamma_w = \frac{G_s + e}{1+e}\gamma_w$$
$$\text{and dry bulk density}, \gamma_d = \frac{G_s}{v}\gamma_w. \tag{1.5}$$

It is useful to remember a relationship between the water content w and specific volume v of a saturated soil

$$v = 1 + G_s w. \tag{1.6}$$

Typical values are as follows: sand with $G_s = 2.65$ when in a *loose* state with $v = 1.8$ will have $\gamma = 1.92\gamma_w$; in a *dense* state with $v = 1.5$ will have $\gamma = 2.10\gamma_w$; clay with $G_s = 2.75$ when at the *liquid* limit might have $w = 0.7$ and then with $v = 1+2.75\times0.7 = 2.92$ it will have $\gamma = 1.60\gamma_w$; at the *plastic* limit it might have $w = 0.3$ and then with $v = 1+2.75\times0.3 = 1.83$ it will have $\gamma = 1.95\gamma_w$. Actual values in any real case will be determined by experiment.

1.6 The Effective Stress Concept

We will discuss stress and strain in more detail in the next chapter, but here we must introduce two topics: (a) the general the treatment of essentially discontinuous material as if it were continuous, and (b) the particular treatment of saturated soil as a two phase continuum.

The first of these topics has a long history.[16] Navier treated elastic material as an assembly of molecular particles with systems of forces which were assumed to be proportional to the small changes of distance between particles. In his computation of the sum of forces on a particle Navier integrated over a sphere of action as if molecular forces were continuously distributed, and ended with a single elastic constant. Subsequently, in 1822 Cauchy replaced the notion of forces between molecular particles with the notion of distributed pressures on planes through the interior of a continuum. This work opened a century of successive developments in continuum mechanics. Cauchy and other early workers retained Navier's belief that the elasticity of a material could be characterized by a single constant but, when Green offered a derivation of the equations of elasticity based on a potential function rather than on a hypothesis about the molecular structure of the material, it became clear that the linear properties of an isotropic material had to be characterized by *two* constants – a bulk modulus and a shear modulus.

Thereafter, in the mathematical theory of elasticity and in other sections of continuum mechanics, success has attended studies which treat a volume of material

simply as a space in which some properties such as strain energy or plastic power are continuously distributed So far the advances in solid state physics which have been accompanied by introduction of new materials and by new interpretations of the properties of known materials, have not led to a revival of Navier's formulation of elasticity. There is a clear distinction between workers in continuum mechanics who base solutions of boundary value problems on equations into which they introduce certain material constants determined by experiment, and workers in solid-state physics who discuss the material constants *per se.*

Words like specific volume, pressure, stress, strain are essential to a proper study of continuum mechanics. Once a sufficient set of these words is introduced all subsequent discussion is judged in the wider context of continuum mechanics, and no plea for special treatment of this or that material can be admitted. Compressed soil, and rolled steel, and nylon polymer, must have essentially equal status in continuum mechanics.

The particular treatment of saturated soil as a *two-phase* continuum, while perfectly proper in the context of continuum mechanics is sufficiently unusual to need comment. We have envisaged a distribution of clean solid particles in mechanical contact with each other, with water wetting everything except the most minute areas of interparticle contact, and with water filling every space not occupied by solids. The water is considered to be an incompressible liquid in which the *pore pressure* may vary from place to place. Pore-water may flow through the structure of particles under the influence of excess pore-pressures: if the structure of particles remains rigid a steady flow problem of *seepage* will arise, and if the structure of particles alters to a different density of packing the transient flow problem of *consolidation* will occur. The stress concept is discussed in chapter 2, and the total stress component σ normal to any plane in the soil is divided into two parts; the pore-pressure u_w and the *effective* stress component σ', which must be considered to be effectively carried by the structure of soil particles. The pore-pressure u_w can be detected experimentally if a porous-tipped tube is inserted in the soil. The total stress component can be estimated from knowledge of the external forces and the weight of the soil body. The effective stress component σ' is simply calculated as

$$\sigma' = \sigma - u_w \tag{1.7}$$

and our basic supposition is that the mechanical behaviour of the effective soil structure depends on all the components of the *effective stress* and is quite independent of u_w.

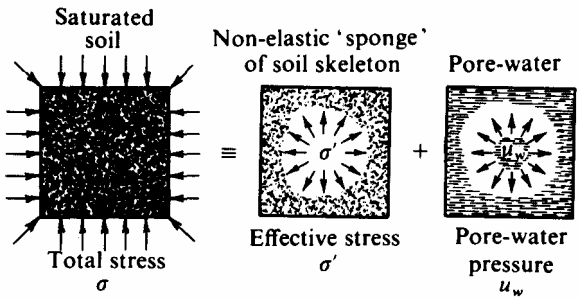

Fig. 1.5 Saturated Soil as Two-phase Continuum

In Fig. 1.5 the different phases are shown diagrammatically: each phase is assumed to occupy continuously the entire space, somewhat in the same manner that two vapours sharing a space are assumed to exert their own partial pressures. In Fig. 1.6 a simple tank is shown containing a layer of saturated soil on which is superimposed a layer of lead shot. The pore-pressure at the indicated depth in the layer is $u_w = \gamma_w \times h_w$, and this applies whether h_w is a metre of water in a laboratory or several kilometres of water in an ocean

abyss. The lead shot is applying the effective stress which of controls the mechanical behaviour of the soil.

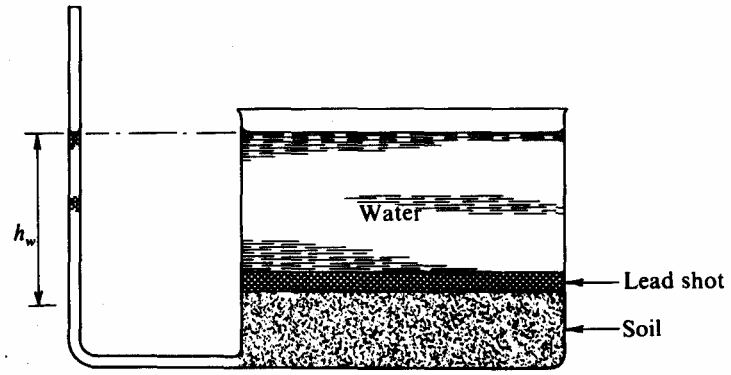

Fig. 1.6 Pore-pressure and Effective Stress

The introduction of this concept of effective stress by Terzaghi, and its subsequent generalization by Rendulic, was the essential first step in the development of a continuum theory of the mechanical behaviour of remoulded saturated soils.

1.7 Some Effects that are 'Mathematical' rather than 'Physical'

Most texts on soil mechanics[17] refer to work of Prandtl which solved the problem of plane punch indentation into perfectly *plastic* material; the same texts also refer to work of Boussinesq which solved various problems of contact stresses in a perfectly *elastic* material. The unprepared reader may be surprised by the contrast between these solutions. In the elastic case stress and strain vary continuously, and every load or boundary displacement causes some disturbance – albeit a subtle one – *everywhere* in the material. In direct contrast, the plastic case of limiting stress distribution leads to regions of *constant* stress set abruptly against fans of *varying* stress to form a crude patchwork.

We can begin to reconcile these differences when we realize that both types of solution must satisfy the same fundamental differential equations of equilibrium, but that the elastic equations are 'elliptic' in character[18] whereas the plastic equations are 'hyperbolic'. A rather similar situation occurs in compressible flow of gases, where two strongly contrasting physical regimes are the mathematical consequence of a *single* differential equation that comes from a single rather simple physical model.

The general differential equation of steady compressible flow in the (x, *y)* plane has the form[19]

$$\left(1-M^2\right)\frac{\partial^2\phi}{\partial x^2}+\frac{\partial^2\phi}{\partial y^2}=0 \tag{1.8}$$

where φ is a potential function, and M (the Mach number) is the ratio u/v_{so} of the flow velocity u and the sonic velocity v_{so} corresponding to that flow. The model is simply one of a fluid with a limiting sonic velocity.

To illustrate this, we have an example in Fig. 1.7(a) of wavefronts emanating at speed v_{so} from a single fixed source of disturbance O in a fluid with uniform low-speed flow $u<v_{so}$. After a time t, the centre of the disturbance has been carried a distance ut downstream,

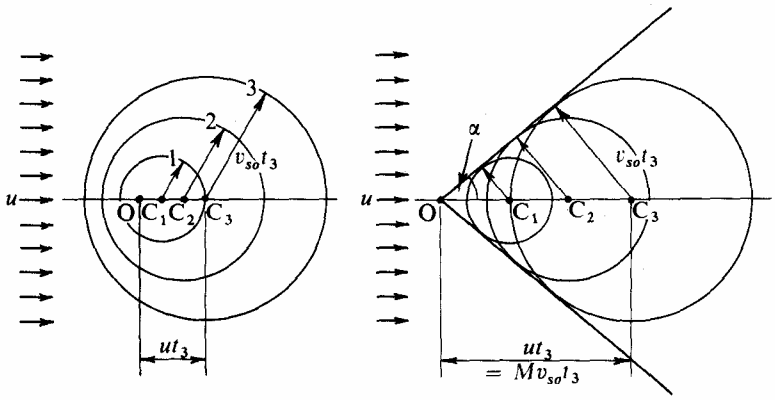

(a) Subsonic case $M < 1$ (b) Supersonic case $M > 1$

Fig. 1.7 Wavefronts Disturbing Uniform Flow

but this is less than the radius $v_{so}t$ of the wavefront. The wavefronts will eventually reach all points of the fluid.

In contrast, in Fig. 1.7(b) we have the same source disturbing a fluid with uniform high-speed flow $u>v_{so}$. In this case the wavefronts are carried so fast downstream that they can never cross the Mach cone (of angle 2α where M sin α = 1) and never reach points of the fluid outside it.

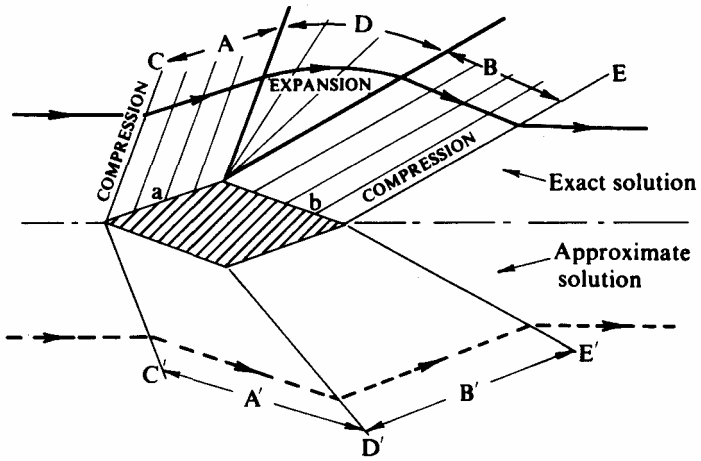

Fig. 1.8 High-speed Flow past an Aerofoil

In the subsonic case where $M<1$ the general differential equation (1.8) is elliptic without real 'characteristic' directions (i.e., there is no real solution for α) and the Mach cone is not generated. In the supersonic case where $M>1$, the general differential equation is hyperbolic with real 'characteristic' directions existing at angles ± α to the direction of flow.

The example of high speed flow past an aerofoil is shown in Fig. 1.8; above the aerofoil we show an 'exact' pattern of characteristics and below the aerofoil an approximation. The directions of the characteristics are found from the local sonic velocity and the flow velocity. Conditions along straight segments 'a' and 'b' of the profile dictate straight supersonic flow in domains A and B. The flow lines have concentrated changes of direction at the compression shocks C and E; in the exact solution a steady change of direction occurs throughout the expansion wave D – a centred fan of characteristics – whereas in the approximation a concentrated expansion D' leads to a concentrated change

of direction. This approximation is valid for calculations of integrated effects near the aerofoil.

Some simple intuitive understanding of a problem of plane plastic flow can be gained from Fig. 1.9, which shows inverted extrusion of a contained metal billet pressed against a square die. The billet A is rigidly contained: the billet advances on the die with a certain velocity but when the metal reaches the fan B, it distorts in shear and it leaves the die as a rigid bar C with twice the billet velocity. Each element of metal is rigid until it enters the fan, it shears and flows within the fan, and on exit it abruptly freezes into the deformed pattern. The effect of the die is severe, and local. The metal in the fan is stressed to its yield limit and it is not possible to transmit more pressure from the billet to the die face through this yielding plastic material. In the mathematically comparable problems of supersonic flow we have regions into which it is not possible to propagate certain disturbances and the inability of the material to disperse these disturbances results in locally concentrated physical effects.

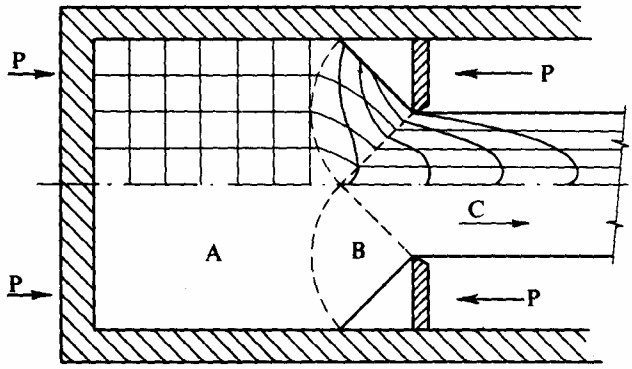

Fig. 1.9 Extrusion of Metal Billet (After Hill)

We have to explain in this book much more complicated models than the models of compressible flow or plastic shear flow. It will take us three more chapters to develop initial concepts of stress and strain and of steady and transient flow of water in soil. When we reach the new models for mechanical behaviour of a soil it will take four more chapters to explain their working, and the last chapter can only begin to review what is already known of the mathematical consequences of older models.

1.8 The Critical State Concept

The kernel of our ideas is the concept that soil and other granular materials, if continuously distorted until they flow as a frictional fluid, will come into a well-defined critical state determined by two equations

$$q = Mp$$

$$\Gamma = v + \lambda \ln p.$$

The constants M, Γ, and λ represent basic soil-material properties, and the parameters q, v, and p are defined in due course.

Consider a random aggregate of irregular ‘solid’ particles of diverse sizes which tear, rub, scratch, chip, and even bounce against each other during the process of continuous deformation. If the motion were viewed at close range we could see a stochastic process of random movements, but we keep our distance and see a continuous flow. At close range we would expect to find many complicated causes of power dissipation and some damage to particles; however, we stand back from the small details and loosely describe the whole process of power dissipation as ‘friction’, neglecting the

possibilities of degradation or of orientation of particles. The first equation of the critical states determines the magnitude of the 'deviator stress' q needed to keep the soil flowing continuously as the product of a frictional constant M with the effective pressure p, as illustrated in Fig. 1.10(a).

Microscopically, we would expect to find that when interparticle forces increased, the average distance between particle centres would decrease. Macroscopically, the second equation states that the specific volume v occupied by unit volume of flowing particles will decrease as the logarithm of the effective pressure increases (see Fig. 1.10(b)). Both these equations make sense for dry sand; they also make sense for saturated silty clay where low effective pressures result in large specific volumes – that is to say, more water in the voids and a clay paste of a softer consistency that flows under less deviator stress.

Specimens of remoulded soil can be obtained in very different states by different sequences of compression and unloading. Initial conditions are complicated, and it is a problem to decide how rigid a particular specimen will be and what will happen when it begins to yield. What we claim is that the problem is not so difficult if we consider the *ultimate* fully remoulded condition that might occur if the process of uniform distortion were carried on until the soil flowed as a frictional fluid. The *total change* from any initial state to an ultimate critical state can be precisely predicted, and our problem is reduced to calculating just how much of that total change can be expected when the distortion process is not carried too far.

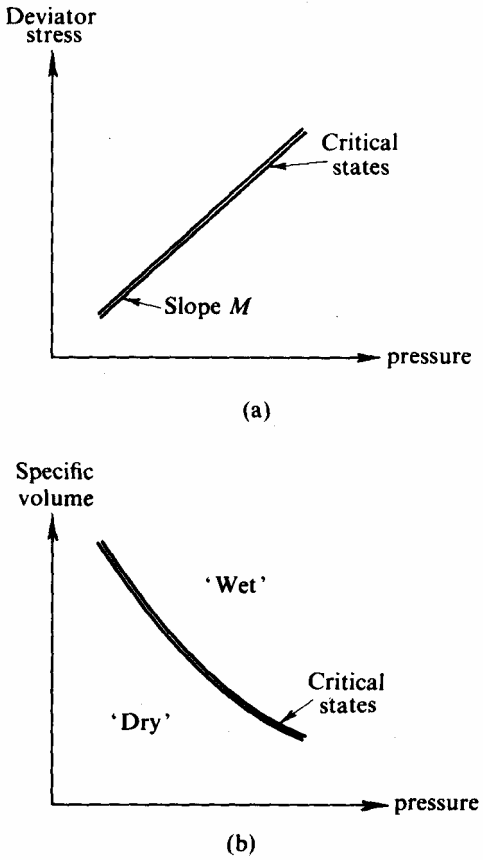

Fig. 1.10 Critical States

The critical states become our base of reference. We combine the effective pressure and specific volume of soil in any state to plot a single point in Fig. 1.10(b): when we are looking at a problem we begin by asking ourselves if the soil is looser than the critical states. In such states we call the soil 'wet', with the thought that during deformation the effective soil structure will give way and throw some pressure into the pore-water (the

amount will depend on how far the initial state is from the critical state), this positive pore-pressure will cause water to bleed out of the soil, and in remoulding soil in that state our hands would get wet. In contrast, if the soil is denser than the critical states then we call the soil 'dry', with the thought that during deformation the effective soil structure will expand (this expansion may be resisted by negative pore-pressures) and the soil would tend to suck up water and dry our hands when we remoulded it.

1.9 Summary

We will be concerned with isotropic mechanical properties of soil-material, particularly remoulded soil which lacks 'fabric'. We will classify the solids by their mechanical grading. The voids will be saturated with water. The soil-material will possess certain 'index' properties which will turn out to be significant because they are related to important soil properties – in particular the plasticity index PI will be related to the constant λ from the second of our critical state equations.

The current state of a body of soil-material will be defined by specific volume *v,* effective stress (loosely defined in eq. (1.7)), and pore-pressure u_w. We will begin with the problem of the definition of stress in chapter 2. We next consider, in chapter 3, *seepage* of water in steady flow through the voids of a rigid body of soil- material, and then consider unsteady flow out of the voids of a body of soil-material while the volume of voids alters during the transient *consolidation* of the body of soil-material (chapter 4).

With this understanding of the well-known models for soil we will then come, in chapters *5, 6,* 7, and 8, to consider some models based on the concept of critical states.

References to Chapter 1

1 Coulomb, C. A. Essai sur une application des règles de maximis et minimis a quelques problèmes de statique, relatifs a l'architecture. *Mémoires de Mathématique de I'Académie Royale des Sciences,* Paris, *7,* 343 – 82, 1776.

2 Prandtl, **L.** *The Essentials of Fluid Dynamics,* Blackie, *1952,* p. 106, or, for a fuller treatment,

3 Rosenhead, L. *Laminar Boundary Layers,* Oxford, 1963.

4 Krumbein, W. C. and Pettijohn, F. J. *Manual of Sedimentary Petrography,* New York, 1938, PP. 97 – 101.

5 British Standard Specification (B.S.S.) 1377: 1961. *Methods of Testing Soils for Civil Engineering Purposes,* pp. 52 – 63; *alternatively* a test using the hydrometer is standard for the 6American Society for Testing Materials (A.S.T.M.) Designation D422-63 adopted 1963.

6 Hvorslev, M. J. *(Iber die Festigkeirseigenschafren Gestörter Bindiger Böden,* Køpenhavn, 1937.

7 Eldin, A. K. Gamal, *Some Fundamental Factors Controlling the Shear Properties of Sand,* Ph.D. Thesis, London University, 1951.

8 Penman, A. D. M. 'Shear Characteristics of a Saturated Silt, Measured in Triaxial Compression', *Gèotechnique* 3, 1953, pp. 3 12 – 328.

9 Gilbert, G. D. *Shear Strength Properties of Weald Clay,* Ph.D. Thesis, London University, *1954.*

10 Plant, J. R. *Shear Strength Properties of London Clay,* M.Sc. Thesis, London University, 1956.

11 Wroth, C. P. *Shear Behaviour of Soils,* Ph.D. Thesis, Cambridge University, 1958.

[12] British Standard Specification (B.S.S.) 410:1943, *Test Sieves;* or American Society for Testing Materials (A.S.T.M.) E11-61 adopted 1961.
[13] Skempton, A. W. 'Soil Mechanics in Relation to Geology', *Proc. Yorkshire Geol. Soc.* 29, 1953, pp. 33 – 62.
[14] Grim, R. E. *Clay Mineralogy,* McGraw-Hill, 1953.
[15] Bjerrum, L. and Rosenqvist, I. Th. 'Some Experiments with Artificially Sedimented Clays', *Géotechnique 6, 1956,* pp. 124 – 136.
[16] Timoshenko, S. P. *History of Strength of Materials,* McGraw-Hill, 1953, pp. 104 – 110 and 217.
[17] Terzaghi, K. *Theoretical Soil Mechanics,* Wiley, 1943.
[18] Hopf, L. *Introduction to the Differential Equations of Physics,* Dover, 1948.
[19] Hildebrand, F. B. *Advanced Calculus for Application,* Prentice Hall, 1963, p. 312.
[20] Lambe, T. W. *Soil Testing for Engineers,* Wiley, *1951,* p. 24.

2
Stresses, strains, elasticity, and plasticity

2.1 Introduction

In many engineering problems we consider the behaviour of an *initially unstressed* body to which we apply some *first* load-increment. We attempt to predict the consequent distribution of stress and strain in key zones of the body. Very often we assume that the material is perfectly elastic, and because of the assumed linearity of the relation between stress-increment and strain-increment the application of a *second* load-increment can be considered as a separate problem. Hence, we solve problems by applying each load-increment to the unstressed body and superposing the solutions. Often, as engineers, we speak loosely of the relationship between stress-increment and strain-increment as a 'stress – strain' relationship, and when we come to study the behaviour of an inelastic material we may be handicapped by this imprecision. It becomes necessary in soil mechanics for us to consider the application of a stress-increment to a body that is *initially stressed,* and to consider the actual sequence of load-increments, dividing the loading sequence into a series of small but discrete steps. We shall be concerned with the changes of configuration of the body: each *strain-increment* will be dependent on the *stress* within the body at that particular stage of the loading sequence, and will also be dependent on the particular *stress-increment* then occurring.

In this chapter we assume that our readers have an engineer's working understanding of elastic stress analysis but we supplement this chapter with an appendix A (see page 293). We introduce briefly our notation for *stress* and *stress-increment,* but care will be needed in §2.4 when we consider *strain-increment.* We explain the concept of a *tensor* being divided into *spherical* and *deviatoric* parts, and show this in relation to the elastic constants: the axial compression or extension test gives engineers two elastic constants, which we relate to the more fundamental bulk and shear moduli. For elastic material the properties are independent of stress, but the first step in our understanding of inelastic material is to consider the representation of possible states of stress (other than the unstressed state) in *principal stress space.* We assume that our readers have an engineer's working understanding of the concept of 'yield functions', which are functions that define the combinations of stress at which the material yields plastically according to one or other theory of the strength of materials. Having sketched two yield functions in principal stress space we will consider an aspect of the theory of plasticity that is less familiar to engineers: the association of a plastic strain-increment with yield at a certain combination of stresses. Underlying this associated 'flow' rule is a *stability* criterion, which we will need to understand and use, particularly in chapter *5*.

2.2 Stress

We have defined the effective stress component normal to any plane of cleavage in a soil body in eq. (1.7). In this equation the pore-pressure u_w, measured above atmospheric pressure, is subtracted from the (total) normal component of stress σ acting on the cleavage plane, but the tangential components of stress are unaltered. In Fig. 2.1 we see the total stress components familiar in engineering stress analysis, and in the following Fig. 2.2 we see the effective stress components written with *tensor-suffix* notation.

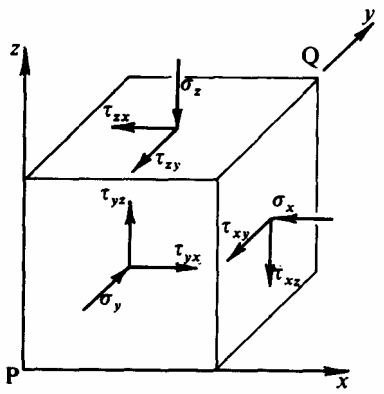

Fig. 2.1 Stresses on Small Cube: Engineering Notation

The equivalence between these notations is as follows:

$$\sigma_x = \sigma'_{11} + u_w \qquad \tau_{xy} = \sigma'_{12} \qquad \tau_{xz} = \sigma'_{13}$$
$$\tau_{yx} = \sigma'_{21} \qquad \sigma_y = \sigma'_{22} + u_w \qquad \tau_{yz} = \sigma'_{23}$$
$$\tau_{zx} = \sigma'_{31} \qquad \tau_{zy} = \sigma'_{32} \qquad \sigma_z = \sigma'_{33} + u_w .$$

We use *matrix* notation to present these equations in the form

$$\begin{bmatrix} \sigma_x & \tau_{xy} & \tau_{xz} \\ \tau_{yx} & \sigma_y & \tau_{yz} \\ \tau_{zx} & \tau_{zy} & \sigma_z \end{bmatrix} = \begin{bmatrix} \sigma'_{11} & \sigma'_{12} & \sigma'_{13} \\ \sigma'_{21} & \sigma'_{22} & \sigma'_{23} \\ \sigma'_{31} & \sigma'_{32} & \sigma'_{33} \end{bmatrix} + \begin{bmatrix} u_w & 0 & 0 \\ 0 & u_w & 0 \\ 0 & 0 & u_w \end{bmatrix}.$$

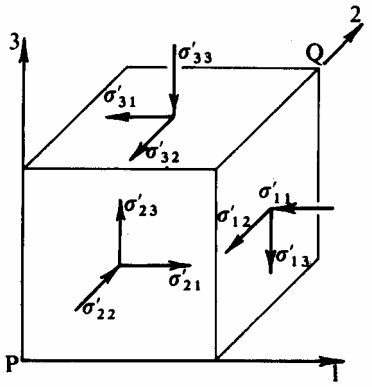

Fig. 2.2 Stresses on Small Cube: Tensor Suffix Notation

In both figures we have used the *same* arbitrarily chosen set of Cartesian reference axes, labelling the directions (x, y, *z*) and (1, 2, 3) respectively. The stress components acting on the cleavage planes perpendicular to the 1-direction are σ'_{11}, σ'_{12} and σ'_{13}. We have exactly similar cases for the other two pairs of planes, so that each stress component can be written as σ'_{ij} where the first suffix *i* refers to the direction of the normal to the cleavage plane in question, and the second suffix *j* refers to the direction of the stress component itself. It is assumed that the suffices *i* and *j* can be permuted through all the values 1, 2, and 3 so that we can write

$$\sigma'_{ij} = \begin{bmatrix} \sigma'_{11} & \sigma'_{12} & \sigma'_{13} \\ \sigma'_{21} & \sigma'_{22} & \sigma'_{23} \\ \sigma'_{31} & \sigma'_{32} & \sigma'_{33} \end{bmatrix}. \qquad (2.1)$$

The relationships $\sigma'_{ij} \equiv \sigma'_{ji}$ expressing the well-known requirement of equality of complementary shear stresses, mean that the array of nine stress components in eq. (2.1) is symmetrical, and necessarily degenerates into a set of only six independent components.

At this stage it is important to appreciate the sign convention that has been adopted here; namely, *compressive* stresses have been taken as *positive,* and the shear stresses acting on the faces containing the reference axes (through P) as *positive* in the *positive* directions of these axes (as indicated in Fig. 2.2). Consequently, the *positive* shear stresses on the faces through Q (i.e., further from the origin) are in the opposite direction.

Unfortunately, this sign convention is the exact opposite of that used in the standard literature on the Theory of Elasticity (for example, Timoshenko and Goodier[1], Crandall and Dahl[2]) and Plasticity (for example, Prager[3], Hill[4], Nadai[5]), so that care must be taken when reference and comparison are made with other texts. But because in soil mechanics we shall be almost exclusively concerned with compressive stresses which are universally assumed by all workers in the subject to be positive, we have felt obliged to adopt the same convention here.

It is always possible to find three mutually orthogonal *principal* cleavage planes through any point P which will have zero shear stress components. The directions of the normals to these planes are denoted by (*a, b, c*), see Fig. 2.3. The array of *three principal effective stress components* becomes

$$\begin{bmatrix} \sigma'_a & 0 & 0 \\ 0 & \sigma'_b & 0 \\ 0 & 0 & \sigma'_c \end{bmatrix}$$

and the directions (*a*, *b*, *c*) are called principal stress directions or principal stress axes. If, as is common practice, we adopt the principal stress axes as permanent reference axes we only require three data for a complete specification of the state of stress at P. However, we require three data for relating the principal stress axes to the original set of arbitrarily chosen reference axes (1, 2, 3). In total we require *six* data to specify stress relative to arbitrary reference axes.

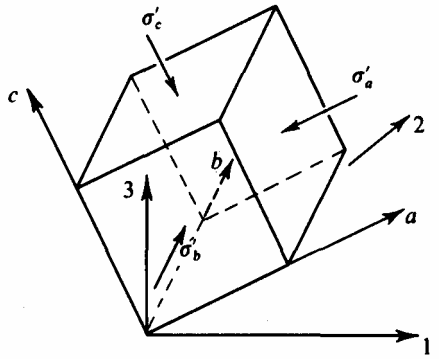

Fig. 2.3 Principal Stresses and Directions

2.3 Stress-increment

When considering the application of a small increment of stress we shall denote the resulting *change* in the value of any parameter x by $\dot{x}$. This convention has been adopted in preference to the usual notation & because of the convenience of being able to express, if need be, a reduction in x by $+\dot{x}$ and an increase by $-\dot{x}$ whereas the mathematical convention demands that $+\delta x$ always represents an increase in the value of x. With this notation care will be needed over signs in equations subject to integration; and it must be noted that a dot does *not* signify rate of change with respect to *time.*

Hence, we will write *stress-increment* as

$$\dot{\sigma}'_{ij} = \begin{bmatrix} \dot{\sigma}'_{11} & \dot{\sigma}'_{12} & \dot{\sigma}'_{13} \\ \dot{\sigma}'_{21} & \dot{\sigma}'_{22} & \dot{\sigma}'_{23} \\ \dot{\sigma}'_{31} & \dot{\sigma}'_{32} & \dot{\sigma}'_{33} \end{bmatrix}. \tag{2.2}$$

where each component $\dot{\sigma}'_{ij}$ is the difference detected in effective stress as a result of the small load-increment that was applied; this will depend on recording also the change in pore-pressure $\dot{u}_w$. This set of nine components of stress-increment has exactly the same properties as the set of stress components σ'_{ij} from which it is derived. Complementary shear stress-increments will necessarily be equal $\dot{\sigma}'_{ij} \equiv \dot{\sigma}'_{ji}$; and it will be possible to *find* three principal directions *(d,e,f)* for which the shear stress-increments disappear $\dot{\sigma}'_{ij} \equiv 0$ and the three normal stress-increments $\dot{\sigma}'_{ij}$ become principal ones.

In general we would expect the data of principal stress-increments and their associated directions *(d,e,f)* at any interior point in our soil specimen to be six data quite independent of the original stress data: there is no a *priori* reason for their principal directions to be identical to those of the stresses, namely, *a,b,c.*

2.4 Strain-increment

In general at any interior point P in our specimen before application of the load-increment we could embed three extensible fibres PQ, PR, and PS in directions (1, 2, 3), see Fig. 2.4. For convenience these fibres are considered to be of unit length. After application of the load-increment the fibres would have been displaced to positions P'Q', P'R', and P'S'. This total displacement is made up of three parts which must be carefully distinguished:

(a) *body displacement*
(b) body rotation
(c) body distortion.

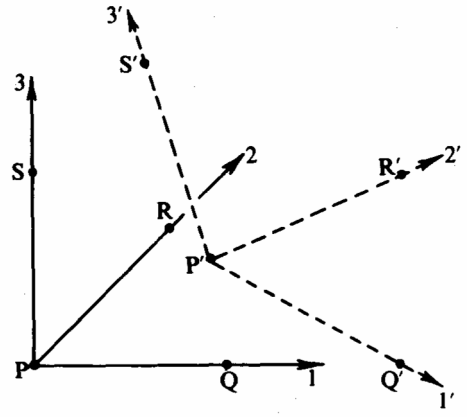

Fig. 2.4 Total Displacement of Embedded Fibres

We shall start by considering the much simpler case of two dimensional strain in Fig. 2.5. Initially we have in Fig. 2.5(a) two orthogonal fibres PQ and PR (of unit length) and their bisector PT (this bisector PT points in the spatial direction which at all times makes equal angles with PQ and PR; PT is not to be considered as an embedded fibre). After a small increment of plane strain the final positions of the fibres are P'Q' and P'R' (no longer orthogonal or of unit length) and their bisector P'T'. The two fibres have moved

respectively through anticlockwise angles α and β, with their bisector having moved through the average of these two angles. This strain-increment can be split up into the three main components:

(a) body displacement represented by the vector PP' in Fig. 2.5(b);

(b) body rotation of $\dot{\theta} = \frac{1}{2}(\alpha + \beta)$ shown in Fig. 2.5(c);

(c) body distortion which is the combined result of *compressive strain-increments* $\dot{\varepsilon}_{11}$ and $\dot{\varepsilon}_{22}$ (being the shortening of the unit fibres), and a relative *turning* of the fibres of amount $\dot{\varepsilon}_{12} \equiv \dot{\varepsilon}_{21} \equiv \frac{1}{2}(\beta - \alpha)$, as seen in Fig. *2.5(d).*

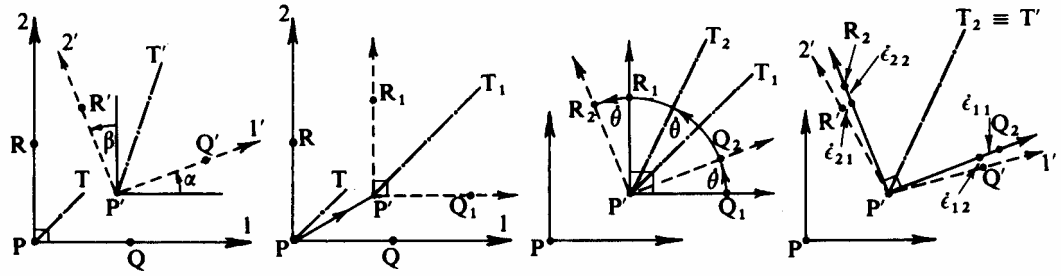

(a) Total displacement ≡ (b) Body displacement + (c) Body rotation + (d) Body distortion

Fig. 2.5 Separation of Components of Displacement

The latter two quantities are the two (equal) *shear strain- increments* of irrotational deformation; and we see that their sum $\dot{\varepsilon}_{12} + \dot{\varepsilon}_{21} \equiv (\beta - \alpha)$ is a measure of the angular *increase* of the (original) right-angle between directions 1 and 2. The definition of shear

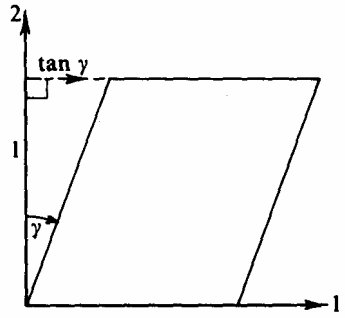

Fig. 2.6 Engineering Definition of Shear Strain

strain, γ,* often taught to engineers is shown in Fig. 2.6 in which $\alpha = 0$ and $\beta = -\gamma$ and use of the opposite sign convention associates positive shear strain with a reduction of the right-angle. In particular we have $\dot{\theta} = -\frac{1}{2}\gamma = \dot{\varepsilon}_{12} = \dot{\varepsilon}_{21}$ and *half* of the distortion γ is really bodily rotation and only *half* is a measure of pure shear.

Returning to the three-dimensional case of Fig. 2.4 we can similarly isolate the body distortion of Fig. 2.7 by removing the effects of body displacement and rotation. The displacement is again represented by the vector PP' in Fig. 2.4, but the rotation is that experienced by the space diagonal. (The space diagonal is the locus of points equidistant from each of the fibres and takes the place of the bisector.) The resulting distortion of Fig. 2.7 consists of the compressive strain-increments $\dot{\varepsilon}_{11}, \dot{\varepsilon}_{22}, \dot{\varepsilon}_{33}$ and the associated shear strain-increments $\dot{\varepsilon}_{23} = \dot{\varepsilon}_{32}, \dot{\varepsilon}_{31} = \dot{\varepsilon}_{13}, \dot{\varepsilon}_{12} = \dot{\varepsilon}_{21}$: and here again, the first suffix refers to the direction of the fibre and the second to the direction of change.

* Strictly we should use tan γ and not γ; but the definition of shear strain can only apply for angles so small that the difference is negligible.

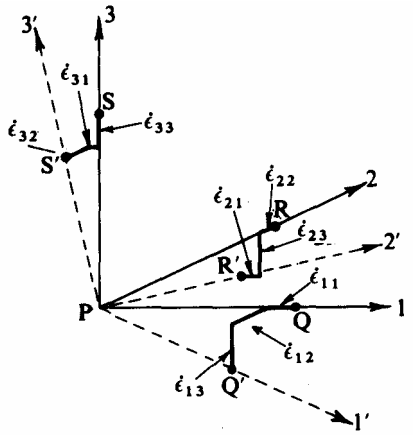

Fig. 2.7 Distortion of Embedded Fibres

We have, then, at this interior point P an array of nine strain measurements

$$\dot{\varepsilon}_{ij} = \begin{bmatrix} \dot{\varepsilon}_{11} & \dot{\varepsilon}_{12} & \dot{\varepsilon}_{13} \\ \dot{\varepsilon}_{21} & \dot{\varepsilon}_{22} & \dot{\varepsilon}_{23} \\ \dot{\varepsilon}_{31} & \dot{\varepsilon}_{32} & \dot{\varepsilon}_{33} \end{bmatrix} \tag{2.3}$$

of which only six are independent because of the equality of the complementary shear strain components. The fibres can be orientated to give directions (*g*, *h*, *i*) of *principal strain-increment* such that there are only compression components

$$\begin{bmatrix} \dot{\varepsilon}_g & 0 & 0 \\ 0 & \dot{\varepsilon}_h & 0 \\ 0 & 0 & \dot{\varepsilon}_i \end{bmatrix}.$$

The sum of these components $\left(\dot{\varepsilon}_g + \dot{\varepsilon}_h + \dot{\varepsilon}_i\right)$equals the increment of volumetric (compressive) strain $\dot{\nu}\left(=-\delta\nu\right)$which is later seen to be a parameter of considerable significance, as it is directly related to density.

There is no requirement for these principal strain-increment directions (*g, h, i*) to coincide with those of either stress (*a*, *b, c*) or stress-increment (*d, e, f*), although we may need to assume that this occurs in certain types of experiment.

2.5 Scalars, Vectors, and Tensors

In elementary physics we first encounter *scalar* quantities such as density and temperature, for which the measurement of a single number is sufficient to specify completely its magnitude at any point.

When *vector* quantities such as displacement d_i are measured, we need to observe three numbers, each one specifying a component (d_1, d_2, d_3) along a reference direction. Change of reference directions results in a change of the numbers used to specify the vector. We can derive a *scalar* quantity $d = \sqrt{\left(d_1^{\,2} + d_2^{\,2} + d_3^{\,2}\right)} = \sqrt{\left(d_i d_i\right)}$ (employing the mathematical summation convention) which represents the distance or magnitude of the displacement vector *d,* but which takes *no* account of its direction.

Reference directions could have been chosen so that the vector components were simply (*d*, 0, 0), but then two direction cosines would have to be known in order to define the new reference axes along which the non-zero components lay, making three data in all. There is no way in which a Cartesian vector can be fully specified with less than three numbers.

The three quantities, stress, stress-increment, and strain-increment, previously discussed in this chapter are all physical quantities of a type called a *tensor.* In measurement of components of these quantities we took note of reference directions *twice,* permuting through them once when deciding on the cleavage planes or fibres, and a second time when defining the directions of the components themselves. The resulting arrays of nine components are symmetrical so that only six independent measurements are required. There is no way in which a symmetrical Cartesian tensor of the second order can be fully specified by less than six numbers.

Just as *one* scalar quantity can be derived from *vector* components so also it proves possible to derive from an array of *tensor* components *three* scalar quantities which can be of considerable significance. They will be independent of the choice of reference directions and unaffected by a change of reference axes, and are termed *invariants* of the tensor.

The simplest scalar quantity is the sum of the diagonal components (or trace), such as $\sigma'_{ii} = (\sigma'_{11} + \sigma'_{22} + \sigma'_{33}) = (\sigma'_a + \sigma'_b + \sigma'_c)$, derived from the stress tensor, and similar expressions from the other two tensors. It can be shown mathematically (see Prager and Hodge[6] for instance) that any strictly symmetrical function of all the components of a tensor must be an invariant; the first-order invariant of the principal stress tensor is $(\sigma'_a + \sigma'_b + \sigma'_c)$, and the second-order invariant can be chosen as $(\sigma'_b\,\sigma'_c + \sigma'_c\,\sigma'_a + \sigma'_a\,\sigma'_b)$ and the third-order one as $(\sigma'_a\,\sigma'_b\,\sigma'_c)$. Any other symmetrical function of a 3 × 3 tensor, such as $(\sigma'_a{}^2 + \sigma'_b{}^2 + \sigma'_c{}^2)$ or $(\sigma'_a{}^3 + \sigma'_b{}^3 + \sigma'_c{}^3)$, can be expressed in terms of these three invariants, so that such a tensor can only have three *independent* invariants.

We can tabulate our findings as follows:

Array of	zero order	first order	second order
Type	scalar	vector	tensor
Example	specific volume	displacement	stress
Notation	υ	d_i	σ'_{ij}
Number of components	$3^0 = 1$	$3^1 = 3$	$3^2 = 9$
Independent data	1	3	9 in general 6 if symetrical
Independent scalar quantities that can be derived	1	1	3

2.6 Spherical and Deviatoric Tensors

A tensor which has only principal components, all equal, can be called *spherical.* For example, hydrostatic or spherical pressure p can be written in tensor form as:

$$\begin{bmatrix} p & 0 & 0 \\ 0 & p & 0 \\ 0 & 0 & p \end{bmatrix} \quad \text{or} \quad p\begin{bmatrix} 1 & 0 & 0 \\ 0 & 1 & 0 \\ 0 & 0 & 1 \end{bmatrix} \quad \text{or} \quad p\begin{bmatrix} 1 & & \\ & 1 & \\ & & 1 \end{bmatrix}.$$

For economy we shall adopt the last of these notations. A tensor which has one principal component zero and the other two equal in magnitude but of opposite sign can be called *deviatoric.* For example, plane (two-dimensional) shear under complementary shear stresses t is equivalent to a purely deviatoric stress tensor with components

$$t\begin{bmatrix} 0 & & \\ & 1 & \\ & & -1 \end{bmatrix}.$$

It is always possible to divide a Cartesian tensor, which has only principal components, into one spherical and up to three deviatoric tensors. The most general case can be divided as follows

$$\begin{bmatrix} \sigma'_a & & \\ & \sigma'_b & \\ & & \sigma'_c \end{bmatrix} = p\begin{bmatrix} 1 & & \\ & 1 & \\ & & 1 \end{bmatrix} + t_a\begin{bmatrix} 0 & & \\ & 1 & \\ & & -1 \end{bmatrix} + t_a\begin{bmatrix} -1 & & \\ & 0 & \\ & & 1 \end{bmatrix} + t_c t_a\begin{bmatrix} 1 & & \\ & -1 & \\ & & 0 \end{bmatrix}$$

where

$$p = \frac{1}{3}(\sigma'_a + \sigma'_b + \sigma'_c), \qquad \left.\begin{aligned} t_a &= \frac{1}{3}(\sigma'_b - \sigma'_c) \\ t_b &= \frac{1}{3}(\sigma'_c - \sigma'_a) \\ t_c &= \frac{1}{3}(\sigma'_a - \sigma'_b) \end{aligned}\right\} \tag{2.4}$$

2.7 Two Elastic Constants for an Isotropic Continuum

A continuum is termed *linear* if successive effects when superposed leave no indication of their sequence; and termed *isotropic* if no directional quality can be detected in its properties.

The linear properties of an elastic isotropic continuum necessarily involve only *two* fundamental material constants because the total effect of a general tensor σ'_{ij} will be identical to the combined effects of one spherical tensor p and up to three deviatoric tensors, t_i. One constant is related to the effect of the spherical tensor and the other to any and all deviatoric tensors.

For an elastic specimen the two fundamental elastic constants relating stress-increment with strain-increment tensors are (a) the *Bulk Modulus K* which associates a spherical pressure increment $\dot{p}$ with the corresponding specific volume change $\dot{v}$

$$\frac{\dot{p}}{K} = (\dot{\varepsilon}_a + \dot{\varepsilon}_b + \dot{\varepsilon}_c) = \frac{\dot{v}}{v} \tag{2.5}$$

and *(b)* the *Shear Modulus G* which associates each deviatoric stress-increment tensor with the corresponding deviatoric strain-increment tensor as follows

$$\begin{matrix}\text{stress}\\ \text{increment}\\ \text{tensor}\end{matrix} \quad \dot{t}\begin{bmatrix} 0 & & \\ & 1 & \\ & & -1 \end{bmatrix} \quad \begin{matrix}\text{gives rise}\\ \text{to strain} -\\ \text{increment}\\ \text{tensor}\end{matrix} \quad \frac{\dot{t}}{2G}\begin{bmatrix} 0 & & \\ & 1 & \\ & & -1 \end{bmatrix}. \tag{2.6}$$

(The factor of *2G* is a legacy from the use of the engineering definition of shear strain γ in the original definition of the shear modulus $t = G\gamma$. We are also making the important assumption that the principal directions of the two sets of tensors coincide.)

It is usual for engineers to derive alternative elastic constants that are appropriate to a specimen in an axial compression (or extension) test, Fig. 2.8(a) in which $\dot{\sigma}'_a = \dot{\sigma}'_l$; $\dot{\sigma}'_b = \dot{\sigma}'_c = 0$. *Young's Modulus E* and *Poisson's Ratio v* are obtained from

$$-\frac{\delta l}{l} = +\frac{\dot{l}}{l} = \dot{\varepsilon}_a = \frac{\dot{\sigma}'_l}{E} \quad \text{and} \qquad \dot{\varepsilon}_b = \dot{\varepsilon}_c = -\frac{\nu \dot{\sigma}'_l}{E}$$

which can be written as

$$\begin{bmatrix} \dot{\varepsilon}_a & & \\ & \dot{\varepsilon}_b & \\ & & \dot{\varepsilon}_c \end{bmatrix} = \frac{\dot{\sigma}'_l}{E} \begin{bmatrix} 1 & & \\ & -\nu & \\ & & -\nu \end{bmatrix}. \tag{2.7}$$

By reference to Fig. 2.8(b) we can split this strain-increment tensor into its spherical and deviatoric parts as follows:

$$\begin{aligned} \begin{bmatrix} \dot{\varepsilon}_a & & \\ & \dot{\varepsilon}_b & \\ & & \dot{\varepsilon}_c \end{bmatrix} &= \frac{1}{3}(\dot{\varepsilon}_a + \dot{\varepsilon}_b + \dot{\varepsilon}_c) \begin{bmatrix} 1 & & \\ & 1 & \\ & & 1 \end{bmatrix} + \frac{1}{3}(\dot{\varepsilon}_b - \dot{\varepsilon}_c) \begin{bmatrix} 0 & & \\ & 1 & \\ & & -1 \end{bmatrix} \\ &\quad + \frac{1}{3}(\dot{\varepsilon}_c - \dot{\varepsilon}_a) \begin{bmatrix} -1 & & \\ & 0 & \\ & & 1 \end{bmatrix} + \frac{1}{3}(\dot{\varepsilon}_a - \dot{\varepsilon}_b) \begin{bmatrix} 1 & & \\ & -1 & \\ & & 0 \end{bmatrix}. \end{aligned} \tag{2.8}$$

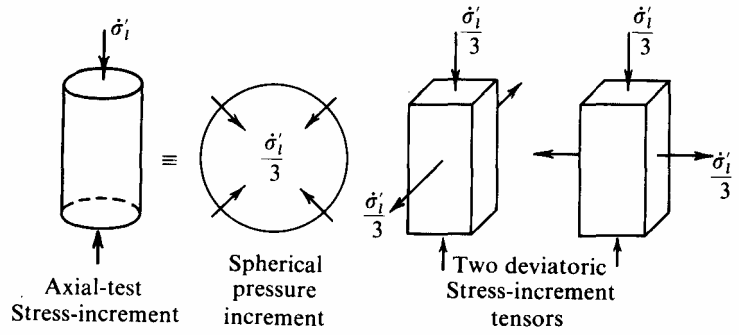

(a) Stress-increment

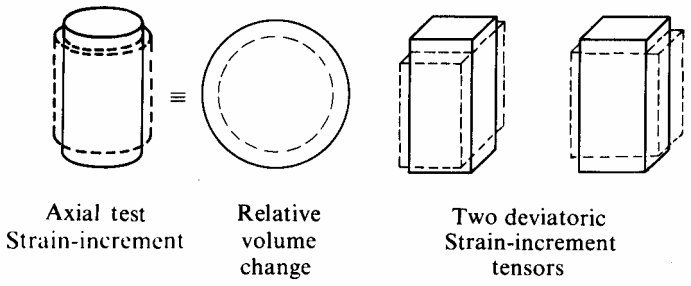

(b) Strain-increment

Fig. 2.8 Unconfined Axial Compression of Elastic Specimen

But from eq. (2.5)

$$\frac{\dot{\sigma}'_l}{3K} = \frac{\dot{\sigma}'_a + \dot{\sigma}'_b + \dot{\sigma}'_c}{3K} = \frac{\dot{p}}{K} = \dot{\varepsilon}_a + \dot{\varepsilon}_b + \dot{\varepsilon}_c$$

and from eq. (2.6)

$$\frac{1}{3}(\dot{\varepsilon}_b - \dot{\varepsilon}_c) \begin{bmatrix} 0 & & \\ & 1 & \\ & & -1 \end{bmatrix} = \frac{1}{6G}(\dot{\sigma}'_b - \dot{\sigma}'_c) \begin{bmatrix} 0 & & \\ & 1 & \\ & & -1 \end{bmatrix} + 2 \text{ similar expressions.}$$

Substituting in eq. (2.8) and using eq. (2.7) we have

$$\frac{\dot{\sigma}'_l}{E}\begin{bmatrix}1 & & \\ & -\nu & \\ & & -\nu\end{bmatrix}=\begin{bmatrix}\dot{\varepsilon}_a & & \\ & \dot{\varepsilon}_b & \\ & & \dot{\varepsilon}_c\end{bmatrix}=\frac{\dot{\sigma}'_l}{9K}\begin{bmatrix}1 & & \\ & 1 & \\ & & 1\end{bmatrix}-\frac{\dot{\sigma}'_l}{6G}\begin{bmatrix}-1 & & \\ & 0 & \\ & & 1\end{bmatrix}+\frac{\dot{\sigma}'_l}{6G}\begin{bmatrix}1 & & \\ & -1 & \\ & & 0\end{bmatrix}$$

which gives the usual relationships

$$\frac{1}{E}=\frac{1}{9K}+\frac{1}{3G}\ \text{and}\ \frac{-\nu}{E}=\frac{1}{9K}-\frac{1}{6G} \tag{2.9}$$

between the various elastic constants.

We see that axial compression of *1/E* is only partly due to spherical compression *1/9K* and mostly caused by shearing distortion *1/3G*; conversely, indirect swelling *v/E* is the difference between shearing distortion *1/6G* and spherical compression *1/9K*. Consequently, we must realize that Young's Modulus alone cannot relate the component of a tensor of stress-increment that is directed across a cleavage plane with the component of the tensor of compressive strain-increment that gives the compression of a fibre embedded along the normal to that cleavage plane. An isotropic elastic body is *not* capable of reduction to a set of three orthogonal coil springs.

2.8 Principal Stress Space

The *principal* stresses $(\sigma'_a,\sigma'_b,\sigma'_c)$ experienced by a point in our soil continuum can be used as Cartesian coordinates to define a point D in a three-dimensional space, called principal stress space. This point D, in Fig. 2.9, although it represents the state of the particular point of the continuum which we are at present considering, only displays the *magnitudes* of the principal stresses and cannot fully represent the stress tensor because the three data establishing the *directions* of the principal stresses are not included.

The division of the principal stress tensor into spherical and deviatoric parts can readily be seen in Figs. 2.9 and 2.10. Suppose, as an example, the principal stresses in question are $\sigma'_a=12,\sigma'_b=6,\sigma'_c=3;$ then, recalling eq. (2.4),

$$\begin{bmatrix}12 & & \\ & 6 & \\ & & 3\end{bmatrix}=\begin{bmatrix}\sigma'_a & & \\ & \sigma'_b & \\ & & \sigma'_c\end{bmatrix}$$

$$=\frac{(\sigma'_a+\sigma'_b+\sigma'_c)}{3}\begin{bmatrix}1 & & \\ & 1 & \\ & & 1\end{bmatrix}+\frac{(\sigma'_b-\sigma'_c)}{3}\begin{bmatrix}0 & & \\ & 1 & \\ & & -1\end{bmatrix}$$

$$+\frac{(\sigma'_c-\sigma'_a)}{3}\begin{bmatrix}-1 & & \\ & 0 & \\ & & 1\end{bmatrix}+\frac{(\sigma'_a-\sigma'_b)}{3}\begin{bmatrix}1 & & \\ & -1 & \\ & & 0\end{bmatrix}$$

$$=7\begin{bmatrix}1 & & \\ & 1 & \\ & & 1\end{bmatrix}+1\begin{bmatrix}0 & & \\ & 1 & \\ & & -1\end{bmatrix}+(-3)\begin{bmatrix}-1 & & \\ & 0 & \\ & & 1\end{bmatrix}+2\begin{bmatrix}1 & & \\ & -1 & \\ & & 0\end{bmatrix}$$

$$= \begin{bmatrix} 7 & & \\ & 7 & \\ & & 7 \end{bmatrix} + \begin{bmatrix} 0 & & \\ & 1 & \\ & & -1 \end{bmatrix} + \begin{bmatrix} 3 & & \\ & 0 & \\ & & -3 \end{bmatrix} + \begin{bmatrix} 2 & & \\ & -2 & \\ & & 0 \end{bmatrix}$$

$$= OA + AB + BC + CD = OD$$

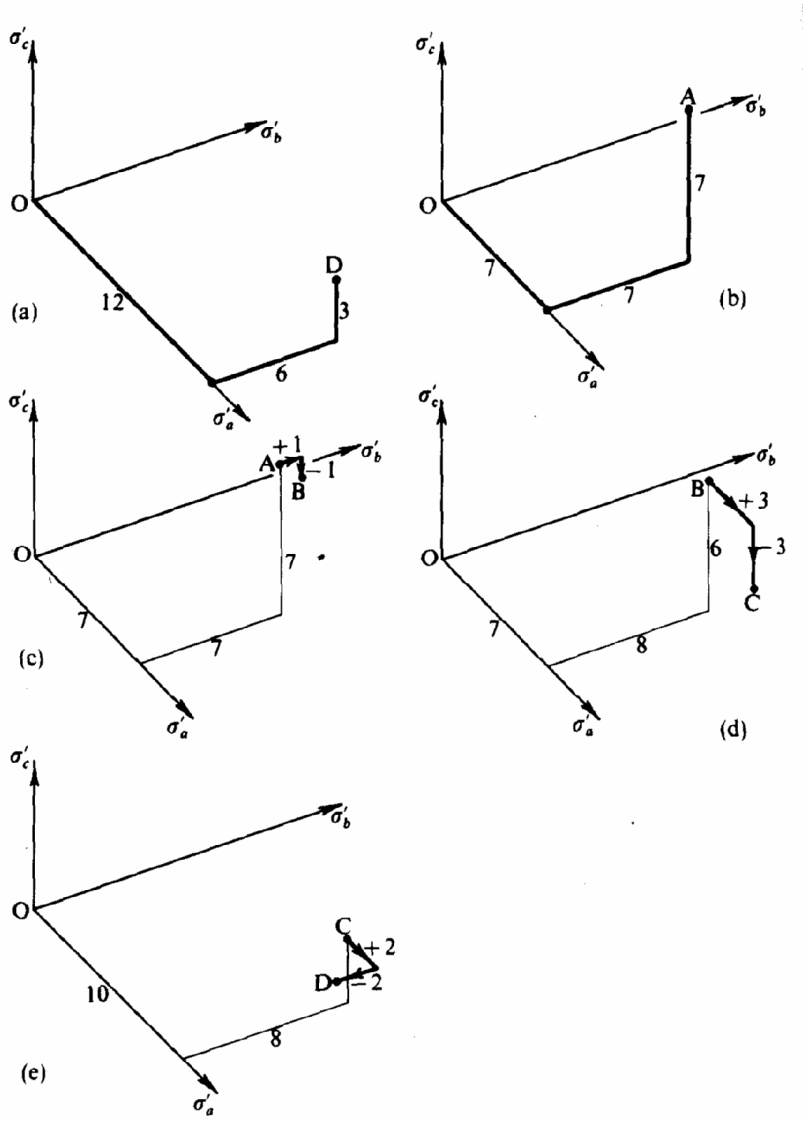

Fig. 2.9 Principal Stress Space

Hence, we see that the point D which represents the state of stress, can be reached *either* in a conventional way, **OD,** by mapping the separate components of the tensor

$$\begin{bmatrix} 12 & & \\ & 6 & \\ & & 3 \end{bmatrix}$$

or by splitting it up into the spherical pressure and mapping **OA**

$$\begin{bmatrix} 7 & & \\ & 7 & \\ & & 7 \end{bmatrix}$$

and three different deviatoric stress tensors and mapping **AB**, **BC,** and **CD:**

$$\begin{bmatrix} 0 & & \\ & 1 & \\ & & -1 \end{bmatrix}, \begin{bmatrix} 3 & & \\ & 0 & \\ & & -3 \end{bmatrix}, \text{and} \begin{bmatrix} 2 & & \\ & -2 & \\ & & 0 \end{bmatrix}.$$

So **AB** is a vector in the plane perpendicular to the u-axis and with equal and opposite components of unity parallel with the other two principal axes: and similarly **BC** and **CD** are vectors as shown.

As mentioned in §2.1, the principal stress space is particularly favoured for representation of theories of the yield strength of plastic materials. Experiments on metals show that large changes of spherical pressure p have no influence on the deviatoric stress combinations that can cause yield. Consequently, for perfectly plastic material it is usual to switch from the principal stress axes to a set of Cartesian axes *(x, y, z)* where

$$\left.\begin{aligned} x &= \frac{1}{\sqrt{3}}\left(\sigma'_a+\sigma'_b+\sigma'_c\right)=\sqrt{(3)}p \\ y &= \frac{1}{\sqrt{2}}=\left(\sigma'_b-\sigma'_a\right) \\ z &= \frac{1}{\sqrt{6}}=\left(2\sigma'_c-\sigma'_b-\sigma'_a\right). \end{aligned}\right\} \tag{2.10}$$

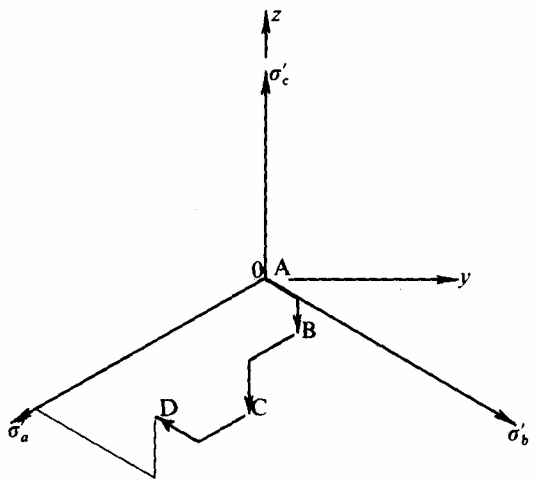

Fig. 2.10 Section of Stress Space Perpendicular to the Space Diagonal

The x-axis coincides with the *space diagonal;* change of spherical pressure has no influence on yielding and the significant stress combinations are shown in a plane *perpendicular* to the space diagonal. In the Fig. 2.10 we look down the space diagonal and see the plane *yz:* the *z*-axis is coplanar with the *x*-axis and the σ'_c-axis, but of course the three axes σ'_a, σ'_b and σ'_c are to be envisaged as rising out of the plane of Fig. 2.10. The mapping of the three different deviatoric stress tensors of our example is shown by the pairs of vectors **AB** and **BC** and **CD** in Fig. 2.10.

When we consider the yielding of perfectly plastic material the alternative theories of strength of materials can be either described by algebraic yield functions or described by symmetrical figures on this *yz*-plane, as we will now see in the next section.

2.9 Two Alternative Yield Functions

Two alternative yield functions are commonly used as criteria for interpretation of tests on plastic behaviour of metals. The first, named after Tresca, suggests that yield occurs when the maximum shear stress reaches a critical value *k*. We can see the effect of the criterion in the sector where in which the function becomes

$$F = \sigma'_a - \sigma'_c - 2k = 0 \tag{2.11}$$

and the intersection of this with the plane $p = \frac{1}{3}(\sigma'_a + \sigma'_b + \sigma'_c) = \text{const.}$ defines one side **IN** of the regular hexagon **INJLKM** in Fig. 2.11. The other sides are defined by appropriate permutation of parameters.

The second function, named after Mises, is expressed as

$$F = (\sigma'_b - \sigma'_c)^2 + (\sigma'_c - \sigma'_a)^2 + (\sigma'_a - \sigma'_b)^2 - 2Y^2 = 0 \tag{2.12}$$

where Y is the yield stress obtained in axial tension. This function together with $p = \frac{1}{3}(\sigma'_a + \sigma'_b + \sigma'_c) = \text{const.}$ has as its locus a circle of radius $\sqrt{\left(\frac{2}{3}\right)}Y$ in Fig. 2.11. Since these two loci are unaffected by the value of the spherical pressure $\frac{1}{3}(\sigma'_a + \sigma'_b + \sigma'_c) = p$, they will generate

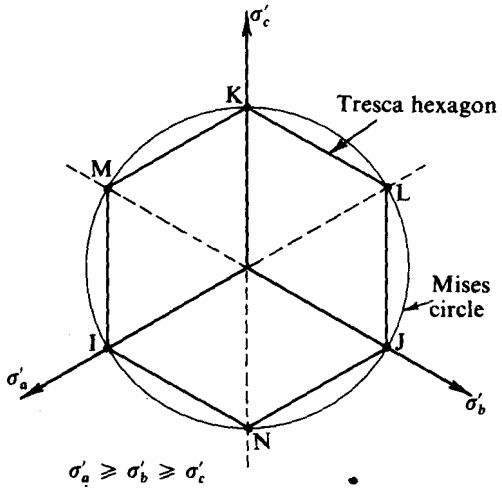

Fig. 2.11 Yield Loci of Tresca and Mises

for various values of p (or x) hexagonal and circular cylinders coaxial with the x-axis. These are illustrated in Fig. 2.12: these cylinders are examples of *yield surfaces,* and all states of stress at which one or other criterion allows material to be in stable equilibrium will be contained inside the appropriate surface.

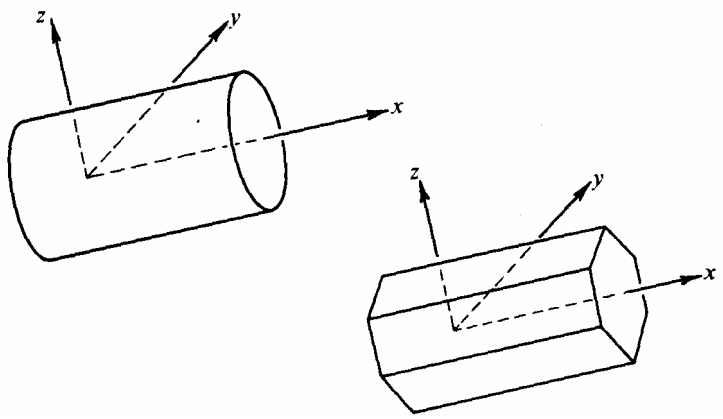

Fig. 2.12 Yield Surfaces in Stress Space

Most tests are what we will call *axial tests,* in which a bar or cylinder of material sustains two radial principal stresses of equal magnitude (often but not always zero) and the axial principal stress is varied until the material yields in compression or extension. Data of stresses in such axial tests will lie in an *axial-test plane* in principal stress space; the three diagonal lines **IL**, **JM**, **KN**, in Fig. 2.11, each lie in one of the three such planes that correspond to axial compression tests with σ'_a *or* σ'_b *or* σ'_c respectively as the major principal stress. Now if we consider, for example, the axial-test plane for which $\sigma'_b = \sigma'_c$, this intersects Tresca's yield surface in the pair of lines $\sigma'_a - \sigma'_c = \pm 2k,$ and it intersects Mises' yield surface in the pair of lines $\sigma'_a - \sigma'_c = \pm Y.$ We cannot use axial-test data to decide which yield function is appropriate to a material – each will fit equally well if we choose 2k = *Y.* More refined tests* on thin-wall tubes of annealed metal in combined tension and torsion do appear to be fitted by Mises' yield function with rather more accuracy than by Tresca's yield function: however, the error in Tresca's function is not sufficient to invalidate its use in appropriate calculations.

2.10 The Plastic-Potential Function and the Normality Condition

As engineers, we concentrate attention on yield functions, because when we design a structure we calculate the factor by which all loads must be multiplied before the structure is brought to collapse. We use elastic theory to calculate deflections under working loads, and generally neglect the calculation of strain-increments in plastic flow. We will find in later chapters that our progress will depend on an understanding of plastic flow.

When any material flows without vorticity it is possible to find a *potential* function, such that the various partial derivatives of that function at any point are equal to the various velocity components at that point. We will meet 'equipotentials' when we discuss seepage in the next chapter, but the idea of a potential is not restricted to flow of water. It is the nature of plastic material to flow to wherever it is forced by the heavy stresses that bring the material to yield, so the potential function for plastic flow must be a function of the components r of stress. The classical formulation of theory of plasticity considers a class of materials for which the *yield* function *F(u)* also serves as the *plastic potential* for the flow. Each of the plastic strain-increments is found from the partial derivatives of the yield function by the equation (which is in effect a definition of plasticity)

$$\nu \dot{\varepsilon}^{p}{}_{ij} = \frac{\partial F}{\partial \sigma'_{ij}} \tag{2.13}$$

* An early set of tests was carried out in the engineering laboratories at Cambridge by G. I. Taylor and H. Quinney.[7]

where v is a scalar factor proportional to the amount of work used in that particular set of plastic strain-increments.

If a material yields as required by Mises' function, eq. (2.12), we can calculate the gradients of this potential function as

$$v\dot{\varepsilon}_a = \frac{\partial F}{\partial \sigma'_a} = 6\left(\sigma'_a - \frac{\sigma'_a+\sigma'_b+\sigma'_c}{3}\right)$$

$$v\dot{\varepsilon}_b = \frac{\partial F}{\partial \sigma'_b} = 6\left(\sigma'_b - \frac{\sigma'_a+\sigma'_b+\sigma'_c}{3}\right)$$

$$v\dot{\varepsilon}_c = \frac{\partial F}{\partial \sigma'_c} = 6\left(\sigma'_c - \frac{\sigma'_a+\sigma'_b+\sigma'_c}{3}\right).$$

For given values of $(\sigma'_a, \sigma'_b, \sigma'_c)$ these equations fix the *relative* magnitudes of the strain-increments, but the number v which adjusts their *absolute* magnitudes will depend on the amount of work used to force that particular set of plastic strain-increments. With given values of $(\sigma'_a, \sigma'_b, \sigma'_c)$ we can equally well associate a point in principal stress space on the yield surface: we can then visualize the plastic strain-increment vector as being normal to the yield surface at that point. Once we have decided upon a yield surface then the associated flow rule of the theory of plasticity obeys a *normality* condition: for Mises' yield function the plastic strain-increments are associated with vectors perpendicular to the cylindrical surface, while for Tresca's yield function the associated vectors are perpendicular to the faces of the hexagonal prism.

2.11 Isotropic Hardening and the Stability Criterion

In the yielding of a metal such as annealed copper we observe, as shown in Fig. 2.13, that once the material has carried an axial stress Y it has hardened and will not yield again until that stress Y is exceeded. We will be particularly interested in a class of *isotropic hardening* plastic materials, for which we can simply substitute the increasing values of Y into equations such as (2.12) and get yield surfaces that expand symmetrically.

Our assumption of isotropic hardening does not mean that we dismiss an apparent occurrence of Bauschinger's effect. Some metal specimens, on hardening in axial tension to a stress Y, will yield on reversal of stress at an axial compressive stress less than Y, as illustrated in Fig. 2.13: in *metals* this indicates some anisotropy. In *soil* the yield strength is found to be a function of spherical pressure

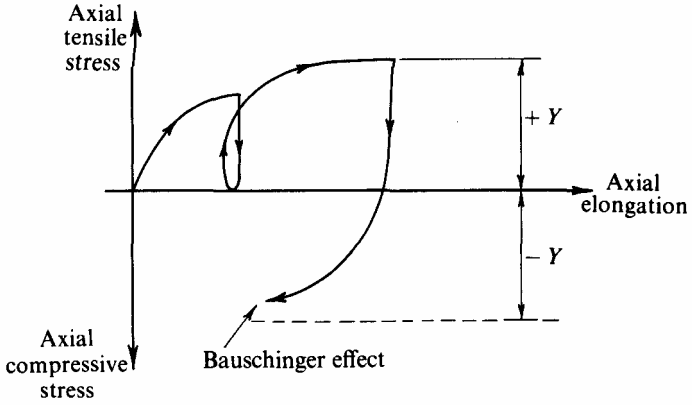

Fig. 2.13 Hardening in an Axial Test

and specific volume, so a major change of yield strength is to be expected on reversal of stress *without* anisotropy.

In Fig. 2.14(a) we have sketched a yield locus $F = 0$. The vector σ'_{ij} represents a combination of stress that brings the material to the point of yielding. The fan of small vectors $\dot{\sigma}'_{ij}$ represent many possible combinations of stress-increment components which would each result in the same isotropic hardening of the material to a new yield locus $F' = 0$. In Fig. 2.14(b) we sketch a normal vector to the yield locus: no matter what stress-increment vector is applied the same associated plastic strain-increments will occur because they are governed by the particular stress combination that has brought the material to yield. The plastic strain-increments are not related directly to the stress-increments, nor are they directly proportional to the stress components (we can see in the figure that the strain- increment vector is *not* sticking out in the same direction as the extension of σ'_{ij}). The plastic strain-increments are found as the gradients of a potential function – the function is F and $\dot{\varepsilon}^p{}_{ij}$ is normal to F.

Engineers have understandably been slow to accept that the materials with which they commonly work really do obey this curious associated flow rule. Recently, D. C. Drucker[8] has introduced the most persuasive concept of 'stability' which illuminates this matter. For all stress-increment vectors directed *outwards* from

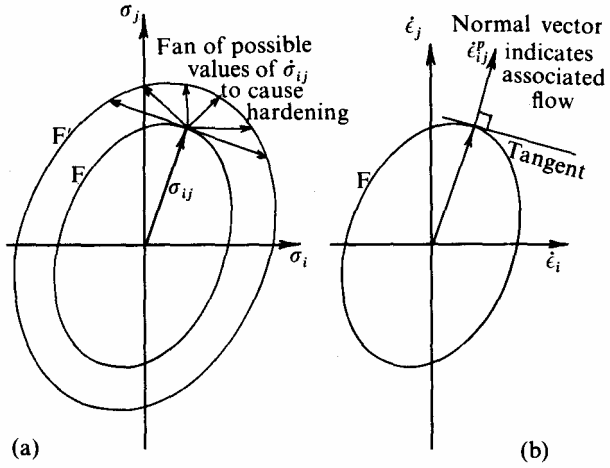

Fig. 2.14 Isotropic Hardening and Associated Plastic Flow

the tangent to the yield locus, the vector product of the stress-increment vector $\dot{\sigma}'_{ij}$ with the associated plastic strain-increment vector $\dot{\varepsilon}^p{}_{ij}$ will be positive or zero

$$\dot{\sigma}'_{ij}\,\dot{\varepsilon}^p{}_{ij} \geq 0. \tag{2.14}$$

Plastic materials are *stable* in the sense that they only yield for stress increments that satisfy eq. (2.14). It is not appropriate for us now to make general statements that go further with the stability concept: it has been the subject of various discussions, and from here on we do best to develop specific arguments that are appropriate to our own topic. Our chapters *5* and 6 will pick up this theme again and go some way towards fulfilment of a suggestion of Drucker, Gibson, and Henkel[9], that soil behaviour can be described by a theory of plasticity.[10,11]

2.12 Summary

Most readers will have some knowledge of the theories of elasticity, plasticity and soil mechanics, so that parts of this chapter will already be familiar to them. As a consequence, the omission and the inclusion of certain material may seem curious on first reading, but the selection and emphasis are deliberate.

We are concerned with the development of a continuum analysis, so that we need to be clear about the manner in which stress and strain components can be defined in the interior of a granular body. It will be found that the current state of a soil depends on the stress and the specific-volume: stress is a second-order symmetrical tensor which requires six numbers for a definition, while specific volume is a scalar and is defined by one number. By emphasizing the importance of the elastic bulk modulus K and shear-modulus G we hope to develop a feeling for these tensor and scalar quantities.

For those who are familiar with Mohr's circle as a representation of stress it may be a surprise to find no mention of it in this chapter, although it will be required as an appendix to chapters 8 and 9. Its omission at this stage is deliberate on the grounds that Mohr's representation of stress imparts no understanding of the interrelation of stress-increment and strain-increment in elastic theory, that it plays little part in continuum theories, and that the uncritical use of Mohr's circle by workers in soil mechanics has been a major obstacle to the progress of our subject.

In contrast, the representation of stress σ'_{ij}, stress-increment $\dot{\sigma}'_{ij}$ and strain-increment $\dot{\varepsilon}_{ij}$, as compact symbols with the tensor suffix is helpful to our progress. Representation of stress in principal stress space is useful and gives an understanding of the difference between spherical pressure and the deviatoric stress tensors. A cautionary word is needed to remind our readers that when a point in principal stress space is defined by three numbers we necessarily assume that we know the three direction cosines of principal directions (needed to make up the six numbers that define a symmetrical 3×3 tensor). When we plot a stress-increment tensor in the same principal stress space, or associate a normal vector to a yield surface with the plastic strain-increment tensor, we necessarily assume that these tensors have the *same principal directions:* if not, then some more information is needed for the definition of these tensors. It will follow that the principal stress space representation is appropriate for discussion of behaviour of isotropic materials in which all principal directions coincide.

We have met yield surfaces that apply to the yielding of elastic/plastic metal. As long as the material is elastic the stress and strain are directly related, so the state of the metal at yield must be a function of stress, and the yield surface can be defined in principal stress space. When metals yield, only plastic distortion occurs, and there is no plastic volume change. The hardening of metal can be defined by a family of successive surfaces in principal stress space and the succession is a function of plastic distortion increment. However, soils and other granular materials show plastic volume change, and we will need to innovate in order to represent this major effect.

We have defined a parameter p, where

$$p = \frac{\sigma'_a + \sigma'_b + \sigma'_c}{3} \qquad \text{from eq. (2.4)}$$

gives an average or mean of the principal stress components, and p is called spherical pressure. One innovation that we will introduce is to propose that soil is a material for which the yield stress first increases and then decreases as spherical pressure increases.

References to Chapter 2

[1] Timoshenko, S. P. and Goodier, J. N. *Theory of Elasticity,* McGraw-Hill, 1951.

[2] Crandall, S. H. and Dahi, N. C. *An Introduction to the Mechanics of Solids,* McGraw-Hill, *1959.*
[3] Prager, W. *An Introduction to Plasticity,* Addison-Wesley, *1959.*
[4] Hill, R. *Mathematical Theory of Plasticity,* Oxford, 1950.
[5] Nadai, A. *Plasticity,* New York, 1931.
[6] Prager, W. and Hodge, P. *G. Theory of Perfectly Plastic Solids,* Wiley,1951, p. 22.
[7] Taylor, G. I. and Quinney, H. 'The Plastic Distortion of Metals', *Phil. Trans. Roy. Soc.,* A. 230, 323 – 363, 1931.
[8] Drucker, D. C. 'On the Postulate of Stability of Material in the Mechanics of Continua', *Journal de Mécanique,* 3,235 – 249, 1964.
[9] Drucker, D. C., Gibson, R. E. and Henkel, D. J. 'Soil Mechanics and Work-hardening Theories of Plasticity', *A.S.C.,* 122, 338 – 346, 1957.
[10] Calladine, C. R. Correspondence, Geotechnique 13, 250 – 255, 1963.
[11] Drucker, D. C. 'Concept of Path Independence and Material Stability for Soils' *Proc. Int. Symp. of Rheology and Soil Mechanics in Grenoble 1964,* Springer-Verlag, 23 – 46, 1966.

3
Seepage

In this chapter the structure of soil particles within our two-phase continuum is considered to be *stationary* and effectively rigid, and we shall study the flow of water through it. This restriction means that we are investigating states of *steady flow* only, and we shall see in chapter 4 that *transient flow* implies change in effective stress which necessarily results in deformation of the soil matrix.

3.1 Excess Pore-pressure

A simple apparatus for investigating the one-dimensional flow of water through a soil is the permeameter of Fig. 3.1. The apparatus consists of a perspex cylinder containing a soil specimen, in this case a saturated sand, supported by a gauze mesh with suitable size of aperture. De-aired water is supplied from a source at a constant head higher than the top of the permeameter, so that water is forced to flow upwards through the sand specimen.

Tappings at two neighbouring points, A and B, in the centre of the cylinder are connected with manometer tubes so that the pressures in the water can be recorded for both these points, with the level of the horizontal upper surface of the sand being used as datum.

Measuring z positively downwards, and h positively upwards from this datum, the *total* pressure in the pore-water u_w at A recorded by the manometer is simply $u_w = \gamma_w(z+h)$. Similarly, the *total* pressure at B is $u_w + \delta u_w = \gamma_w(z+\delta z+h+\delta h)$.

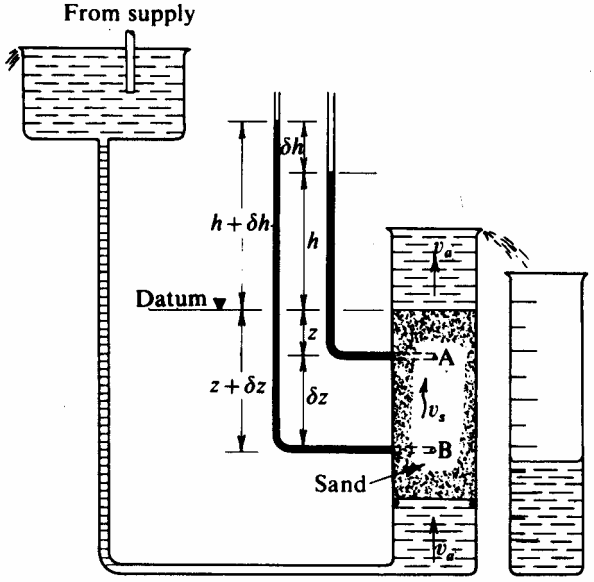

Fig. 3.1 Simple Permeameter

The difference between these two expressions

$$\delta u_w = \gamma_w(\delta z + \delta h) \tag{3.1}$$

is the difference in total pore-pressure between A and B and consists of two terms:

a) $\gamma_w \delta z$ which is the 'elevation' head, solely due to the difference in levels between A and B; it ensures that the total pressures are related to the same datum, and

b) $\gamma_w \delta h$ which will be denoted by δu and termed the *excess pore-pressure* between B and A; it is the sole cause of the (steady) flow of water upwards from B to A.

The quantity, δu, represents the energy loss per unit volume of water that flows from B to A; it is dissipated (a) in viscous drag as the water flows through the individual pores of the soil structure, and *(b)* in change of kinetic energy. In seepage problems in soil mechanics the latter term is negligible, and all the energy is effectively lost in drag, with corresponding reactions being generated in the soil structure, normally termed *seepage forces.*

3.2 Hydraulic Gradient

The points A and B have been chosen to be on the *same flowline* (i.e., water flows from one point on a flowline to the next) which happens to be vertical in this particular apparatus. Generally the flow will not be vertical, and Fig. 3.2 illustrates the case of seepage of groundwater where A and B are still neighbouring points on a flowline separated by a distance δs measured along the flowline but *against* the flow.

The *hydraulic gradient i* at the point A is a vector quantity defined to have magnitude

$$i = -\underset{\delta s \to 0}{Lim}\left(\frac{\delta h}{\delta s}\right) = -\frac{\mathrm{d}h}{\mathrm{d}s} = -\frac{1}{\gamma_w}\frac{\mathrm{d}u}{\mathrm{d}s} \tag{3.2}$$

and to have direction of the flowline at A towards B. This choice of sign convention means that the hydraulic gradient is positive in the direction of the flow that it causes; and we need to note that it is a pseudo-dimensionless quantity, representing the space rate of energy loss per unit weight of water.

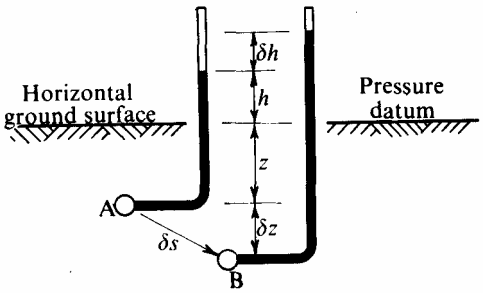

Fig. 3.2 Seepage of Groundwater

3.3 Darcy's Law

Darcy's law (1856) resulted from experiments to establish the relationship between hydraulic gradients and rates of flow of water. If Q is the volume of water flowing through the permeameter during time *t,* then the artificial (or approach and discharge) velocity v_a of the water is given by

$$v_a = \frac{Q}{A_t t}$$

where A_t is the *total* cross-sectional area of the interior of the perspex cylinder.

Darcy's law states that there is a linear relationship between hydraulic gradient and velocity for any given soil (representing a case of steady laminar flow at low Reynolds number)

$$v_a = ki = -k\frac{\mathrm{d}h}{\mathrm{d}s} \tag{3.3}$$

where the constant k is the coefficient of permeability (sometimes called the hydraulic conductivity) and has the dimensions of a velocity. Although the value of k is constant for a particular soil at a particular density it varies to a minor extent with viscosity and temperature of the water and to a major extent with pore size. For instance, for a coarse sand k may be as large as 0.3 cm/s = 3×10^5 ft/yr, and for clay particles of micron size k may be as small as 3×10^{-8} cm/s = 3×10^{-2} ft/yr. This factor of 10^7 is of great significance in soil mechanics and is linked with a large difference between the mechanical behaviours of clay and sand soils.

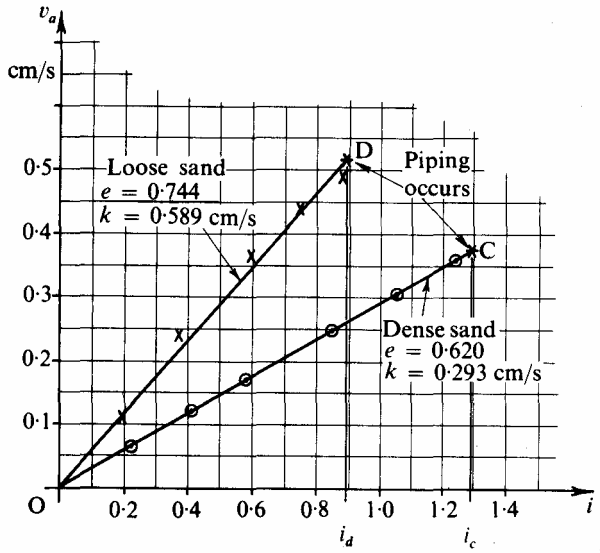

Fig. 3.3 Results of Permeability Test on Leighton Buzzard Sand

Typical results of permeability tests on a sample of Leighton Buzzard sand (between Nos. 14 and 25 B.S. Sieves) for a water temperature of 20°C are shown in Fig. 3.3. Initially the specimen was set up in a dense state achieved by tamping thin layers of the sand. The results give the lower straight line **OC,** which *terminates* at C. Under this hydraulic gradient i_c the upward drag on the particles imparted by the water is sufficient to lift their submerged weight, so that the particles float as a suspension and become a fluidized bed. This *quicksand* condition is also known as piping or *boiling.*

At this critical condition the total drag upwards on the sand between the levels of A and B will be $A_t\ \delta u = A_t\gamma_w\delta h$ and this must exactly balance the submerged weight of this part of the sample, namely $A_t\gamma'\delta s$. Hence, the fluidizing hydraulic gradient should be given by

$$i_f = -\frac{\mathrm{d}h}{\mathrm{d}s} = +\frac{\gamma'}{\gamma_w} = \frac{G_s - 1}{1+e}. \tag{3.4}$$

For the sand in question with e = 0.620 (obtained by measuring the weight and overall volume of the sample) and G_s = 2.65, eq. (3.4), gives a critical hydraulic gradient of 1.02 which is an underestimate of the observed value of 1.29 (which included friction due to the lateral stresses induced in the sand sample in its preparation).

If during piping the supply of water is rapidly stopped the sand will settle into a very loose state of packing. The specific volume is correspondingly larger and the resulting permeability, given by line **OD,** has increased to k=0.589 cm/s from the original value of 0.293 cm/s appropriate to the dense state. As is to be expected from eq. (3.4), the calculated value of the fluidizing hydraulic gradient has fallen to 0.945 because the sample

is looser; any increase in the value of e reduces the value of i_f given by eq. (3.4). We therefore expect $i_c > i_d$.

The variation of permeability for a given soil with its density of packing has been investigated by several workers and the work is well summarized by Taylor[1] and Harr[2]. Typical values for various soil types are given in Table 3.1.

Soil type	*Coefficient of permeability cm/sec*
Gravels	$k > 1$
Sands	$1 > k > 10^{-3}$
Silts	$10^{-3} > k > 10^{-6}$
Clays	$10^{-6} > k$

Table 3.1 Typical values of permeability

The actual velocity of water molecules along their narrow paths through the specimen (as opposed to the smooth flowlines assumed to pass through the entire space of the specimen) is called the seepage velocity, v_s. It can be measured by tracing the flow of dye injected into the water. Its average value depends on the unknown cross-sectional area of voids A_v and equals $Q/A_v t$. But

$$v_s = \left(\frac{Q}{A_v t}\right) = \left(\frac{Q}{A_t t}\right)\left(\frac{A_t}{A_v}\right) = v_a . \frac{v_t}{v_v} = \frac{v_a}{n} = v_a\left(\frac{1+e}{e}\right) \tag{3.5}$$

where V_t and V_v are the total volume of the sample and the volume of voids it contains, and n is the porosity. Hence, for the dense sand sample, we should expect the ratio of velocities to be

$$\frac{v_s}{v_a} = \frac{1+e}{e} = 2.62.$$

It is general practice in all seepage calculations to use the artificial velocity v_a and total areas so that consistency will be achieved.

3.4 Three-dimensional Seepage

In the last section dealing with Darcy's law, we studied the one-dimensional flow of water through a soil sample in the permeameter. We now extend these concepts to the general three-dimensional case, and consider the flow of pore-water through a small cubical element of a large mass of soil, as shown in Fig. 3.4. Let the excess pore-pressure at any point be given by the function $u = f(x, y, z)$ which remains unchanged with time, and let the resolved components of the (artificial) flow velocity v_a through the element be (v_x, v_y, v_z). Since the soil skeleton or matrix remains undeformed and the water is assumed to be incompressible, the bulk volume of the element remains constant with the inflow of water exactly matching the outflow. Remembering that we are using the artificial velocity and total areas then we have

$$v_x \mathrm{d}y\,\mathrm{d}z + v_y \mathrm{d}z\,\mathrm{d}x + v_z \mathrm{d}x\,\mathrm{d}y = \left(v_x + \frac{\partial v_x}{\partial x}\mathrm{d}x\right)\mathrm{d}y\,\mathrm{d}z + \left(v_y + \frac{\partial v_y}{\partial y}\mathrm{d}y\right)\mathrm{d}z\,\mathrm{d}x + \left(v_z + \frac{\partial v_z}{\partial z}\mathrm{d}z\right)\mathrm{d}x\,\mathrm{d}y,$$

i.e.,

$$\frac{\partial v_x}{\partial x} + \frac{\partial v_y}{\partial y} + \frac{\partial v_z}{\partial z} = 0. \tag{3.6}$$

Darcy's law, so far established only for a flowline, is also applicable for resolved components of velocity and hydraulic gradient.

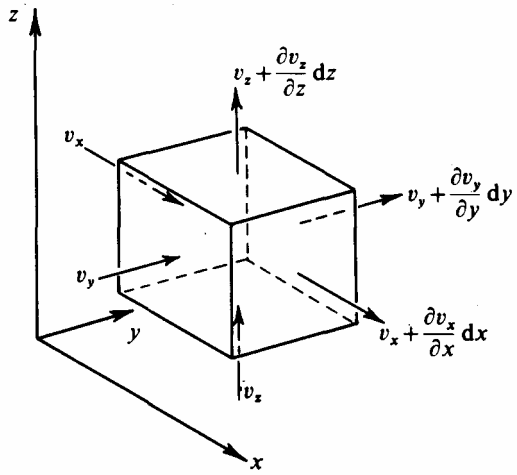

Fig. 3.4 Three-dimensional Seepage

In addition, it is possible for the permeability of the soil not to be isotropic, so that we have as the most general case

$$\left.\begin{aligned} v_x &= k_x i_x = -\frac{k_x}{\gamma_w}\frac{\partial u}{\partial x} \\ v_y &= k_y i_y = -\frac{k_y}{\gamma_w}\frac{\partial u}{\partial y} \\ v_z &= k_z i_z = -\frac{k_z}{\gamma_w}\frac{\partial u}{\partial z} \end{aligned}\right\} \tag{3.7}$$

and on substituting these equalities in eq. (3.6) we obtain

$$k_x \frac{\partial^2 u}{\partial x^2} + k_y \frac{\partial^2 u}{\partial y^2} + k_z \frac{\partial^2 u}{\partial z^2} = 0 \tag{3.8}$$

which is the general differential equation for the excess pore-pressure *u(x,* y, *z)* causing *steady* seepage in three dimensions.

Having derived this equation we have an exact analogy with the corresponding differential equations for the steady flow of electricity and heat through bodies, respectively

$$\frac{1}{R_x}\frac{\partial^2 V}{\partial x^2} + \frac{1}{R_y}\frac{\partial^2 V}{\partial y^2} + \frac{1}{R_z}\frac{\partial^2 V}{\partial z^2} = 0$$

$$C_x \frac{\partial^2 \Theta}{\partial x^2} + C_y \frac{\partial^2 \Theta}{\partial y^2} + C_z \frac{\partial^2 \Theta}{\partial z^2} = 0$$

where V is the electric potential, R_x, R_y, and R_z are electrical resistances, Θ is the temperature, and C_x, C_y, and C_z are thermal conductivities. Consequently, we can use these analogies for obtaining solutions to specific seepage problems.

3.5 Two-dimensional Seepage

In many real problems of soil mechanics the conditions are essentially two-dimensional, as in the case of seepage under a long sheet-pile wall or dam. We shall examine the former of these in the next section.

If we take the y-axis along the sheet-pile wall, there can be no flow or change in excess pore-pressure in the y-direction; hence $\partial u/\partial y \equiv 0$. We can further simplify the problem by taking $k_x = k_z$, because even if this is not the case, we can reduce the problem to its equivalent by distorting the scale in one direction.* To do this we select a new transformed variable

$$x_t = \sqrt{\left(\frac{k_z}{k_x}\right)}x$$

so that the basic equation, (3.8), is reduced to

$$\frac{\partial^2 u}{\partial x_t^{\,2}} + \frac{\partial^2 u}{\partial z^2} = 0. \tag{3.9}$$

This equation (known as Laplace's equation) is satisfied by plane harmonic functions, which are represented graphically by two families of orthogonal curves; one family forms the equipotentials and the other the flowlines, as shown in Figs. 3.5 and 3.6.

However, there will not be many cases of particular boundary conditions for which eq. (3.9) will be exactly soluble in closed mathematical form, and we shall depend on the various approximate methods described in relation to the sheet pile example of the next section, 3.6.

3.6 Seepage Under a Long Sheet Pile Wall: an Extended Example

Figure 3.5 is a section of a sheet pile wall POP' forming one side of a long coffer dam built in a riverbed: the bed consists of a uniform layer of sand overlying a horizontal (impermeable) stratum. The analysis of the cofferdam for any given depth of driving could pose the problems of the quantity of seepage that can be expected to enter the working area from under the wall, or the stability against piping which will be most critical immediately behind the wall. Approximate answers could be obtained from the following alternative methods:

(a) Model experiment in the laboratory. A model of the riverbed is constructed in a narrow tank with glass or perspex sides which are perpendicular to the sheet pile. The different water levels on each side are kept constant, with the downstream level being just above the sandbed to ensure saturation. Probes are placed through these transparent sides at convenient positions, as for the permeameter, to record the excess pore-pressures and thereby indicate the equipotentials. The flowlines can readily be obtained by inserting small quantities of dye at points on the upstream surface of the sand (against one of the transparent faces of the tank) and tracing their subsequent paths. We can also measure the quantity of seepage that occurs in a given time.

There will be symmetry about the centre line P'OP and the imposed boundary conditions are that (i) the upper surface of the sand on the upstream side, AO, is an equipotential $\phi = h$, (ii) the upper surface of the sand on the downstream side, OB, is also an equipotential $\phi = 0$, (iii) the lower surface of the sand is a flowline, and (iv) the buried surface of the sheet pile itself is a flowline. Readings obtained from such a laboratory model have been used to give Fig. 3.5.

* For full treatment of this topic, reference should be made to Taylor1 or Harr2 however, it should be noted that these authors differ in their presentation. Taylor's flownets consist of conjugate functions formed by equipotentials of *head* and of *flux,* whereas Harr's approach has conjugate functions of equal values of *velocity potential* and of *velocity.* There is, in effect, a difference of a factor of permeability between these two approaches which only becomes important for a soil with anisotropic permeability. Here we have an isotropic soil and this distinction need not concern us.

(b) Electrical analogue. A direct analogue of the model can be constructed by cutting out a thin sheet of some suitable conducting material to a profile identical to the section of the sand including a slit, OP, to represent the sheet pile. A potential is applied between the edges AO and OB; and equipotentials can be traced by touching the conducting sheet with an electrical probe connected to a Wheatstone bridge.

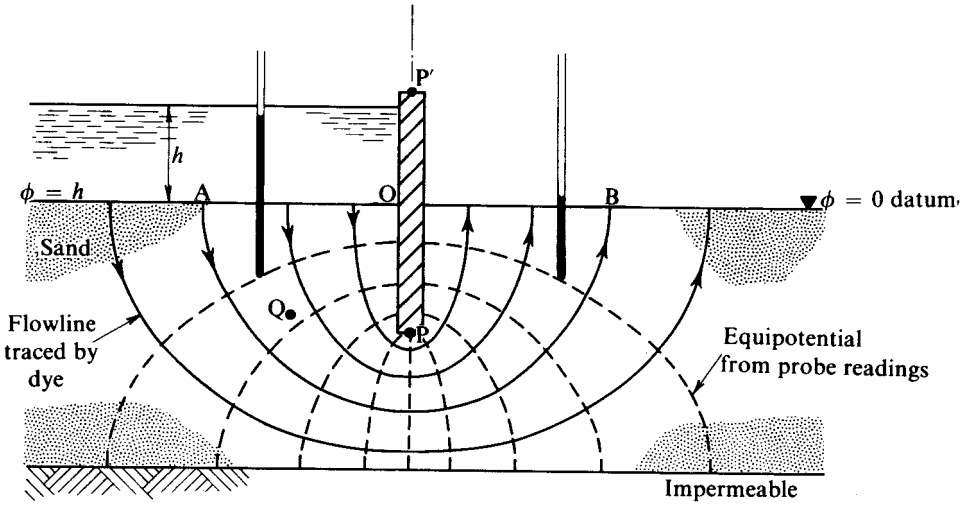

Fig. 3.5 Seepage under Model of Long Sheet Pile Wall

Unlike method (a) above, we cannot trace separately the flow-lines of current. This method can be extended to the much more complicated case of three-dimensional seepage by using an electrolyte as the conducting material.

(c) Graphical flownet. It is possible to obtain a surprisingly accurate two-dimensional flownet (corresponding to that of Fig. 3.5) by a graphical method of trial and error. Certain guiding principles are necessary such as the requirement that the formation of the flownet is only proper when it is composed of 'curvilinear squares': these will not be dealt with here, but are well set out in Taylor's book.[1]

(d) Relaxation methods. These are essentially the same as the graphical approach of *(c)* to the problem, except that the construction of the correct flownet is semi-computational.

3.7 Approximate Mathematical Solution for the Sheet Pile Wall

The boundary conditions of the problem of §3.6 are such that with one relatively unimportant modification an exact mathematical solution can be obtained. This modification is that the sandbed should be not only of infinite extent laterally but also in depth as shown in Fig. 3.6. In this diagram we are taking OB_1B_2 as the x-axis and OPC_1C_2 as the z-axis, and adopting for convenience a unit head difference of water between the outside and inside of the cofferdam; we are taking as our pressure datum the mean of these two, so that the upstream horizontal equipotential $\phi = +\frac{1}{2}$, and the downstream one is $\phi = -\frac{1}{2}$. The buried depth of sheet pile is taken as *d.*

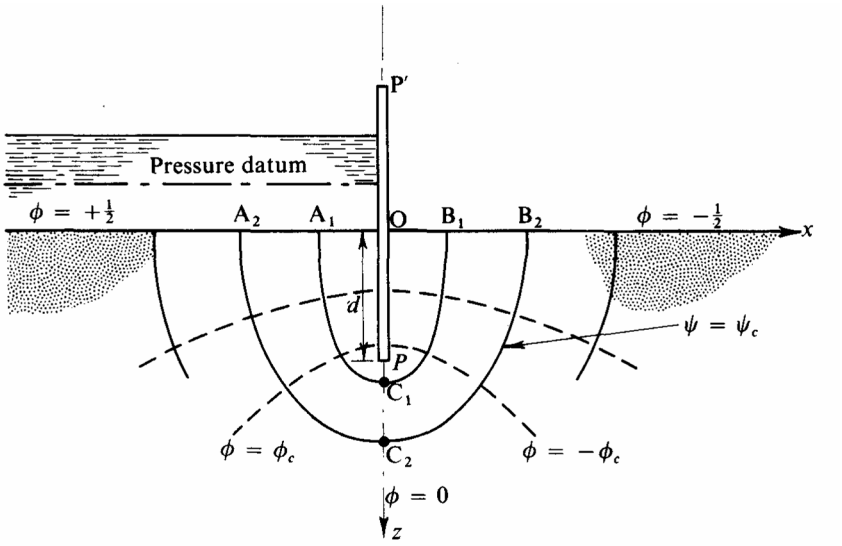

Fig. 3.6 Mathematical Representation of Flownet

We need to find conjugate functions $\phi(x,z)\,and\,\psi(x,z)$ of the general form $(\phi + i\psi) = f(z + ix)$ that satisfy the boundary conditions of our particular problem; the Laplace differential equation, (3.9), will automatically be satisfied by such conjugate functions. (Differentiating we have

$$\frac{\partial \phi}{\partial z} + i\frac{\partial \psi}{\partial z} = f' \text{ and } \frac{\partial \phi}{\partial x} + i\frac{\partial \psi}{\partial x} = if'$$

so that

$$\frac{\partial \phi}{\partial z} = +\frac{\partial \psi}{\partial x} \text{ and } -\frac{\partial \psi}{\partial z} = \frac{\partial \phi}{\partial x}.$$

Differentiating again

$$\frac{\partial^2 \phi}{\partial z^2} + i\frac{\partial^2 \psi}{\partial z^2} = f'' = -\left(\frac{\partial^2 \phi}{\partial x^2} + i\frac{\partial^2 \psi}{\partial x^2}\right)$$

from which we have

$$\frac{\partial^2 \phi}{\partial x^2} + \frac{\partial^2 \phi}{\partial z^2} = 0 = -\left(\frac{\partial^2 \psi}{\partial x^2} + \frac{\partial^2 \psi}{\partial z^2}\right)$$

i.e., Laplace's equation is satisfied.)

Consider the relationship

$$\pi(\phi + i\psi) = \cos^{-1}\frac{(z + ix)}{d} \tag{3.10}$$

i.e.,

$$\frac{z + ix}{d} = \cos\pi(\phi + i\psi) = \cos\pi\phi\cosh\pi\psi - i\sin\pi\phi\sinh\pi\psi.$$

Equating real and imaginary parts

$$\left.\begin{aligned} x &= -d\sin\pi\phi\sinh\pi\psi \\ z &= d\cos\pi\phi\cosh\pi\psi. \end{aligned}\right\} \tag{3.11}$$

Eliminating ϕ we obtain

$$\frac{x^2}{d^2\sinh^2\pi\psi} + \frac{z^2}{d^2\cosh^2\pi\psi} = 1 \tag{3.12}$$

which defines a family of confocal ellipses, each one being determined by a fixed value of $\psi = \psi_c$ and describing a streamline. The joint foci are given by the ends of the limiting 'ellipse' $\psi = 0$ which from eq. (3.11) are $x = 0, z = \pm d$.

Similarly, eliminating ψ we obtain

$$\frac{z^2}{d^2 \cos^2 \pi\phi} + \frac{x^2}{d^2 \sin^2 \pi\phi} = 1 \tag{3.13}$$

which defines a family of confocal hyperbolae, each one being determined by a fixed value of $\phi = \phi_c$ and describing an equipotential. The limiting 'hyperbola' corresponding to $\phi = 0$ leads to the same foci as for the ellipses.

We have yet to establish that the boundary conditions are exactly satisfied, which will now be done.

For $x = 0$ eq. (3.11) demands that either

$$\psi = 0$$

leading to, $z = d \cos \pi\phi$, i.e., P'OP; or

$$\phi = 0$$

leading to $z = d \cosh \pi\psi$, i.e., **PZ** (or positive z-axis below P).

(The possibility of $\phi = 1$ gives the negative z-axis above P'.)

For $z = 0$ eq. (3.11) demands that either

$$\phi = \tfrac{1}{2}$$

leading to $x = -d \sinh \pi\psi$; or

$$\phi = -\tfrac{1}{2}$$

leading to $x = d \sinh \pi\psi$.

If we arbitrarily restrict ψ to being positive then

$\phi = \tfrac{1}{2}, \psi \geq 0$ gives the negative x-axis OA_1A_2

$\phi = -\tfrac{1}{2}, \psi \geq 0$ gives the positive x-axis OB_1B_2.

We have therefore established a complete solution, and in effect if we plot the result in the (ϕ, ψ) plane in Fig. 3.7 we see that we have re-mapped the infinite half plane of the sand into the infinitely long thin rectangle. This process is known as a conformal transformation, and has transformed the flownet into a simple rectilinear grid. In particular it can be seen that the half ellipse *with slit* $POA_1A_2C_2B_2B_1OP$ has been distorted into the rectangle $PO_1A'_2B'_2O_2P$ and the process can be visualized in Fig. 3.7 as a simultaneous rotation in opposite directions of the top corners of the slit about the bottom, P.

At any general point **Q** of the sandbed the hydraulic gradient is given by $-\left(\mathrm{d}\phi/\mathrm{d}s\right)$ which in *magnitude* (but not necessarily sign) equals

$$\left|\mathrm{grad}\,\phi\right| = \sqrt{\left\{\left(\frac{\partial\phi}{\partial x}\right)^2 + \left(\frac{\partial\phi}{\partial z}\right)^2\right\}}$$

where s is measured 'up' a streamline. Appropriate differentiation and manipulation of eqs. (3.11) leads to the expression

$$|i| = \frac{1}{\pi d\sqrt{\sinh^2 \pi\psi + \sin^2 \pi\phi}} = \frac{1}{\pi\left\{\left(d^2 + x^2 - z^2\right)^2 + 4x^2z^2\right\}^{\frac{1}{4}}}. \tag{3.14}$$

Hence we can calculate the hydraulic gradient and resulting flow velocity at any point in the sandbed, and compare the predictions with experimental values obtained from the model.

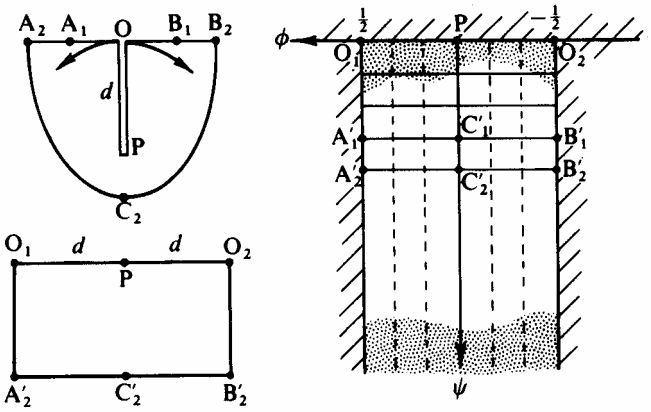

Fig. 3.7 Transformed Flownet

Typical experimental readings obtained from the laboratory model are:

Depth of sheet pile in sand = 6.67 in.; depth of sand bed 12 in.; breadth of model b = 6.55 in.; upstream head of water h = 3.85 in.; average voids ratio of sand e = 0.623 for which the specific gravity G_s=2.65 and the permeability k=0.165 in./s; rate of seepage **Q** = 1.75 in.^{3}/s; and time for dye to travel from x = - 5 , z = 7 to x = - 3.7, z = 8 was 30 s.

(a) Comparison of seepage velocity. The coordinates of Q, the mean point of the measured dye path, are x = - 4.35, z = 7.5 and substituting in eq. (3.14) we get for *unit head* $|i_q| = 1/\pi \times 8.1$. Hence predicted *seepage velocity* at Q will be

$$v_s = \frac{v}{n} = \frac{v(1+e)}{e} = k|i_q|h\frac{(1+e)}{e}$$

$$= \frac{0.165 \times 3.85 \times 1.623}{\pi \times 8.1 \times 0.623} = 0.065 \ in./s.$$

This compares with a measured value of

$$\frac{\sqrt{(1^2 + 1.3^2)}}{30} = 0.0547 \ in./s.$$

and is an overestimate by 18 per cent.

(b) Total seepage. The mathematical solution gives an infinite value of seepage since the sand bed has had to be assumed to be of infinite depth. But as a reasonable basis of comparison we can compute the seepage passing under the sheet pile, $z = d$, down to a depth z = 18d which corresponds with the bottom of the sand in the model. This is equivalent to taking the boundary of the sand as a half ellipse such as $A_2C_2B_2$ where $0C_2$ = 1.8d.

$$Q = \int_d^{1.8d} v_a b \, dz = kbh \int_d^{1.8d} \frac{i}{h} dz.$$

But on the line $x = 0$, the streamlines are all in the positive x-direction and $i/h = +\partial\phi/\partial s = -\partial\phi/\partial x$ since $\delta s = -\delta x$, and the properties of the conjugate functions are such that $\partial\phi/\partial x = -\partial\psi/\partial z$.

Hence,

$$Q = kbh\int_d^{1.8d}\frac{\partial\psi}{\partial z}dz = kbh\left[\psi\right]_{z=d}^{z=1.8d} = \frac{kbh}{\pi}\left[\cosh^{-1}\left(\frac{z}{d}\right)\right]_d^{1.8d}$$

$$= \frac{0.165\times 6.55\times 3.85\times 1.195}{\pi} = 1.59\,in.^3/s.$$

This compares with a measured value of 1.75 in.^{3}/s and is as expected an underestimate, by an order of 9 per cent.

The effect of cutting off the bottom of the infinite sand bed below a depth $z = 1.8d$ in the model, is to crowd the flowlines closer to the sheet-pile wall; consequently, we expect in the model a higher measured seepage velocity and a higher total seepage. The comparatively close agreement between the model experiment and the mathematical predictions is because the modification to the boundary conditions has little effect on the flownet where it is near to the sheet pile wall and where all the major effects occur.

A further important prediction concerns the stability against piping. The predicted hydraulic gradient at the surface of the sand immediately behind the sheet-pile wall $\left(\psi = 0, \phi = -\frac{1}{2}\right)$ is $h/\pi d$. Hence the predicted factor of safety against piping under this difference of head is

$$\frac{\gamma'}{i\gamma_w} = \frac{(G_s - 1)}{\left(h/\pi d\right)(1+e)} = \frac{1.65\times\pi\times 6.67}{3.85\times 1.623} = 5.5.$$

3.8 Control of Seepage

In the previous sections we have explained the use of a conceptual model for seepage: the word ‘model’ in our usage has much the same sense as the word ‘law’ that was used a couple of hundred years ago by experimental workers such as Darcy. We only needed half a chapter to outline the simple concepts and formulate the general equations, and in the rest of the chapter we have gone far enough with the solution of a two-dimensional problem to establish the status of the seepage problem in continuum mechanics. Rather than going on to explain further techniques of solution, which are discussed by Harr[2], we will turn to discuss the simplifications that occur when a designer controls the boundaries of a problem.

Serious consequences may attend a failure to impound water, and civil engineers design major works against such danger. There is a possibility that substantial flow of seepage will move soil solids and form a pipe or channel through the ground, and there is also danger that substantial pore-pressures will occur in ground and reduce stability even when the seepage flow rate is negligibly small. The first risk is reduced if a *graded filter* drain is formed in the ground, in which seepage water flows under negligible hydraulic gradient. The materials of such filters are sands and gravels, chosen to be stable against solution, and made to resist movement of small particles by choosing a succession of gradings which will not permit small particles from any section of the filter to pass through the voids of the succeeding section.

These *drains* have a most important role in relieving pore-pressure and, for example, reducing uplift below a dam: wells serve the same function when used to lower

groundwater levels and prevent artesian pressure of water in an underlying sand layer bursting the floor of an excavation in an overlying clay layer. The technical possibilities could be to insert a porous tipped pipe and cause local spherical flow, or to insert a porous-walled pipe and cause local radial flow, or to place or insert a porous-faced layer and cause local parallel flow. These three possibilities correspond to more simple solutions than the two-dimensional problem discussed above:

(a) The Laplace equation for spherical flow is

$$\frac{1}{r^2}\frac{\partial}{\partial r}\left(r^2\frac{\partial h}{\partial r}\right)=0$$

which can be integrated to give

$$(h_1-h_2)\propto\left(\frac{1}{r_2}-\frac{1}{r_1}\right);$$

and *(b)* the Laplace equation for radial flow is

$$\frac{1}{r}\frac{\partial}{\partial r}\left(r\frac{\partial h}{\partial r}\right)=0$$

which can be integrated to give

$$(h_1-h_2)\propto\ln\left(\frac{r_1}{r_2}\right)$$

and *(c)* the Laplace equation for parallel flow is

$$\frac{\partial^2 h}{\partial r^2}=0$$

which can be integrated to give

$$(h_1-h_2)\propto(r_1-r_2);$$

where (h_1-h_2) is the loss of head between coordinates r_1 and r_2.

A contrasting technical possibility is to make a layer of ground relatively impermeable. Two or three lines of holes can be drilled and grout can be injected into the ground; a trench can be cut and filled with clay slurry or remoulded 'puddled' clay; or a blanket of rather impermeable silty or clayey soil can be rolled down. Seepage through these *cut-off* layers is calculated as a parallel flow problem.

In 'seepage space' a cut-off is immensely large and a drain is extremely small. The designer can vary the spatial distribution of permeability and adjust the geometry of seepage by introducing cut-offs and drains until the mathematical problem is reduced to simple calculations. Applied mathematics can play a useful role, but engineers often carry solutions to slide-rule accuracy only and then concentrate their attention on (a) the actual observation of pore-pressures and *(b)* the actual materials, their permeabilities, and their susceptibility to change with time.

References to Chapter 3

1 Taylor, D. W. *Fundamentals of Soil Mechanics,* Wiley, 1948.

2 Harr, M. E. *Groundwater and Seepage,* McGraw-Hill, 1962.

4
One-dimensional consolidation

In the previous chapter we studied briefly the conditions of the steady flow of water through a stationary soil structure; in this chapter we shall be concerned with the more general conditions of *transient* flow of water from and through soil-material. The seepage forces experienced by the soil structure will vary with time, and the soil structure itself may deform under the varying loads it sustains.

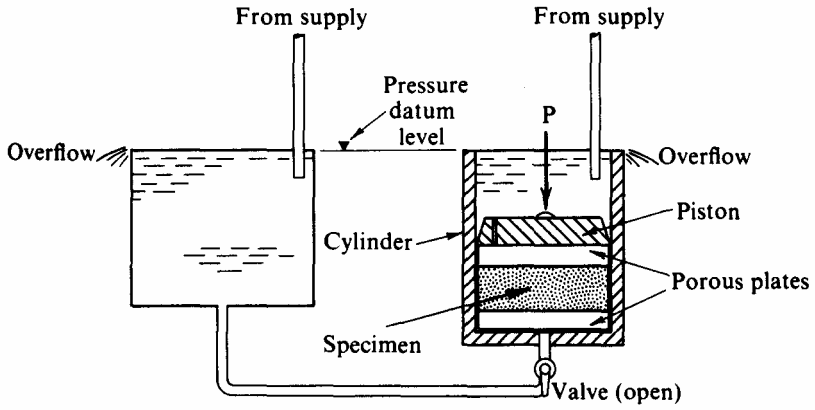

Fig. 4.1 Consolidometer

While the soil structure will exhibit compressibility, its response to an external compressive load will take time – the time necessary for the transient flow of pore-water to cease as the excess pore- pressures dissipate.

The time-dependent process during which a soil specimen responds to compression is commonly called the *process of consolidation.* Laboratory tests for measuring such compressibility of a soil are conducted either in a consolidometer (sometimes known as an oedometer) or in an axial compression cell (usually known as a 'triaxial' cell). We shall here confine our attention to a consolidometer, the principles of which are illustrated in Fig. 4.1. The apparatus consists essentially of a rigid metal cylinder with closed base, containing a soil sample in the shape of a thick circular plate sandwiched between two thin porous plates. The porous plates, generally made of ceramic or some suitable stone, allow the passage of water into or (more usually) out of the soil sample, but their pores are not sufficiently large to allow any of the soil particles to pass through them. Both porous plates are connected to constant head reservoirs of water, and vertical loads are applied to the sample by means of a closely fitting piston. A test consists of the instantaneous application of a constant increment of load and observation of the consequent settlement of the piston (and hence consolidation of the sample) with time.

4.1 Spring Analogy

The soil sample in the consolidometer is at all times carrying the total vertical load transmitted by the piston; and, as such, forms a load-carrying system. But the soil is a two-phase continuum, and it contains two separate materials (water and the structure of soil particles) which can be thought of as two independent structural members in parallel, as, for example, two members in parallel could make a double strut. The two members have markedly different stress – strain characteristics, and we can only discover the share of the

total load taken by each (at any one instant) by considering both their statical equilibrium *and* strain compatibility, just as we have to do in the example of a composite member such as a double strut. We shall continue to assume that the water is *incompressible* compared with the soil structure. (Typical values are compressibility of water = 48×10^{-6} cm^2/kg and compressibility of London clay = 3000×10^{-6} cm^2/kg.)

There is an analogy between the behaviour of the soil sample in the consolidometer, and that of the spring in Fig. 4.2. (Note our caveat that an isotropic elastic continuum cannot properly be represented by a system of springs.) The spring is also in a consolidometer, fully surrounded by water and supporting a similar piston, except that it is assumed to be frictionless, weightless, and leakproof. The lead connecting the bottom of the cylinder to the reservoir above the piston contains a valve and is of small bore so that the water can only flow very slowly between the cylinder and reservoir, with a resulting pressure difference between the two containers.

Let us carry out a test in parallel on both soil sample and spring by applying a total vertical load P to both pistons. This additional load P will act at all levels within

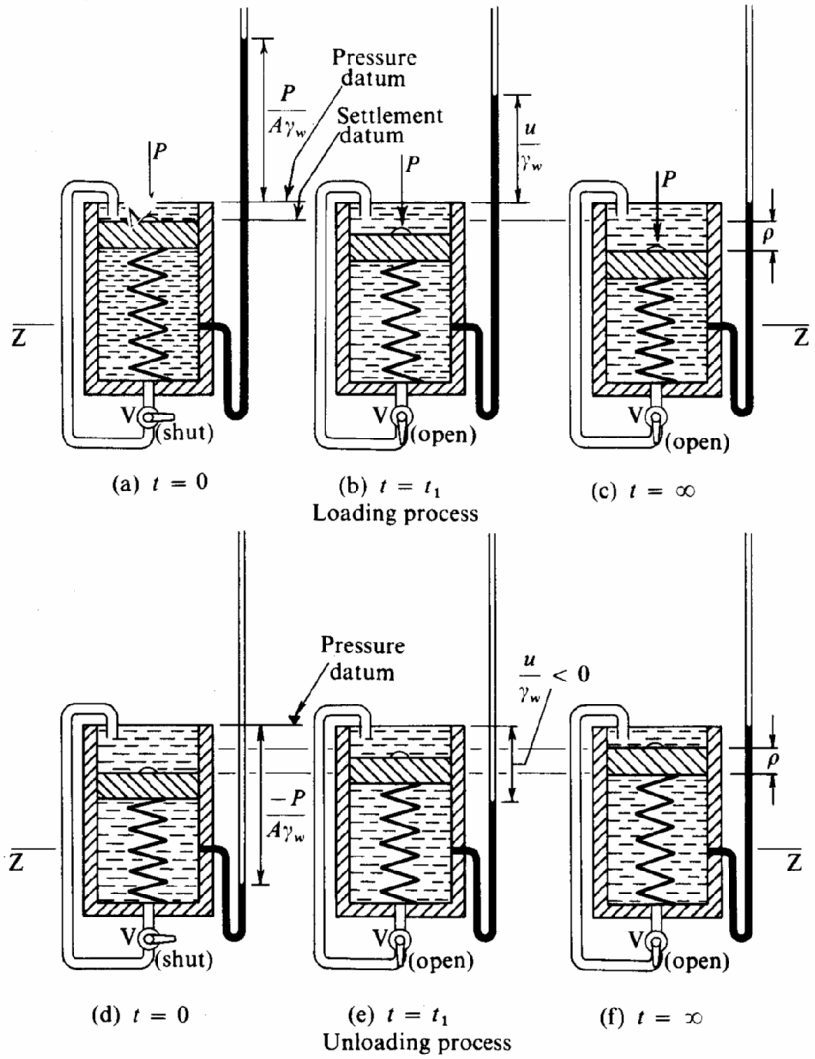

Fig. 4.2 Spring Analogy of Consolidation Process

the cylinder, but the proportions carried by the two structural members (water and soil) will vary not only with time but also with the particular level being considered. At any instant and at a certain level **ZZ** let the vertical load carried by the soil or spring be P_s, and that by the water P_w; then simple statics demands that at all times $P_s+P_w=P$. The load

carried by the water is measured as excess pore-pressure *u,* recorded by the pressure tapping and manometer tube shown in Fig. 4.2.

If we divide these forces by the total cross-sectional area *A* of the cylinder (as for seepage) we have

$$\sigma' = {}^{P_s}\!/_{A} = effective\ stress$$

$$u = {}^{P_w}\!/_{A} = excess\ pore-pressure\ (neglecting\ the\ self\ weight\ of\ the\ soil\ and\ piston)$$

$$\sigma = (\sigma' + u) = {}^{P}\!/_{A} = total\ applied\ stress$$

Loading process

Before the start of the test the valve *V* is closed so that immediately the load *P* is applied, no water can escape from the cylinder, the piston cannot move, the soil or spring cannot be strained and cannot therefore experience any stress. Hence, at the very start, when $t = 0, \sigma' = 0, u = \sigma = {}^{P}\!/_{A}$ and we have the case of Fig. 4.2(a).

We now open the valve and observe that the water flows out of the cylinder into the reservoir, that the piston settles, and by so doing starts to compress the spring. At time $t = t_1$ after the valve is opened we have the situation of Fig. 4.2(b).

$0 < \sigma' = (\sigma - u)$; σ' increasing with time

$\sigma > u > 0$; u decreasing with time.

The rate of flow of water, and hence of settlement, will decay with time, and eventually after infinite time all excess pore-pressure will have dissipated, all settlement ceased, and all the load will be carried by the spring or soil. We have then at $t = \infty$ the case of Fig. 4.2(c)

$$\sigma' = \sigma = \frac{P}{A}\ and\ u = 0$$

and a total settlement of the piston recorded as ρ.

Unloading process

We now attempt to reverse the process by removing the total applied load *P.* Immediately after having done this, no time has elapsed for water to be sucked into the cylinder and for the piston to rise, so the spring will still be compressed by p and exerting an upward force *P.* Since the total load is zero, this force must be matched by a 'negative' one provided by 'tension' or a drop in pressure in the water. Consequently, at $t = 0$ we shall observe Fig. 4.2(d)

$$\sigma' = {}^{P}\!/_{A};\ u = -\sigma';\ \sigma = (\sigma' + u) = 0.$$

As time elapses, the spring stretches and pushes the (weightless) piston upwards as water is sucked into the cylinder from the reservoir. At time $t = t_1$ after the start of this unloading process we have the situation of Fig. 4.2(e)

${}^{P}\!/_{A} > \sigma'$ decreasing with time

$-{}^{P}\!/_{A} < u (= -\sigma') < 0$; u increasing with time.

Finally, after infinite time the system will have reached equilibrium with $\sigma' = 0 = u$, and the piston will have regained its original position having risen by ρ, see Fig. 4.2(f). We shall find in the next section that the soil sample often does not unload with the same characteristics as for the loading process, and that not all the settlement ρ may be recovered.

4.2 Equilibrium States

If we carry out a consolidation test on a real soil, and observe the settlement of the piston as a function of time we shall obtain results which when plotted give a curve of the form of Fig. 4.3, that at first sight appears to have a 'horizontal' asymptote and to reach a maximum settlement which remains fixed at some point such as E.

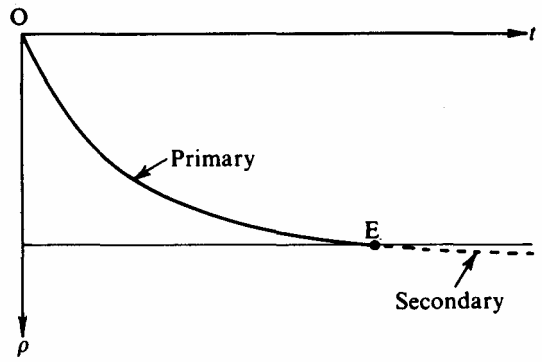

Fig. 4.3 Settlement of Piston

A second, closer look will show that after E is reached the piston will continue to settle indefinitely by a very small amount exhibiting the well-known phenomenon of creep. The settlement from O to E is known as *primary consolidation* and that after E as *secondary consolidation;* the choice of the position of E is not entirely arbitrary and a suitable definition will be given in §4.5. Throughout this chapter we shall be concerned only with primary consolidation, totally ignoring all secondary consolidation, so that we can consider E to represent effectively an *equilibrium state* marking the end of settlement under a given loading increment.

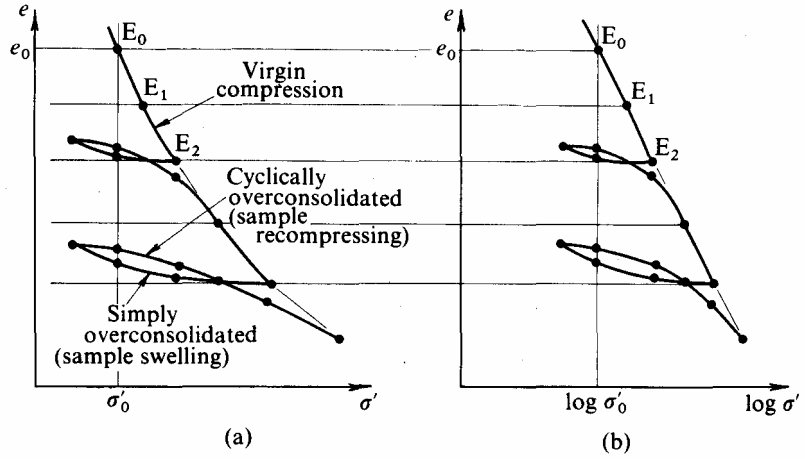

Fig. 4.4 Terzaghi Equilibrium States

If a series of load-increments is applied to a specimen which is initially very wet, the resulting equilibrium states will appear when plotted, as in Fig. 4.4. In Fig. 4.4(a) with the effective vertical stress σ' to a natural scale are the results of a sequence of loading and unloading processes, showing hysteresis loops where the specimen has been allowed to swell and then be reconsolidated. The outermost curve connecting the points when the specimen is in the loosest possible states is often called the virgin consolidation line, but will be referred to here as the *virgin compression line,* because it is strictly the line connecting equilibrium states whereas consolidation is a term used only for the time-dependent process between any pair of equilibrium states.

In Fig. 4.4(b), the same results are plotted with σ' on a logarithmic scale in which the virgin compression line becomes straight. Terzaghi1 fitted such data by a line of equation

$$e = e_0 - C_c \log_{10} \frac{\sigma'}{\sigma'_0} \tag{4.1}$$

in which the constant C_c, is called the compression index; it should be noted that the base 10 is used in this definition rather than the natural logarithm, which we denote by *ln*.

Later in this book instead of Terzaghi's expression, eq. (4.1), the virgin compression line will be denoted by the equation

$$v = v_0 - \lambda \ln \frac{p}{p_0}$$

and each swelling and recompression loop will be represented by a single straight line of the form

$$v = v_0 - \kappa \ln \frac{p}{p_0},$$

where λ and κ are characteristic constants for the soil. We suppose that the virgin compression λ-line represents an *irreversible* process, whereas the swelling and recompression κ-lines represent *reversible* processes.

4.3 Rate of Settlement

The rate of settlement of the piston that will occur inside the consolidometer will be governed by the speed with which water can be expelled from the innermost pores of the soil specimen: it will depend both on the permeability and on the length of drainage path. In the case of sand, the permeability is so high that the process of consolidation is effectively instantaneous, whereas for a clay layer in the ground, settlement may continue for years. The following analysis is relevant to clays.

In Fig. *4.5* we consider a suitably thin horizontal layer of the soil specimen and investigate its condition at some instant during the consolidation process during virgin compression. We assume that the process is entirely one-dimensional (with no lateral variations) so that the velocity and pressure of the pore-water are only functions of the depth *z* measured vertically downwards from the surface of the specimen, and of the time *t.* We imagine that two small probes are inserted so that the pore-pressures of the top and bottom surfaces of the layer are known. Our sign convention will require that the artificial velocity v_a is taken as positive *downwards* in the direction of *z,* and opposite to that of the permeameter in Fig. 3.1; also a positive increment of excess head *h* is shown which will cause an upward velocity, i.e., negative v_a.

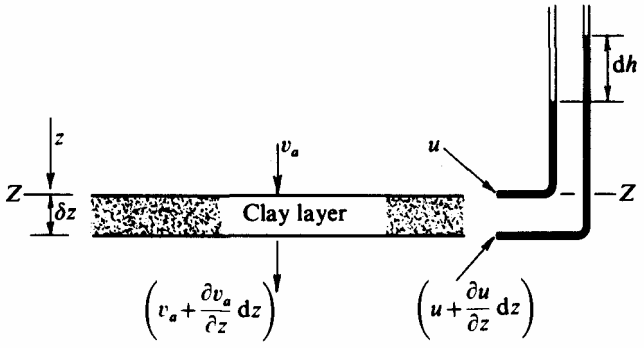

Fig. 4.5 Specimen Layer of Clay

The loading increment $\dot{\sigma}(=\delta\sigma)$ applied to the specimen is such that the initial and final equilibrium states are E_0 and E_1, shown in Fig. 4.6. At the present time *t* after the start of the consolidation process, the state of the thin layer will be represented by some point T between E_0 and E_1. The conventional assumption introduced by Terzaghi in his classic theory* of primary consolidation is that T always lies on the straight line joining E_0 and E_1. The slope of this straight line, which will change for different initial states E_0, is defined as

$$-\frac{\mathrm{d}e}{\mathrm{d}\sigma'} = (1+e_0)m_{vc} \tag{4.2}$$

where m_{vc} is the coefficient of volume compressibility. A similar constant m_{vs} but of much smaller value will be required for steps in the swelling and recompression loops of Fig. 4.4.

This definition allows us to relate settlement with change in effective stress. Let δp be the settlement experienced by the thin layer during time δt. The reduction in volume of the layer will be $A\,\delta p$ which can be expressed as

$$A\delta z\left(-\frac{\delta e}{1+e_0}\right),$$

by reference to Fig. 1.4

$$\therefore \qquad \frac{\delta p}{\delta z} = -\frac{\delta e}{1+e_0} = m_{vc}\delta\sigma'. \tag{4.3}$$

Because of continuity, the reduction in volume of the thin layer must be exactly matched by the volume of water expelled, which during time δt will be $(\partial v_a / \partial z)A\delta z\delta t$. Hence, in the limit we have

$$\frac{\partial v_a}{\partial z} = \frac{-1}{1+e_0}\frac{\partial e}{\partial t} = m_{vc}\frac{\partial \sigma'}{\partial t}. \tag{4.4}$$

Since the loading increment is a *fixed* one of $\dot{\sigma} = \delta\sigma$ we have $\delta\sigma' = \delta u = \sigma' =$ constant so that $\partial\sigma'/\partial t = -\partial u/\delta t$, and eq. (4.4) can be taken a step further to give

$$\frac{\partial v_a}{\partial z} = -m_{vc}\frac{\partial u}{\partial t}. \tag{4.5}$$

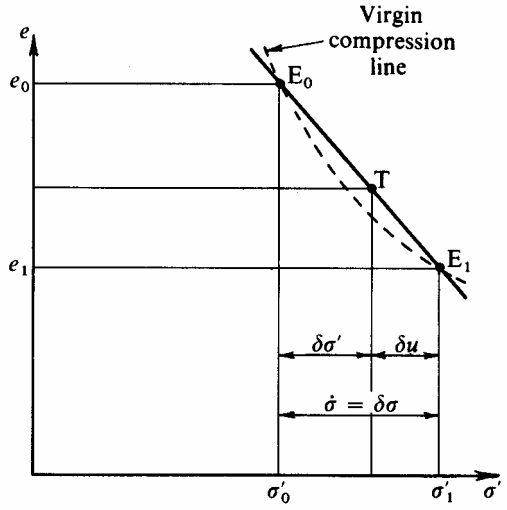

Fig. 4.6 Loading Increment

* We continue to use the parameter *e* here as in eq. (4.1) although in subsequent chapters we will use exclusively the parameter $v = 1 + e$.

Finally, we can obtain another relationship between v_a and u by employing Darcy's law,

$$v_a = ki = -k\frac{\mathrm{d}h}{\mathrm{d}s} = \frac{-k}{\gamma_w}\frac{\partial u}{\partial z}. \tag{4.6}$$

Differentiating this with respect to z, and combining with eq. (4.5)

$$\frac{+k}{\gamma_w}\frac{\partial^2 u}{\partial z^2} = -\frac{\partial v_a}{\partial z} = +m_{vc}\frac{\partial u}{\partial t}.$$

This is Terzaghi's fundamental differential equation for one- dimensional consolidation, usually written as

$$\frac{\partial u}{\partial t} = c_{vc}\frac{\partial^2 u}{\partial z^2} \tag{4.7}$$

where $c_{vc} = k/\gamma_w m_{vc}$ is the coefficient of consolidation; a typical value for a stiff clay is 2×10^{-3} in.^{2}/min. Once having solved the consolidation equation for a particular set of boundary conditions, we can calculate for any given time the total settlement ρ, the excess pore-pressure u, and effective stress σ' at any depth. In the next two sections an approximate and an exact solution will be derived for the one-dimensional consolidation of a clay layer under the same conditions as occur in the consolidometer.

4.4 Approximate Solution for Consolidometer

We have made an approximation to the physical problem in the construction of the model for one-dimensional consolidation. Before we become involved in Fourier's analysis in *§4.5,* we set out in this section an approximate solution[2] which fits the boundary conditions, but only has terms in z and z^2 so that it does not satisfy exactly the (already approximate) differential equation (4.7). We believe this solution to be helpful in providing an intuitive understanding of the various aspects of the problem.

Figure 4.7 represents part of a clay layer of large area A and depth H resting on an *impermeable* stratum so that no drainage can occur at the base: the boundary conditions are identical with that of the consolidometer when drainage is prevented at the base by closing the lead to the reservoir (Fig. 4.1). If we place a series of imaginary probes along the line AB at 45° to the horizontal to act as standpipes, their levels at any instant will provide a distribution of the excess pore-pressure u with depth z.

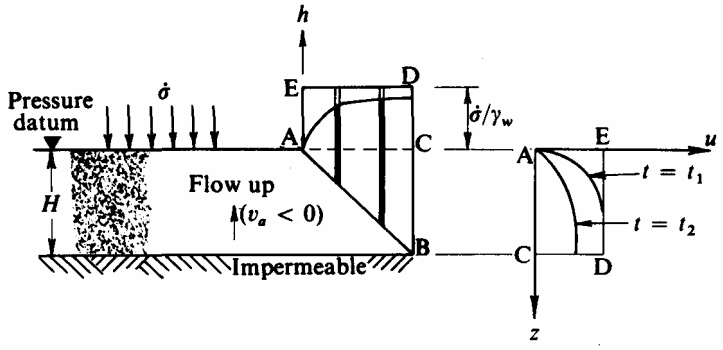

Fig. 4.7 Case of Consolidometer with no Drainage at Base

Immediately after the application of the increment of vertical load $\dot{\sigma}$ at t =0, the excess pore-pressure everywhere will be $\dot{\sigma}$ and all standpipes will show a level of $\dot{\sigma}/\gamma_w$ above pressure datum at the top of the clay layer. As time elapses, the excess pore-pressures dissipate as load is transferred to the soil structure and a series of lines

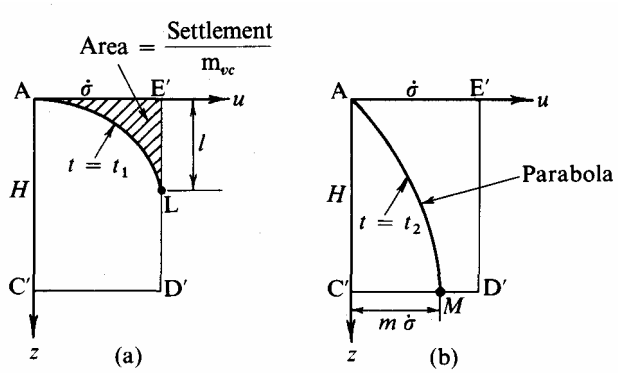

Fig. 4.8 Parabolic Isochrones

at $t = t_1$, $t = t_2$, etc., will be obtained. Each one is known as an *isochrone* (from the Greek 'equal time '), and since the length AC is equal to the depth H the gradient of the isochrone at any point is equal to d*h*/d*z* and represents the hydraulic gradient *i* that is acting upwards. In this case *i* is positive upwards and causing the flow of water to be vertically upwards everywhere in the clay layer. It is usual and convenient to depict the isochrones all rotated clockwise through 90° as seen in the right-hand part of Fig. 4.7.

We can obtain an approximate but fairly accurate solution by assuming that the isochrones are all parabolas and distinguishing two stages of consolidation as shown in Fig. 4.8. Immediately consolidation starts the pore-pressure at the surface A must drop to zero, and a typical isochrone for the first stage will be as AL in Fig. 4.8(a). Since the hydraulic gradient must be continuous (this is not a necessary condition in a layered soil) the parabola must have its apex at L with a vertical tangent there. The apex L rapidly moves down $E'D'$ and on reaching D' the first stage is complete.

During the second stage, a typical isochrone will appear as AM. This must have its apex at M with a vertical tangent there, because the boundary conditions at the base $D'C'$ demand no flow and hence zero hydraulic gradient. The point M gradually traverses $D'C'$ and eventually reaches C' when all consolidation is complete.

First stage

The isochrone AL for $t = t_1$ is given by

$$u = \dot{\sigma}\left(2\frac{z}{l} - \frac{z^2}{l^2}\right), \qquad 0 \le z \le l(t). \tag{4.8}$$

The settlement that has occurred will be, from eq. (4.3)

$$\rho_{t_1} = \int_0^l m_{vc}\sigma' \,\mathrm{d}\, z = \int_0^l m_{vc}(\dot{\sigma} - u)\mathrm{d}z$$

which is m_{vc} times the shaded area ALE'. This can readily be calculated to be $\frac{1}{3}m_{vc}\dot{\sigma}\, l$; so that the rate of settlement will be $\frac{1}{3}m_{vc}\dot{\sigma}\frac{\mathrm{d}\, l}{\mathrm{d}\, t}$, which must be equal (and opposite) to the rate of flow of water out of the surface. But this is the value of v_a for $z = 0$, i.e., from eq. (4.8) the upwards velocity is

$$(-v_a)_{z=0} = (-ki)_{z=0} = \frac{k}{\gamma_w}\left(\frac{\partial u}{\partial z}\right)_{z=0} = \frac{k\dot{\sigma}}{\gamma_w}\frac{2}{l}. \tag{4.9}$$

Hence

$$\frac{1}{3}m_{vc}\dot{\sigma}\frac{\mathrm{d}\,l}{\mathrm{d}\,t}=\frac{\mathrm{d}\rho}{\mathrm{d}\,t}=(-v_a)_{z=0}=\frac{k\dot{\sigma}}{\gamma_w}\frac{2}{l} \tag{4.10}$$

and integrating for the appropriate limits

$$l^2=12c_{vc}t_1. \tag{4.11}$$

It is convenient here to introduce two useful parameters. The first is the proportion of the total settlement that has occurred so far, defined by

$$U=\frac{\rho_t}{\rho_\infty}. \tag{4.12}$$

The second is a dimensionless time factor defined by

$$T_v=\frac{c_{vc}t}{H^2}. \tag{4.13}$$

During this first stage of consolidation,

$$U=\frac{\rho_t}{\rho_\infty}=\frac{\frac{1}{3}m_{vc}\dot{\sigma}\,l}{m_{vc}\dot{\sigma}\,H}=\frac{\frac{1}{3}\sqrt{12c_{vc}t}}{H}=\sqrt{4T_v/3} \tag{4.12}$$

and the first stage will end when $l=H$, i.e., $T_v=\frac{1}{12}$.

Second stage $\left(T_v\geq\frac{1}{12}\right)$

The isochrone AM for $t=t_2$ is given by

$$u=\dot{\sigma}\,m\left(2\frac{z}{H}-\frac{z^2}{H^2}\right),\quad 1\geq m(t)\geq 0. \tag{4.15}$$

Proceeding exactly similarly as for the first stage we have

$$\rho_{t_2}=m_{vc}\dot{\sigma}\,H\left(1-\frac{2m}{3}\right) \tag{4.16}$$

$$(-v_a)_{z=0}=\frac{k\dot{\sigma}}{\gamma_w}\frac{2m}{H} \tag{4.17}$$

leading to

$$m_{vc}\dot{\sigma}H\left(-\frac{2}{3}\frac{\mathrm{d}\,m}{\mathrm{d}\,t}\right)=\frac{\mathrm{d}\rho}{\mathrm{d}\,t}=(-v_a)_{z=0}=\frac{k\dot{\sigma}}{\gamma_w}\frac{2m}{H} \tag{4.18}$$

and after integration

$$m=\exp\left(\frac{1}{4}-3T_v\right). \tag{4.19}$$

The proportion of settlement

$$U=\frac{m_{vc}\dot{\sigma}\,H\left(1-\frac{2m}{3}\right)}{m_{vc}\dot{\sigma}\,H}=1-\frac{2}{3}\exp\left(\frac{1}{4}-3T_v\right). \tag{4.20}$$

If we now put the two stages of consolidation together and plot U against T_v we obtain Fig. 4.9 where in the first stage we have a straight line of slope $2/\sqrt{3}$ and the second a curve decaying exponentially.

Should the clay layer rest on a permeable stratum, as in Fig. 4.10, and drainage occur from both top and bottom surfaces, as will be the more usual case in laboratory

experiments in the consolidometer, we can make immediate use of the above solution for the case of single drainage. This case of double drainage has symmetry about the mid-plane with all flow being upwards above this, and all flow being downwards below it. Typical isochrones are as shown, and we see that the top *half* has identical conditions with that of the case of single drainage. Hence we adopt the solution for single drainage, and *double* the settlements. In particular, in order to make use of the time factor, we must evaluate H as *half* of the depth in Fig. 4.10, and we can avoid any ambiguity by redefining it as the maximum drainage path, i.e., the longest path that any water particle has to travel to be expelled.

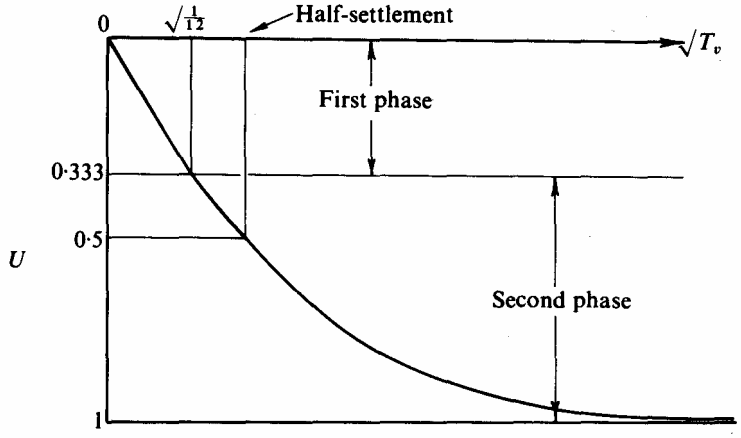

Fig. 4.9 Settlement Results from Parabolic Isochrones

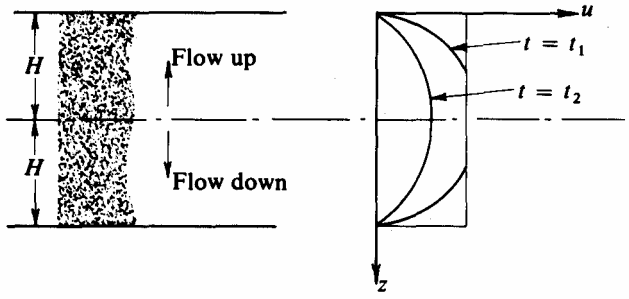

Fig. 4.10 Case of Consolidometer with Drainage at Both Surfaces

4.5 Exact Solution for Consolidometer

The above approximate solutions, although exactly fitting the boundary conditions, do not satisfy exactly the differential equation, (4.7). We can obtain an exact solution of the differential equation satisfying the relevant boundary conditions which for single drainage are

$$\left.\begin{array}{lll} t = 0, & 0 \le z \le H, & u = \dot{\sigma} \\ 0 < t \le \infty, & z = 0, & u = 0 \\ 0 \le t \le \infty, & z = H, & v = -\dfrac{k}{\gamma_w}\dfrac{\partial u}{\partial z} = 0 \\ t = \infty, & 0 \le z \le H, & u = 0. \end{array}\right\} \tag{4.21}$$

Our experience with the parabolic isochrones suggests that we separate variables and assume that u is the product of independent functions of z and t. We try $u = \phi(t)f(z)$ and substitution in eq. (4.7) then gives us

$$\frac{\phi'(t)}{\phi(t)} = c_{vc}\frac{f''(z)}{f(z)}. \tag{4.22}$$

Since this must hold for all z and all t, each side of this equation must be constant. For convenience let each side be equal to $-c_{vc}A^2$, and then by integrating we find

$$\left.\begin{aligned}\phi(t) &= \alpha\, e^{-A^2 c_{vc} t}\\ f(z) &= \beta\cos Az + \gamma \sin Az\end{aligned}\right\} \tag{4.23}$$

where α, β and γ are constants of integration. To satisfy the boundary conditions we might start by putting

$$u = \phi(t) f(z) = A' e^{-Mt}\sin\left(\frac{\pi z}{2H}\right)$$

where

$$Mt = \frac{\pi^2 c_{vc} t}{4H^2} = \frac{\pi^2 T_v}{4}$$

but this could never satisfy the first boundary condition as it is. So we have to employ Fourier analysis and take the infinite series

$$u = \sum_{m=1,2,\ldots}^{\infty} A_m e^{-m^2 Mt}\sin\left(\frac{m\pi z}{2H}\right)$$

requiring that

$$\dot{\sigma} = (u)_{t=0} = \sum A_m \sin\left(\frac{m\pi z}{2H}\right).$$

To solve this we adopt the standard procedure; we multiply by sin *(nπz/2H)* where *n* is an integer and integrate over a range of π to find

$$A_m = \frac{2\dot{\sigma}}{m\pi}(1-\cos m\pi).$$

The complete solution then becomes

$$u = \sum_{m=1,2,\ldots}^{\infty}\frac{2\dot{\sigma}}{m\pi}(1-\cos m\pi)\sin\left(\frac{m\pi z}{2H}\right)e^{-m^2 Mt} \tag{4.24}$$

and

$$U = 1 - \sum\frac{4}{m^2\pi^2}(1-\cos m\pi)\sin\left(\frac{m\pi}{2}\right)e^{-m^2 Mt.} \tag{4.25}$$

Fortunately, because of the exponential factor both of these series are rapidly convergent and only two or three of their terms need be evaluated. For small values of t or T_v, the latter expression approximates to the straight line $U = \sqrt{4T_v/\pi}$ having a slope of $2/\sqrt{\pi}$ compared with $2/\sqrt{3}$ for the parabolic isochrones.

Figure 4.11 shows the resulting curve obtained from eq. (4.25) compared both with experimental results obtained in the laboratory on specimens of saturated remoulded Gault Clay, and with the comparable approximate solution. The agreement is very close principally because with small thin laboratory specimens the assumptions and conditions implicit in Terzaghi's classic theory are fulfilled.

A method for establishing the end of primary consolidation suggested by Taylor[3] is as follows, as indicated in Fig. 4.11. The best straight line possible, E_0A, is drawn through the initial experimental points, and a second line, E_0B, with a slope 15 per cent less is drawn through the initial point, E_0. This line will cut the theoretical curve at $U = 0.9$, so that its intersection with the experimental curve is taken to be this point; hence the scale on the U-axis can be fixed together with the value of 100 per cent primary consolidation at E_1.

Further settlement after E_1, called secondary consolidation, is the topic of much current research.[4-6]

4.6 The Consolidation Problem

This chapter has considered transient flow of pore-water in one dimension, using the heat equation. The mathematically inclined reader may now expect us to generalize Terzaghi's model in some manner that leads us to an equation resembling that of three-dimensional heat transfer. Unfortunately, we cannot solve the consolidation problem with the same ease as was possible for the seepage problem. Terzaghi's model has a spring constant which is comparable to Young's modulus for an elastic body, and soil is no more capable of being reduced to a model with three orthogonal springs than is an isotropic elastic body. Terzaghi's model has one spring constant for virgin compression and a different constant for swelling, so we have to model a material with an elastic/plastic hardening character; we have to model the behaviour of the soil structure both in compression and in distortion; and if we can meet these difficulties we will be so far from the linear heat-transfer model that we shall not be able to make use of the elegant solution of problems of transient heat-transfer in three dimensions. However, we can make some general comments on the problem of transient flow in three dimensions by reference to what we now know of one-dimensional transient flow.

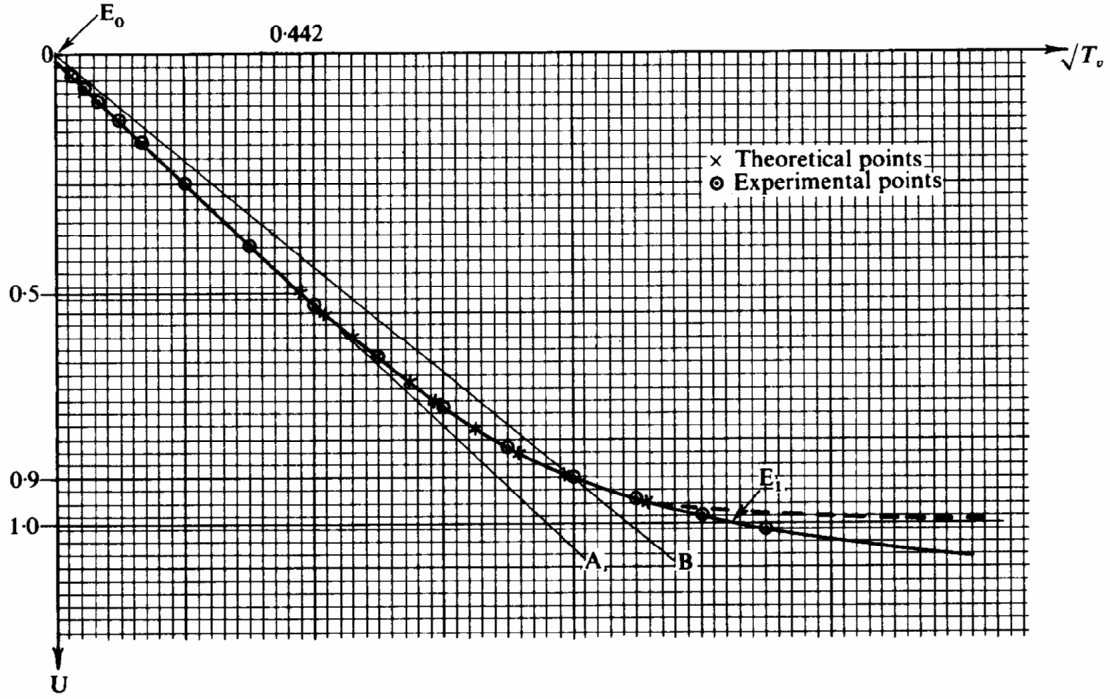

Fig. 4.11 Experimental Laboratory Results

In the one-dimensional problem the relative displacement of the two opposite surfaces (ends) of the body was called 'settlement' and equalled the total quantity of drainage out of the body per unit cross-sectional area. In general, an engineer will want to know a 'differential settlement', that is the relative displacement of two adjacent points of a three-dimensional body such as one point at the centre of an oil tank and another point at the edge of the tank. In this general case, the normal component of the rate of displacement of a point on the surface of the loaded soil body will not equal the rate of flow of seepage water through the surface at that point, and the rate of change of differential settlement of two points need not equal the rate of total flow of water out of the body.

Although an engineer might like to categorize any consolidation problem .by numerical values of two parameters:

(a) a maximum differential settlement, and

(b) the time required before halfsettlement* occurs,

the exact calculation of these two parameters will clearly be a formidable problem in any non-trivial case. However, approximate estimates may be made with less difficulty.

Let us calculate the half-settlement time factor $T_{1/2}$ for the problem of one-dimensional consolidation. We had an approximate solution using parabolic isochrones in eq. (4.20), into which we can introduce *U = 1/2* to give our first estimate

$$T_{1/2} = \frac{1}{3}\left(\frac{1}{4} - \ln\frac{3}{4}\right) = 0.18. \tag{4.26}$$

The curve of U against $\sqrt{T_v}$ for this solution has an initial slope

$$\frac{U}{\sqrt{T_v}} = \frac{2}{\sqrt{3}}. \tag{4.27}$$

We also had an exact series solution in eq. (4.25): the curve of U against $\sqrt{T_v}$ for that solution has a comparable initial slope

$$\frac{U}{\sqrt{T_v}} = \frac{2}{\sqrt{\pi}}, \tag{4.28}$$

and gives an exact half-settlement time factor

$$T_{1/2} = 0.20 \tag{4.29}$$

which is only 10 per cent different from the value estimated by the approximate solution.

For further comparison let us note results from exact solutions of two different problems. In the first case consider a layer where initial excess pore-pressure decreases linearly from some value at the drained surface to zero at $z = H$; this sort of distribution is generated when a vertical load is applied somewhere on the horizontal surface of a clay layer, and in known[1] solutions of this problem the half-settlement time factor is found to be

$$T_{1/2} \cong 0.09. \tag{4.30}$$

In contrast, consider a second case of a layer where initial excess pore-pressure increases linearly from zero at the drained surface to some value at depth; this sort of distribution is generated when a body of soil is placed as a slurry in 'hydraulic fill', and for this case the half-settlement time factor is known[1] to be

$$T_{1/2} \cong 0.29. \tag{4.30}$$

Comparison of these three values of $T_{1/2}$ suggests that a useful range of problems will have

$$0.1 < T_{1/2} < 0.3 \tag{4.31}$$

which is a much smaller range of variation than is likely in H^2 and in c_{vc}.

We may generally calculate the time required before half-settlement occurs as

$$t_{1/2} = \frac{H^2 T_{1/2}}{c_{vc}}, \tag{4.32}$$

and for a useful range of problems a crude numerical estimate can be made using $T_{1/2} = 0.2$.

* We have chosen the half-factor arbitrarily: some practicing engineers regard 80 per cent as significant. In limiting equilibrium calculations dissipation of 90 per cent of maximum excess pore-pressures is considered significant. Although these differences are important we will not discuss them here.

If we accept as a proper approximation that

$$t_{1/2} = 0.2\frac{H^2}{c_{vc}} \tag{4.34}$$

then we can draw a useful distinction between *undrained* and *drained* problems. For any given soil body let us suppose we know a certain time t_l in which a proposed load will gradually be brought to bear on the body; construction of an embankment might take a time t_l of several years, whereas filling of an oil tank might involve a time t_l, of less than a day. Then we can distinguish *undrained* problems as having $t_{1/2} >> t_l$, and *drained* problems as having $t << t_l$.

Equation (4.34) can be written

$$t_{1/2} = \frac{0.2\gamma_w H^2 m_{vc}}{k} \tag{4.35}$$

in which form we can see directly the effects of the different parameters m_{vc}, k, and H. More compressible bodies of virgin compressed soft soil will have values of m_{vc} associated with λ and longer half-settlement times than less compressible bodies of overcompressed firm soil having values of associated with k (elastic swelling or recompression). Less permeable clays will have much smaller values of k and hence longer half-settlement times than more permeable sands. Large homogeneous bodies of plastically deforming soft clay will have long drainage paths H comparable to the dimension of the body itself, whereas thin layers of soft clay within a rubble of firm clay will have lengths H comparable to the thinness of the soft clay layer. This distinction between those soils in which the undrained problem is likely to arise and those in which the drained problem is likely to arise will be of great importance later in chapter 8.

The engineer can control consolidation in various ways. The soil body can be pierced with sand-drains that reduce the half-settlement time. The half-settlement time may be left unaltered and construction work may be phased so that loads that are rather insensitive to settlement, such as layers of fill in an embankment, are placed in an early stage of consolidation and finishing works that are sensitive to settlement are left until a later stage; observation of settlement and of gradual dissipation of pore-pressure can be used to control such operations. Another approach is to design a flexible structure in which heavy loads are free to settle relative to lighter loads, or the engineer may prefer to underpin a structure and repair damage if and when it occurs. A different principle can be introduced in 'pre-loading' ground when a heavy pre-load is brought on to the ground, and after the early stage of consolidation it is replaced by a lighter working load: in this operation there is more than one ultimate differential settlement to consider.

In practice undetected layers of silt[6], or a highly anisotropic permeability, can completely alter the half-settlement time. Initial 'elastic' settlement or swelling can be an important part of actual differential settlements; previous secondary consolidation[7], or the pore-pressures associated with shear distortion may also have to be taken into account. Apart from these uncertainties the engineer faces many technical problems in observation of pore-pressures, and in sampling soil to obtain values of c_{vc}. While engineers are generally agreed on the great value of Terzaghi 's model of one- dimensional consolidation, and are agreed on the importance of observation of pore-pressures and settlements, this is the present limit of general agreement. In our opinion there must be considerable progress with the problems of quasi-static soil deformation before the general consolidation problem, with general transient flow and general soil deformation, can be discussed. We will now turn to consider some new models that describe soil deformation.

References to Chapter 4

1 Terzaghi, K. and Peck, R. B. *Soil Mechanics in Engineering Practice,*Wiley, 1951.

2 Terzaghi, K. and Fröhlich, 0. K. *Theorie der Setzung von Tonschich ten,* Vienna Deuticke, 1936.

3 Taylor, D. W. *Fundamentals of Soil Mechanics,* Wiley, 1948, 239 – 242.

4 Christie, I. F. 'A Re-appraisal of Merchant's Contribution to the Theory of Consolidation', *Gèotechnique,* 14, 309 – 320, 1964.

5 Barden, L. 'Consolidation of Clay with Non-Linear Viscosity', *Gèotechnique,* 15, 345 – 362, *1965.*

6 Rowe, P. W. 'Measurement of the Coefficient of Consolidation of Lacustrine Clay', *Géotechnique, 9,* 107 – 118, *1959.*

7 Bjerrum, L. 'Engineering Geology of Norwegian Normally Consolidated Marine Clays as Related to Settlements of Buildings, *Gèotechnique,* **17,** 81 – 118, 1967.

5
Granta-gravel

5.1 Introduction

Previous chapters have been concerned with models that are also discussed in many other books. In this and subsequent chapters we will discuss models that are substantially new, and only a few research workers will be familiar with the notes and papers in which this work was recently first published. The reader who is used to thinking of 'consolidation' and 'shear' in terms of two dissimilar models may find the new concepts difficult, but the associated mathematical analysis is not hard.

The new concepts are based on those set out in chapter 2. In §2.9 we reviewed the familiar theoretical yield functions of strength of materials: these functions were expressed in algebraic form $F = 0$ and were displayed as yield surfaces in principal stress space in Fig. 2.12. We could compress the work of the next two chapters by writing a general yield function $F=0$ of the same form as eq. (5.27), by drawing the associated yield surface of the form shown in Fig. 5.1, and by directly applying the associated flow rule of §2.10 to the new yield function. But although this could economically generate the algebraic expressions for stress and strain-increments it would probably not convince our readers that the use of the theory of plasticity makes sound mechanical sense for soils. About fifteen years ago it was first suggested[1] that Coulomb's failure criterion (to which we will come in due course in chapter 8) could serve as a yield function with which one could properly associate a plastic flow: this led to erroneous predictions of high rates of change of volume during shear distortion, and research workers who rejected these predictions tended also to discount the usefulness of the theory of plasticity. Although Drucker, Gibson, and Henkel[2] subsequently made a correct start in using the associated flow rule, we consider that our arguments make more mechanical sense if we build up our discussion from Drucker's concept[3] of 'stability', to which we referred in §2.11.

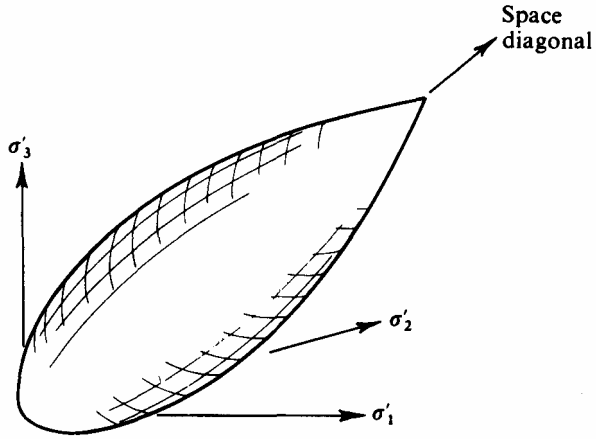

Fig. 5.1 Yield Surface

The concept of a 'stable material' needs the setting of a 'stable system': we will begin in §5.2 with the description of a system in which a cylindrical specimen of ideal material is under test in axial compression or extension. We will devote the remainder of chapter 5 to development of a conceptual model of an ideal rigid/plastic continuum which has been given the name Granta-gravel. In chapter 6 we will develop a model of an ideal

elastic/plastic continuum called Cam-clay[4], which supersedes Granta-gravel. (The river which runs past our laboratory is called the Granta in its upper reach and the Cam in the lower reach. The intention is to provide names that are unique and that continually remind our students that these are conceptual materials – not real soil.) Both these models are defined only in the plane in principal stress space containing axial-test data: most data of behaviour of soil-material which we have for comparison are from axial tests, and the Granta-gravel and Cam-clay models exist only to offer a persuasive interpretation of these axial-test data. We hope that by the middle of chapter 6 readers will be satisfied that it is reasonable to compare the mechanical behaviour of real soil-material with the ideal behaviour of an isotropic-hardening model of the theory of plasticity. Then, and not until then, we will formulate a simple critical state model that is an integral part of Granta-gravel, and of Cam-clay, and of other critical state model materials which all flow as a frictional fluid when they are severely distorted. With this critical state model we can clear up the error of the early incorrect application of the associated flow rule to 'Coulomb's failure criterion', and also make a simple and fundamental interpretation of the properties by which engineers currently classify soil.

The Granta-gravel and Cam-clay models only define yield curves in the axial-test plane as shown in Fig 5.2: this curve is the section of the surface of Fig. 5.1 on a diametrical plane that includes the space diagonal and the axis of longitudinal effective stress o (similar sections of Mises' and Tresca's yield surfaces in Fig. 2.12 would show two lines running parallel to the *x*-axis in the *xz*-plane). The obvious features of the pear-shaped curve of Fig. 5.2 are the pointed tip on the space diagonal at relatively high pressure, and the flanks parallel to the space diagonal at a lower pressure. A continuing family of yield curves shown faintly in Fig. 5.2 indicates occurrence of stable isotropic hardening. Our first goal in this chapter is to develop a model in the axial-test system that possesses yield curves of this type.

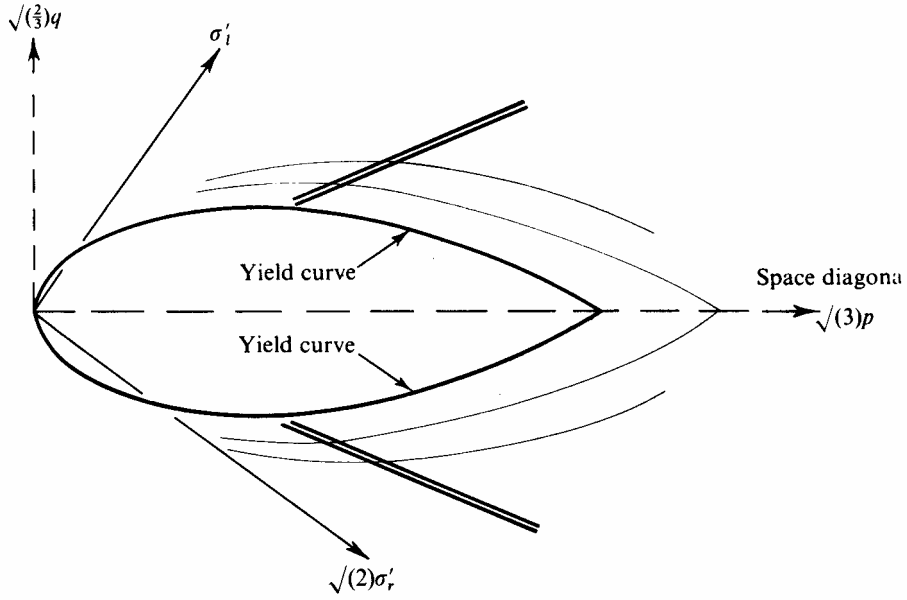

Fig. 5.2 Yield Curves

5.2 A Simple Axial-test System

We shall consider a real axial test in detail in chapter 7: for present purposes a much simplified version of the test system will be described with all dimensions chosen to make the analysis as easy as possible.

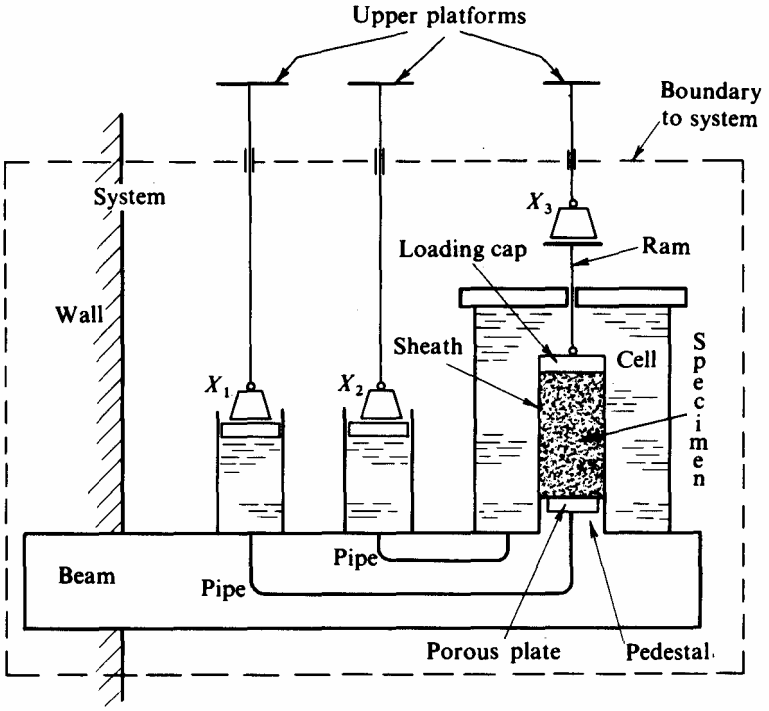

Fig. 5.3 Test System

Let us suppose that we enter a laboratory and find a specimen under test in the apparatus sketched in Fig. 5.3. We first examine the test system and determine the current state of the specimen, which is in *equilibrium* under static loads in a uniform vertical gravitational field. We see that we may probe the equilibrium of the specimen by slowly applying load-increments to some accessible loading platforms. We shall hope to learn sufficient about the mechanical properties of the material to be able to predict its behaviour in any general test.

The specimen forms a right circular cylinder of axial length l, and total volume v, so that its cross-sectional area, $a = v/l$. The volume v is such that the specimen contains unit volume of solids homogeneously mixed with a volume $(v - 1)$ of voids which are saturated with pore-water and free from air.

The specimen stands, with axis vertical, on a pedestal containing a porous plate. The porous plate is connected by a rigid pipe to a cylinder, all full of water and free of air. The pressure in the cylinder is controlled by a piston at approximately the level of the middle of the specimen which is taken as datum. The piston which is of negligible weight and of unit cross-sectional area supports a weight X_1 so that the *pore-pressure* in the specimen is simply $u_w = X_1$.

A stiff impermeable disc forms a loading cap for the specimen. A flexible, impermeable, closely fitting sheath of negligible thickness and strength envelops the specimen and is sealed to the load-cap and to the pedestal. The specimen, with sheath, loading cap, and pedestal, is immersed in water in a transparent cell. The cell is connected by a rigid pipe to a cylinder where a known weight X_2 rests on a piston of negligible weight and unit cross-sectional area. The cell, pipe, and cylinder are full of water and free from air, so that the cell pressure is simply $\sigma_r = X_2$ which is related to the same datum as the pore-pressure. The cell pressure is the principal *radial total stress* acting on the cylindrical specimen.

A thin stiff ram of negligible weight slides freely through a gland in the top of the cell in a vertical line coincident with the axis of the specimen. A weight X_3 rests on this

ram and causes a vertical force to act on the loading cap and a resulting axial pressure to act through the length of the specimen. In addition, the cell pressure σ_r acts on the loading cap and, together with the effect of the ram force X_3, gives rise to the principal *axial total stress* σ_l experienced by the specimen, so that

$$X_3 = a(\sigma_l - \sigma_r).$$

Hence, three stress quantities u_w, σ_r and $(\sigma_l - \sigma_r)$, and two dimensional quantities v, and l, describe the state of the specimen as it stands in equilibrium in the test system.

5.3 Probing

The *test system* of Fig. *5.3* is encased by an imaginary boundary which is penetrated by three stiff, light rods of negligible weight shown attached to the main loads X_1, X_2, and X_3. These rods can slide freely in a vertical direction through glands in the boundary casing, and they carry upper platforms to which small load-increments can be applied or removed. The displacement of any load- increment is identical to that of its associated load within the system, being observed as the movement of the upper platform.

We imagine ourselves to be an *external agency* standing in front of this test system in which a specimen is in equilibrium under relatively heavy loads: we test its stability by gingerly prodding and poking the system to see how it reacts. We do this by conducting a *probing* operation which is defined to be the slow application and slow removal of an infinitesimally small load-increment. The *load-increment* itself consists of a set of loads $\dot{X}_1, \dot{X}_2, \dot{X}_3$ (any of which may be zero or negative) applied simultaneously to the three upper platforms, see Fig. 5.4.

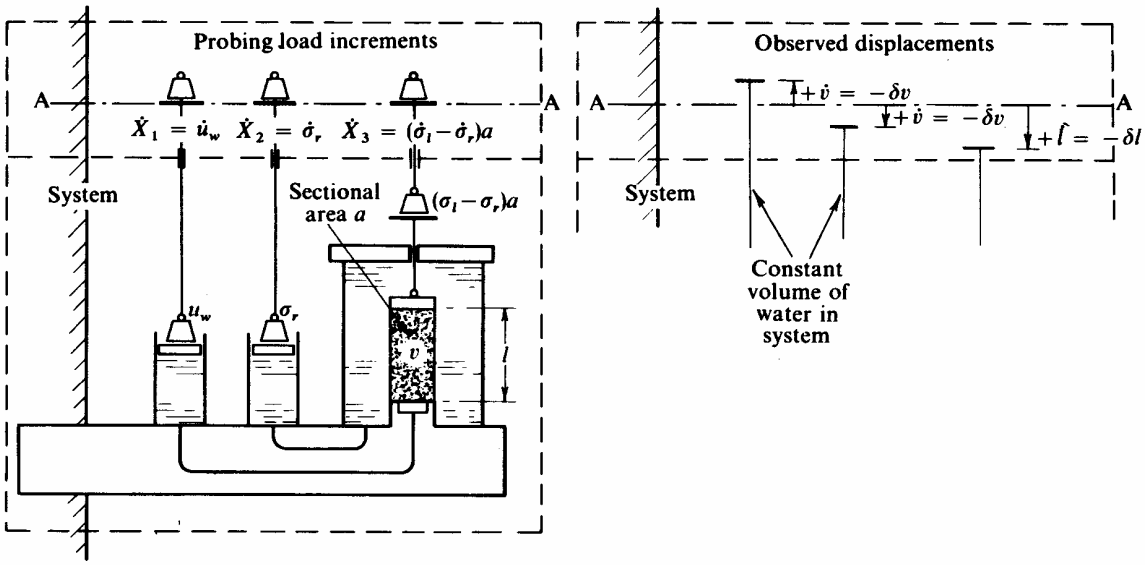

Fig. 5.4 Probing Load-increments

Each application and removal of load-increment will need to be so slow that it is at all times fully resisted by the effective stresses in the specimen, and at all times excess pore-pressures in the specimen are negligible. If increments were suddenly placed on the platforms work would be done making the pore-water flow quickly through the pores in the specimen.

We use the term *effectively stressed* to describe a state in which there are no excess pore-pressures within the specimen, i.e., load and load-increment are both acting with full

effect on the specimen. In Fig. 5.5(a) **OP** represents the slow application of a single load-increment $\dot{X}$ fully resisted by the slow compression of an effectively stressed specimen, and **PO** represents the slow removal of the load-increment $\dot{X}$ exactly matched by the slow swelling of the effectively stressed specimen. It is clear that, in the cycle **OPO,** by stage P the external agency has slowly transferred into the system a small quantity of work of magnitude $(1/2)\dot{X}\delta$, and by the end **O** of the cycle this work has been recovered by the external agency without loss.

In contrast in Fig. 5.5(b) **OQ** represents a sudden application of a load-increment $\dot{X}$ at first resisted by excess pore-pressures and only later coming to stress effectively the specimen at R. During the stage **QR** a quantity of work of magnitude $\dot{X}\delta$ is transferred into the system, of which a half (represented by area OQR) has been dissipated within the system in making pore-water flow quickly and the other half (area ORS) remains in store in the effectively stressed specimen. Stage **RS** represents the sudden removal of the whole small load-increment $\dot{X}$ from the loading platform when it is at its low level. Negative pore-pressure gradients are generated which quickly suck water back into the specimen, and by the end of the cycle at O the work which was temporarily stored in the specimen has all been dissipated. At the end of the loading cycle the small load increment is removed at the lower level, and the external agency has transferred *into* the system the quantity of work $\dot{X}\delta$ indicated by the shaded area **OQRS** in Fig. 5.5(b), although the effectively stressed material structure of the specimen has behaved in a reversible manner. In a study of work stored and dissipated in effectively stressed specimens it is therefore essential to displace the loading platforms slowly.

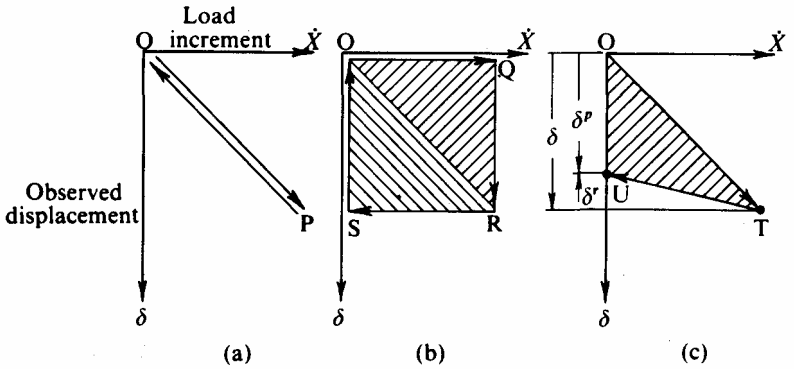

Fig. 5.5 Work Done during Probing Cycle

For the most general case of probing we must consider the situation shown in Fig. 5.5(c) in which the loading platform does not return to its original position at the end of the cycle of operations, and the specimen which has been effectively stressed throughout has suffered some permanent deformation. The total displacement δ observed after application of the load-increment has to be separated into a component δ^r which is *recovered* when the load-increment is removed and a *plastic* component δ^p which is not.

Because we shall be concerned with quantities of *work* transferred into and out of the test system, and not merely with displacements, we must take careful account of signs and treat the displacements as *vector* quantities. Since we can only discover the plastic component as a result of applying and then removing a load-increment, we must write it as the resultant of initial, total, and subsequently recovered displacements

$$\delta^p = \delta + \delta^r.$$

When plastic components of displacement occur we say that the specimen *yields.* As we have already seen in §2.9 and §2.10 we are particularly interested in the states in which the specimen will yield, and in the nature of the infinitesimal but irrecoverable displacements that occur when the specimen yields.

5.4 Stability and Instability

Underlying the whole previous section is the tacit assumption that it is within our power to make the displacement diminishingly small: that if we do virtually nothing to disturb the system then virtually nothing will happen. We can well recall counter-examples of systems which failed when they were barely touched, and if we really were faced with this axial-test system in equilibrium under static loads we would be fearful of failure: we would not touch the system without attaching some buffer that could absorb as internal or potential or inertial energy any power that the system might begin to emit.

If the disturbance is small then, whatever the specimen may be, we can calculate the net quantity of work transferred across the boundary *from* the external agency *to* the test system, as

$$\sum \frac{1}{2} \dot{X}_i \delta_i^p .$$

For example, with the single probing increment illustrated in Fig. 5.5(c) this net quantity of work equals the shaded area ΔAOTU. If the specimen is *rigid,* then $\delta_i^p \equiv 0 \equiv \delta_i^r$, and the probe has no effect. If the specimen is *elastic* (used in the sense outlined in chapter 2) then $\delta_i^p \equiv 0$, all displacement is recoverable and there is no net transfer of work at the completion of the probing cycle. If the specimen is *plastic* (also used in the sense outlined in chapter 2) then some net quantity of work will be transferred to the system. In each of these three cases the system satisfies a *stability criterion* which we will write as

$$\sum \dot{X}_i \delta_i^p \geq 0, \tag{5.1}$$

and we will describe these specimens as being made of *stable material.*

> In a recent discussion Drucker5 writes of
> 'the term *stable material,* which is a specialization of the rather ill-defined term *stable system.*
> A stable system is, qualitatively, one whose configuration is determined by the history of loading in the sense that small perturbations produce a small change in response and that no spontaneous change in configuration will occur. Quantitative definition of the terms stable, small, perturbation, and response are not clear cut when irreversible processes are considered, because a dissipative system does not return in general to its original equilibrium configuration when a disturbance is removed. Different degrees of stability may exist.'

Our choice of the stability* criterion (5.1) enables us to distinguish two classes of response to probing of our system:

I *Stability,* when a cycle of probing of the system produces a response satisfying the criterion (5.1), and

II *Instability,* when a cycle of probing of the system produces a response violating the criterion (5.1).

* This word will only be used in one sense in this text, and will always refer to material stability as discussed in §2.11 and here in *§5.4.* It will *not* be used to describe limiting-stress calculations that relate to failure of soil masses and are sometimes called 'slope-stability' or 'stability-of-foundation' calculations. These limiting-stress calculations will be met later in chapter 9.

The role of an external attachment in moderating the consequence of instability can be illustrated in Fig. 5.6. The axial-test system in that figure has attached to it an arrangement in which instability of the specimen permits the transfer of work out of the system: Fig. 5.6(a) shows a pulley fixed over the relatively large ram load with a relatively small *negative* load-increment $(\dot{X}_3 < 0)$ applied by attaching a small weight to the chord round the pulley. At the same time a small *positive* load-increment $(\dot{X}_1 > 0)$ is applied to the pore pressure platform, and we suppose that, for some reason which need not be specified here, the change in pore-pressure happens to result, as shown in Fig. 5.6(b), in unstable compressive failure of the specimen at constant volume. The large load on the ram will fall as the specimen fails, and in doing so will raise the small load-increment. The external probing agency has thus provoked a release of usable *work from the system.* In general, the loading masses within the system would take up energy in acceleration, and we would observe a sudden uncontrollable displacement of the loading platforms which we would take to indicate *failure* in the system.

The study of systems at failure is problematical. The load-increment sometimes brings parts of a test system into an unstable configuration where failure occurs, even though the specimen itself is in a state which would not appear unstable in another test in another system. In contrast, the study of stable test systems leads in a straightforward manner, as is shown below, to development of stress – strain relationships for the specimen under test. Once these relationships are known they may be used to solve problems of failure.

It is essential to distinguish *stable* states from the wider class of states of static *equilibrium* in general. A simple calculation of virtual work within the system boundary based on some virtual displacement of parts of a system, would be sufficient to check that the system is in static equilibrium, but additional calculations are needed to guarantee stability. Engineers generally must design systems not only to perform a stated function but also to continue to perform properly under changing conditions. A small change of external conditions must only cause a small error in predicted performance of a well engineered system. For each state of the system, we check carefully to ensure that there is no accessible alternative state into which probing by an external agency can bring the system and cause a net emission of power in a probing cycle.

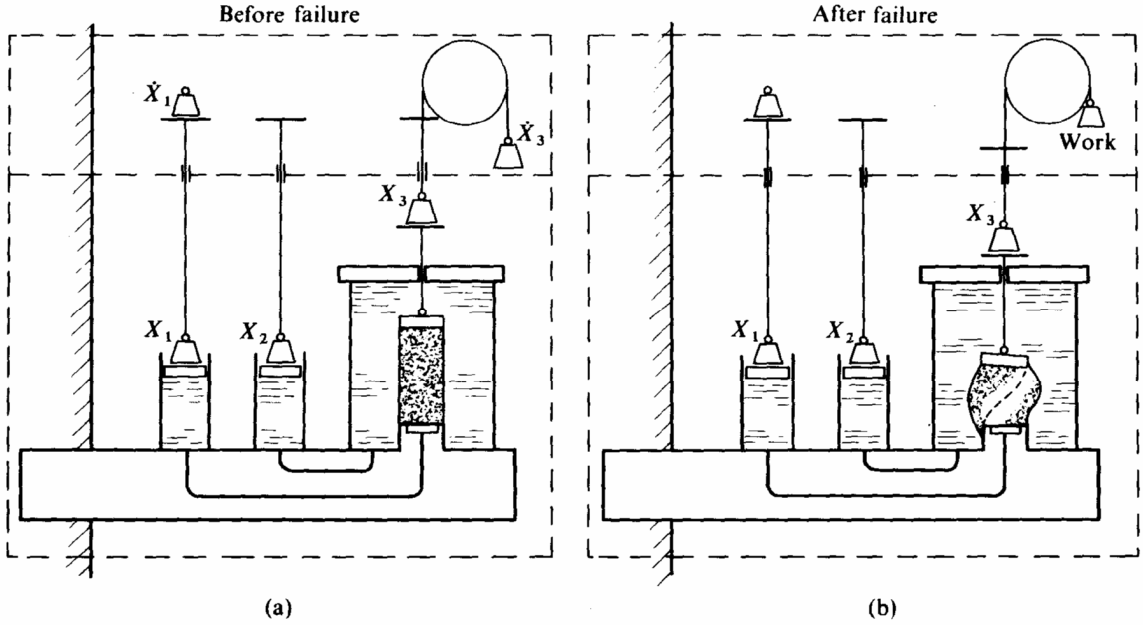

Fig. 5.6 Unstable Yielding

In the following sections we begin by considering the stressed state of the specimen and the increments of stress and strain. Then come calculations about power, and the use of power in the system. This leads to certain interesting calculations, but in §5.10 we will return to this stability criterion and make use of it to explain why it is that in some states some load-increments make the specimens yield and others do not. The stability criterion is essential to this chapter, but before developing it in detail we must select appropriate parameters.

5.5 Stress, Stress-increment, and Strain-increment

Let the state of effective stress experienced by the specimen be separated into *spherical* and *deviatoric* components, in the same manner that proved helpful to an understanding of the mechanical behaviour of elastic material in §2.6 and §2.7. The *total* stresses acting on the specimen u_w, σ_r, and σ_l can be used to define parameters somewhat similar to eq. (2.4):
effective spherical pressure

$$p = \frac{\sigma_l + 2\sigma_r}{3} - u_w > 0 \tag{5.2}$$

and axial-deviator stress

$$q = \sigma_l - \sigma_r. \tag{5.3}$$

In Fig. *5.2* the space diagonal axis has units of $\sqrt{(3)}p$ and the perpendicular axis has units $\sqrt{(2/3)}q$; an alternative and simpler representation of the state of stress of the axial-test specimen is now given in Fig. 5.7 where axes p and q are used directly without the multiplying factors $\sqrt{(3)}$ and $\sqrt{(2/3)}q$.

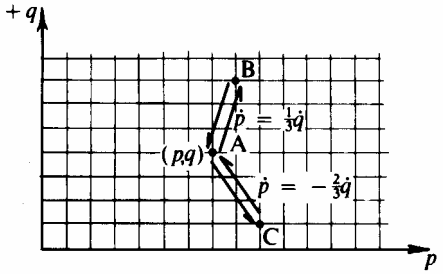

Fig. 5.7 Stress Paths Applied by Probes

In a corresponding manner, parameters of stress-increment can be calculated and used to describe any load-increment, namely:
effective spherical pressure increment

$$\dot{p} = \frac{\dot{\sigma}_l + 2\dot{\sigma}_r}{3} - \dot{u}_w \tag{5.4}$$

and axial-deviator stress-increment

$$\dot{q} = \dot{\sigma}_l - \dot{\sigma}_r. \tag{5.5}$$

The parameters $(\dot{p}, \dot{q})$ define a vector in the (p, q) plane, and Fig. 5.7 illustrates two examples. In each example the specimen drains into the pore-pressure cylinder with no pore-pressure load-increment, $\dot{u}_w \equiv 0$. One example, AB, (equivalent to a conventional drained compression test) involves load-increment only on the ram platform and not on the cell pressure platform so that

$$\dot{\sigma}_r = 0, \qquad \dot{\sigma}_l = \frac{\dot{X}_3}{a} > 0.$$

In this example, eqs. (5.4) and (5.5) give

$$\dot{p} = \frac{1}{3}\dot{\sigma}_l \qquad \dot{q} = \dot{\sigma}_l \qquad \frac{\dot{p}}{\dot{q}} = \frac{1}{3}$$

so that the load-increment brings the specimen into a state of stress represented on the (*p, q*) plane by some point B on the line through A of slope 3 given by $\dot{p} = \frac{1}{3}\dot{q}$. The probing cycle would be completed by removal of the load-increment and return of the specimen to the original stress state at A (though not necessarily to the original lengths and volumes).

The second example, AC (equivalent to a drained extension test), involves load-increment on the cell pressure platform and an equal but opposite negative stress-increment on the ram platform, so that $\dot{\sigma}_l = 0, \dot{\sigma}_r = \dot{X}_2 = -\dot{X}_3 / a > 0$. In that case eqs. (5.4) and (5.5) give

$$\dot{p} = \frac{1}{3}\dot{\sigma}_r \qquad \dot{q} = -\dot{\sigma}_r \qquad \frac{\dot{p}}{\dot{q}} = -\frac{2}{3}$$

so that the load-increment brings the specimen into a state represented in the (*p, q*) plane by some point C on a line through A of slope $-\frac{3}{2}$ given by $\dot{p} = -\frac{2}{3}\dot{q}$. As before, completion of the probing cycle requires removal of load increments, and a return to a state represented by point A.

The choice of strain-increment parameters to correspond to $(p, \dot{p})$ and $(q, \dot{q})$ requires care. It is essential that when the corresponding stress and strain-increments are multiplied together they correctly give the incremental work per unit volume performed by stresses on the specimen. This essential check will be carried out in the next section, §5.6. But in introducing the strain-increment parameters an appeal to intuition is helpful. Clearly, change in specimen volume can be chosen to correspond with effective spherical pressure and pressure increment. The choice of a strain parameter to correspond with axial-deviator stress and stress-increment is not so obvious. The ram displacement *I* does not correspond simply to axial-deviator stress; indeed, if an elastic specimen is subjected to effective spherical pressure increment without any axial- deviator stress there will be a longitudinal strain of one third of the volumetric strain. This suggests the possibility of defining a parameter[6] called axial-distortion increment

$$+\dot{\varepsilon} = \frac{\dot{l}}{l} - \frac{1}{3}\frac{\dot{v}}{v} \tag{5.6}$$

to correspond to axial-deviator stress. The correctness of this choice will be shown in §5.6.

Care must be taken with signs of these parameters. Since stress is defined to be positive in compression, it is necessary to define length *reduction* and radius *reduction* as *positive* strain-increments, $\dot{\varepsilon}_l$ and $\dot{\varepsilon}_r$ respectively. Then defining longitudinal strain-increment as

$$\left.\begin{aligned} &\dot{\varepsilon}_l = \frac{\dot{l}}{l} = -\frac{\delta l}{l} \\ &\text{and radial strain-increment as} \\ &\dot{\varepsilon}_r = \frac{\dot{r}}{r} = -\frac{\delta r}{r} \end{aligned}\right\} \tag{5.7}$$

we have volumetric strain-increment,

$$\frac{\dot{v}}{v} = -\frac{\delta v}{v} = \dot{\varepsilon}_l + 2\dot{\varepsilon}_r \tag{5.8}$$

and eq. (5.6) can be re-written

$$\dot{\varepsilon} = \tfrac{2}{3}(\dot{\varepsilon}_l - \dot{\varepsilon}_r). \tag{5.9}$$

It will be appropriate to distinguish between deformations called

length reduction when $\dot{\varepsilon} > 0$

and *radius reduction* when $\dot{\varepsilon} < 0$.

A little conceptual difficulty may be met later because volumetric strain-increment has been defined in eq. (5.8) to be positive when the volume v is being reduced.

It should be noted that for this choice of parameters to be meaningful principal axes of stress, stress-increment, and strain- increment must coincide.

5.6 Power

The rate (with respect to strain*) of working of the main loading *within the system* on the specimen during the displacements provoked by the external agency will be called the *loading power* of the system. It can be simply calculated from the observed displacements of Fig. 5.4 to be

$$\dot{E} = -u_w \dot{v} + \sigma_r \dot{v} + (\sigma_l - \sigma_r) a \dot{l}. \tag{5.10}$$

The upward displacement of the pore-pressure piston is equal and opposite to the downward displacement of the cell-pressure piston, and so the loading power depends only on the effective stresses

$$\sigma'_r = \sigma_r - u_w \qquad \sigma'_l = \sigma_l - u_w$$

and eq. (5.10) can be re-written

$$\dot{E} = \sigma'_r \dot{v} + (\sigma'_l - \sigma'_r) a \dot{l}.$$

Introducing eqs. (5.7) and (5.8), the loading power per unit volume of specimen becomes

$$\begin{aligned} \frac{\dot{E}}{v} &= \sigma'_r \frac{\dot{v}}{v} + (\sigma'_l - \sigma'_r) \frac{\dot{l}}{l} \\ &= \sigma'_r (\dot{\varepsilon}_l + 2\dot{\varepsilon}_r) + (\sigma'_l - \sigma'_r) \dot{\varepsilon}_l \\ &= \sigma'_l \dot{\varepsilon}_l + 2\sigma'_r \dot{\varepsilon}_r, \end{aligned} \tag{5.1}$$

in which form the rate of working of effective stresses moving at their respective strain rates is directly evident.

But from eqs. (5.2), (5.3), (5.8), and (5.9) we obtain

$$\left.\begin{aligned} p\frac{\dot{v}}{v} &= \left(\frac{\sigma'_l + 2\sigma'_r}{3}\right)(\dot{\varepsilon}_l + 2\dot{\varepsilon}_r) = \frac{\sigma'_l \dot{\varepsilon}_l}{3} + \frac{4\sigma'_r \dot{\varepsilon}_r}{3} + \frac{2\sigma'_r \dot{\varepsilon}_l}{3} + \frac{2\sigma'_l \dot{\varepsilon}_r}{3} \\ \text{and} \\ q\dot{\varepsilon} &= \frac{2}{3}(\sigma'_l - \sigma'_r)(\dot{\varepsilon}_l - \dot{\varepsilon}_r) = \frac{2\sigma'_l \dot{\varepsilon}_l}{3} + \frac{2\sigma'_r \dot{\varepsilon}_r}{3} - \frac{2\sigma'_r \dot{\varepsilon}_l}{3} - \frac{2\sigma'_l \dot{\varepsilon}_r}{3} \end{aligned}\right\}$$

which when added give

$$p\frac{\dot{v}}{v} + q\dot{\varepsilon} = \sigma'_l \dot{\varepsilon}_l + 2\sigma'_r \dot{\varepsilon}_r. \tag{5.12}$$

This confirms the correctness of the choice of strain-increment parameters, because comparison of eqs. (5.11) and (5.12) shows that

$$\frac{p\dot{v}}{v} + q\dot{\varepsilon} = \frac{\dot{E}}{v} \tag{5.13}$$

which is clearly necessary.

* Equations of the theory of plasticity are independent of time.[7]

At this juncture we must recall the mechanical working of the system and the external agency, see Fig. 5.4. The loads within the casing of the test system are relatively heavy and they may well have brought the specimen to the point of yielding. The object of the tests is to learn how this loaded specimen will adjust itself when it is gently probed. During the small displacements that are provoked by the external agency the heavy loads moving within the system generate power $\dot{E}$ which the specimen must either store or dissipate: in the following section §5.7 we will define the nature of the Granta-gravel material by stating the manner in which it disposes of this loading power. All this is taking place *within* the system. In addition, there is the small power input $\dot{P}$ by which the external agency is controlling, and at the same time provoking, the displacements of the system, given by

$$\frac{\dot{P}}{v} = \frac{1}{2}\left(\dot{p}\frac{\dot{v}}{v} + q\dot{\varepsilon} \right).$$

This power is transmitted across the casing or boundary of the system during application of the load-increment, but it is altogether smaller than the power of the heavy loads that are causing the specimen to deform. We think of $\dot{P}$ as a small input signal that controls the powerful heavy loads within the system.

During application of the load-increment the loading power per unit volume transferred from the heavy loads to the specimen is, from eq. (5.13),

$$\frac{\dot{E}}{v} = \left(\frac{p\dot{v}}{v} + q\dot{\varepsilon} \right).$$

During subsequent unloading the recoverable power per unit volume returned by the specimen to the heavy loads within the system is

$$+\frac{\dot{U}}{v} = -\left(\frac{p\dot{v}^r}{v} + q\dot{\varepsilon}^r \right). \tag{5.14}$$

The remainder of the loading power which is not transferred back and has been dissipated within the specimen is

$$\frac{\dot{W}}{v} = \frac{\dot{E}}{v} - \frac{\dot{U}}{v} = -\left(\frac{p\dot{v}^p}{v} + q\dot{\varepsilon}^p \right). \tag{5.15}$$

Of course transfers from heavy loads to specimen and back again do not involve any transfer across the casing that surrounds the system. However, there may be some *net* work transferred by the external probing agency across the boundary to the system in the complete probing cycle, which is the small quantity

$$\frac{1}{2}\left(\dot{p}\frac{\dot{v}^p}{v} + \dot{q}\dot{\varepsilon}^p \right) = \sum \frac{1}{2}\dot{X}_i \delta_i^{\,p}$$

corresponding to the shaded area in Fig. 5.5(c). We have already discussed the importance of this in §5.4 and seen that our criterion of stability (5.1) requires

$$\dot{p}\frac{\dot{v}^p}{v} + \dot{q}\dot{\varepsilon}^p \geq 0. \tag{5.16}$$

5.7 Power in Granta-gravel

To specify the mechanical behaviour of a material it is necessary to prescribe the nature of the four terms on the right of eqs. (5.14) and (5.15). For example, if a gas were tested only the first term of the first equation $p\dot{v}^r/v$ would be significant and all the other terms would be negligible. Again, if a perfectly elastic material were tested $\dot{v}^p$ and

$\dot{\varepsilon}^p$ would be zero, and $\dot{v}^r$ and $\dot{\varepsilon}^r$ might be prescribed functions of $p, \dot{p}$ and $q, \dot{q}$. In formulating an artificial material we are free to choose what ingredients we like for the recipe provided by these two equations. We require Granta-gravel to be an *ideal rigid/plastic material* and so we shall take as our first and major simplification the requirement that it *never displays any recoverable strains,* i.e.,

$$\dot{v}^r \equiv \dot{\varepsilon}^r \equiv 0. \tag{5.17}$$

This means that the application of a probing load-increment either meets with a rigid response, or causes yield, but that the subsequent removal of the load-increment has no effect at all. There can be no recoverable power $\dot{U}$ and all loading power $\dot{E}$ is dissipated within the specimen as $\dot{W}$.

We need to specify how this work $\dot{W}$ is dissipated, and as Granta-gravel is intended to be as simple a model as possible of a frictional granular material we shall assume that

$$\frac{\dot{W}}{v} = Mp|\dot{\varepsilon}| > 0. \tag{5.18}$$

In this equation M (capital μ) is a simple frictional constant so that $\dot{W}$ is linearly dependent on $p > 0$. The modulus sign is required for $\dot{\varepsilon}$ because frictional work is always dissipated and $\dot{W}$ must always be positive. This property of Granta-gravel is a sort of 'friction' in the sense loosely defined in §1.8.

Combining these assumptions and re-writing eqs. (5.14), (5.15), and (5.16) we have specified for Granta-gravel

$$\dot{v}^r \equiv \dot{\varepsilon}^r \equiv 0 \qquad \dot{v} \equiv \dot{v}^p \qquad \dot{\varepsilon} \equiv \dot{\varepsilon}^p \qquad \dot{U} \equiv 0$$

$$\frac{p\dot{v}}{v} + q\dot{\varepsilon} = \frac{\dot{W}}{v} = Mp|\dot{\varepsilon}| \tag{5.19}$$

and the stability criterion becomes

$$\frac{\dot{p}\dot{v}}{v} + \dot{q}\dot{\varepsilon} \geq 0. \tag{5.20}$$

5.8 Responses to Probes which cause Yield

If we have a specimen of Granta-gravel of specific volume v_1 under test, in equilibrium at the stressed state (p_1, q_1), and we apply a series of different probes $(\dot{p}, \dot{q})$, we can now use eq. (5.19) to predict responses of the system. Generally, the specimen remains *rigid* but there may be certain probes which cause it to *yield,* and when yielding occurs the power equation (5.19) tells us what ratio of (permanent) increments of strain the specimen will experience.

For the case of length reduction, $\dot{\varepsilon} > 0$, we have

$$\frac{\dot{v}}{v_1\dot{\varepsilon}} = +M - \frac{q_1}{p_1} \tag{5.21a}$$

and for radius reduction, $\dot{\varepsilon} < 0$,

$$\frac{\dot{v}}{v_1\dot{\varepsilon}} = -M - \frac{q_1}{p_1}. \tag{5.21b}$$

These equations provide relationships between stress ratio $\eta_1 = (q_1/p_1)$ and strain-increment ratio $\dot{v}/v_1\dot{\varepsilon}$, and reveal the importance of the constant M. We will describe specimens which yield when $|q_1| < Mp_1$ as being *weak at yield,* and those which yield when $|q_1| > Mp_1$ as

being *strong at yield,* and those which yield when $|q_1| = Mp_1$ as being in a *critical state* at yield.

At this stage, in order to develop the argument economically, we shall confine our attention to specimens that are experiencing a *positive* deviator stress, $q_1 > 0$, and subject to reduction of length $\dot{\varepsilon} \geq 0$. This is equivalent to conducting conventional axial compression tests only, but we shall see later that this restriction does not cause loss of generality, as similar results can be obtained for extension tests where $q_1 < 0$ and $\dot{\varepsilon} \leq 0$.

5.9 Critical States

Although we are taking $q_1 > 0$ and $\dot{\varepsilon} \geq 0$ we still have three distinct classes of specimen to consider:

a) $q_1 < Mp_1$ for which eq. (5.21a) shows that $\dot{v} = -\delta v > 0$ so that all specimens weak at yield must be *compacting,*

b) $q_1 > Mp_1$ for which we must have $\dot{v} = -\delta v < 0$ so that all specimens strong at yield must be *dilating,*

c) $q_1 = Mp_1$ for which $\dot{v} = 0$ so that specimens yielding in what we call 'critical states' remain at constant volume, $\dot{\varepsilon}$ is indeterminate, and in these states yield can continue to occur without change in q_1, p_1, or v_1. The material behaves as a *frictional fluid* rather than a yielding *solid;* it is as though the material had melted under stress.

The behaviour of each of these three classes *(a)*, *(b),* and *(c)* is indicated in Fig. 5.8 from which it is clear that when the states of

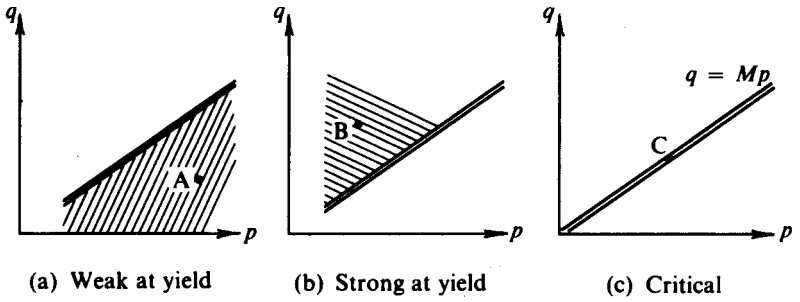

Fig. 5.8 Condition of Specimens at Yield in Relation to Line of Critical States

specimens are represented by the parameters (*p*, *v)* in Fig. 5.9 a distinct curve separates an area in which yielding specimens compact, from one in which they dilate. In addition, any point such as C appropriate to a specimen yielding in a critical state with $q_1 = Mp_1, v = v_1$ must lie on this curve.

Experimental evidence [8-11] supports the assumption that for specimens of Granta-gravel in tests with length reduction there exists a unique curve of *critical states* in (*p*, *v, q*) space. This curve, which will always be shown in diagrams as a double line, is given by the pair of equations

$$q = Mp \tag{5.22}$$

defining the straight line projection in Figs. 5.8(a), (b), and (c),

and $$v = \Gamma - \lambda \ln p \tag{5.23}$$

defining the projected *critical curve* of Fig. 5.9. (We shall expect a mirror image of this critical state curve on the negative side of the $q = 0$ plane for tests with radius reduction.)

It is experimentally difficult to keep a specimen under control as it approaches the critical state and tends towards frictional fluid behaviour. Axial-test specimens have closely defined right-cylindrical shape at the start of a test, but we can clearly see them lose shape and we must expect that the test system will become unstable and exhibit 'failure' before average conditions in the specimen correspond closely to critical conditions. However, leaving to one side at present the difficulties of the specific system of Figs. 5.3, 5.4, 5.6, it is necessary to idealize and assume that specimens of Granta-gravel can reach a critical state.

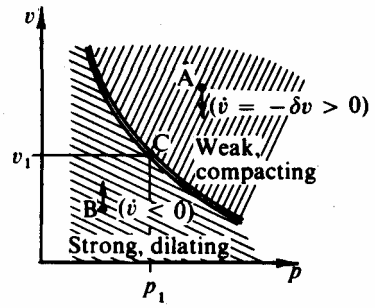

Fig. 5.9 Line of Critical States for Length Reduction

5.10 Yielding of Granta-gravel

From our outline of theory of plasticity in chapter 2 we expect the permissible stressed states of a particular specimen of Granta-gravel to be bounded by a convex closed *yield curve* in the axial-test plane or the (p, q) plane of Fig. 5.10. We expect that under changes of states of stress represented by paths within the boundary, such as from L to K, the specimen of Granta-gravel will remain rigid with no displacements and with its specific volume unchanged at v_1.

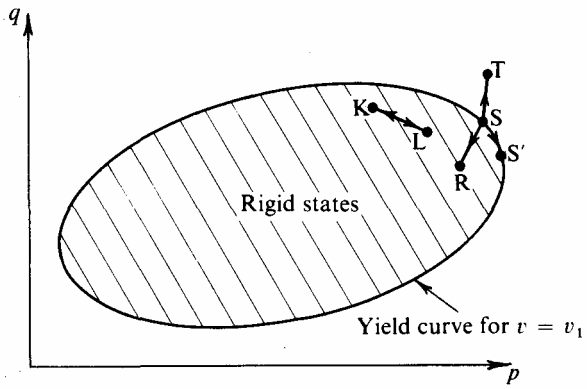

Fig. 5.10 Closed Convex Yield Curve

Let us examine in detail the behaviour of a specimen under the state of stress given by S, which is on the yield curve with coordinates (p_s, q_s). We can apply a variety of infinitesimal probes $(\dot{p}, \dot{q})$, as a result of which the specimen either remains rigid or yields with permanent deformations satisfying eq. (5.19). The inequality (5.20) tells us whether such yielding is stable or unstable. Combining these and eliminating $\dot{v}$ we obtain the inequality

$$\dot{p}(Mp_s|\dot{\varepsilon}| - q_s\dot{\varepsilon}) + p_s\dot{q}\dot{\varepsilon} \geq 0$$

and since we have previously specified $\dot{\varepsilon} \geq 0$ we have the requirement for *stable yielding*

$$\left(M-\frac{q_s}{p_s}\right)\dot{p}+\dot{q}>0, \quad \dot{\varepsilon}>0. \tag{5.24}$$

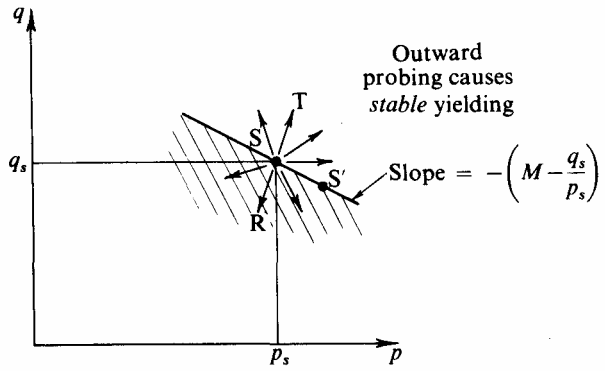

Fig. 5.11 Probing Vectors at Point on Yield Curve

Considering in Fig. 5.11 all possible probing vectors at the point S, we can now distinguish between those such as ST which are directed *outwards* from a line through S of slope

$$\frac{\mathrm{d}q}{\mathrm{d}p}=\frac{\dot{q}}{\dot{p}}=-\left(M-\frac{q_s}{p_s}\right) \tag{5.25}$$

those such as SR which are directed *inwards* from the line, and those such as SS' which are directed *along* the line. Under the first of these probings yielding would satisfy the stability criterion and inequality (5.24): under the second of these probings rigidity must be postulated so that $\dot{\varepsilon}$ is zero if the stability criterion is to be satisfied: under the third of these probings the specimen experiences a *neutral* change of state in which it moves into an adjacent state of limiting rigidity, still on the point of yielding.

In this manner we can link the stability criterion with the theory of plasticity, as also set out in chapter 2. We can integrate eq. (5.25) to give

$$\frac{q}{Mp}=\ln p=\text{const.} \tag{5.26}$$

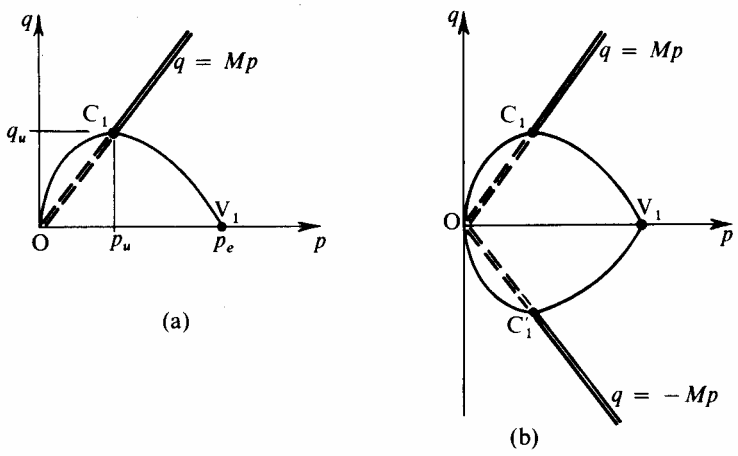

Fig. 5.12 Yield Curve for Specimens of Granta-gravel of Volume v_1

We can evaluate the constant of integration as we know that the yield curve must pass through the critical state C_1 appropriate to this specimen of specific volume v_1. Let this be denoted by $(p_u, q_u = Mp_u)$ so that the yield curve becomes

$$\frac{q}{Mp} + \ln\left(\frac{p}{p_u}\right) = 1 \ (q > 0). \tag{5.27}$$

Our argument has been confined so far to loads with $q > 0$ so the yield curve given by eq. (5.27) is confined to the positive quadrant as shown in Fig. 5.12(a). If the argument of this and the last section (5.9) is now repeated for specimens subject to negative deviator stress $q < 0$ and reduction of radius $\dot{\varepsilon} \le 0$ (equivalent to a conventional extension test) we shall get exactly similar expressions but with appropriate changes of sign throughout, and derive a yield curve which is the mirror image of that above, i.e.,

$$-\frac{q}{Mp} + \ln\left(\frac{p}{p_u}\right) = 1 \ (q > 0). \tag{5.28}$$

Putting the two together we have established a symmetrical closed convex curve, Fig. 5.12(b). The main features of this curve are that it passes through the origin (with the q-axis as tangent), has zero gradient at the critical states C_1 and C'_1, and has a vertex at V_1 where the gradients are $\pm M$. In particular, the pressure at the vertex denoted by P_e is such that $\ln(p_e / p_u) = 1$, i.e.,

$$p_e = 2.718 p_u. \tag{5.29}$$

It must be remembered that the yield curve *only* applies to specimens of the particular specific volume $v = v_1$ that we have considered, and that it is a boundary containing *all* permissible equiiibrium states of stress for this set of specimens. Mathematically, in eqs. (5.27) and (5.28) it is the parameter p_u which is a unique function of v_1. In the next section we will consider the family of yield curves that apply to sets of specimens of other specific volumes.

5.11 Family of Yield Curves

In the last section we established the yield curve of Fig. 5.12(b) for specimens of specific volume v_1. If instead we have a specimen of different specific volume v_2, the appropriate critical states C_2 and C'_2 will have moved to a different position (p_u, v_u) on the critical curve of Figs. 5.9 and 5.13 dictated by

$$v = \Gamma - \lambda \ln p. \tag{5.23 bis}$$

We shall have a second yield curve of identical shape but of different size, with the position of C (and C') acting as a scaling factor. Both of these curves clearly belong to a nest or family of yield curves.

This family of curves generates a closed surface in the three-dimensional space (p, v, q) which must contain all permissible states of specimens; it will not be possible for a specimen to be in stable equilibrium in a state represented by a point outside this surface. Hence it is called[9] the *stable-state boundary surface* and is represented by the single equation

$$|q| = Mp\left(1 + \frac{\Gamma - v}{\lambda} - \ln p\right) \tag{5.30}$$

obtained from eqs. (5.23) and the pair (5.27) and (5.28). A view of the surface is best seen in the direction of the arrow of Fig. 5.13; and the upper half is shown thus in Fig. 5.14.

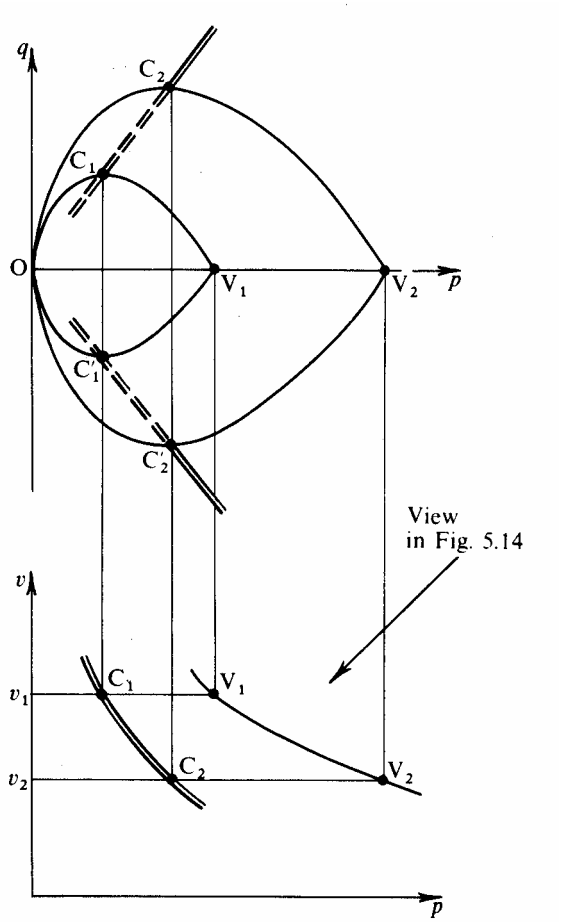

Fig. 5.13 Separate Yield Curves for Specimens of Different Volumes

If we consider a set of specimens all at the same ratio $\eta = q/p > 0$ at yield, we see from substitution in eq. (5.30) that their states must lie on the line

$$v + \lambda \ln p = \lambda\left(1 - \frac{\eta}{M}\right) + \Gamma = \text{const.} \tag{5.31}$$

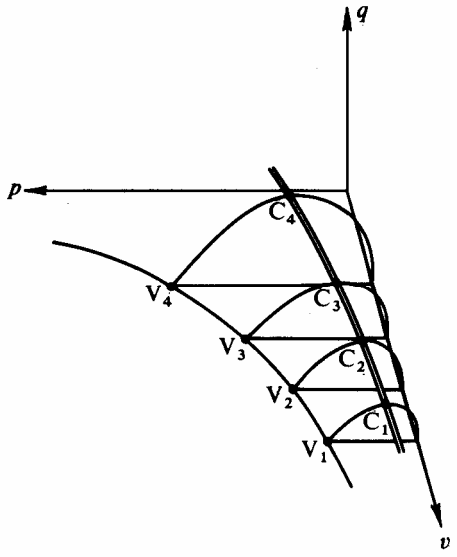

Fig. 5.14 Upper Half of State Boundary Surface

This is illustrated in Fig. 5.15; where each curve, $v + \lambda \ln p = \text{constant}$, corresponds to one value of η and vice versa. The critical curve $C_1C_2C_3$ and the curve joining the vertices $V_1V_2V_3$ are seen to be special members of this set. If the lower diagram, Fig. 5.15(b), is plotted with p on a logarithmic scale the set of curves become a set of parallel lines of slope – λ, in Fig. 5.15(c).

5.12 Hardening and Softening

At this stage we must return to consider certain special circumstances in which an inward probing vector must be associated with *unstable* yielding of Granta-gravel.

Whenever yielding does occur the specimen will suffer permanent deformation $(\dot{v}, \dot{\varepsilon})$ so that after removal of the probe the specimen will have (marginally) changed its specific volume from v_1 to $(v_1 + \delta v) = (v_1 - \dot{v})$ and it will then be in state $(p_s, v_1 - \dot{v}, q_s)$. From the point of view of the observations that can be made by the external agency the specimen will have been distorted into a different rigid specimen of specific volume $(v_1 - \dot{v})$, which in effect is a different material with its own distinct yield curve. It will not be possible to reverse this process to return the specimen to its original state at S.

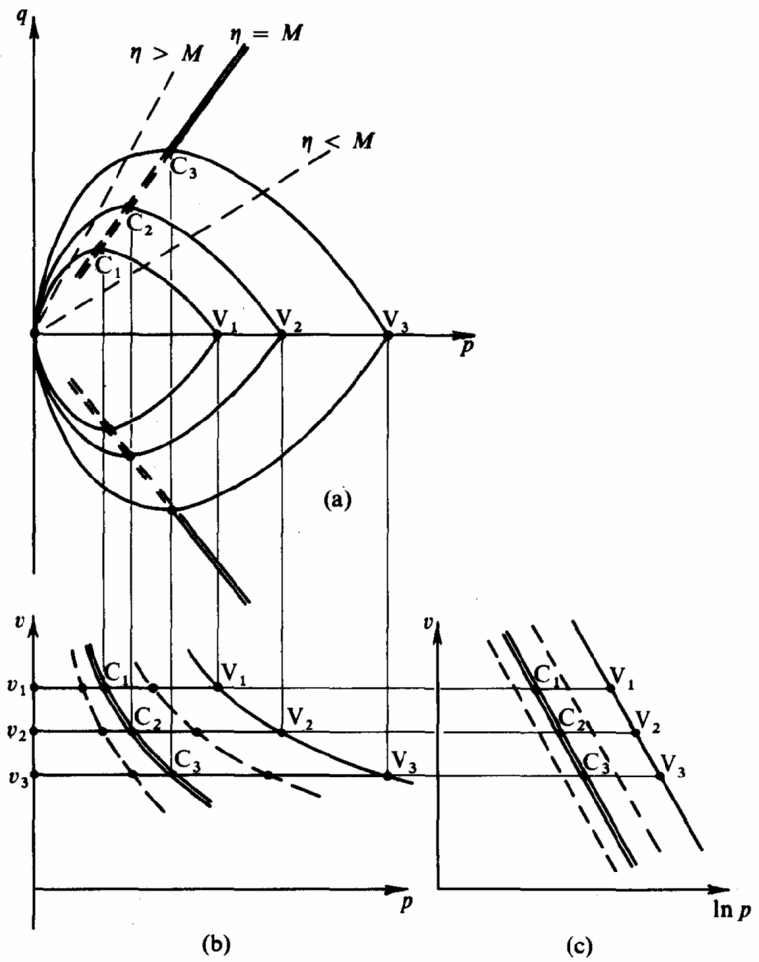

Fig. 5.15 Set of Specimens Yielding at Same Stress Ratio

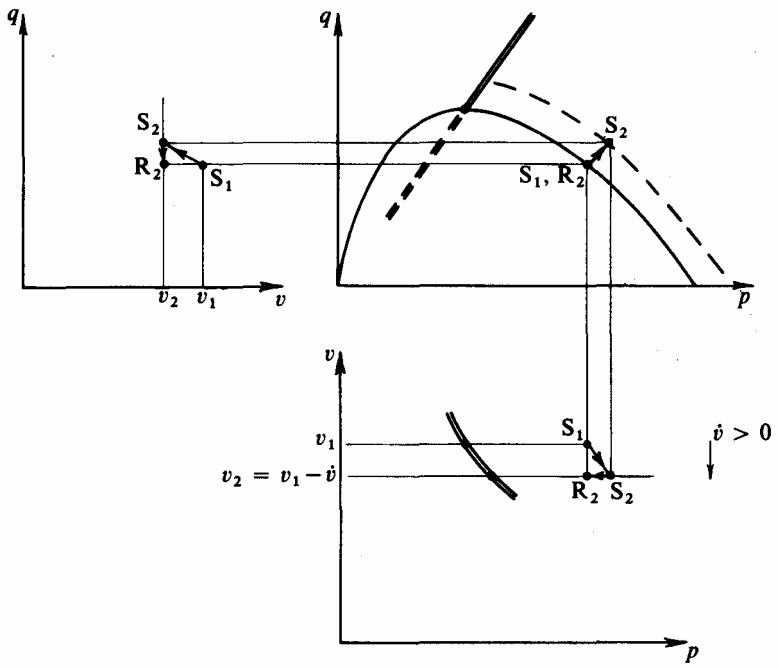

Fig. 5.16 Hardening

From §5.9 it is apparent that the critical curve divides all possible states of a specimen into two distinct categories. Let us first concentrate on specimens which are *weak at yield* for which $0 < q_s < Mp_s$, and show that the application of a small outward probing cycle is consistent with *stable yielding* and permanent deformation $(\dot{v}, \dot{\varepsilon} > 0)$ to an isotropically hardened state.

From eq. (5.12a) we know that this volumetric strain-increment $\dot{v}$ must be positive, thus δv is negative and the specimen will compact to a smaller total volume $v_2 = (v_1 + \delta v) = (v_1 - \dot{v})$, at which it has a new larger yield curve. On removal of the load-increment to complete the probing cycle as illustrated in Fig. 5.16, the specimen is left in the rigid stressed state $(p_r = p_s, v_2 = v_1 - \dot{v}, q_r = q_s)$ which is represented by the point R_2, *inside* the dotted yield curve that is appropriate to specimens of specific volume v_2. We could now add a *permanent* load-increment of $(\dot{p}, \dot{q})$ to our new 'denser' specimen at R_2 before bringing it to the verge of yielding again at some point S_2 on the *larger* yield curve. The effect of our probe has been to deform the specimen into one that is slightly stronger or harder, so that our original assumption of stable yielding is valid. This phenomenon is known as *hardening* and will be the consequence of any outward probe that we choose to apply to a specimen with stressed state $0 < q_s < Mp_s$.

In contrast, let us now consider a similar specimen which is in a stressed state F_1 given by (p_f, v_1, q_f) in Fig. 5.17, where it is *strong* at *yield* with $q_f > Mp_f$. We will now find that yielding has to be associated with application of an inward probe, and this is consistent with *instability*. If the probing causes the specimen to yield and undergo permanent deformation $(\dot{v}, \dot{\varepsilon} > 0)$ then in this case the volumetric strain-increment $\dot{v}$ must be negative, the sample must expand to a *larger* volume $v_3 = v_1 + \delta v > v_1$, and in this condition at H_3 the new 'looser' specimen is just in equilibrium governed by a *smaller* yield curve. Hence the probing cycle had to be directed *inwards* and it will now be impossible to complete the cycle and restore the state to (p_f, q_f) because this state lies outside the dotted yield curve and the specimen can no longer sustain these stresses in

equilibrium. This means that the effect of probing has been to deform the specimen into one that is weaker or softer: we will call this process *softening.*

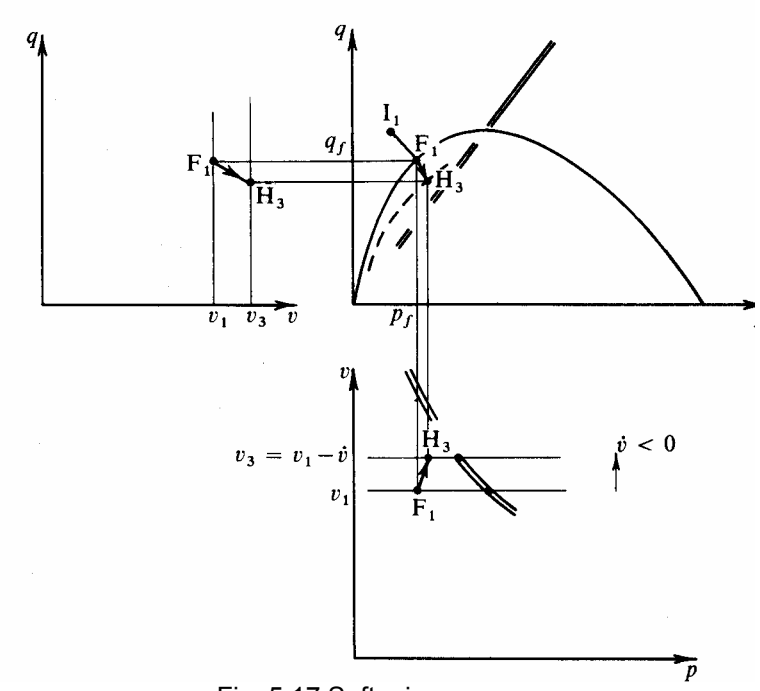

Fig. 5.17 Softening

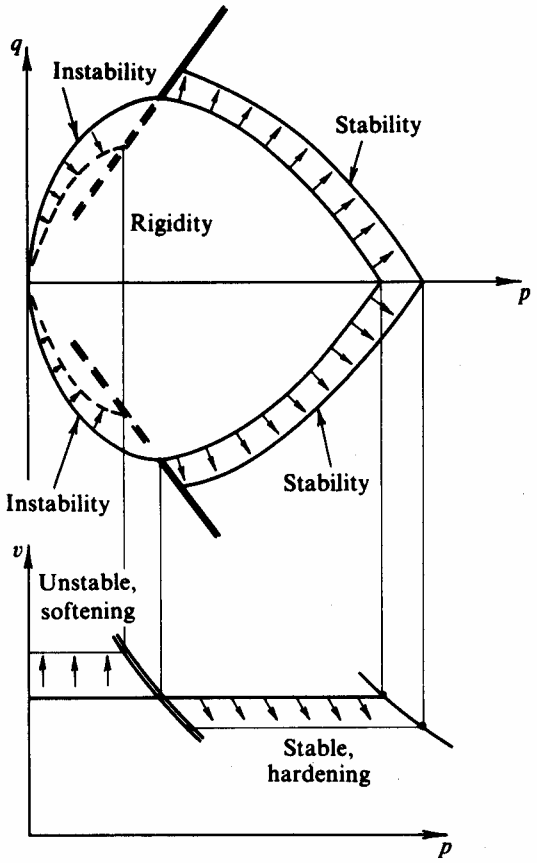

Fig. 5.18 Rigidity, Stability, and Instability

In engineering terms the condition of the specimen at F is what we would recognize as a state of incipient failure, and we would need some buffer to arrest displacements if we were to try to control the specimen and reduce loads during the softening process. Of course if we hàd tried to apply an outward probe such as F_1I_1 to the original specimen we should have observed catastrophic uncontrollable failure.

The results of probing both categories of specimen are summarized in Fig. 5.18.

5.13 Comparison with Real Granular Materials

At this stage we need to take stock of the development of Granta-gravel as an ideal artificial material and see whether it has developed into a useful model and whether its behaviour bears meaningful and worthwhile resemblance to that of real granular materials. We have established certain important features of its behaviour and seen what a dominant role the line of critical states plays in dividing the states of the material into those in which it will display continuous stable yielding and 'harden' from those in which it will 'fail' in unstable yielding and 'soften'.

In our test system we are considering the application of small fixed increments of load and imitating a stress controlled test. In reality most modern laboratory testing is conducted in a strain-controlled manner, but for the results to be valid the rate of strain must be sufficiently slow that pore-pressure gradients are negligible at all times. This will be equivalent to applying a continuous sequence of infinitesimal load-increments of different intensity so that the rate of strain is constant, i.e., $\dot{\varepsilon} \propto \dot{t}$. It will consequently be legitimate for us to predict what the results of strain-controlled tests on Granta-gravel would be, from our 'stress-controlled theory'.

For simplicity, let us consider a compression test on a specimen of initial state (p_0, v_0, $q=0$) in which at all times the effective spherical pressure p is held constant at p_0, so that $\dot{p} \equiv 0$. The state of the specimen throughout the test must lie in the $p = p_0$ plane, which intersects the positive half of the state boundary surface in the straight line

$$p = p_0 \qquad \frac{\lambda q}{M p_0} = (\lambda + \Gamma - \lambda \ln p_0) - v \tag{5.32}$$

obtained directly from eq. (5.30), and shown in Fig. 5.19 in the three projected views of the stable-state boundary surface containing all the points A, B, C, D, E, F, G, and V.

If the initial condition is such that $v_0 > (\Gamma - \lambda \ln p_0)$ the specimen will start at state A, in a condition looser or wetter than critical. As the axial-deviator stress is increased the specimen will remain rigid until it yields at B (when it reaches the yield curve corresponding to $v = v0$) and then continue to yield in a stable *hardening* manner up BDC until it eventually reaches the critical state at C after infinite strain.

Conversely, a specimen with $v_0 < (\Gamma - \lambda \ln p_0)$ will start at state E in a condition denser or drier than critical. The specimen remains rigid until it reaches state F and thereafter exhibits unstable *softening* down FGC until it reaches the critical state at C, after infinite strain.

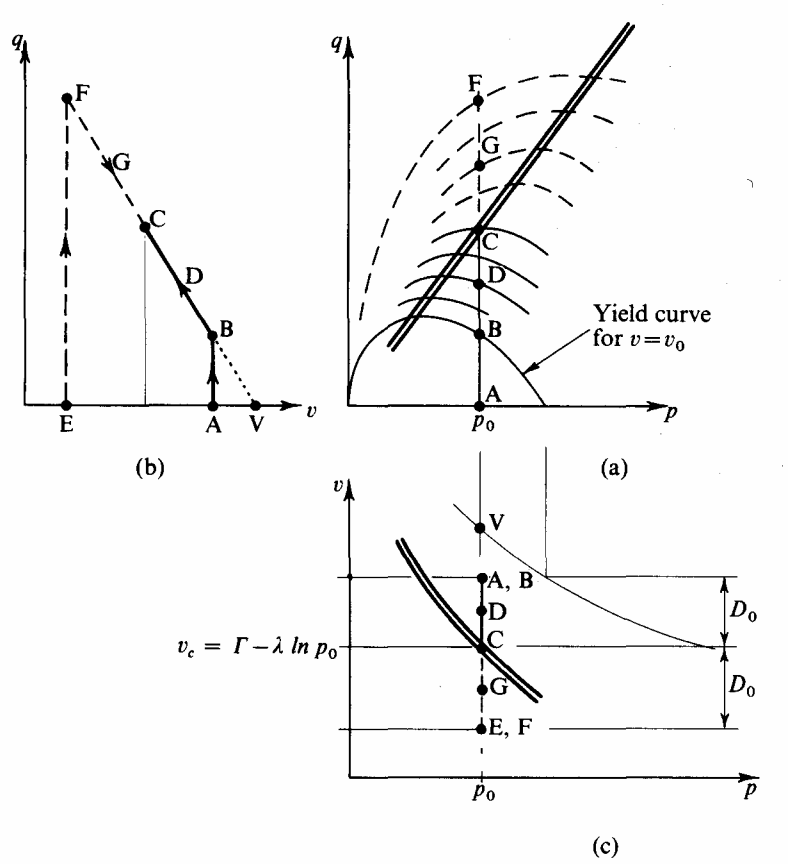

Fig. 5.19 Constant-p Test Paths

For convenience, let Z always be used to denote the point in *(p, v, q)* space representing the current state of the specimen at the particular stage of the test under consideration. As the test progresses the passage of Z on the state boundary surface either from B up towards C, or from F down towards C will be exactly specified by the set of three equations:

$$\left.\begin{aligned} &\frac{p\dot{v}}{v} + q\dot{\varepsilon} = Mp\dot{\varepsilon} && (\dot{\varepsilon} > 0)\ (5.19\,\text{bis}) \\ &q = \frac{Mp}{\lambda}(\lambda + \Gamma - v - \lambda \ln p) && (q > 0)\ (5.30\,\text{bis}) \\ &p = \text{constant} = p_0. \end{aligned}\right\} \qquad (5.33)$$

The first two equations govern the behaviour of all specimens and the third is the restriction on the test path imposed by our choice of test conditions for this specimen. We will find it convenient in a constant-p test to relate the initial state of the specimen to its ultimate critical state by the total change in volume represented by the distance AC (or EC) in Fig. 5.19(c) and define

$$D_0 = v_0 - v_c = v_0 - \Gamma + \lambda \ln p_0. \qquad (5.34)$$

The conventional way of presenting the test data would be in plots of axial-deviator stress q against cumulative shear strain ε and total volumetric strain $\Delta v/v_0$ against ε, and this can be achieved by manipulating equations (5.33) as follows. From the last two equations and (5.34) we have

$$\lambda q = Mp_0(v_0 - v + \lambda - D_0)$$

and substituting in the first equation

$$\frac{p_0\dot{v}}{v} = (Mp_0 - q)\dot{\varepsilon} = \frac{Mp_0\dot{\varepsilon}}{\lambda}(v - v_0 + D_0).$$

Remembering that $\dot{\varepsilon} = +\delta\varepsilon$ whereas $\dot{v} = -\delta v$ this becomes

$$\frac{M}{\lambda}\frac{\mathrm{d}\varepsilon}{\mathrm{d}v} = \frac{-1}{v(v - v_0 + D_0)} = \frac{1}{(v_0 - D_0)}\left\{\frac{1}{v} - \frac{1}{(v - v_0 + D_0)}\right\}. \tag{5.35}$$

Integrating $\frac{M}{\lambda}\varepsilon = \frac{1}{v_0 - D_0}\ln\left\{\frac{v}{v - v_0 + D_0}\right\} + \text{constant}$

and if ε is measured from the beginning of the test

$$M\varepsilon = \frac{\lambda}{v_0 - D_0}\ln\left\{\frac{D_0 v}{v_0(v - v_0 + D_0)}\right\}$$

i.e.,

$$\exp\left\{-\frac{M(v_0 - D_0)}{\lambda}\varepsilon\right\} = \frac{v_0(v - v_0 + D_0)}{D_0 v} = \frac{v_0(\Delta v + D_0)}{D_0(\Delta v + v_0)} \tag{5.36}$$

which is the desired relationship between $\Delta v / v_0$ and ε.

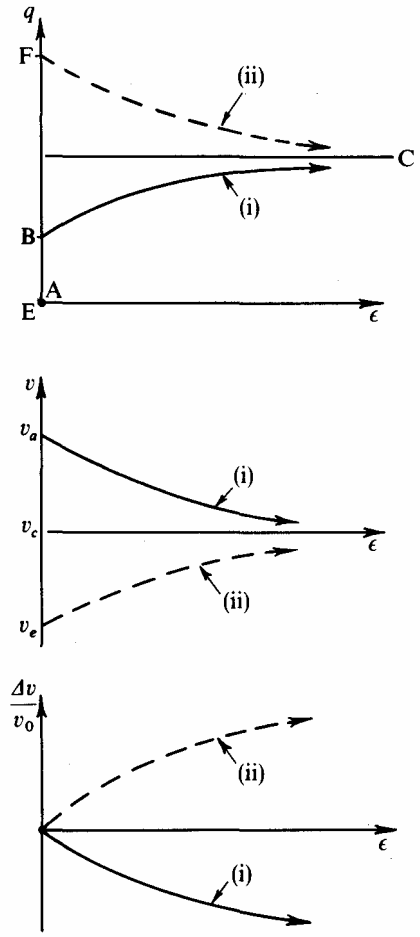

Fig. 5.20 Constant-p Test Results

Similarly we can obtain q as a function of ε

$$\exp\left\{-\frac{M(v_0 - D_0)}{\lambda}\varepsilon\right\} = \frac{v_0\lambda(Mp_0 - q)}{D_0\left[Mp_0(v_0 - D_0 + \lambda) - \lambda q\right]}. \tag{5.37}$$

These relationships for (i) a specimen looser than critical and (ii) a specimen denser than critical are plotted in Fig. 5.20 and demonstrate that we have been able to describe a complete strain-controlled constant-p axial-compression test on a specimen of Granta-gravel.

In a similar manner we could describe a conventional drained test in which the cell pressure σ_r is kept constant and the axial load varies as the plunger is displaced at a constant rate. In §5.5 we saw that throughout such a test $\dot{p} = \frac{1}{3}\dot{q}$, so that the state of the specimen, Z, would be confined at all times to the plane $p = p_0 + \frac{1}{3}q$. Hence the section of this 'drained' plane with the state boundary surface is very similar to the constant-p test of Fig. 5.19 except that the plane has been rotated about its intersection with the $q = 0$ plane to make an angle of $\tan^{-1} 3$ with it.

The differential equation corresponding to eq. (5.35) is not directly integrable, but gives rise to curves of the same form as those of Fig. 5.20.

An attempt to compare these with actual test results on cohesion-less granular materials is not very fruitful. Such specimens are rarely in a condition looser than critical; when they are, it is usually because they are subject to high confining pressures outside the normal range of standard laboratory axial-test equipment. Among the limited published data is a series of drained tests on sand and silt by Hirschfeld and Poulos[12], and the 'loosest' test quoted on the sand is reproduced in Fig. 5.21 showing a marked resemblance to the behaviour of constant-p tests for Granta-gravel.

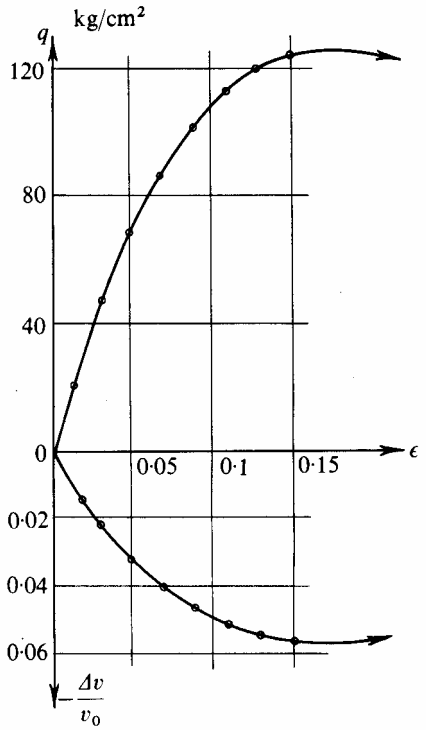

Fig. 5.21 Drained Axial Test on Sand (After Hirschfeld & Poulos)

For the case of specimens denser than critical, Granta-gravel is rigid until peak deviator stress is reached, and we shall not expect very satisfactory correlation with experimental results for strains after peak on account of the instability of the test system

and the non-uniformity of distortion that are to be expected in real specimens. This topic will be discussed further in chapter 8.

However, it is valuable to compare the predictions for peak conditions such as at state F of Fig. 5.19 and this will be done in the next section.

5.14 Taylor's Results on Ottawa Sand

In chapter 14 of his book[13] *Fundamentals of Soil Mechanics* Taylor discusses in detail the shearing characteristics of sands and uses the word 'interlocking' to describe the effect of dilatancy. He presents results of direct shear tests in which the specimen is essentially experiencing the conditions of Fig. 5.22(a); the direct shear apparatus is described in Taylor's book, and the main features can be seen in the Krey shear apparatus of Fig. 8.2. In these tests the vertical effective stress σ' was held constant, and the specimens all apparently denser than critical were tested in a fully air-dried condition, i.e., there was no water in the pore space. (It is well established that sand specimens will exhibit similar behaviour to that illustrated in Fig. 5.22(b) with voids either completely empty or completely full of water, provided that the drainage conditions are the same.)

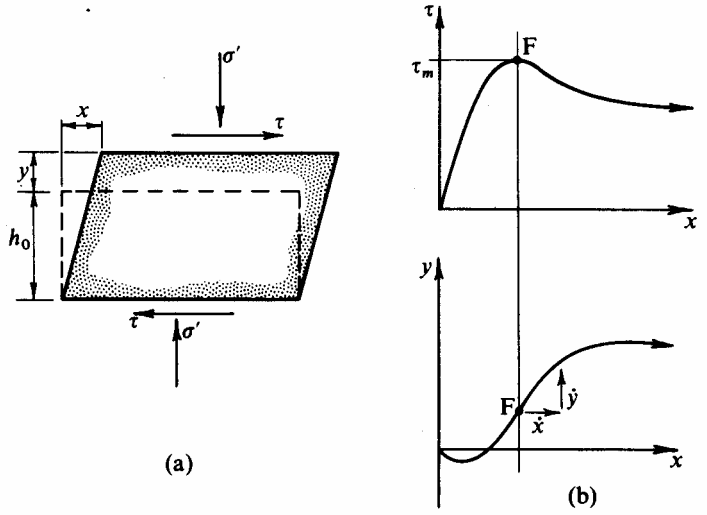

Fig. 5.22 Results of Direct Shear Tests on Sand

On page 346 of his book, Taylor calculates the loading power being supplied to the specimen making due allowance for the external work done by the interlocking or dilatation. In effect, he calculates for the peak stress point F the expression

$$\tau A\dot{x} - \sigma' A\dot{y} = \mu\sigma' A\dot{x} \qquad (5.38)$$

(total loading power = frictional work)

which has been written in our terminology, and where A is the cross-sectional area of the specimen. This is directly analogous to eq. (5.19),

$$q\dot{\varepsilon} + \frac{p\dot{v}}{v} = Mp|\dot{\varepsilon}|$$

which relates true stress invariants p and q, and which expresses the loading power per unit volume of specimen. The parameters are directly comparable: q with τ, p with σ', $\dot{\varepsilon}$ with $\dot{x}$, and $\dot{v}/v$ with $-\dot{y}$ (opposite sign convention); and so we can associate Taylor's approach with the Granta-gravel model.

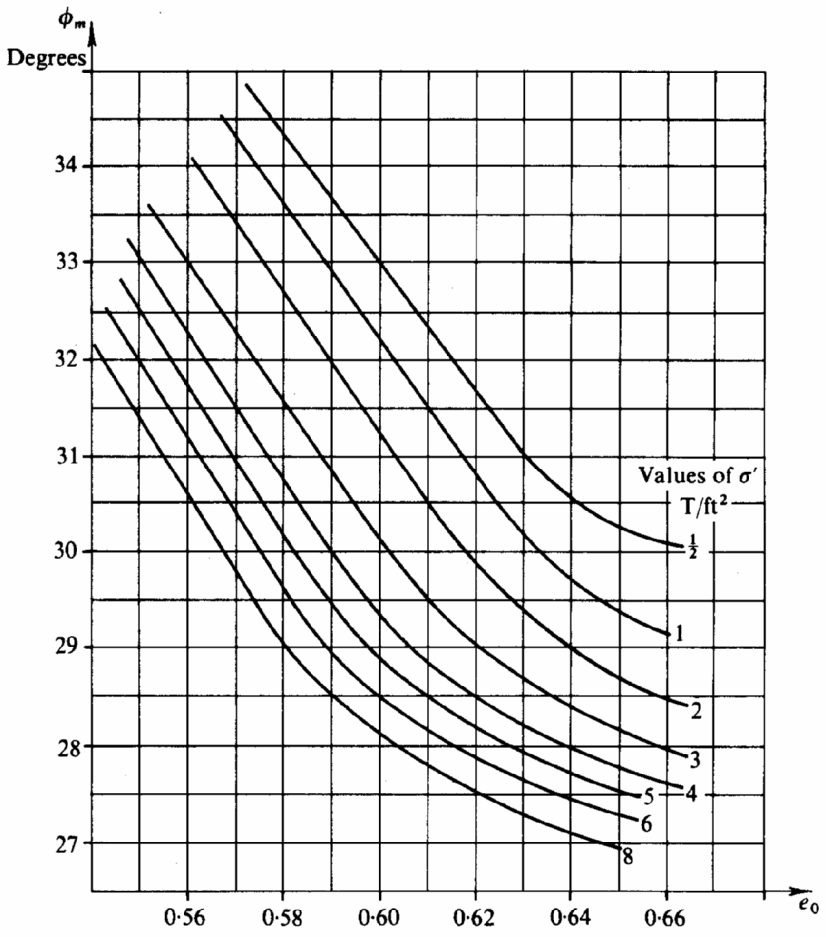

Fig. 5.23 Friction Angle Data from Direct Shear Tests (Ottawa Standard Sand) (After Taylor)

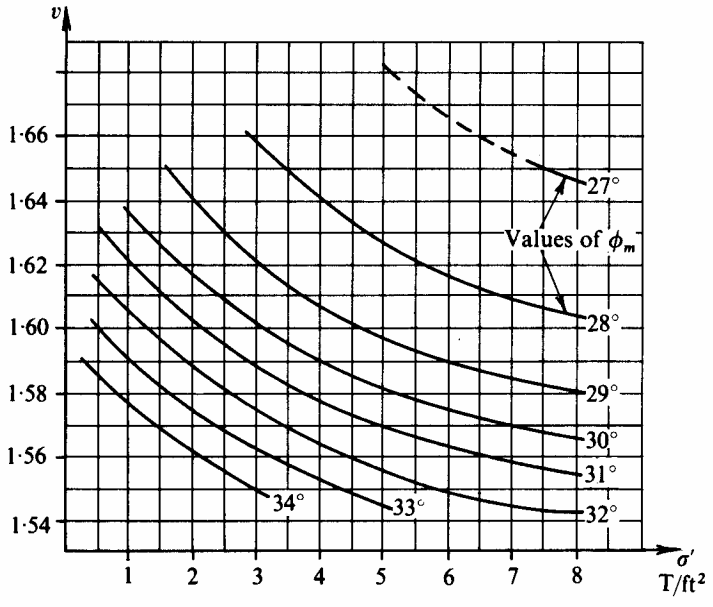

Fig. 5.24 Friction Angle Data from Direct Shear Tests replotted from Fig. 5.23

The comparison can be taken a stage further than this. In his Fig. 14.10, reproduced here as Fig. 5.23, Taylor shows the variation of peak friction angle ϕ_m (where $\tan\phi_m = {}^{\tau_m}/_{\sigma'}$) with initial voids ratio e_0 for different values of fixed normal stress σ'. These results have

been directly replotted in Fig. 5.24 as curves of constant ϕ_m (or peak stress ratio τ_m/σ') for differing values of $v = (1 + e)$ and σ'.

There is a striking similarity with Fig. 5.15(b) where each curve is associated with a set of Granta-gravel specimens that have the same value of *q/p* at yield. Taylor suggests an ultimate value of ϕ for his direct shear tests of 26.7° which can be taken to correspond to the critical state condition, so that all the curves in Fig. 5.24 are on the dense side of the critical curve.

5.15 Undrained Tests

Having examined the behaviour of Granta-gravel in constant-*p* and conventional drained tests, we now consider what happens if we attempt to conduct an undrained test on a specimen. In doing so we shall expose a deficiency in the model formed by this artificial material.

It is important to appreciate that in our test system of Fig. 5.4, although there are three separate platforms to each of which we can apply a load-increment, $\dot{X}_i$, we only have two degrees of freedom regarding our choice of probe $(\dot{p}, \dot{q})$ experienced by the specimen. This is really a consequence of the principle of effective stress, in that the behaviour of the specimen in our test system is controlled by two effective stress parameters which can be either the pair (σ'_l, σ'_r) or (*p, q*). The effects of the loads on the cell-pressure and pore-pressure platforms are *not* independent; they combine to control the effective radial stress σ'_r experienced by the specimen.

Throughout a conventional *drained* test we choose to have zero load-increments on the pore-pressure and cell-pressure platforms $(\dot{X}_1 = \dot{X}_2 \equiv 0)$ and to deform the specimen by means of varying the axial load-increment $\dot{X}_3$, and allowing it to change its volume.

In contrast, in a conventional *undrained* test we choose to have zero load-increment $\dot{X}_2$ on the cell-pressure platform only, and to deform the specimen by means of varying the axial load-increment $\dot{X}_3$. However, we can only keep the specimen at constant volume by applying a simultaneous load-increment $\dot{X}_1$ of a specific magnitude which is *dictated* by the response of the specimen. Hence for any choice of made by the external agency, the specimen will require an associated $\dot{X}_1$ if its volume is to be kept constant.

Let our specimen of Granta-gravel be in an initial state $(p_1, v_0, q = 0)$ represented by I in Fig. 5.25. As we start to increase the axial load by a series of small increments $\dot{X}_3$, the specimen remains rigid and has no tendency to change volume so that the associated $\dot{X}_1$ are all zero. Under these conditions there is no change in pore-pressure and $\dot{p} = \frac{1}{3}\dot{q}$ so that the point Z representing the state of the sample starts to move up the line IJ of slope 3.

This process will continue until Z reaches the yield curve, appropriate to $v = v_0$, at point K. At this stage of the test in order that the specimen should remain at constant volume, Z cannot go outside the yield curve (otherwise it would result in permanent $\dot{v}$ and $\dot{\varepsilon}$); thus as *q* further increases the only possibility is for Z to progress *along* the yield curve in a series of steps of *neutral change.* Once past the point K, the shape of the yield curve will dictate the magnitude of $\dot{X}_1$ that is required for each successive $\dot{X}_3$. At a point such as L the required $\sum \dot{X}_1$ will be represented by the distance $\mathrm{LM} = \mathrm{p}_0 + \frac{1}{3}q - p$, so that this offset indicates the total increase of pore- pressure experienced by the specimen.

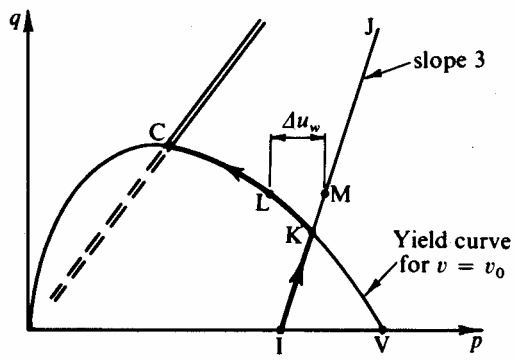

Fig. 5.25 Undrained Test Path for Loose Specimen of Granta-gravel

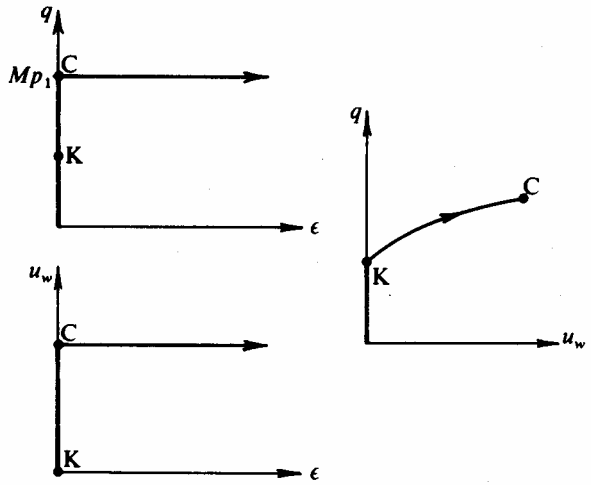

Fig. 5.26 Undrained Test Results for Loose Specimen of Granta-gravel

Eventually the specimen reaches the critical state at C when it will deform at constant volume with indeterminate distortion ε. The conventional plots of deviator stress and pore-pressure against shear strain ε will be as shown in Fig. 5.26, indicating a rigid/perfectly plastic response.

As mentioned in §5.13, when comparing the behaviour in drained tests of Granta-gravel with that of real cohesionless materials, it is rare to find published data of tests on specimens in a condition looser than critical. However, some undrained tests on Ham River sand in this condition have been reported by Bishop[14]; and the results of one of these tests have been reproduced in Fig. 5.27. (This test is No. 9 on a specimen of porosity 44.9 per cent, i.e., $v = 1.815$; it should be noted that for an *undrained* test $\dot{v}/v = \dot{\varepsilon}_1 + 2\dot{\varepsilon}_3 \equiv 0$ so that $\dot{\varepsilon} = \frac{2}{3}(\dot{\varepsilon}_1 - \dot{\varepsilon}_3) = \dot{\varepsilon}_1 = \text{axial strain.}$)

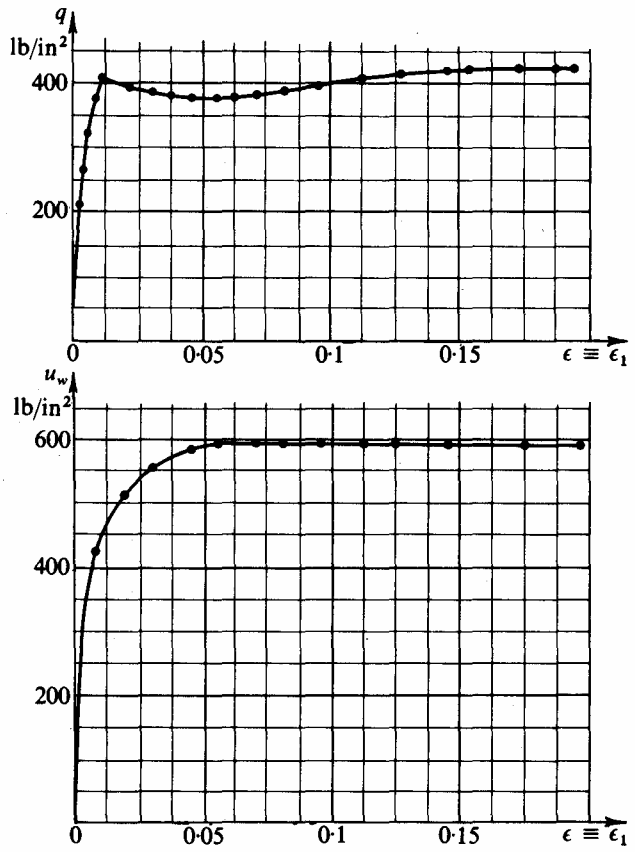

Fig. 5.27 Undrained Test Results on very Loose' Specimen of Ham River Sand (After Bishop)

The results show a close similarity to that of Fig. 5.26. In particular it is significant that axial-deviator stress reaches a peak at a very small axial strain of only about 1 per cent, whereas in a drained test on a similar specimen at least 15–20 per cent axial strain is required to reach peak. We can compare Bishop's test results of Fig. 5.27 with Hirschfeld and Poulos'[12] test results of Fig. 5.21. These figures may be further compared with Fig. 5.26 and 5.20 which predict extreme values for Granta-gravel which are respectively zero strain and infinite strain to reach peak in undrained and drained tests.

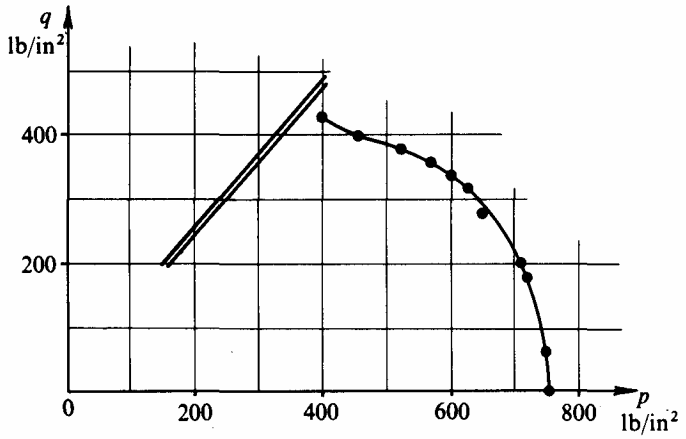

Fig. 5.28 Undrained Test Path for very 'Loose' Specimen of Ham River Sand

Although the Granta-gravel model is seen to be deficient in not allowing us to estimate any values of strains during an undrained test, we can get information about the stresses. The results of Fig. 5.27 have been re-plotted in Fig. 5.28 and need to be compared

with the path IKLC of Fig. 5.25. An accurate assessment of how close the actual path in Fig. 5.28 is to the shape of the yield curve is presented in Fig. 5.29 where *q/p* has been plotted against $\ln(p/p_u)$, and the yield curve becomes the straight line

$$q/p = M[1 - \ln(p/p_u)] \qquad (5.27 \text{ bis})$$

The points obtained for the latter part of the test lie very close to a straight line and indicate a value for *M* of the order of 1.2, but this value will be sensitive to the value of p_u chosen to represent the critical state.

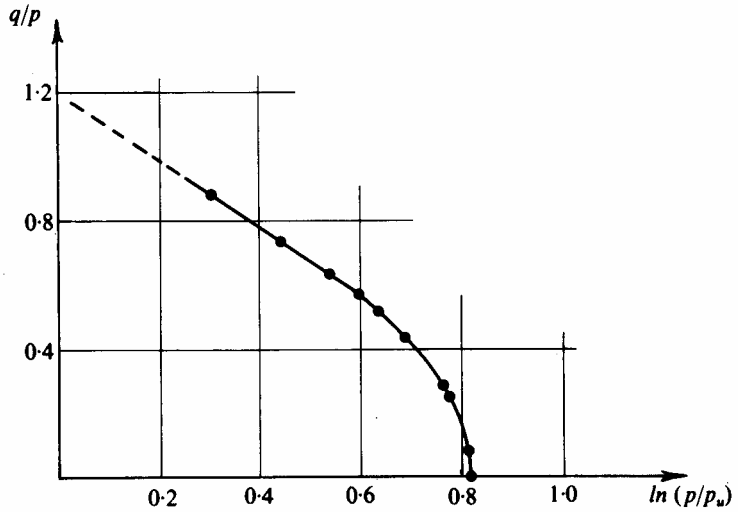

Fig. 5.29 Undrained Test Path Replotted from Fig. 5.28

Consideration of undrained tests on specimens denser than critical leads to an anomaly. If the specimen is in an initial state at a point such as I in Fig. 5.30 we should expect the test path to progress up the line IJ until the yield curve is reached at K and then move round the yield curve until the critical state is reached at C. However, experience suggests that the test path for real cohesionless materials turns off the line IJ at N and progresses up the straight line NC which is collinear with the origin.

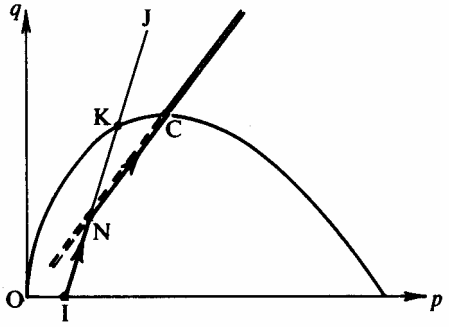

Fig. 5.30 Undrained Test Path for Dense Specimen of Granta-gravel

At the point N, and anywhere on NC, the stressed state of the specimen $q = Mp$ is such that in the initial specification of Granta-gravel, we have the curious situation in which the power eq. (5.19) (for $\dot{\varepsilon} \geq 0$)

$$\frac{p\dot{v}}{v} + q\dot{\varepsilon} = Mp\dot{\varepsilon}$$

is satisfied for *all* values of $\dot{\varepsilon}$, since $\dot{v} \equiv 0$. Moreover, the stability criterion is also satisfied so long as $\dot{q} > 0$, which will be the case. Hence it is quite possible for the test path to take

a short cut by moving up the line NC while still fulfilling the conditions imposed on the test system by the external agency. This, together with the occurrence of instability when specimens yield with $q > Mp$ (as shown in Fig. 5.18), lead us to regard the plane $q = Mp$ as forming a boundary to the domain of stable states. Our Fig. 5.14 therefore must be modified: the plane containing the line $C_1C_2C_3C_4$ and the axis of v will become a boundary of the stable states instead of the curved surface shown in Fig. 5.14. This modification has the fortunate consequence of eliminating any states in which the material experiences a *negative* principal stress, and hence we need not concern ourselves with the possibility of tension-cracking.

5.16 Summary

In this chapter we have investigated the behaviour of the artificial material Granta-gravel and seen that in many respects this does resemble the general pattern of behaviour of real cohesionless granular materials. The model was seen to be deficient (5. 15) regarding undrained tests in that no distortion whatsoever occurs until the stresses have built up to bring the specimen into the critical state appropriate to its particular volume. This difficulty can be overcome by introducing a more sophisticated model, Cam-clay, in the next chapter, which is not rigid/perfectly plastic in its response to a probe.

In particular, the specification of Granta-gravel can be summarized as follows:

(a) No recoverable strains

$$\dot{v}^r \equiv \dot{\varepsilon}^r \equiv 0$$

(b) Loading power all dissipated

$$\frac{p\dot{v}}{v} + q\dot{\varepsilon} = Mp|\dot{\varepsilon}| \qquad (5.19 \text{ bis})$$

(c) Equations of critical states

$$|q| = Mp \qquad (5.22 \text{ bis})$$

$$v = \Gamma - \lambda \ln p \qquad (5.23 \text{ bis})$$

References to Chapter 5

1. Prager, W. and Drucker, D. C. Soil Mechanics and Plastic Analysis or Limit Design', *Q. App!. Mathematics,* **10: 2**, 157 – 165, 1952.
2. Drucker, D. C., Gibson, R. E. and Henkel, D. J. 'Soil Mechanics and Work hardening Theories of Plasticity', *A.S.C.E.,* **122**, 338 – 346, 1957.
3. Drucker, D. C. 'A Definition of Stable Inelastic Material', *Trans. A.S.M.E. Journal of App!. Mechanics,* **26: 1**, 101 – 106, 1959.
4. Roscoe, K. H., Schofield, A. N. and Thurairajah, A. Correspondence on 'Yielding of clays in states wetter than critical', *Gêotechnique,* **15**, 127 – 130, 1965.
5. Drucker, D. C. 'On the Postulate of Stability of Material in the Mechanics of Continua', *Journal de M'canique,* Vol. **3**, 235 – 249, 1964.
6. Schofield, A. N. *The Development of Lateral Force during the Displacement of Sand by the Vertical Face of a Rotating Mode/Foundation,* Ph.D. Thesis, Cambridge University, 1959. pp. 114 – 141.
7. Hill, R. *Mathematical Theory of Plasticity,* footnote to p. 38, Oxford, 1950.
8. Wroth, C. P. *Shear Behaviour of Soils,* Ph.D. Thesis, Cambridge University, 1958.
9. Poorooshasb, H. B. *The Properties of Soils and Other Granular Media in Simple Shear,* Ph.D. Thesis, Cambridge University. 1961.

[10] Thurairajah, A. *Some Shear Properties of Kaolin and of Sand.* Ph.D. Thesis, Cambridge University. 1961.
[11] Bassett, R. H. Private communication prior to submission of Thesis, Cambridge University, 1967.
[12] Hirschfeld, R. C. and Poulos, S. J. 'High-pressure Triaxial Tests on a Compacted Sand and an Undisturbed Silt', *A.S.T.M. Laboratory Shear Testing of Soils Technical Publication No. 361,* 329 – 339, 1963.
[13] Taylor, D. W. *Fundamentals of Soil Mechanics,* Wiley, 1948.
[14] Bishop, A. W. 'Triaxial Tests on Soil at Elevated Cell Pressures', *Proc. 6th Int. Conf. Soil Mech. & Found. Eng.,* Vol. 1, pp. 170 – 174, 1965.

6
Cam-clay and the critical state concept

6.1 Introduction

In the last chapter we started by setting up an ideal test system (Fig. 5.4) and investigating the possible effects of a probing load-increment $(\dot{p},\dot{q})$ applied to *any* specimen within the system. By considering the power transferred between the heavy loads and the specimen within the system boundary we were able to establish two key equations, (5.14) and (5.15). These need to be recalled and repeated:
(*a*) the recoverable power per unit volume returned to the heavy loads during the *unloading* of the probe is given by

$$\frac{\dot{U}}{v} = -\left(\frac{p\dot{v}^r}{v} + q\dot{\varepsilon}^r \right) \tag{6.1}$$

and (*b*) the remainder of the loading power per unit volume (applied during the *loading* of the probe) is dissipated within the specimen

$$\frac{\dot{W}}{v} = \frac{\dot{E}}{v} - \frac{\dot{U}}{v} = \frac{p\dot{v}^p}{v} + q\dot{\varepsilon}^p \tag{6.2}$$

For the specification of Granta-gravel we assumed that there would be no recoverable strains $(\dot{v}^r \equiv \dot{\varepsilon}^r \equiv 0)$ and that the dissipated power per unit volume was $\dot{W}/v = Mp|\dot{\varepsilon}|$. With the further assumption of the existence of critical states, we had then *fully* prescribed this model material, so that the response of the loaded axial-test system to any probe was known. The behaviour of the specimen was found to have a general resemblance to the known pattern of behaviour of cohesionless granular materials.

In essence the behaviour of a specimen of Granta-gravel is typified by Fig. 6.1(a, b, c). If its specific volume is v_0, then it remains *rigid* while its stressed state (p, q) remains within the $v = v_0$ yield curve; if, and only if, a load increment is applied that would take the stressed state outside the yield curve does the specimen *yield* to another specific volume (with a marginally smaller or larger yield curve). The stable-state boundary surface in effect contains a pack of spade-shaped leaves of which the section of Fig. 6.1(a) is a typical one. Each such leaf is a section made by a plane $v = \text{constant}$, and is of identical shape but with its size determined by a scaling factor proportional to exp v.

The modification which is to be introduced in the first half of this chapter in development of a more sophisticated model[1,2], is that Cam-clay displays recoverable (but non-linear) volumetric strains. This has the effect of slightly 'curling' the leaves formed by the family of yield curves so that in plan view each appears as a curved line in Fig. 6.1(e), which is straight in the semi-logarithmic plot of Fig. 6.1(f).

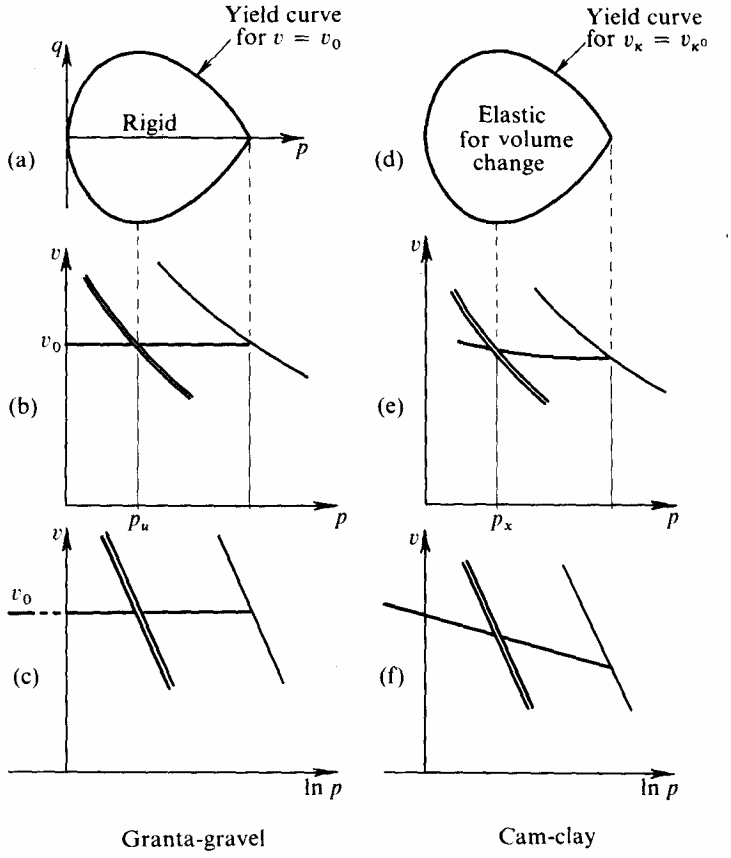

Fig. 6.1 Yield Curves for Granta-gravel and Cam-clay

Recalling the results of one-dimensional consolidation tests described in chapter 4 and in particular Fig. 4.4, we shall assume for a specimen of Cam-clay that during isotropic ($q = 0$) swelling and recompression its equilibrium states will lie on the line given by

$$v = v_0 - \kappa \ln(p/p_0) \tag{6.3}$$

in which κ is considered to be a characteristic soil constant. This line is straight in the plot of Figs. 6.1(f) and 6.2, and will be referred to as the κ-line of the specimen. It will be convenient later to denote the intercept of this κ-line with the unit pressure line p=1, by the symbol v_κ so that

$$v_\kappa = v + \kappa \ln p \tag{6.4}$$

We have seen for the Granta-gravel model the important role that lines of slope $-\lambda$ play in determining its behaviour. We shall also find it useful to denote by the symbol v_λ the intercept of the particular λ-line on which the specimen's state lies, with the unit pressure line, so that

$$v_\lambda = v + \lambda \ln p \tag{6.5}$$

As a test progresses on a yielding specimen of Cam-clay both these parameters v_κ and v_λ will vary, and they can be used instead of the more conventional parameters, v and p, for defining the state of the specimen. Each value of v_κ is associated with a particular density of random packing of the solids within a Cam-clay specimen; the packing can swell and be recompressed without change of v_κ during change of effective spherical pressure p.

We will carry our theoretical discussion of the Cam-clay model only as far as §6.7 where we show that the model can predict stress and strain in an undrained axial test. At that point we will interrupt the natural line of argument and delay the close comparison of experimental data with the theoretical predictions until chapter 7. Refined techniques are needed to obtain axial-test data of a quality that can stand up to this close scrutiny, and engineers at present get sufficient data for their designs from less refined tests. Although we expect that research studies of stress and strain will in due course lead to useful design calculations, at present most engineers only need to know soil 'strength' parameters for use in limiting-stress design calculations. We will suggest in chapter 8 that only the data of critical states of soil are fundamental to the choice of soil strength parameters. We outlined the critical state concept in general terms in §1.8, and we will return to expand this concept as a separate model in its own right in the second half of this chapter. Certain qualitative interpretations based on the critical state concept will follow, but the strong confirmation of the validity of this concept will be the closeness with which the Cam-clay model can predict the experimental data of the refined tests that are the subject of chapter 7. We do not regard this interpretation of axial-test data as an end in itself; the end of engineering research is the rationalization and improvement of engineering design. In due course the accurate calculation of soil displacements may become part of standard design procedure, but the first innovation to be made within *present* design procedure is the introduction of the critical state concept. We will see that this concept allows us to rationalize the use of index properties and unconfined compression test data in soil engineering.

6.2 Power in Cam-clay

As in §5.7 for Granta-gravel, we have to specify the four terms on the right-hand sides of eqs. (6.1) and (6.2). If we consider the application of a probe $\dot{p}$ (in the absence of any deviator stress) which takes the sample from A to B in Fig. 6.2 then the work done during loading is $p(v_a - v_b) = -p\delta v$; this is stored internally in the specimen as elastic energy which can be fully recovered as the probe is unloaded and the specimen is returned to its original state at A. The process is reversible and the amount of recoverable energy, denoted by $-p\dot{v}^r$, can be calculated from eq. (6.3) to be

$$-p\dot{v}^r = p(v_a - v_b) = \kappa\delta p = \kappa\dot{p} \tag{6.6}$$

We shall assume that Cam-clay *never displays any recoverable shear strain* so that

$$\dot{\varepsilon}^r \equiv 0 \tag{6.7}$$

Combining these, the recoverable power per unit volume

$$\frac{\dot{U}}{v} = -\left(\frac{p\dot{v}^r}{v} + q\dot{\varepsilon}^r\right) = +\frac{\kappa\dot{p}}{v} \tag{6.8}$$

We shall also assume, exactly as before, that the frictional work is given by

$$\frac{\dot{W}}{v} = Mp|\dot{\varepsilon}| > 0 \tag{6.9}$$

and so we can write

$$\frac{p\dot{v}}{v} + q\dot{\varepsilon} - \frac{\kappa\dot{p}}{v} = \frac{\dot{E}}{v} - \frac{\dot{U}}{v} = \frac{\dot{W}}{v} = Mp|\dot{\varepsilon}| \tag{6.10}$$

or (for unit volume) *loading power* less *stored energy* equals *frictional loss.*

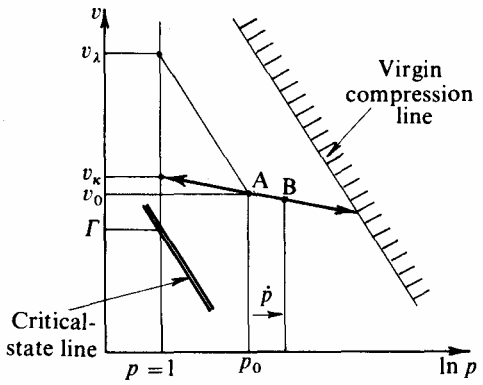

Fig. 6.2 Elastic Change of State

6.3 Plastic Volume Change

Let us suppose we have a specimen in a state of stress on the verge of yield, represented by point D in Fig. 6.3. We apply a loading increment $(\dot{p},\dot{q})$ which causes it to *yield* to state E, and on removal of the load-increment which completes the probing cycle it is left in state F having experienced permanent volumetric and shear strains. Because we have applied a full probing cycle the state of *stress* of the specimen is the same at F as at D, so these points have the same ordinate $p_f = p_d$. Because of our assumptions that Cam-clay exhibits no recoverable shear strain, and that its recoverable volumetric strain occurs *along* a κ-line, the points E and F must lie on the same κ-line, and have the same value of v_κ.

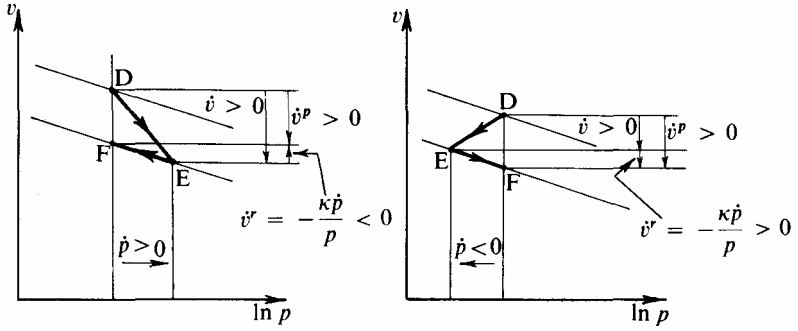

(a) 'Positive' probe ($\dot{p} > 0$) (b) 'Negative' probe ($\dot{p} < 0$)

Fig. 6.3 Plastic Volume Change during Yield

One of the unfortunate consequences of our original sign convention (compression taken as positive) is now apparent, and to avoid difficulty later the position is set out in some detail. In Fig. 6.3(a) and (b) two situations are considered, one with a probe with $\dot{p} > 0$ and the other with $\dot{p} < 0$. Remembering our sign convention, and since strain-increments must be treated as vector quantities, we have for both cases

Total volumetric strain	$\dot{v} = -(v_e - v_d)$
Recoverable volumetric strain	$\dot{v}^r = -(v_f - v_e) = -\dfrac{\kappa\dot{p}}{p}$
Resulting Plastic volumetric strain	$\dot{v}^p = -(v_f - v_d)$

Adding, and noting that $(v_f - v_d)$ is also the permanent change of v_κ experienced by the specimen, we have

$$-\delta v_\kappa = \dot{v}_\kappa = \dot{v}^p = \dot{v} + \dot{v}^r = \dot{v} - \frac{\kappa \dot{p}}{p} \tag{6.11}$$

which can be derived directly from eq. (6.4), defining v_κ.

It is important for us to appreciate that yield of the specimen has permanently moved its state from one κ-line with associated yield curve to another κ-line having a different yield curve: it is the *shift* of κ-line, measured as $\dot{v}_\kappa$, that always represents the plastic volume change $\dot{v}^p$ and governs the amount of distortion that occurs (cf. eq. (6.13) to follow).

6.4 Critical States and Yielding of Cam-clay

So far the specification of Cam-clay is

$$\dot{\varepsilon}^r \equiv 0 \qquad \dot{\varepsilon} \equiv \dot{\varepsilon}^p \qquad \dot{v}^r = \frac{\kappa \dot{p}}{p} \qquad \dot{v}^p = \dot{v}_\kappa$$

$$\frac{p\dot{v}}{v} + q\dot{\varepsilon} - \frac{\kappa \dot{p}}{v} = Mp|\dot{\varepsilon}| \qquad (\dot{\varepsilon} \neq 0) \tag{6.10 bis}$$

with the stability criterion becoming

$$\dot{p}\frac{\dot{v}^p}{v} + \dot{q}\dot{\varepsilon} \geq 0 \tag{6.12}$$

Comparison with eq. (5.19) and (5.20) confirms that Granta-gravel is merely a special case of Cam-clay when $\kappa = 0$. This distinction between the two model materials is the only one to be made; and we shall now examine the behaviour of Cam-clay in exactly the same way as the procedure of chapter 5.

Re-writing eq. (6.10) and using (6.11)

$$\frac{p\dot{v}_\kappa}{v} = \frac{p\dot{v}}{v} - \frac{\kappa \dot{p}}{v} = Mp|\dot{\varepsilon}| - q\dot{\varepsilon} \tag{6.13}$$

For the case of length reduction, $\dot{\varepsilon} > 0$, we have

$$\frac{\dot{v}_\kappa}{v\dot{\varepsilon}} = M - \frac{q}{p} \tag{6.14a}$$

and for radius reduction, $\dot{\varepsilon} < 0$,

$$\frac{\dot{v}_\kappa}{v\dot{\varepsilon}} = -M - \frac{q}{p} \tag{6.14b}$$

As a consequence we distinguish between specimens:

(a) those that are weak at yield when $(|q|/p) < M$ and $\dot{v}_\kappa = -\delta v_\kappa > 0$,

(b) those that are strong at yield when $(|q|/p) > M$ and $\dot{v}_\kappa = -\delta v_\kappa < 0$; and

(c) those that are at the critical states given by

$$|q| = Mp \tag{6.15}$$

and

$$v = \Gamma - \lambda \ln p \tag{6.16}$$

6.5 Yield Curves and Stable-state Boundary Surface

Let us consider a particular specimen of Cam-clay in equilibrium in the stressed state $\mathrm{I} \equiv (p_i, v_i, q_i)$ in Fig. 6.4, so that the relevant value of $v_\kappa = v_i + \kappa \ln p_i = v_{\kappa i}$ say. As before, we shall expect there to be a yield curve, expressible as a function of p and q, which is a boundary to all permissible states of stress that this specimen can sustain *without yielding.* In general, a small probe $(\dot{p}, \dot{q})$ will take the state of the specimen to some neighbouring point within the yield curve such as J; its effect will be to cause no shear strain $(\dot{\varepsilon} = 0)$, but a volumetric strain $\dot{v}$ which is *wholly recoverable,* and of sufficient magnitude to keep the specimen on the same κ-line, so that

$$\dot{v}_\kappa = \dot{v}^p = 0; \qquad \dot{v} = -\dot{v}^r = +\frac{\kappa \dot{p}}{p}$$

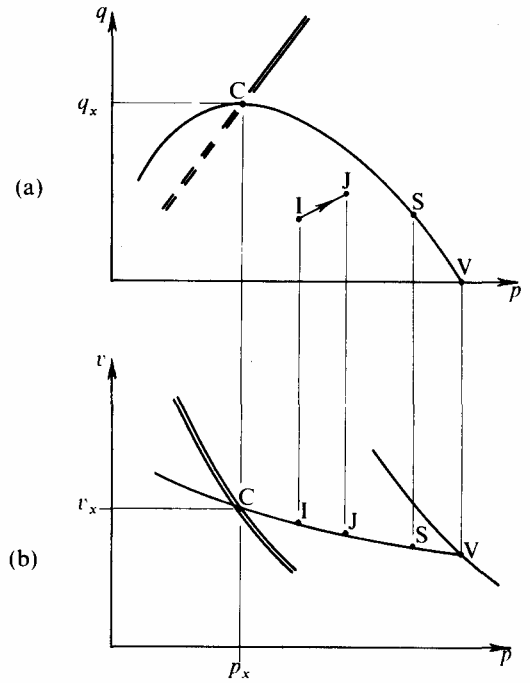

Fig. 6.4 Yield Curve for Specimen of Cam-clay

and

$$v_{\kappa i} = v_{\kappa j} = v_j + \kappa \ln p_j = (v_i - \dot{v}) + \kappa \ln(p_i + \dot{p})$$

All states *within* the yield curve are accessible to the specimen, with it displaying a rigid response to any change of shear stress q, and a (non-linear) elastic response to any change of effective spherical pressure p, so as to keep the value of v_κ constant. Probes which cross the yield curve cause the specimen to yield and experience a change of v_κ, so that it will have been permanently distorted into what in effect is a new specimen of a different material with its own distinct yield curve.

Following the method of §5.10 we find that probes which cause neutral change of a specimen at state S on the yield curve, satisfy

$$\frac{\mathrm{d}q}{\mathrm{d}p} = \frac{\dot{q}}{\dot{p}} = -\left(M - \frac{q_s}{p_s}\right) \tag{5.25bis}$$

and we can integrate this to derive the complete yield curve as

$$\frac{|q|}{Mp} + \ln\left(\frac{p}{p_x}\right) = 1 \tag{6.17}$$

In chapter 5 (p_u, q_u) were used as coordinates of the critical state on any particular yield curve, which was *planar* and therefore an *undrained* section of the state boundary surface. For Cam-clay the yield curves are no longer planar and to avoid later confusion the relevant critical state will be denoted by (p_x, q_x)—as in Fig. 6.1— and (p_u, q_u) will be reserved for the undrained section. The yield curve is only completely described in (p, v, q) space by means of the additional relationship

$$v_\kappa = v + \kappa \ln p = \text{constant} \tag{6.18}$$

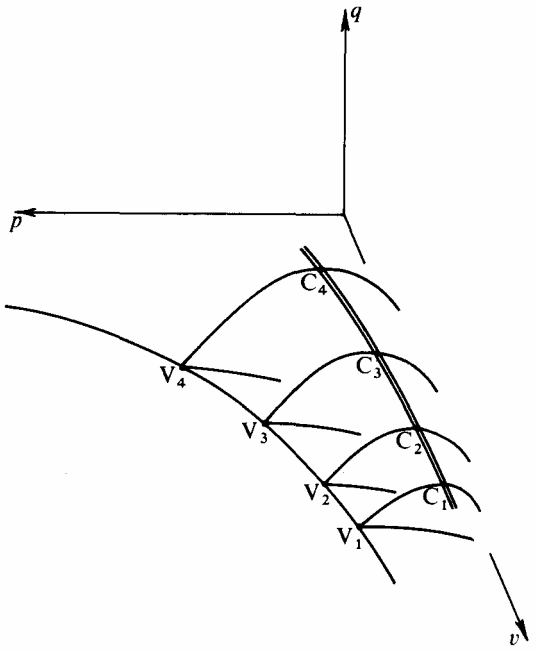

Fig. 6.5 Upper Half of State Boundary Surface for Cam-clay

The critical state point (p_x, q_x) for this one yield curve is given by the intersection of the κ-line and critical curve in Fig. 6.4(b) so that

$$\left.\begin{aligned} v + \kappa \ln p &= v_x + \kappa \ln p_x \\ \text{and} \qquad v_x &= \Gamma - \lambda \ln p_x \end{aligned}\right\}$$

Eliminating p_x and v_x from this pair of equations and eq. (6.17) we get

$$|q| = \frac{Mp}{\lambda - \kappa}(\Gamma + \lambda - \kappa - v - \lambda \ln p) \tag{6.19}$$

as the equation of the stable-state boundary surface sketched in Fig. 6.5. As a check, if we put κ=0 it must reduce to eq. (5.30) for the Granta-gravel stable-state boundary surface. Continuing the argument, as in §5.12, we find that specimens looser or wetter than critical $(v_\lambda = v + \lambda \ln p > \Gamma$; see Fig. 6.2) will exhibit stable yielding and harden, and specimens denser or dryer than critical $(v_\lambda < \Gamma)$ will exhibit unstable yielding and soften: Fig. 5.18 will also serve for Cam-clay except that in plan view in Fig. 5.18(b) the yield curve should now appear curved being coincident with a κ-line.

6.6 Compression of Cam-clay

If we consider a set of specimens all at the same ratio $\eta = (q/p) > 0$ at yield, we find from eq. (6.19) that their states must all be on the line:

$$v_\lambda = v + \lambda \ln p = (\lambda - \kappa)\left(1 - \frac{\eta}{M}\right) + \Gamma = \text{constant} \tag{6.20}$$

This is illustrated in Fig. 6.6 where each curve given by v_λ = constant corresponds to the set of specimens with one fixed value of η and vice versa. This curve becomes a straight line in the semi-logarithmic plot of Fig. 6.6(c), which is *parallel* to the line of critical states and offset from it by a distance $(v_\lambda - \Gamma) = (\lambda - \kappa)\{a - (\eta/M)\}$ measured parallel to the v-axis.

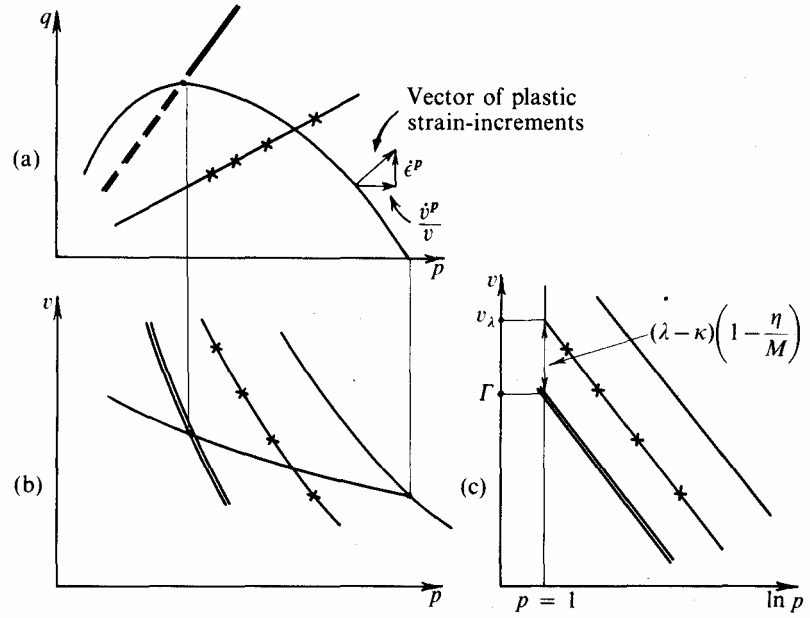

Fig. 6.6 Set of Specimens Yielding at Same Stress Ratio

If we choose to make one of this set of specimens yield continuously under a succession of load-increments chosen so that

$$\frac{\dot{q}}{\dot{p}} = \frac{q}{p} = \eta = \text{constant} > 0 \tag{6.21}$$

then its state point will progress along this line (given by eqs. (6.20) and (6.21)). As this specimen yields, the ratio of volumetric strain to shear strain is governed by eq. (6.13) for the case $\dot{\varepsilon} > 0$, i.e.,

$$\frac{p\dot{v}}{v} - \frac{\kappa\dot{p}}{v} = (Mp - q)\dot{\varepsilon} \tag{6.22}$$

but from eq. (6.20)

$$\dot{v} = -\delta v = +\frac{\lambda \delta p}{p} = \frac{\lambda \dot{p}}{p}$$

so substituting for $\dot{p}$, we get

$$\frac{\dot{v}}{v}\left(1 - \frac{\kappa}{\lambda}\right) = (M - \eta)\dot{\varepsilon} \tag{6.23}$$

For convenience we shall denote $\{(1-(\kappa/\lambda)\}$ by Λ, so that it is another soil constant (but not an independent one). Re-writing this in terms of the principal strain-increments $\dot{\varepsilon}_l$ and $\dot{\varepsilon}_r$ we have

$$\Lambda(\dot{\varepsilon}_l + 2\dot{\varepsilon}_r) = (M-\eta)\tfrac{2}{3}(\dot{\varepsilon}_l - \dot{\varepsilon}_r), \qquad (\dot{\varepsilon}_l > \dot{\varepsilon}_r)$$

or for length reduction

$$\frac{\dot{\varepsilon}_l}{\dot{\varepsilon}_r} = \frac{2M - 2\eta + 6\Lambda}{2M - 2\eta - 3\Lambda} \tag{6.24}$$

Similarly, for a case of radius reduction when $\eta < 0, \dot{\varepsilon} < 0, \dot{\varepsilon}_l < \dot{\varepsilon}_r$, we obtain

$$\frac{\dot{\varepsilon}_l}{\dot{\varepsilon}_r} = \frac{2M + 2\eta - 6\Lambda}{2M + 2\eta + 3\Lambda} \tag{6.25}$$

The values of these ratios depend on the material constants and on η, but for a given ratio of principal stresses Cam-clay undergoes compression with successive principal strain-increments in constant ratio.

One special case is isotropic compression in the axial-test apparatus where the *imposed* boundary conditions are that $q \equiv 0$, i.e., $\eta \equiv 0$. From experience we expect there not to be any distortion (in the absence of deviator stress) so that the loading increments of $\dot{p}$ would only produce volumetric strain. Unfortunately, the mathematical prescription of Cam-clay produces uncertainty for this particular case; if we take the limit as $\eta \to 0$ for eqs. (6.24) and (6.25) we have

$$\left.\begin{aligned} \frac{\dot{\varepsilon}_l}{\dot{\varepsilon}_r} &\to \frac{2M + 6\Lambda}{2M - 3\Lambda} && \text{for } \dot{\varepsilon}_l > \dot{\varepsilon}_r \\ \frac{\dot{\varepsilon}_l}{\dot{\varepsilon}_r} &\to \frac{2M - 6\Lambda}{2M + 3\Lambda} && \text{for } \dot{\varepsilon}_l < \dot{\varepsilon}_r \end{aligned}\right\}$$

These limiting ratios do not allow the possibility that $\dot{\varepsilon}_l$ is equal to 4 (unless $\kappa = \lambda$ which is unacceptable). This is an example of a difficulty met in the theory of plasticity when a yield curve has a corner: there are always two alternative limiting plastic strain increment vectors, depending on the direction from which the corner was approached. It is usual to associate any plastic strain- increment vector that lies *between* these two limiting vectors with yielding *at* the state of stress at the corner. Amongst these permissible vectors is the one *along* the *p-axis* corresponding to $\dot{\varepsilon}^p = 0$, i.e., $\dot{\varepsilon}_l = \dot{\varepsilon}_r$.

Although there is uncertainty about distortions, the volumetric strains associated with this condition are directly given by eq. (6.20) from which $v = \lambda\dot{p}/p$. These Cam-clay specimens are metastable; yielding under *any* increment $\dot{p} > 0$ of effective spherical pressure, they exist in a state of isotropic compression at the corners of successive yield curves. It has been usual to call real soil specimens 'normally consolidated' under these conditions: such specimens of Cam-clay are in a very special and abnormal condition and (because the term 'consolidation' is reserved for the transient process of drainage) we prefer to call them *virgin compressed.*

Above, we chose a particular stress ratio η and then calculated the associated vector of plastic strain-increments. We could equally well have chosen a particular combination of strain-increments and then located a point on the Cam-clay yield curve where that given vector is normal to the curve. This method is necessary for the analysis of one-dimensional compression in the consolidometer where the boundary conditions imposed are such that $\dot{\varepsilon}_r \equiv 0$ and hence $\dot{v}/v\dot{\varepsilon} = 3/2$. From eq. (6.23) we find that $\eta = M - \frac{3}{2}\Lambda$ and this determines

one point on the curve if $M > \frac{3}{2}\Lambda$. However, if $M \le \frac{3}{2}\Lambda$, then we must associate this particular strain-increment vector with yielding at the corner where $\eta = 0$. Thus, if the coefficient of earth pressure 'at rest' is defined as $K_0 = \sigma'_r / \sigma'_l$, we have

$$K_0 = \frac{\sigma'_r}{\sigma'_l} = \frac{3-\eta}{3+2\eta} = \begin{cases} 1 & for \quad M \le \frac{3}{2}\Lambda \\ \dfrac{6-2M+3\Lambda}{6+4M-6\Lambda} < 1 & for \quad M > \frac{3}{2}\Lambda \end{cases} \tag{6.26}$$

Values of K_0 predicted by eq. (6.26) are higher than those measured in practice. In recent research,[3] to resolve this difficulty, a modified form of the Cam-clay model has been suggested.

6.7 Undrained Tests on Cam-clay

We have now reached a stage where we can imagine an undrained test on a specimen of Cam-clay, and justify its existence as a model and its superiority over Granta-gravel. Let us consider a specimen virgin compressed in an initial state $(p_0, v_0, q = 0)$ represented by point V in Fig. 6.7 so that $v_{\lambda_0} = v_0 + \lambda \ln p_0 = \Gamma + \lambda - \kappa$. This is already on the yield curve (at the vertex) corresponding to its particular structural packing, v_{κ_0}, so that as soon as any load-increment is applied yielding will occur at once.

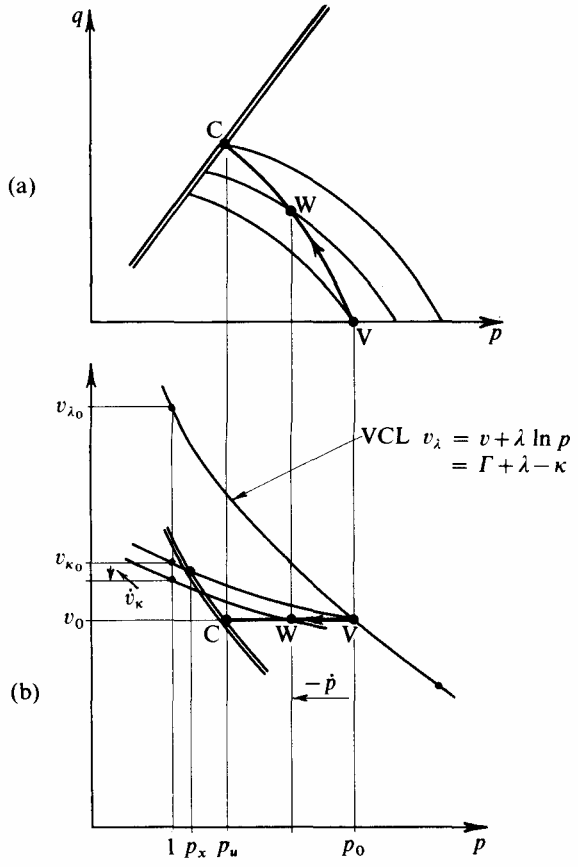

Fig. 6.7 Undrained Test Path for Virgin Compressed Specimen of Cam-clay

The volumetric strains must satisfy eq. (6.11) viz. $\dot{v}_\kappa = \dot{v}^p = \dot{v} - (\kappa \dot{p}/p)$ and also the added restriction $\dot{v} \equiv 0$ imposed by the requirement that our test should be undrained.

Hence, as the point representing the state of the sample moves across the stable-state boundary surface from V to a neighbouring point W, the shift $\dot{v}_\kappa$ of κ-line must be exactly matched by a reduction of effective spherical pressure of amount $-\kappa\dot{p}/p$. This compensating change of effective spherical pressure will be brought about by an increase of pore-pressure, as was discussed in §5.15.

This process will continue with the test path moving obliquely through successive yield curves until the critical state (p_u, v_0, q_u) is reached at C. The equation of the test path is obtained by putting $v = v_0 = \Gamma + \lambda - \kappa - \lambda \ln p_0$ into eq. (6.19) of the stable-state boundary surface

$$|q| = \frac{Mp}{\lambda - \kappa}(\lambda \ln p_0 - \lambda \ln p) = \frac{Mp}{\Lambda} \ln\left(\frac{p_0}{p}\right) \tag{6.27}$$

This is related to the initial effective spherical pressure p_0 and can be alternatively expressed in terms of the critical effective spherical pressure p_u, since

$$\left.\begin{aligned} v_0 + \lambda \ln p_u &= \Gamma \\ \text{and} \quad v_0 + \lambda \ln p_0 &= \Gamma + \lambda - \kappa \end{aligned}\right\} \text{ or } \ln\left(\frac{p_0}{p_u}\right) = \Lambda,$$

$$\text{i.e.,} \qquad |q| = \frac{Mp}{\Lambda}\left\{\Lambda - \ln\left(\frac{p}{p_u}\right)\right\} \tag{6.28}$$

Either of these equations represents the test path in the plot of Fig. 6.7(a).

The rate of distortional strain experienced along the test path comes directly from eq. (6.13) with

$$\left.\begin{aligned} \dot{v} &= 0 \\ v &\equiv v_0 \end{aligned}\right\}, \qquad \text{i.e.,} \qquad -\frac{\kappa\dot{p}}{v_0} = Mp|\dot{\varepsilon}| - q\dot{\varepsilon}$$

Choosing the conventional case of length reduction $\dot{\varepsilon} > 0, q > 0$ this becomes

$$\frac{-\dot{p}}{p\dot{\varepsilon}} = \frac{Mv_0}{\kappa}\left(1 - \frac{q}{Mp}\right) = \frac{Mv_0}{\kappa\Lambda} \ln\left(\frac{p}{p_u}\right) \tag{6.29}$$

Integrating

$$\frac{Mv_0}{\kappa\Lambda}\varepsilon = \int \frac{-\mathrm{d}p}{p \ln(p/p_u)} = -\ln\left[\ln\left(\frac{p}{p_u}\right)\right] + \text{const.}$$

and measuring ε from the beginning of the test we have

$$\ln\left(\frac{p}{p_u}\right) = \Lambda \exp\left(-\frac{Mv_0}{\kappa\Lambda}\varepsilon\right) \tag{6.30}$$

Substituting back into equation (6.28) we obtain

$$\frac{q}{Mp} = 1 - \exp\left(-\frac{Mv_0}{\kappa\Lambda}\varepsilon\right) \tag{6.31}$$

Both of these relationships are illustrated in Fig. 6.8 and provide a complete description of an undrained test on a virgin compressed specimen of Cam-clay. Detailed comparison with experimental resuits is made in the next chapter, but reference to Fig. 5.26 for Granta-gravel shows that the introduction of recoverable volumetric strains in Cam-clay has allowed us to conduct meaningful undrained tests.

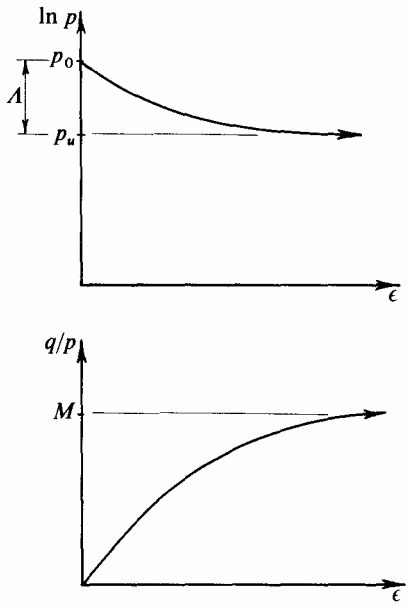

Fig. 6.8 Undrained Test Results for Virgin Compressed Specimen of Cam-clay

6.8 The Critical State Model

The critical state concept was introduced in §1.8 in general terms. We are now in a position to set up a model for critical state behaviour, postulating the existence of an ideal material that flows as a frictional fluid at constant specific volume v when, and only when, the effective spherical pressure p and axial-deviator stress q satisfy the eqs. $q = Mp$ (5.22 bis) and $v = \Gamma - \lambda \ln p$ (5.23 bis).

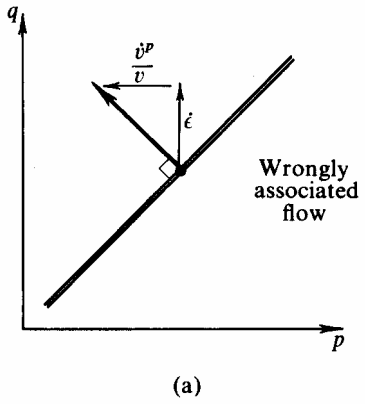

(a)

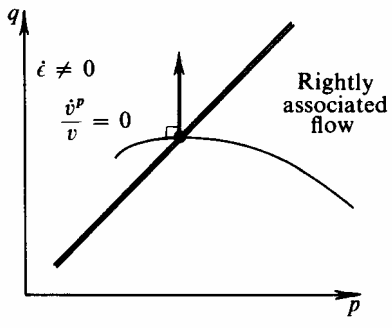

(b)

Fig. 6.9 Associated Flow for Soil at Critical State

This concept was stated in 1958 by Roscoe, Schofield and Wroth[4] in a slightly different form, but the essential ideas are unaltered. Two hypotheses are distinguished: first is the concept of *yielding* of soil through progressively severe distortion, and second is the concept of *critical states* approached after severe distortion. Two levels of difficulty are recognized in testing these hypotheses: specimens *yield* after a slight distortion when the magnitudes of parameters *(p, v, q*) as determined from mean conditions in a specimen can be expected to be accurate, but specimens only approach the *critical state* after severe distortion and (unless this distortion is a large controlled shear distortion) mean conditions in the specimen can- not be expected to define accurately a point on the critical state line.

It seems to us that the simple critical state concept has validity in relation to two separate bodies of engineering experience. *First,* it gives a simple working model that, as we will see in the remainder of this chapter, provides a rational basis for discussion of plasticity index and liquid limit and unconfined compression strength; this simple model is valid with the same accuracy as these widely used parameters. *Second,* the critical state concept forms an integral part of more sophisticated models such as Cam-clay, and as such it has validity in relation to the most highly accurate data of the best axial tests currently available. Certain criticisms[5,6] of the simple critical state concept have drawn attention to the way in which specimens 'fail' before they reach the critical state: we will discuss failure in chapter 8.

The error introduced in the early application of the associated flow rule in soil mechanics can now be cleared up. It was wrongly supposed that the critical state line in Fig. 6.9(a) was a yield curve to which a normal vector could be drawn in the manner of §2.10: such a vector would predict very large volumetric dilation rates $\dot{v}^p / v\dot{\varepsilon} = M$. However, we have seen that the set of points that lie along the critical state line are *not* on one yield curve: through each critical state point we can draw a segment of a yield curve parallel to the *p*-axis in Fig. 6.9(b). Hence it is correct to associate a flow vector which has $\dot{v}^p = 0$ with each of the critical states. At any critical state very large distortion can occur without change of state and it is certainly not possible to regard the move from one critical state to an adjacent critical state as only a neutral change: the critical state curve is not a yield curve.

6.9 Plastic Compressibility and the Index Tests

If we have a simple laboratory with only a water supply, a drying oven, a balance and a simple indentation test equipment (such as the falling cone test widely used in Scandinavia), we can find a value of λ for a silty clay soil. We mix the soil with water and remould it into a soft paste: we continually remould the soil and as it dries in the air it becomes increasingly strong. There will be a surface tension in the water of the menisci in the wet soil surface that naturally compresses the effective soil structure as water evaporates. As long as the soil is continually being remoulded it must remain at the critical state. We use the simple indentation test equipment to give us an estimate of the 'strength' of the soil, and we prepare two specimens A and B such that their strengths q_a and q_b, are in the ratio

$$\frac{q_b}{q_a} = 100$$

within the accuracy of our simple test equipment.

While we are handling the specimens in the air the external *total* stress is small, but the water tensions generate effective spherical pressures p_a and p_b. We can not measure the

effective spherical pressure directly, but from the critical state model we know in Fig. 6.10(a) that

$$q_a = Mp_a \qquad \text{and} \qquad q_b = Mp_b$$

so that

$$\frac{q_b}{q_a} = 100 = \frac{p_b}{p_a}$$

and the ratio of indentation test strengths gives an indirect measure of the increase in effective spherical pressure that has occurred during the drying out of the soil specimens.

We find the water contents (expressing them as ratios and not percentages) of each specimen w_a and w_b using the drying oven and balance. Assuming that the specific gravity G_s of the soil solids is approximately 2.7 we have

$$v_a - v_b = G_s(w_a - w_b) \cong 2.7(w_a - w_b)$$

From the critical state model we have from Fig. 6.10(b) and eq. (5.23 bis)

$$v_a + \lambda \ln p_a = \Gamma = v_b + \lambda \ln p_b$$

Hence $$2.7(w_a - w_b) \cong v_a - v_b = \lambda \ln \frac{p_b}{p_a} = \lambda \ln 100 = 4.6\lambda,$$

i.e., $$\lambda \cong 0.585(w_a - w_b) \qquad (6.32)$$

so that we can readily calculate λ from the measured water contents. The loss of water content that corresponds to a certain proportional increase in strength is a measure of the plastic compressibility of the soil.

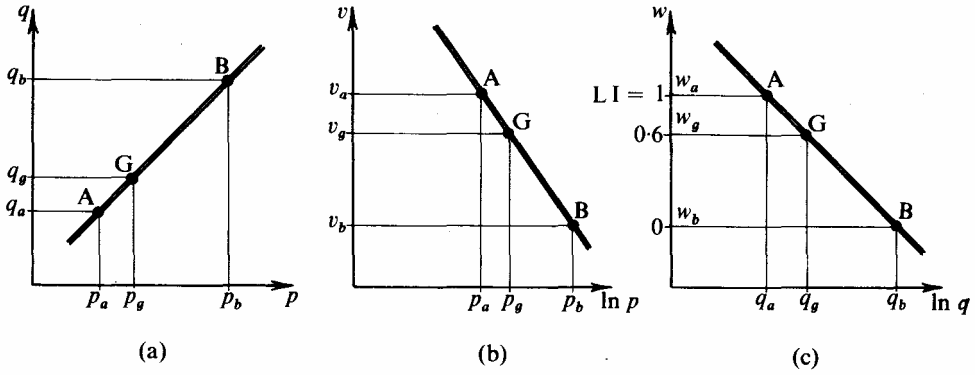

Fig. 6.10 Critical State Line and Index Tests

If we prepare further specimens that have intermediate values of indentation test strength, then we will expect in Fig. 6.10(c) to be able to plot general points such as G on the straight line AB on the graph of water content against 'strength' (on a logarithmic scale). If we arbitrarily choose to define the state of the soil at A as *liquid* and the state of the soil at B as *plastic* then we can define a *liquidity index* $=(w_g\text{-}w_b)/(w_a\text{-}w_b)$ which gauges the position of the specimen G in the range between B and A. We can then add a second set of numbers to the left of Fig. 6.10(c), giving zero liquidity to B, about 0.6 liquidity to G (in the particular case shown) and unit liquidity to A. It is a direct consequence of the critical state model that a plot of this liquidity index against the logarithm of strength should give a straight line.

In §1.3 we discussed the widely used and well-respected index tests of soil engineering. In the liquid limit test it seems that high decelerations cause a miniature slope-failure in the banks of the groove of Fig. 1.3: the conditions of the test standardize

this failure, and we might expect that it corresponds with some fixed value of shear strength q.

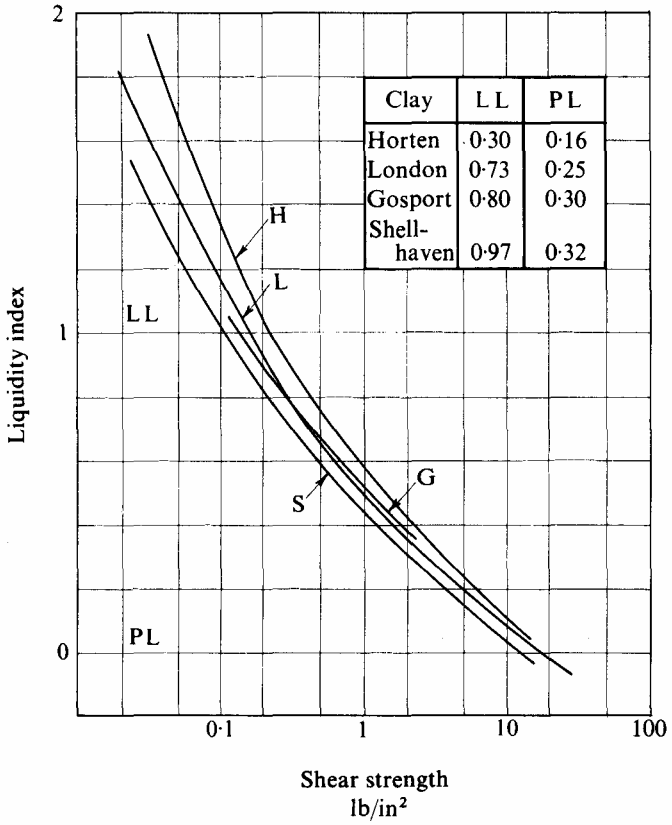

Fig. 6.11 Relation between Liquidity Index and Shear Strength of Remoulded Clays (After Skempton & Northey)

In the plastic limit test the 'crumbling' of soil implies a tensile failure, rather like the split-cylinder[7] or Brazil test of concrete cylinders: it would not seem that conditions in this test could be associated with failure at a specific strength or pressure.

However, in a paper by Skempton and Northey[8] experimental results with four different clays give similar variation of strength with liquidity index as shown in Fig. 6.11. From these data it appears that the liquid limit and plastic limit do correspond approximately to fixed strengths which are in the proposed ratio of 1:100, and so we can reasonably adopt A as the liquid limit and B as the plastic limit.

The measured difference of water contents $(w_a - w_b)$ then corresponds to *the plasticity index* of real silty clay, and we can generalize eq. (6.32) as

$$\lambda \cong 0.585\text{PI} \cong 0.217\Delta v_{\text{PI}} \tag{6.33}$$

where Δv_{PI} denotes the plasticity index expressed as a change of specific volume instead of the conventional change of water content $\Delta w\{= (\Delta v)/(G_s)\}$. Similarly, it will be useful to denote the liquid and plastic limits as v_{LL} and v_{PL}. (In eq. (6.33) and subsequent equations, PI, LL and PL are expressed as ratios and not percentages of water content.)

In Fig. 6.12 the critical state lines for several soils are displayed, and these have been drawn from the experimental data assembled in Table 6.1. Each line has been continued as an imaginary straight dashed line[9] beyond the range of experimental data at present available; this extrapolation is clearly unlikely to be justified experimentally because besides any question of fracture and degradation of the soil particles under such

high pressures, the lines cannot cross and must be asymptotic to the line $v = 1$ which represents a specimen with zero voids.

However, this geometrical extension allows some interesting analysis to be developed since these dashed lines all pass through, or very near, the single point Ω given by $v_\Omega \cong 1.25, p_\Omega \cong 1500$ lb/in^2. In addition, the points on each critical state line corresponding to the liquid and plastic limits have been marked. Those associated with the plastic limit are all very close to the same effective spherical pressure $p = p_{PL} \cong 80$ lb/in^2. The pressures p_{LL} associated with the liquid limits show a much wider range of values but this scatter is exaggerated by the logarithmic scale.

In Fig. 6.13 these experimental observations have been idealized with all lines passing through Ω, and p_{LL} and p_{PL} assumed to have fixed values. This means that in Fig. 6.14, where the liquidity index has replaced specific volume as the ordinate, all critical state lines *coincide* to one unique straight line.

For any one critical state line in Fig. 6.13 (that is for any one soil) we have

$$v_{PL} - v_\Omega = \lambda \ln\left(\frac{\Omega}{p_{PL}}\right) \tag{6.34a}$$

$$v_{LL} - v_\Omega = \lambda \ln\left(\frac{\Omega}{p_{LL}}\right) \tag{6.34b}$$

$$\Delta v_{PI} = v_{LL} - v_{PL} = \lambda \ln\left(\frac{p_{PL}}{p_{LL}}\right) \tag{6.34c}$$

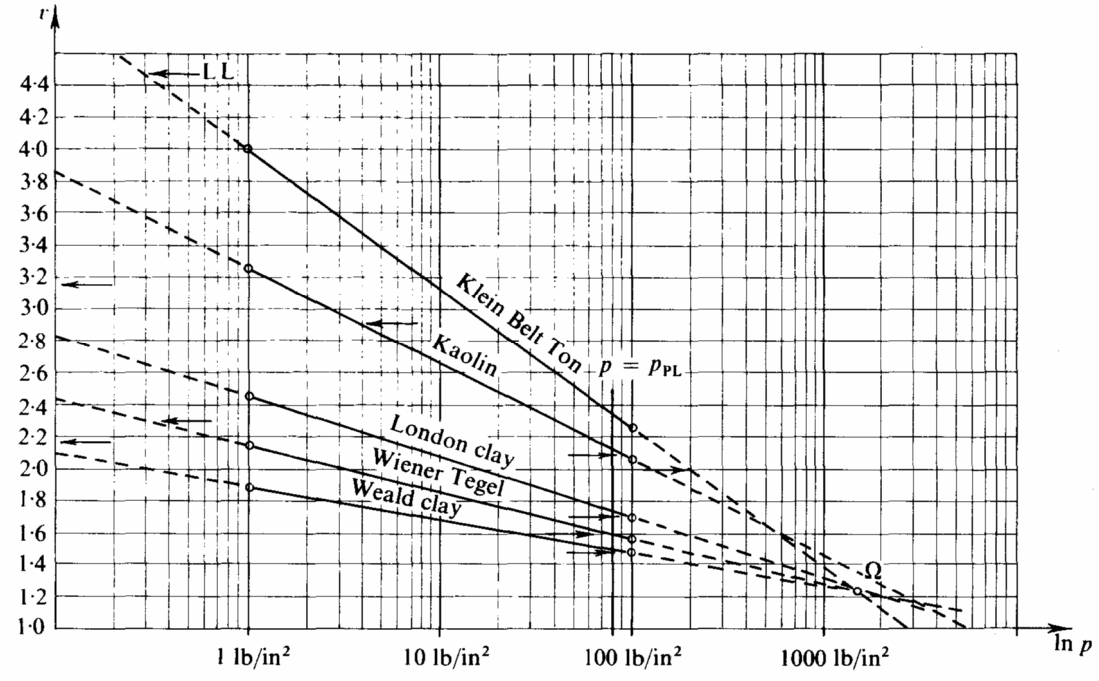

Fig. 6.12 Family of Experimental Critical State Lines

Properties		Klein Belt Ton	Wiener Tegel V	London Clay	Weald Clay	Kaolin
Critical state values	λ	0·356	0·122	0·161	0·093	0·26
	Γ	3·990	2·130	2·448	1·880	3·265
	v for $p=100$ lb/in^2	2·350	1·558	1·700	1·480	2·065
	M	0·845	1·01	0·888	0·95	1·02
Equivalent friction angle		$21\frac{3}{4}°$	$25\frac{3}{4}°$	$22\frac{1}{2}°$	$24\frac{1}{4}°$	26°
Average κ		0·184	0·026	0·062	0·035	0·05
$\Lambda=(\lambda-\kappa)/\lambda$		0·483	0·788	0·614	0·628	0·807
Liquid limit	w_{LL}	1·27	0·47	0·78	0·43	0·74
	v_{LL}	4·520	2·300	3·144	2·180	2·930
Plastic limit	w_{PL}	0·36	0·22	0·26	0·18	0·42
	v_{PL}	2·00	1·607	1·715	1·495	2·108
Plasticity index	Δw_{PI}	0·91	0·25	0·52	0·25	0·32
	Δv_{PI}	2·52	0·693	1·429	0·685	0·822
	G_s	2·77	2·76	2·75	2·75	2·61
Source of data		Hvorslev		Parry		Loudon

Table 6.1 Typical values of soil constants for a wide range of clays

Note. The critical-state values for Klein Belt Ton and Wiener Tegel V are based on results of Shearbox tests on the assumption that $\sigma'_2=\frac{1}{2}(\sigma'_1+\sigma'_3)$ at the critical state; evidence of this has been observed by Bassett, reference 11 of chapter 5.

Substituting the quoted values for Ω and p_{PL} in the first of these equations we get

$$v_{PL}-1.25=\lambda\ln\frac{1500}{80}=2.93\lambda,$$

i.e., $$\lambda=0.341(v_{PL}-1.25)\cong 0.92(PL-0.09) \qquad (6.35)$$

This predicted linear relationship is drawn as a dashed line in Fig. 6.15 where the experimental point for each soil is also plotted.

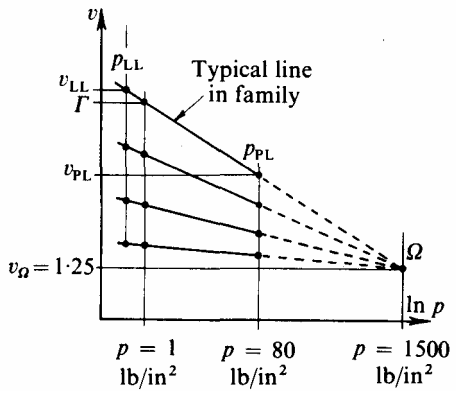

Fig. 6.13 Idealized Family of Critical State Lines

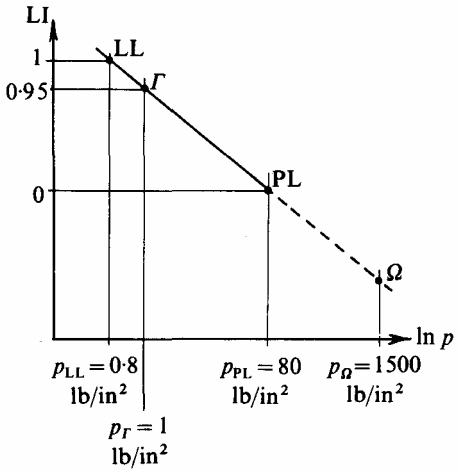

Fig. 6.14 Idealized Critical State Line

Similarly, we can predict from eq. (6.34b) the linear relationship

$$\lambda = 0.133(v_{LL} - 1.25) \cong 0.36(LL - 0.09) \tag{6.36}$$

on the basis that $p_{PL} \cong 100 p_{LL}$, so that eq. (6.34c) is identical with (6.33).

The best correlation of these predicted results with the quoted data is that between λ and the plastic limit simply because p_{PL} seems to be conveniently defined by the test conditions as approximately

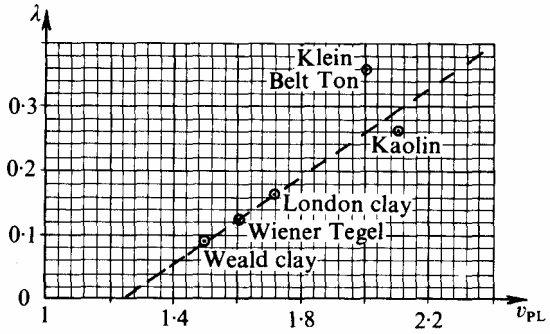

Fig. 6.15 Relationship between λ and Plastic Limit

80 lb/in^2. This suggests that the plastic limit test may be more consistent than the liquid limit test in measuring associated soil properties.

From this simple approach we can deduce two further simple relationships. The first connects plasticity index with the liquid limit; by elimination of λ from eqs. (6.33) and (6.36)

$$PI \cong 1.71\lambda \cong 0.615(LL - 0.09) \tag{6.37}$$

This relationship has been drawn as the heavy straight line 'B' in Casagrande's plasticity chart[10] in Fig. 6.16 and should be compared with his 'A' line

$$PI \cong 0.73(LL - 0.2)$$

The second relationship connects the compression index C'_c for a remoulded clay with the liquid limit. In eq. (4.1) the virgin compression curve was defined by $e = e_0 - C'_c \log_{10}(\sigma'/\sigma'_0)$, which is comparable to $v = v_0 - \lambda \ln(p/p_0)$ except that the logarithm is to the base of ten. Hence,

$$C'_c = \lambda \ln 10 = 2.303\lambda \cong 0.83(LL - 0.09) \tag{6.38}$$

which compares well with Skempton's empirical relationship[11]

$$C'_c = 0.7(\mathrm{LL} - 0.1)$$

The parameter Γ was defined as the specific volume of the point on the critical state line corresponding to unit pressure which we have adopted as 1 lb/in^2. We must be careful to realize that the value of Γ for any soil will be associated with the particular unit chosen for pressure (and will change if we alter our system of units).

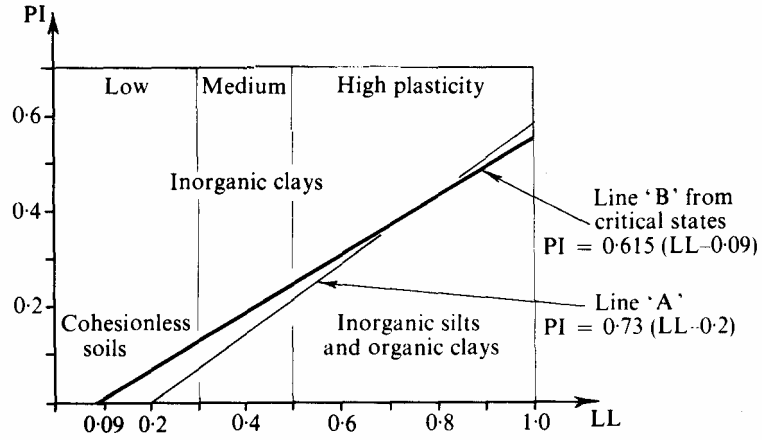

Fig. 6.16 Plasticity Chart (After Casagrande)

From the idealized situation of Fig. 6.14 we can predict that

$$\Gamma \cong v_\Omega + \lambda \ln 1500 = 1.25 + 7.3\lambda$$

which from eqs. (6.33) and (6.35) can be written in the forms

$$\Gamma \cong 1.25 + 6.7(\mathrm{PL} - 0.09) = 0.65 + 6.7\mathrm{PL}$$

$$\cong 1.25 + 4.27\mathrm{PI} \qquad (6.39)$$

At the bottom of the family of critical state lines in Fig. 6.13 we have the silty sandy soils that are almost non-plastic with low values of λ. These soils show almost no variation of critical specific volume with pressure, and it is for such soils that Casagrande first introduced[12] his original concept of a *critical void ratio* independent of pressure.

In contrast, at the top of the family of lines we have the more plastic silty clays and clays. It was for such soils that Casagrande later used[13] data of undrained axial-tests to derive a modified concept of critical 'conditions at failure' with voids ratio dependent on pressure.

In this section we have suggested various relationships between the constants of the critical state model and the index tests which are in general agreement with previous empirical findings. We also see that we could obtain a reasonably accurate value of λ from a simple apparatus such as that of the falling cone test, and can confirm this by establishing the plastic limit for the soil, which can also give us an estimate of the value of Γ.

6.10 The Unconfined Compression Strength

The critical state model is the natural basis for interpretation of the unconfined compression test. It is a simple test in which a cylindrical specimen of saturated clayey soil sustains no total radial stress $\sigma_r = 0$, and the total axial stress σ_l is rapidly increased until the specimen yields and fails. The unconfined compressive strength q_u is defined to equal the ultimate total axial stress σ_l. No attempt is made to measure pore-pressure, and no sheath is used to envelop the specimen, but the whole operation is so rapid relative to the

drainage of the specimen that it is assumed that there is no time for significant change of volume. Thus the specimen still has its *initial* specific volume v_0 when it attains its *ultimate* total axial stress $\sigma_l = q_u = 2c_u$.

We have already discussed in §6.7 the close prediction of changes of pore-pressure during the yielding of undrained specimens of Cam-clay: in the unconfined compression test no measurement is taken until the termination of yielding at what we will assume to be the critical state. So a simple prediction of the ultimate *effective* stresses can be made by introducing the initial specific volume v_0 into the equations for the critical state line

$$q = Mp \; and \qquad v_0 = \Gamma - \lambda \ln p$$

With $\sigma_r = 0$ and $\sigma_l = 2c_u$, $q = \sigma_l - \sigma_r = 2c_u$ so that

$$c_u = \frac{M}{2}\exp\left(\frac{\Gamma - v_0}{\lambda}\right) \tag{6.40}$$

This equation expresses c_u in terms of v_0, the soil constants λ, Γ, M and the same units of pressure as that used in the definition of Γ (i.e., lb/in^2). In Fig. 6.7 this is equivalent to disregarding the stress history of the specimen along the path VWC and assuming that the path merely ends at the point C.

Let us apply this result to samples of soil taken at various depths from an extensive stratum of 'normally consolidated' or virgin compressed clay. At a particular depth let the vertical effective pressure due to the overburden be σ'_v and the horizontal effective

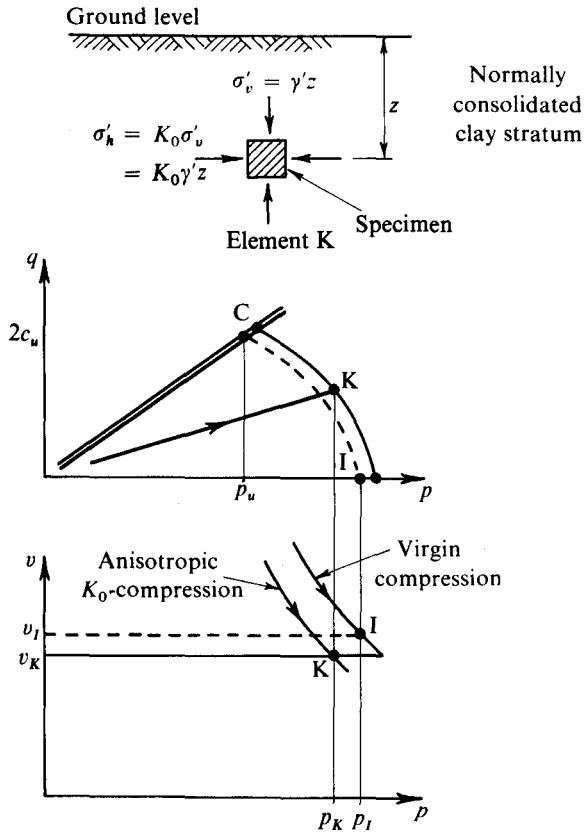

Fig. 6.17 Specific Volumes of Anisotropically Compressed Specimens

pressure be $\sigma'_h = K_0\sigma'_v$ so that the state of the specimen before extraction is represented by point K in Fig. 6.17, where

$$p_K = \frac{\sigma'_v + 2\sigma'_h}{3} = \frac{\sigma'_v}{3}(1 + 2K_0) \qquad \text{and} \qquad q_K = \sigma'_v - \sigma'_h = \sigma'_v(1 - K_0)$$

From eq. (6.20) the specific volume of the specimen v_K is given by

$$v_K = -\lambda \ln p_K + (\lambda - \kappa)\left(1 - \frac{\eta_K}{M}\right) + \Gamma$$

$$= -\lambda \ln \frac{\sigma'_v(1 + 2K_0)}{3} + (\lambda - \kappa)\left(1 - \frac{3(1 - K_0)}{M(1 + 2K_0)}\right) + \Gamma \qquad (6.41)$$

It will prove helpful to compare this specimen with an imaginary one which has been isotropically virgin compressed under the *same* vertical effective pressure $p = \sigma'_v$, so that its state is represented by point I. Its specific volume will be given by putting $K_0 = 1$ in eq. (6.41) or directly from eq. (6.20)

$$v_I = -\lambda \ln \sigma'_v + (\lambda - \kappa) + \Gamma$$

The difference in specific volume of the two specimens will be

$$v_I - v_K = \lambda \ln\left(\frac{1 + 2K_0}{3}\right) + \frac{(\lambda - \kappa)}{M} \frac{3(1 - K_0)}{1 + 2K_0}$$

$$= \lambda\left\{\ln\left(\frac{1 + 2K_0}{3}\right) + \frac{3\Lambda(1 - K_0)}{M(1 + 2K_0)}\right\} \qquad (6.41)$$

The value of Λ appears to be approximately $\frac{2}{3}M$ for most clays, so that for specimens with a minimum value of K_0 of 0.6, say, the maximum value of

$$v_I - v_K \cong \lambda\left(\ln\frac{2.2}{3} + \frac{2 \times 0.4}{2.2}\right) = \lambda(-0.3075 + 0.364) = 0.0565\lambda \qquad (6.43)$$

which even for kaolin with λ as high as 0.26 is equivalent to a difference in specific volume of only 0.0147 or only $\frac{1}{2}$ per cent water content.

Therefore, in relation to the accuracy of the unconfined compression test and this analysis we can ignore this small difference in specific volume and assume that both specimens I and K have the same v_0, and hence will be expected to reach the *same* value of c_u in a test. But we have a simple relation for the isotropically compressed sample I between its initial effective spherical pressure p_I and its final value p_u at the critical state, given by eq. (6.28)

$$\frac{p_I}{p_u} = \exp \Lambda$$

Hence, the unconfined compressive strength of both specimens is

$$2c_u = q_u = Mp_u = Mp_I \exp(-\Lambda) = M\sigma'_v \exp(-\Lambda)$$

and we have arrived at a very simple expression for the ratio of unconfined shear strength to overburden pressure of a 'normally consolidated' specimen as a *constant* for any one soil:

$$\frac{c_u}{\sigma'_v} = \tfrac{1}{2} M \exp(-\Lambda) \qquad (6.44)$$

This agrees with Casagrande's working hypothesis[13] which led to the well-established result that undrained shear strength increases linearly with depth for a 'normally consolidated' deposit. If we adopt numerical values for Weald clay of $M \cong 0.95$ and $\Lambda \cong 0.628$ this gives

$$\frac{c_u}{\sigma'_v} = 0.254$$

which agrees well with the figure of 0.27 quoted by Skempton and Sowa[14].

This result is also in general agreement with the empirical relationship presented by Skempton[15] between c_u/σ'_v (denoted as c_u/p by him) and plasticity index reproduced in Fig. 6.18, and represented by the straight line

$$\frac{c_u}{\sigma'_v} = 0.11 + 0.37\text{PI} \tag{6.45}$$

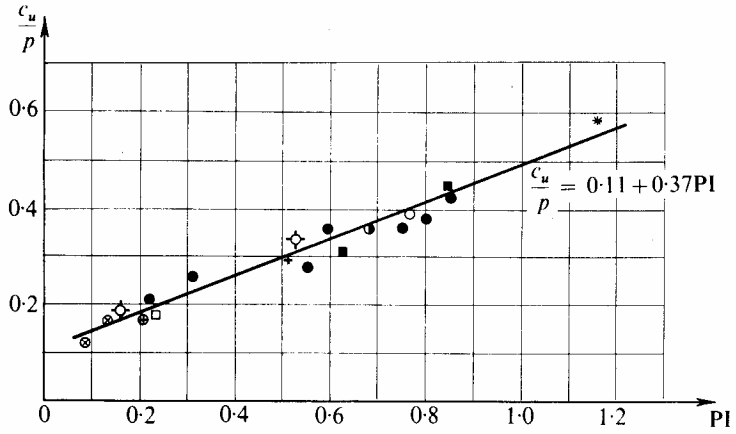

Fig. 6.18 Relationship between *cjp* and Plasticity Index for Normally Consolidated Clays (After Skempton)

If we adopt this we can use it in conjunction with eq. (6.44) to obtain another relationship between soil properties

$$M \cong (0.22 + 0.74\text{PI})\exp\Lambda \cong (0.22 + 1.267\lambda)\exp\Lambda$$

6.11 Summary

In summarizing this chapter we are aware of the point at which we decided not to introduce at this stage further theoretical developments of the critical state models. We have not introduced the generalization of the stress parameters p and q that turns eq. (6.17) into a function $F=0$ and following Mises' method of eq. (2.13) can be used to derive general plastic strain rates, but we will introduce this in appendix C. We have not introduced a research modification of the Cam-clay model that generates a corner that is less sharp for virgin compression, and shifts one-dimensional consolidation to correspond more closely with observed coefficients of lateral soil pressure. At §6.8 we called a halt to further theoretical developments, and introduced the simplified *critical state model.* With this model we have been able to interpret the simple index tests which engineers have always rightly regarded as highly significant in practice[16] but which have not previously been considered so significant in theory. In the next chapter we consider the precise interpretation of the best axial-test data and will begin by describing the sort of test for which this interpretation is possible.

References to Chapter 6

1 Roscoe, K. H. and Schofield, A. N. Mechanical Behaviour of an Idealised Wet Clay', *Proc. 2nd European Conf Soil Mech.,* pp *47 – 54 ,* 1963.

2 Roscoe, K. H., Schofield, A. N. and Thurairajah, A. Yielding of Clays in States Wetter than Critical, *Geotechnique* 13, 211 – 240, 1963.

[3] Burland, J. B. Correspondence on 'The Yielding and Dilation of Clay', *Géotechnique* 15, 211 – 214, 1965.
[4] Roscoe, K. H., Schofield, A. N. and Wroth, C. P. On the Yielding of Soils, *Géotechnique* 8, 22 – 53, 1958.
[5] Henkel, D. J. Correspondence on 'On the Yielding of Soils', *Géotechnique* 8, 134 – 136, 1958.
[6] Bishop, A. W., Webb, D. L. and Lewin, P. I. Undisturbed Samples of London Clay from the Ashford Common Shaft: Strength Effective Stress Relationships, *Géotechnique* 15, 1 – 31, 1965.
[7] Wright, P. J. F. Comments on an Indirect Tensile Test on Concrete Cylinders, *Mag. of Concrete Research 7,* 87 – 96, 1955.
[8] Skempton, A. W. and Northey, R. D. The Sensitivity of Clays, *Géotechnique* 3, 30 – 53, 1953.
[9] Skempton, A. W. Soil Mechanics in Relation to Geology, *Proc. Yorkshire Geol. Soc.* 29, 33 – 62, 1953.
[10] Casagrande, A. Classification and Identification of Soils, *Proc. A.S.C.E.,* 73, 783 – 810, 1947.
[11] Skempton, A. W. Notes on the Compressibility of Clays, *.1. Geol. Soc.,* 100, 119 – 135, 1944.
[12] Casagrande, A. Characteristics of Cohesionless Soils affecting the Stability of Slopes and Earth Fills, *J. Boston Soc. Civ. Eng.,* pp 257 – 276, 1936.
[13] Rutledge, P. C. *Progess Report on Triaxial Shear Research,* Waterways Experiment Station, pp 68 – 104, 1947.
[14] Skempton, A. W. and Sowa, V. A. The Behaviour of Saturated Clays during Sampling and Testing, *Geotechnique* 13, 269 – 290, 1963.
[15] Skempton, A. W. Discussion on the 'Planning and Design of the New Hong Kong Airport', *Proc. Inst. Civ. Eng. 7,* 306, 1957.
[16] Casagrande, A. Research on the Atterburg Limits of Soils, *Public Roads* 13, 121 – 136, 1932.

7
Interpretation of data from axial tests on saturated clays

7.1 One Real Axial-test Apparatus

In conventional *strain-controlled* tests the loading ram of the axial-test cell is driven down at a constant rate: we will distinguish between the more usual *slow* tests in which the strain rates are chosen to achieve negligible pore-pressure gradients by the time of *ultimate* failure, and the rarer *very slow* tests in which the strain rates are chosen to achieve negligible pore-pressure gradients at *all stages* of yielding. The slow tests give ultimate data which we can interpret in terms of the critical state model for engineering design purposes: the very slow tests give data of yielding *before* the ultimate states which we can interpret by the Cam-clay model, and although this interpretation is too refined for use in practical engineering at present we consider that some understanding is helpful for correct use of the critical state model.

The Cam-clay model is based on a conceptual axial-test system that we introduced in chapter 5. We will now describe briefly a *stress-controlled* test apparatus that closely resembles the conceptual system. We do not regard this apparatus as ideal, but it does provide the standard of comparison by which we can judge whether published data of strain-controlled tests are or are not fully satisfactory for our particular purpose.

The original text[1] *The Measurement of Soil Properties in the Triaxial Test* by Bishop and Henkel of Imperial College, University of London, contains a detailed exposition of axial testing on the basis of extensive work by them and their students. A variation[2] of this original equipment by research workers at the Norwegian Geotechnical Institute with some slight modifications[3] introduced at Cambridge is illustrated in Fig. 7.1. We will describe one class of test only, the stress-controlled test; since our aim is not to present a general review of the many varieties of axial-test apparatus but to introduce a new approach to the analysis of the data, we will merely describe one test technique in sufficient detail to draw attention to the problems that must be overcome.

In Fig. 7.1 is shown a cylindrical specimen K of soil 4 in. long, 2 in. diameter standing on a 2¼ in. diameter pedestal P and supporting a loading cap I of the same diameter. A natural rubber latex membrane L of 0.01 in. thickness and 2 in. diameter when unstretched, envelopes the specimen and is closely bound to the loading cap and to the pedestal by highly stretched rubber **O**-rings J of 1½ in. internal diameter and $\frac{3}{16}$ in. (unstretched) cross-sectional diameter. A mirror polish on the vertical surfaces of the pedestal and the loading cap minimizes the possibility of leakage of cell water past the bindings and into the pore-water.

The cell consists of a transparent plexiglass cylinder O permanently clamped between a top-plate F and a middle plate R by three lengths of threaded tube H. The cell is bolted down to the bottom-plate S by three long bolts with wing-nuts D. When the cell is assembled, the loading ram G that passes through a bushing E in the centre of the top plate is accurately co-axial with the pedestal P that is in the centre of the bottom plate. The bushing E is rotated at a constant rate by a small auxiliary motor, so there is effectively no friction resisting vertical movement of the ram through the bushing.

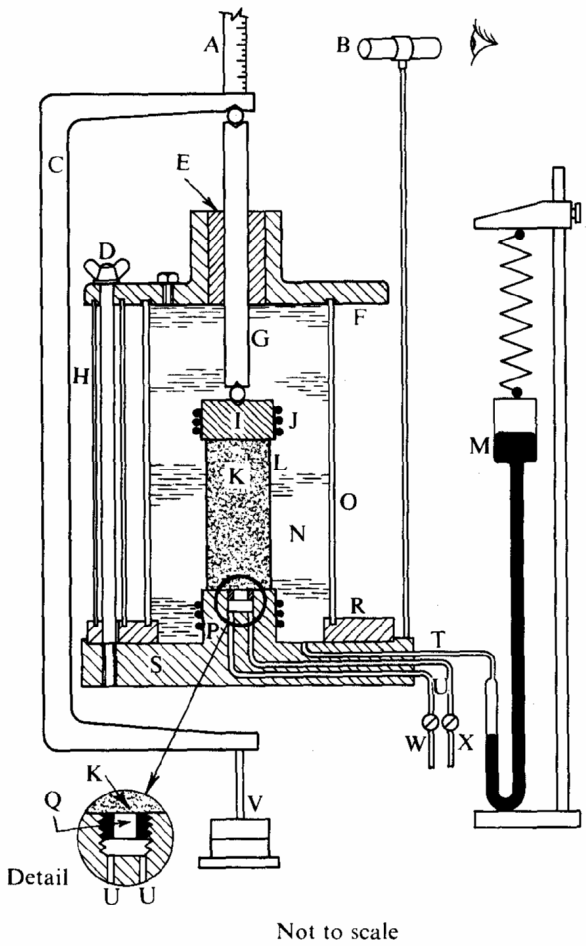

Fig. 7.1 Stress-controlled Axial-test Apparatus

The cell-water N fills the cell and surrounds the sheath, loading cap, and pedestal. A thin tube T connects the cell-water to a constant pressure device M of a type devised by Bishop and described by him (*loc. cit.*) as the self-compensating mercury control. This consists of a pot of mercury suspended by a spring, with leakage of water out of the cell causing the mercury to flow from the hanging pot; the consequent reduction in weight of the pot causes a shortening of the spring length which is so designed to maintain the mercury level constant and exactly sustain a constant pressure in the cell-water.

The bottom of the loading cap has a mirror polish and is lightly greased. The top of the pedestal also has a mirror polish and is lightly greased, except in the centre where a ¼ in. diameter porous stone Q allows drainage of pore-water from the specimen. Thus the ends of the specimen are effectively free to expand laterally[4] by about 12 per cent. The porous stone is itself mounted in a short length of threaded tube (see detail in Fig. 7.1) which is screwed down into a small recess in the top of the pedestal. From the recess two lengths of $\frac{1}{16}$ in. diameter 'hypodermic' steel tube U connected the pore-water with two devices outside the cell.

One device W is a back-pressured burette shown in Fig. 7.2(a). This burette Y is enclosed in a cylinder in which a constant water pressure is maintained by a second self-compensating mercury control. Changes in the silicone oil levels in the top of the cylinder and the burette show clearly the volume of pore-water that drains out of the specimen. The second device X is an accurate pore-pressure transducer which measures the change of pore-pressure that occurs when drainage is prevented. In Fig. 7.2(b) we show the system that was introduced by Bishop and has been widely used. Change of pore-pressure tends to

alter the level of the mercury Z in the 1 mm bore glass tube: this tendency is observed and counteracted by adjustment of the control cylinder so that the mercury level and hence the volume of pore-water within the specimen are kept constant. The pore-pressure u_w is indicated directly on the Bourdon gauge.

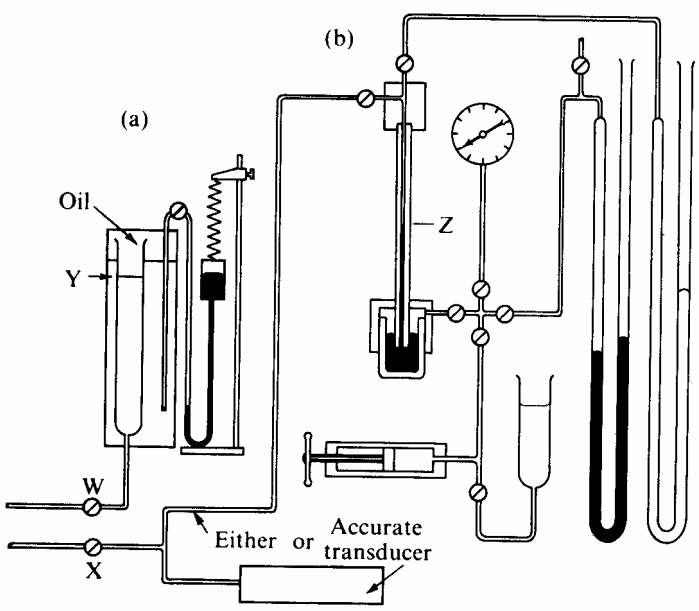

Fig. 7.2 Devices for Measuring Volume and Pressure of Pore-water

The loading ram G tends to be blown out of the bushing by the cell pressure; it is held down by a hanger C carrying a load V. A measuring telescope B fixed to a vertical bar that rises above the cell from the base is focussed on to a vertical scale A fixed to the hanger, so that change of the axial length of the specimen can be observed directly.

This particular apparatus permits study of specimens in a stress- controlled manner similar to that outlined in §5.2, etc. Each successive load-increment can be left long enough for the specimen to attain 100 per cent primary consolidation, and to be considered to be in equilibrium, because we have assumed that secondary phenomena are to be neglected.

The small but significant secondary displacements that occur over long periods after primary consolidation form a difficult topic of current research interest. We are faced with a rate process that is something other than Terzaghi's primary diffusion of water out of soil: it does appear that the best axial tests at a constant very slow strain rate give data that are more useful in this research than the standard stress-controlled test that we are describing.

7.2 Test Procedure

Two alternative test procedures commonly adopted are those for (*a*) the undrained test with pore-pressure measurement, and (*b*) the drained test. Both have much in common; the following brief account outlines the main features of what is a complicated technique and is only supposed to be a typical (but not perfect) test procedure. Readers of Bishop and Henkel (*loc. cit.*) will find much more on this point.

The first requirement is to ensure that the measuring devices W and X are free of air. The porous stone Q is removed from the base P, placed in a small evaporating dish and boiled. A temporary plug is screwed in its place and the pore-water system is checked by

forcing de-aired water from the hand-operated ram of the apparatus X without detectable changes of the pore-water levels Y and Z.

When this check is complete the back-pressured burette is then set to a desired level, and the connecting tube W is closed. A thin film of silicone grease is smeared over the base P, the plug is removed, the recess is flooded with water, and the saturated porous stone is screwed into the recess without trapping any air. A small quantity of water is forced up through the stone to ensure saturation and then the connecting tube X to the pore-pressure measuring apparatus is closed. Any excess water is removed from the surface of the porous stone, and if possible the base is then placed in a humid compartment.

The soil specimen is trimmed in the humid compartment and placed centrally on the pedestal. The rubber membrane, which has been soaked in water, is expanded by external suction back against a tube of 2½ in. internal diameter and placed round the specimen. The greased loading cap is carefully placed on the specimen, and firmly held against vertical movement by a clamp. The rubber membrane is released from the expander so that it embraces the specimen, cap, and pedestal. Any air bubbles trapped between the specimen and membrane are worked out, and three bindings rings are then placed at each end. The specimen and base are removed from the humid compartment, and the specimen's length and diameter are accurately measured.

The cell is then placed round the specimen, filled with de-aired water and a little oil is introduced below the loading ram. A pressure of 100 lb/in.^{2}, say, is applied simultaneously both to the cell-water and back-pressured burette and the valve W opened; if there is any air in the pore-water system it is detected by observing movement of the level Y in the burette.

The specimen can now be consolidated, if necessary, to some predetermined condition by reducing the back pressure on the burette to some value u_w. The specimen is then experiencing an effective spherical pressure $\sigma'_l = \sigma'_r = (100 - u_w)$ and as consolidation takes place pore-water will drain into the burette. For some specimens the back pressure may need to be raised again to allow the specimen to swell to an over-compressed state.

The specimen having experienced the required consolidation history is ready for shearing. If the specimen is to undergo an undrained test the connection to the burette W is closed and that to the pore-pressure device X opened, whereas for a drained test the connection to the burette is left open. Successive increments of load are applied to the hanger and after each increment sufficient time is allowed for primary consolidation to occur. Observations are made of the axial load, the consequent axial displacement of the loading cap, and either of (*a*) the pore-pressure, or of (*b*) the level of pore-water in the back-pressured burette.

The succession of load-increments concludes (after failure) with removal of loads from the hanger. The back pressure is raised to equal the cell pressure and, after sufficient time for swelling, the level in the burette is observed. The back pressure and cell pressure are then reduced to that of the atmosphere and again the level in the burette is observed. The apparatus is dismantled and finally, in the humid compartment, the sheath is removed and the specimen removed for determination of its final weight and water content.

7.3 Data Processing and Presentation

The data of an axial test fall into three main categories:

(*a*) the measurements of specimen length, diameter, weight, etc., and readings of any

consolidation which must be applied to the specimen to bring it to the desired initial condition (p_0, v_0, q_0);
(*b*) test constants such as calibration of proving ring (or load transducer), thickness and strength of membrane, specific gravity of specimen, etc.; and
(*c*) readings of time, axial load, axial displacement, change of volume and/or pressure of pore-water, and change of cell pressure, which occur during the test proper.

From this information we want to evaluate a variety of parameters, such as $p, v, q, \sigma'_l/\sigma'_r, \varepsilon$, etc., and repetitive calculations such as these are ideally performed by electronic digital computers. A suitable computer program can readily be devised to meet the special requirements of a particular laboratory or investigation, and will depend on what computer is available so we shall not attempt to set out a 'standard' program.

Typical input and output data from such a program are included in appendix B (see page 209). These are for a very slow *strain-controlled* undrained axial compression test on a specimen of virgin compressed kaolin which forms one of a recent series of tests.[5] The particular choice of parameters was:

(*a*) Axial train $\sum \dot{\varepsilon}_l = \sum(-\delta l/l)$
(*b*) Volumetric strain $\sum(\dot{v}/v) = \sum(-\delta V/V)$
(*c*) Cumulative shear strain $\sum \dot{\varepsilon} = \sum \dot{\varepsilon}_l - \frac{1}{3}\sum \dot{v}/v$
(*d*) Voids ratio $e = v - 1$
(*e*) Pore-pressure u_w
(*f*) Axial-deviator stress q
(*g*) Mean normal stress p
(*h*) Stress ratio $\eta = q/p$
(*i*) q/p_e where p_e is Hvorslev's equivalent pressure
(*j*) p/p_e
(*k*) v_λ
(*l*) v_κ
(*m*) $\dot{v}_\kappa/v\dot{\varepsilon}$
(*n*) $\dot{q}/p_e\dot{\varepsilon}$
(*0*) $\dot{p}/p_e\dot{\varepsilon}$
(*p*) $\dot{v}^p/v\dot{\varepsilon}$

7.4 Interpretation of Data on the Plots of *v* versus ln p

One assumption of the Cam-clay model is that recoverable compression and swelling should be governed by one constant κ and take the form given by eq. (6.3)

$$v = v_0 - \kappa \ln(p/p_0).$$

Data of swelling and recompression of remoulded London clay specimens from Henkel[6] are shown in Fig. 7.3. (The technique of remoulding used in these tests involved severe handling of specimens at relatively low water-content. The general character of these data differs from that of data from tests where specimens are consolidated from a slurry in that different values of Γ are indicated.) Some hysteresis occurs but the curves can be approximated by eq. (6.3) taking as numerical value for London clay $\kappa = 0.062 \pm 0.016$.

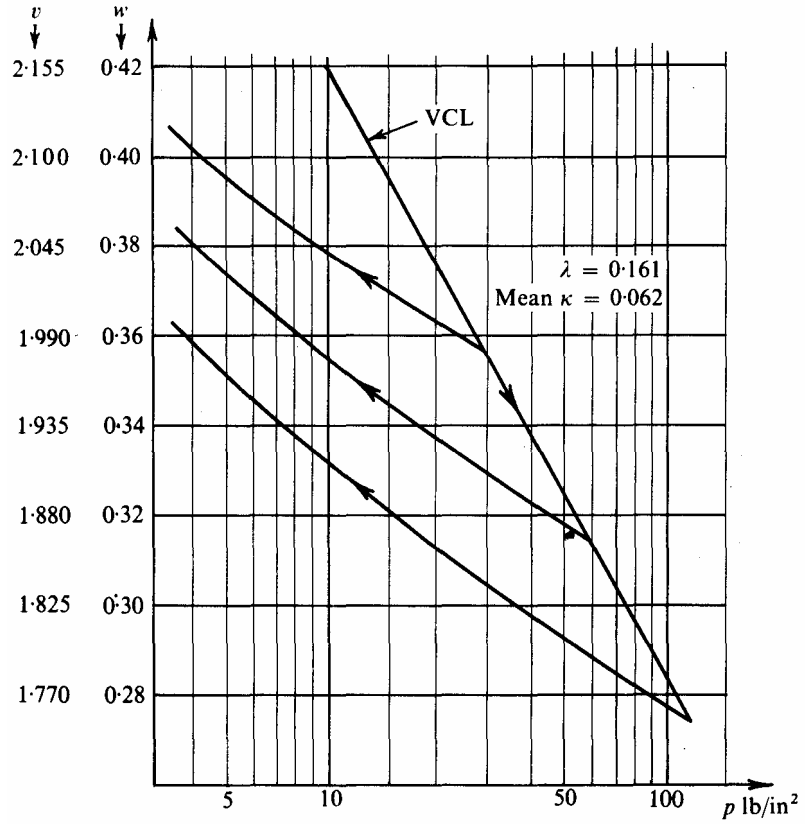

Fig. 7.3 Isotropic Consolidation and Swelling Curves for London Clay (After Henkel)

Having found values of κ and λ that are appropriate to the set of soil specimens under consideration we can compute v_κ and v_λ. We then know the coordinates of any point S in Fig. 7.4 either by values of v and p, or values of v_κ and v_λ which fix the κ-line and λ-line passing through the point S. We will be interested in changes of state of the specimen and can think of the current *state point* such as S and of a *state path* followed by a specimen during test.

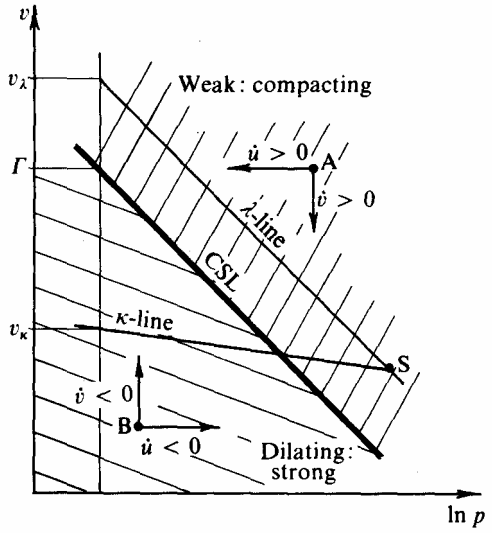

Fig. 7.4 Critical State Line Separating Differences in Behaviour of Specimens

One prediction shared by the Granta-gravel and Cam-clay models — see §5.9 — is that on the plot of v versus ln p (Fig. 7.4) there should be a clear division between an area

of the plot in which specimens are weak at yield and either develop positive pore-pressures or compact, and another area in which specimens are strong at yield and either develop negative pore-pressures or dilate. These areas lie either side of a critical state curve, which should be one of the λ-lines for which $v_\lambda = \Gamma$.

Data of slow strain-controlled tests by Parry[7] on remoulded London clay specimens are shown in Fig. 7.5. For each specimen a moment of 'failure' occurs in the test when the system has become unstable and although the specimen is not wholly in a critical state, as will be discussed further in chapter 8, it is seen to be tending to come into the critical state. In Fig. 7.5(a) the data are points representing the following classes of specimens:
(*a)* drained but showing zero rate of volume change at failure,
(*b*) drained and showing continuing volume decrease at failure,
(*c*) undrained but showing zero rate of pore-pressure change at failure,
(*d*) undrained and showing continuing pore-pressure increase at failure.

All these points in Fig. 7.5(a) lie on the *wet* side of a certain straight A-line on the v versus ln p plot. In contrast, in Fig. 7.5(b) the data are points representing the following classes of specimens:
(*a*) drained and showing continuing volume increase at failure,
(*b*) undrained and showing continuing pore-pressure decrease at failure.

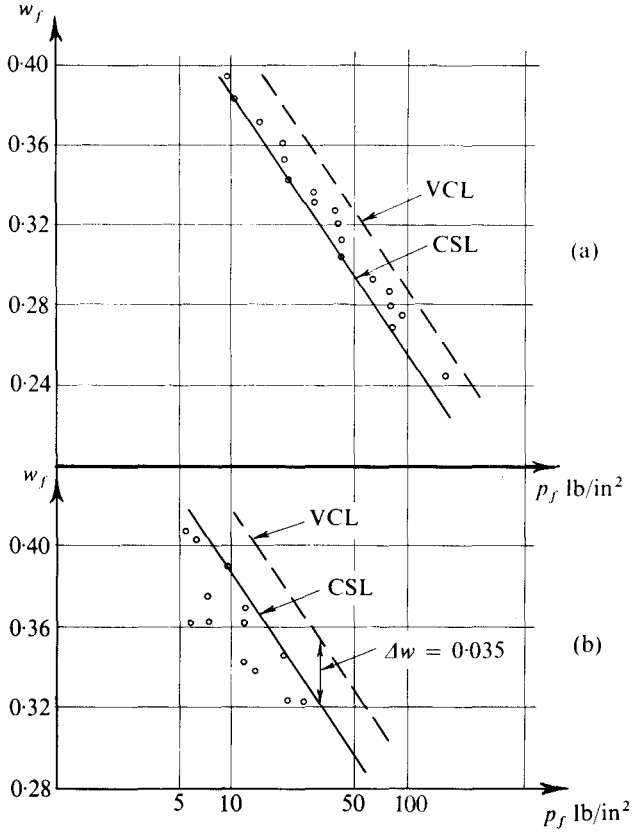

Fig. 7.5 Data of Tests on Remoulded London Clay at failure (After Parry)

All these points in Fig. 7.5(b) lie on the *dry* side of a certain λ-line on the v versus ln p plot. We see that we have the *same* λ-line in Fig. 7.5(a) and (b). It closely resembles the predicted critical state line of Fig. 7.4.

A prediction of the Cam-clay model (§6.6) is that during compression under effective spherical pressure p the virgin compression curve is, from eq. (6.20) when $\eta \to 0$,

$$v_\lambda = v + \lambda \ln p = \Gamma + (\lambda - \kappa) \tag{7.1}$$

so that it is displaced an amount $\Delta v = (\lambda - \kappa)$ to the wet side of the critical state curve. In Fig. 7.5 the position of the virgin compression curve is indicated by Parry. It is displaced an amount $\Delta v = G_s \Delta w \cong 2.75 \times 0.035 = 0.096$ to the wet side of the critical state curve: this is comparable with the prediction $(\lambda - \kappa) = 0.099$.

7.5 Applied Loading Planes

Having looked at the changing states of specimens on the v versus ln p graph we now need to move away from the plane of v and p into the projections of (p, v, q) space in which we can see q. It is possible to relate geometrically the method of loading that we apply to the specimen, with the plane in which the state path of the test must lie, regardless of the material properties of the specimen.

In §5.5 it was shown that a specimen in equilibrium under some effective stress (p, q) will shift to a state $(p + \dot{p}, q + \dot{q})$ when subject to a stress-increment. If the stress-increment is simply $\dot{\sigma}_r = 0, \dot{\sigma}_l > 0,$ and if there is no pore-pressure change $\dot{u}_w = 0,$ as in a drained test, then

$$\dot{p} = \frac{1}{3}\dot{\sigma}_l, \qquad \dot{q} = \dot{\sigma}_l \tag{7.2}$$

giving the vector AB indicated in Fig. 5.7. We can thus introduce the idea of an applied loading plane in Fig. 7.6. Consider first in Fig. 7.6(a) the case of a drained compression test in which initially $\sigma_l = p_0 = \sigma_r$ and then later $\sigma_l > p_0$. From eq. (7.2) $\mathrm{d}q/\mathrm{d}p = 3$ and with initial conditions $q = 0, p = p_0,$ we find

$$p = p_0 + \frac{1}{3}q, \tag{7.3}$$

which is the equation of the inclined plane of Fig. 7.6(a). The imposed conditions in the drained compression test are such that the state point (p, v, q) must lie in this plane.

Next consider the conditions imposed in §6.6, where we considered a drained yielding process with

$$\frac{\dot{q}}{\dot{p}} = \frac{q}{p} = \text{constant} = \eta > 0. \tag{6.21 bis}$$

In this case the principal effective stresses remain in constant ratio $\sigma'_r/\sigma'_l = K$ where

$$K = \frac{3 - \eta}{3 + 2\eta}.$$

The imposed conditions in such a test require the state point to lie in the plane illustrated in Fig. 7.6(b).

The conditions imposed in the undrained test are such that $\dot{v} = 0,$ and for this specimen the state points must lie in the plane $v = v_0$ illustrated in Fig. 7.6(c).

Alternatively, it is possible to conduct extension tests in the axial-test apparatus for which $\sigma_r > \sigma_l$ and $q < 0$. For a drained test of this type we have (from §5.5 and Fig. 5.7)

$$\frac{\dot{q}}{\dot{p}} = \frac{\mathrm{d}p}{\mathrm{d}q} = -\frac{2}{3}$$

and the applied loading plane becomes

$$p = p_0 - \frac{2}{3}q. \tag{7.4}$$

This is illustrated in Fig. 7.7; other examples could be found from tests in which the specimen is tested under conditions of constant p, or of constant q (as the mean normal

pressure is reduced), etc. At this stage we must emphasize that the applied loading planes are an indication only of the loading conditions applied by the external agency, and they are totally independent of the material properties of the soil in question.

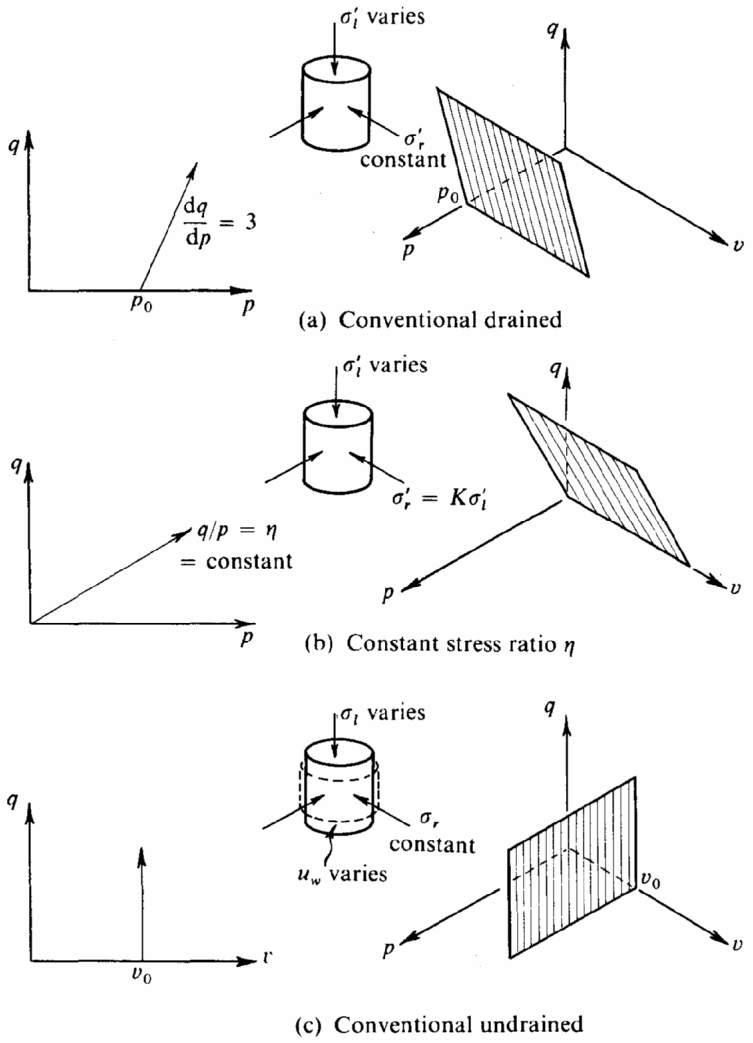

Fig. 7.6 Applied Loading Planes for Axial Compression Tests

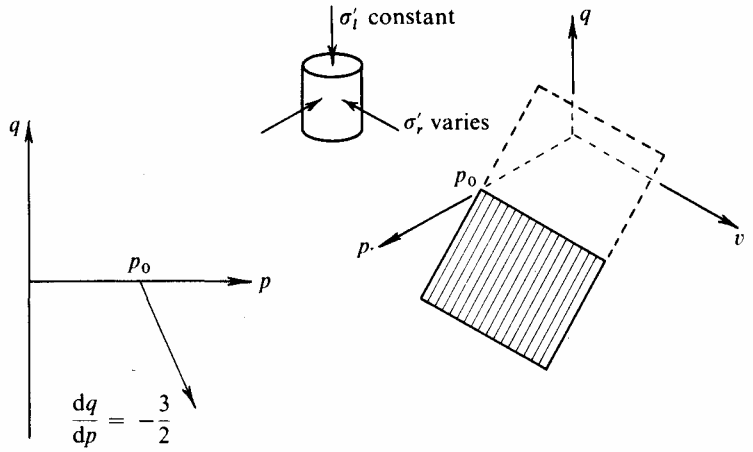

Fig. 7.7 Applied Loading Plane for Drained Axial Extension Test

7.6 Interpretation of Test Data in (*p*, *v*, *q*) Space

The material properties of Cam-clay are defined in the surface shown in Fig. 6.5. If we impose on a specimen the test conditions of the *drained* compression test, the actual state path followed by the specimen must lie in the intersection of a plane such as that of Fig. 7.6(a) and the surface of Fig. 6.5. This intersection is illustrated in Fig. 7.8.

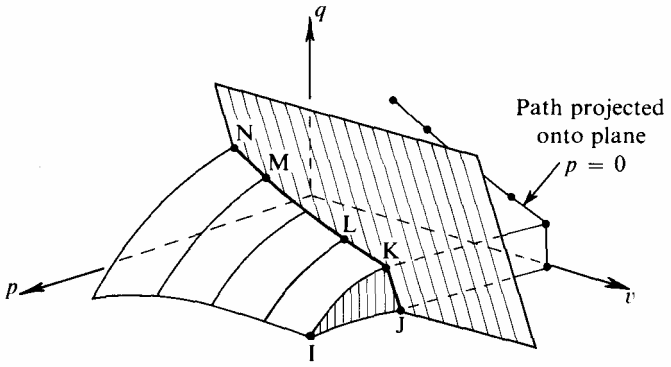

Fig. 7.8 State Path for Drained Axial Compression Test

The prediction of the Cam-clay model is fully projected in Fig. 7.9. We are considering a specimen virgin compressed to a pressure represented by point I and then allowed to swell back to a lightly overcompressed state represented by point J. The test path in Fig. 7.9(a) is the line JKLMN. The portion JK represents reversible behaviour before first yield at K; and in Fig. 7.9(b) this portion JK is seen to follow a re-compression curve (or κ-line). At K the material yields and hardens as it passes through states on successive (lightly drawn) yield curves. Simple projection locates points L, M, and N which then permit plotting of Fig. 7.9(c), which predicts the equilibrium values of the specific volume of a specimen under successive values of q.

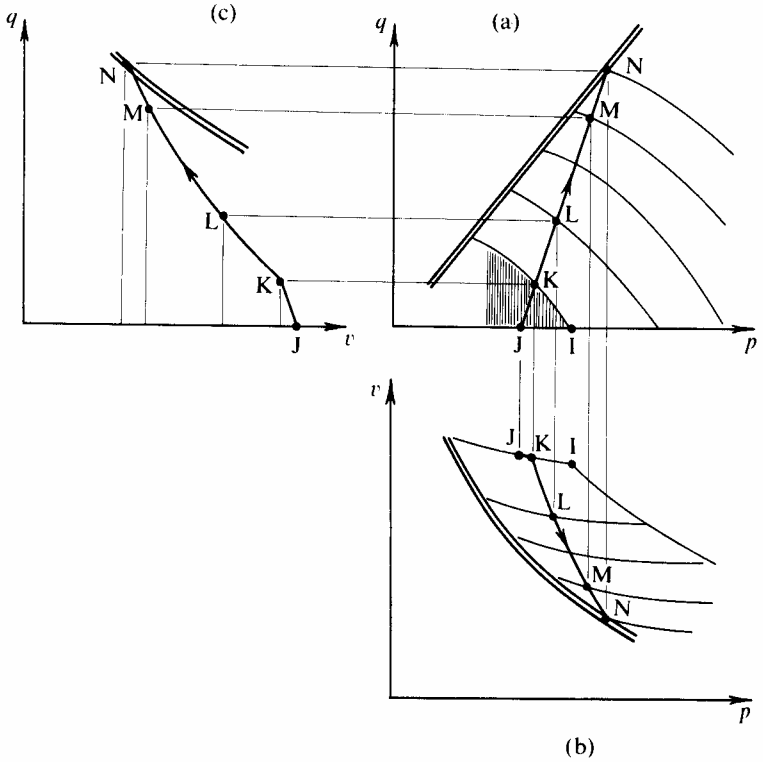

Fig. 7.9 Projections of State Path for Drained Axial Compression Test

In a similar manner, we appreciate in Fig. 7.10 that the intersection of the loading plane for an *undrained* compression test with the stable-state boundary surface must give the state path JFGH experienced by a similar specimen, which is shown projected in Fig. 7.11. Figure 7.11(a) and (b) show the plane $v = v_0 = \text{const.}$ crossing various yield curves at F, G, H, and by simple projection we can plot the predicted stress path in Fig. 7.11(c).

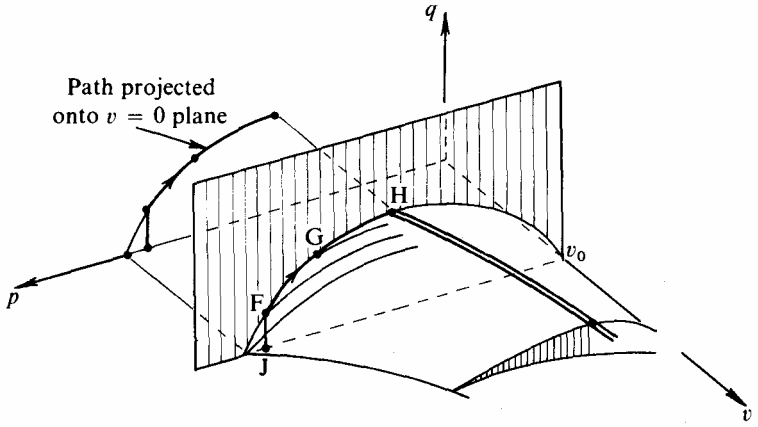

Fig. 7.10 State Path for Undrained Axial Compression Test

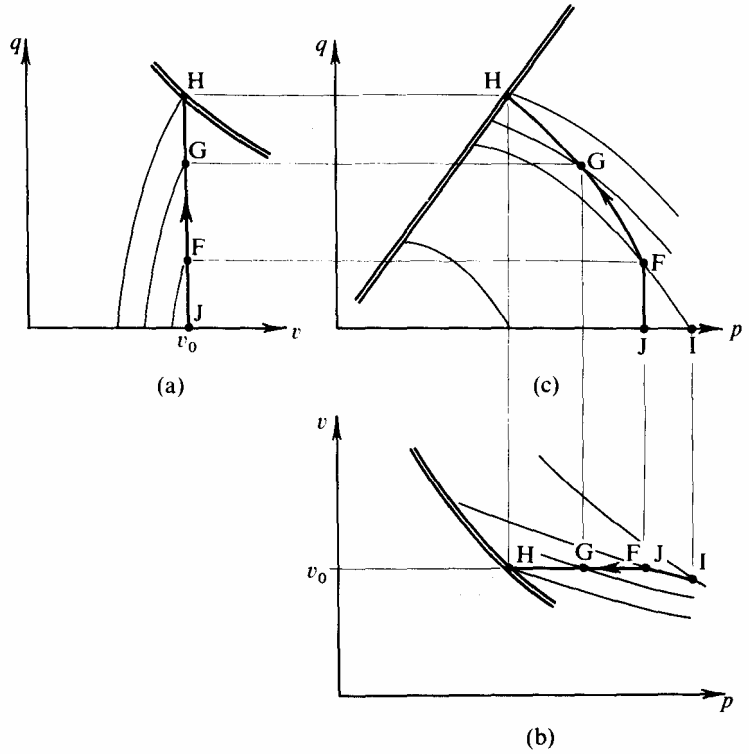

Fig. 7.11 Projections of State Path for Undrained Axial Compression Test

Data of a very slow strain-controlled undrained axial test are shown in Fig. 7.12: the specimen* of London clay was initially in a state of virgin compression at the point E. The experimental points have been taken from results quoted by Bishop, Webb, and Lewin[8] (Test No. 1 of Fig. 17 of their paper) and replotted in terms of the stress parameters p and q. A prediction for this curve can be obtained from eq. (6.27)

* In this case the specimen was prepared as a slurry at high water content and then consolidated, rather than being remoulded at relatively low water content. However, the form of this curve is similar to that found for remoulded specimens subject to the same test.

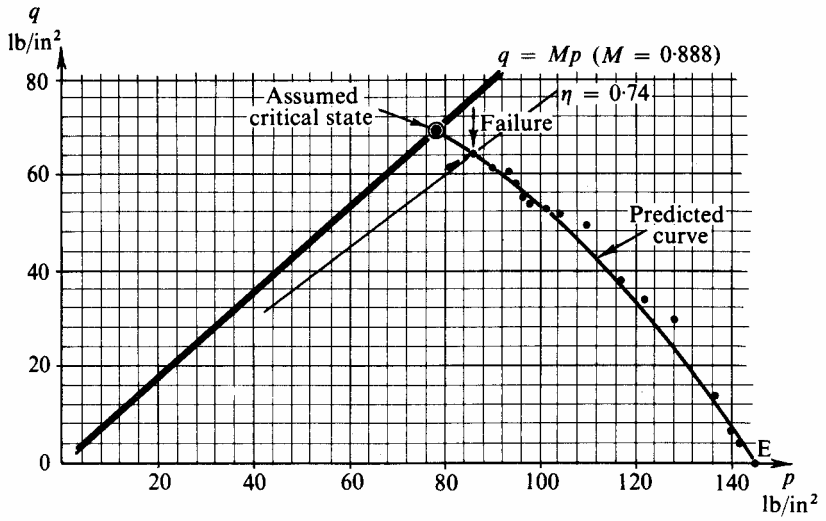

Fig. 7.12 Test Path for Undrained Axial Compression Test on Virgin Compressed Specimen of London Clay (After Bishop *et al.)*

$$|q| = \frac{Mp}{\Lambda}\ln\left(\frac{p_0}{p}\right) \qquad (6.27\text{ bis})$$

which was discussed in §6.7 and sketched in Fig. 6.7. Accepting previously quoted values of $\lambda = 0.161$ and $\kappa = 0.062$ for London clay, we find that with p_0 = 145 lb/in^2 and a choice of M = 0.888 we can then predict an undrained test path which fits closely the observed test data. It is to be noted that the test terminates with a failure condition (defined by maximum q) before an ultimate critical state is reached: we will have more to say about 'failure' in chapter 8.

7.7 Interpretation of Shear Strain Data

From the Cam-clay model we can predict the cumulative (permanent) distortional strain ε experienced by a specimen. Examples where calculations can be made in a closed form are for *undrained* tests and p-constant tests which have already been discussed briefly in §6.7 and §5.13 respectively. The discussion in §5.13 is strictly limited to Granta-gravel, but exactly similar development for Cam- clay leads to similar results for constant-p tests, i.e.,

$$M\varepsilon = \frac{\lambda - \kappa}{v_0 - D_0}\ln\left\{\frac{D_0 v}{v_0(v - v_0 + D_0)}\right\}$$

which reduces to eq. (5.36) when $\kappa = 0$.

If we consider the case of the test on a virgin compressed specimen of London clay (prepared from a slurry) of Fig. 7.12, the relevant equations for an undrained test are:

$$\left.\begin{aligned} |q| &= \frac{Mp}{\Lambda}\ln(p_0/p) && (6.27\text{bis})\\ \ln(p_0/p) + \Lambda &= \ln(p/p_u) = \Lambda\exp\left(\frac{-Mv_0}{\kappa\Lambda}\varepsilon\right) && (6.30\text{bis})\\ \frac{|q|}{Mp} &= 1 - \exp\left(\frac{-Mv_0}{\kappa\Lambda}\varepsilon\right). && (6.31\text{bis}) \end{aligned}\right\}$$

Using the numerical values of κ, λ, M, p_0, already quoted, we get the curves of Fig. 7.13 where the points corresponding to total distortion of 1, 2, 3, 4, and 8 per cent are clearly marked.

In comparison, we can reason that relatively larger strains will occur at each stage of a *drained* test. In Fig. 7.14(a) we consider both drained and undrained compression tests when they have reached the same stress ratio $\eta > 0$. From eq. (6.14) we have

$$\frac{\dot{v}^p}{v} = \frac{\dot{v}_\kappa}{v} = (M - \eta)\dot{\varepsilon} \quad (\dot{\varepsilon} > 0)$$

so that in each test there will be the same shift of swelling line $\dot{v}_\kappa$ for the same increment of distortion $\dot{\varepsilon}$. The yield curves relevant to the successive shifts of swelling line are lightly sketched in Fig. 7.14(a). We see the undrained test slanting across them from U_1 to U_2 while the drained test goes more directly from D_1 to D_2. It follows that for the same increment of distortion $\dot{\varepsilon}$ there will be a greater increment of $\dot{\eta}$ in an undrained test than in a drained test, which explains the different curves of q/p versus ε, in Fig. 7.14(b).

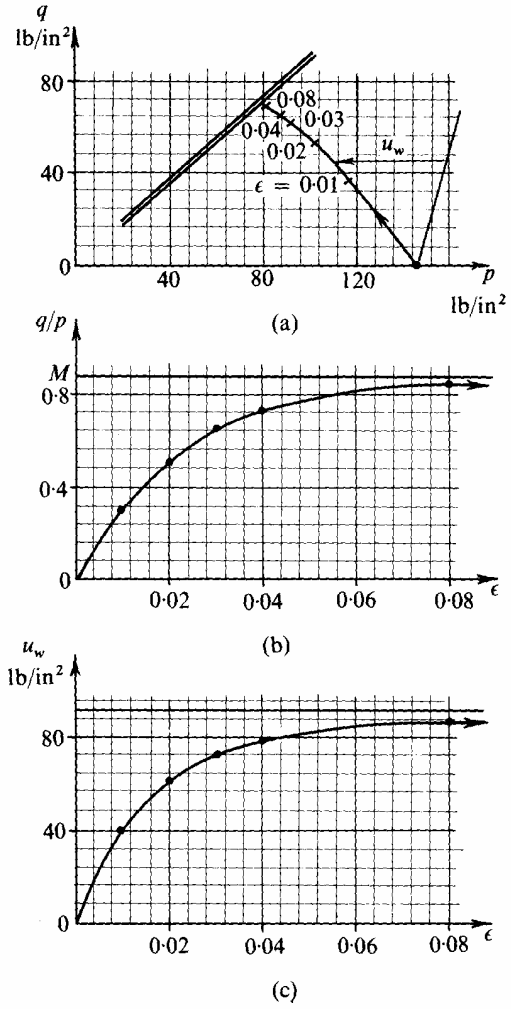

Fig. 7.13 Predicted Strain Curves for Undrained Axial Compression Test of Fig. 7.12

* For the *undrained* test, differentiating eq. (6.27) we get $(\Lambda\dot{\eta}/M) = -\dot{p}/q$ which equals the plastic volume change $\dot{v}_\kappa/v_0$ (since $\dot{v} \equiv 0$) and hence we have eq. (7.5). For the *drained* test, differentiating eq. (6.19) we get $\dot{\eta} = (M/\lambda - \kappa)\{+\dot{v} - (\lambda\dot{p}/p)\}$ and since $\dot{q}/\dot{p} = 3$ we also have $\dot{\eta} = \dot{q}/\dot{p} - q\dot{p}/p^2 = (3 - \eta)\,\dot{p}/p = (3 - \eta)(\dot{v} - \dot{v}_\kappa)$. Eliminating $\dot{p}$ and $\dot{v}$ we obtain eq. (7.6).

We can, in fact, derive expressions for these quantities. It can readily be shown* that for the increment U_1U_2 in the *undrained* test

$$\frac{\kappa\Lambda}{M}\dot{\eta} = (M-\eta)v_0\dot{\varepsilon}_{\text{undrained}} \qquad (v = v_0) \tag{7.5}$$

whereas for D_1D_2 in the *drained* test

$$\lambda\Lambda\left(\frac{1}{M}+\frac{1}{3-\eta}\right)\dot{\eta} = (M-\eta)v_0\dot{\varepsilon}_{\text{drained}} \tag{7.6}$$

(where v varies as the test progresses and is $\leq v_0$).

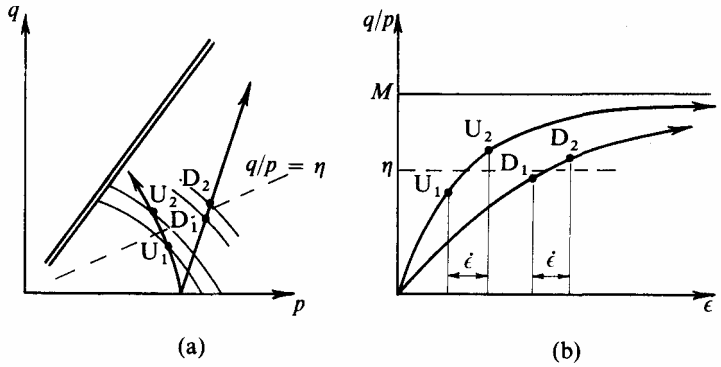

Fig. 7.14 Relative Strains in Undrained and Drained Tests

Hence the ratio of distortional strains required for the *same increment of* η is

$$\frac{\dot{\varepsilon}_d}{\dot{\varepsilon}_u} = \frac{\lambda(3-\eta+M)v_0}{\kappa(3-\eta)v_{\text{d}}}; \tag{7.7}$$

and we shall expect for specimens of remoulded London clay (*a*) at the start of a pair of tests when

$$\left.\begin{array}{l}\eta = 0\\ \\ v_{\text{d}} = v_0\end{array}\right\} \frac{\dot{\varepsilon}_{\text{d}}}{\dot{\varepsilon}_{\text{u}}} \cong 3.37$$

and (*b*) by the end when $\eta \to M$ and $v_{\text{d}} \cong 0.95v_0, \left(\dot{\varepsilon}_{\text{d}}/\dot{\varepsilon}_{\text{u}}\right) \cong 3.52$. It so happens that the minor influences of changing values of η and v during a pair of complete tests almost cancel out; and to all intents and purposes the ratio $\dot{\varepsilon}_{\text{d}}/\dot{\varepsilon}_{\text{u}}$ remains effectively constant (3.45 in this case).

This constant ratio between the increments of shear strain $\dot{\varepsilon}_{\text{d}}/\dot{\varepsilon}_{\text{u}}$ will mean that the cumulative strains should also be in the same ratio. This is illustrated in Fig. 7.15 where results are presented from strain controlled tests by Thurairajah[9] on specimens of virgin compressed kaolin. The strains required to reach the same value of the stress ratio η in each test are plotted against each other, giving a very flat curve which marginally increases in slope as expected.

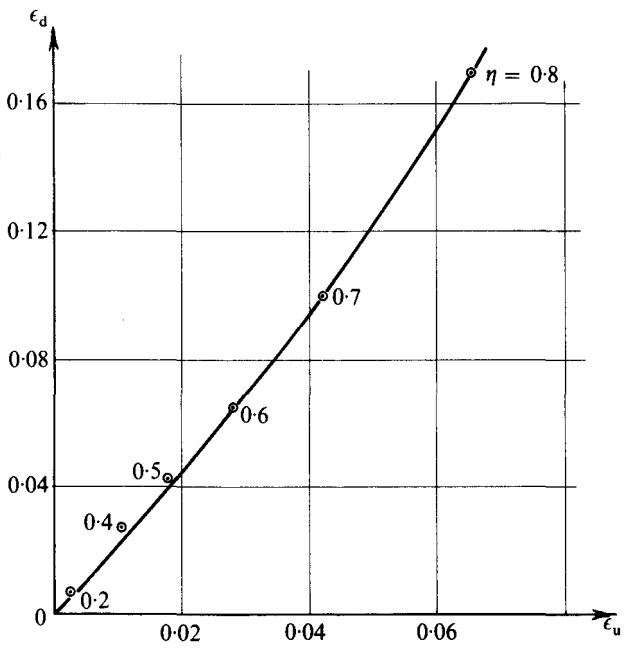

Fig. 7.15 Comparison of Shear Strains in Drained and Undrained Axial Compression Tests on Virgin Compressed Kaolin (After Thurairajah)

However, in general, plots with cumulative strain ε as base are unsatisfactory for two reasons. First, ε increases without limit and so each figure is unbounded in the direction of the ε-axis: this contrasts strikingly with the plots in (p, v, q) space where the parameters have definite physical limits and lie in a compact and bounded region. Secondly, and of greater importance, different test paths ending at one particular state (p, v, q) will generally require different magnitudes ε, so that the *total* distortion experienced by a specimen depends on its stress history and is not an absolute parameter. In contrast, the strain *increment* $\dot{\varepsilon}$ is a fundamental parameter and is uniquely related at all stages of a test on Cam-clay to the current state of the specimen (p, v, q) and the associated stress-increments $(\dot{p},\dot{q})$. In effect, a soil specimen, unlike a perfectly elastic body, is unaware of the datum for ε chosen by the external agency. In the following section we will consider the possibilities of working in terms of relative strain rates.

7.8 Interpretation of Data of $\dot{\varepsilon}$, and Derivation of Cam-clay Constants

In §7.4 we mentioned work by Parry which gave support to the critical state concept. He also plotted two sets of data as shown in Fig. 7.16 where rates of change of pore-pressure or volume change occurring at *failure* have been plotted against (p_u/p_f). (Failure is defined as the condition of maximum deviator stress q.) This ratio is that of the critical state pressure p_u, (corresponding to the specimen's water content w_f in Fig. 7.5*)* to its actual effective spherical pressure at failure p_f*;* this ratio is a measure of how near failure occurs to the critical state, and could just as well be measured by the difference between v_λ at failure and the value $v_\lambda \cong \Gamma$ for the critical state λ-line.

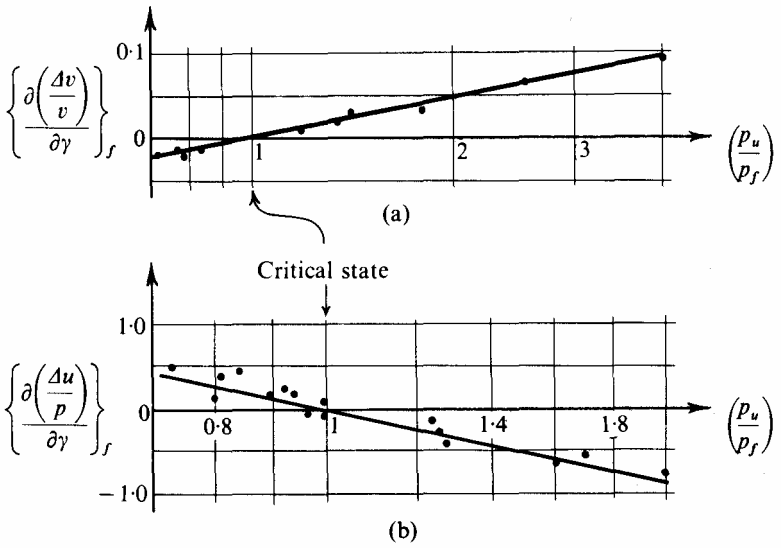

Fig. 7.16 Rates of Volume Change at Failure in Drained Tests, and Rates of Pore-pressure change at Failure in Undrained Tests on London clay (After Parry) Critical state

In the upper diagram, Fig. 7.16(a), results of drained tests are given in terms of the rate of volume change expressed by

$$\left\{\frac{\partial\left(\frac{\Delta v}{v}\right)}{\partial\gamma}\right\}_f$$

which is equivalent to

$$-\frac{2}{300}\left(\frac{\dot{v}}{v\dot{\varepsilon}}\right)_f.$$

This clearly shows that the further failure occurs from the critical state the more rapidly the specimen will be changing its volume.

Conversely, in Fig. 7.16(b) the results of undrained tests are presented in terms of rate of pore-pressure change expressed by

$$\left\{\frac{\partial\left(\frac{\Delta u}{p}\right)}{\partial\gamma}\right\}_f$$

which is equivalent to

$$+\frac{2}{300}\left(\frac{\dot{u}}{p\dot{\varepsilon}}\right)_f.$$

This clearly shows that the further failure occurs from the critical state the more rapidly the specimen will be experiencing change of pore-pressure.

In each case the existence of the critical state has been unequivocably established, together with the fact that the further the specimen is from this critical state condition at failure the more rapidly it is tending towards the critical state.

In the case of Cam-clay it is possible to combine these two sets of results. Our processing of data in §7.3 has provided values of v_λ which tell us on which λ-line the state

of a specimen is at any stage of a test. We also know values of v_κ and $\dot{v}_\kappa/v\dot{\varepsilon}$ which represent the current κ-line and the rate (with respect to distortion) at which the specimen is moving across κ-lines. The prediction of the Cam-clay model is that for *all* compression tests (whether drained, undrained, constant-*p*.. .) the data after yield has begun should obey eq. (6.14a)

$$\frac{\dot{v}_\kappa}{v\dot{\varepsilon}} = M - \frac{q}{p} = M - \eta \tag{7.8}$$

and while the state of the specimen is crossing the stable-state boundary surface we have from eq. (6.19)

$$\eta = \frac{M}{(\lambda - \kappa)}(\Gamma + \lambda - \kappa - v_\lambda). \tag{7.9}$$

Combining these we have

$$\frac{\dot{v}_\kappa}{v\dot{\varepsilon}} = \frac{M}{(\lambda - \kappa)}(v_\lambda - \Gamma) \tag{7.10}$$

which is a simple linear relationship between the rate of movement towards the critical state $\dot{v}_\kappa/v\dot{\varepsilon}$ with the distance from it $(v_\lambda - \Gamma)$, and one which effectively expresses Parry's results of Fig. 7.16. It is possible to express the predictions for Cam-clay in terms of Parry's parameters and obtain relationships which are very nearly linear on the semi-logarithmic plots of Fig. 7.16. The relationships are for undrained tests

$$\frac{3\dot{u}}{p\dot{\varepsilon}} = \frac{\dot{v}_\kappa}{\dot{\varepsilon}} \frac{M + (3 - \eta)\Lambda}{\Lambda}$$

and for drained tests

$$\frac{\dot{v}}{v\dot{\varepsilon}} = -\frac{\dot{v}_\kappa}{v\dot{\varepsilon}} \frac{M + (3 - \eta)\Lambda}{M(1 - \Lambda)}.$$

The experimental data are such that values of η and v_λ are determined to much greater accuracy than $\dot{v}_\kappa/v\dot{\varepsilon}$ and it is better to present them in the two separate relationships of eqs. (7.8) and (7.9) than the combined result of (7.10). The predicted results will be as in Fig. 7.17; a specimen of Cam-clay in an undrained test starting at some state such as A will remain rigid (without change of v_λ, v_κ or ε) until B, and then yield until C is reached. Similarly, we shall have the theoretical path DEC for a specimen denser (or dryer) than critical.

We shall expect real samples to deviate from these ideal paths and are not surprised to find real data lying along the dotted paths, which cut the corners at B and particularly at E. We also know that we have taken no account of the small permanent distortions that really occur between A and B or between D and E, and some large scatter is to be expected in the calculation of $\dot{v}_\kappa/v\dot{\varepsilon}$ when $\dot{\varepsilon}$ is small. However, the plot of Fig. 7.17 will allow us to make a reasonable estimate of a value of *M* which we may otherwise find difficult. A direct assessment from the final value of *q/p* of Fig. 7.14(b) could only be approximate on account of the inaccuracies in measurement of the stress parameters at large strain, and would underestimate *M* because failure intervenes before the critical state is reached.

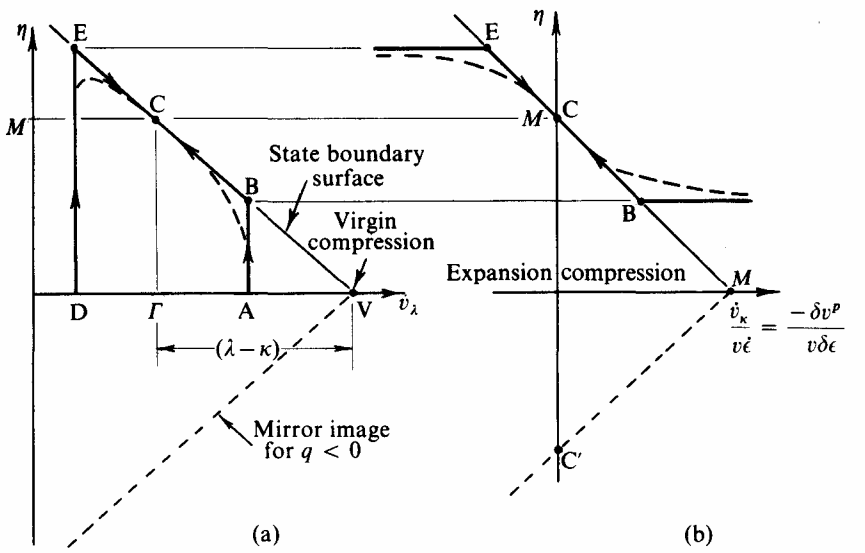

Fig. 7.17 Predicted Test Results for Axial Compression Tests on Cam- clay

Results of a very slow strain-controlled undrained test on kaolin by Loudon are presented in Figs. 7.18 and 7.19 and are tabulated in appendix B. This specimen was initially under virgin compression, but experimentally we can not expect that the stress is an absolutely uniform effective spherical pressure. Any variation of stress through the interior of the specimen must result in mean conditions that give a point A not quite at the very corner V. These initial stress problems are soon suppressed and over the middle range of the test the data in Fig. 7.18 lie on a well defined straight line which should be of slope $(M)/(\lambda-\kappa)$. As we have already established values for κ and λ, we can use them to deduce the value of M. For the quoted case of kaolin $\lambda = 0.26, \kappa = 0.05$ and so $M \cong 1.02$ and $\Gamma \cong 3.265$.

For a series of similar tests we shall expect some scatter (even in specially prepared laboratory samples) and it will be necessary to take mean values for M and Γ. It should be noted that failure as defined by the condition of maximum deviator stress q, occurs well before the condition of maximum stress ratio η, is reached.

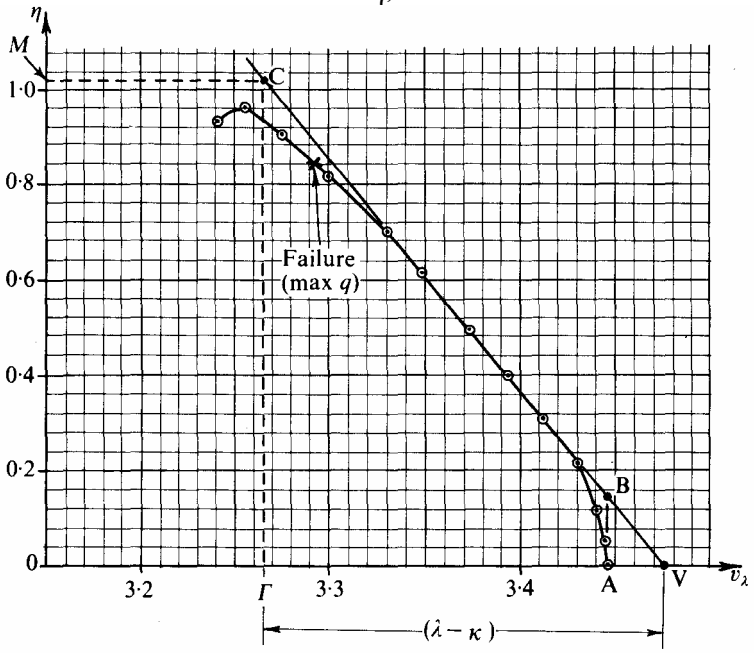

Fig. 7.18 Test Path for Undrained Axial Compression Test on Virgin Compressed Kaolin (After Loudon)

Turning to Fig. 7.19, the results indicate the general pattern of Fig. 7.17(b) but in detail they show some departure from the behaviour predicted by the Cam-clay model. The intercepts of the straight line BC should be M on both axes; but along the abscissa axis the scale is directly proportional to κ so that any uncertainty in measurement of its value will directly affect the position of the intercept.

Thus, in order to establish Cam-clay constants for our interpretation of real axial-test data we need two plots as follows:

(*a*) Results of isotropic consolidation and swelling to give v against ln p as Fig. 7.3 and hence values for κ and λ.

(*b*) Results of conventional undrained compression test on a virgin compressed specimen to give v_λ against η as Fig. 7.18 and hence values of M and Γ.

Having established reasonable mean values for these four constants we can draw the critical state curve, the virgin compression curve, and the form of the stable-state boundary surface, and in Fig. 7.20 we can use these predicted curves as a fundamental background for interpretation of the real data of subsequent tests.

At this stage we must emphasize that the interpretation is concerned with stress–strain relationships, and *not* with failure which we will discuss in chapter 8. We also note that there are *two* alternative ways of estimating the critical state and Cam-clay constants. The data of ultimate states in *slow* tests, in sufficient quantity, will define a critical state line such as is shown in Fig. 7.5. The slow tests cannot be used for close interpretation of their early stages when the data look like Fig. 7.21 and indicate a specimen that is not in equilibrium. However, from the data of slow axial tests and of the semi-empirical index tests, we can obtain a reasonable estimate of the critical state and Cam-clay constants. The second alternative is to use a few *very slow* tests and subject the data to a close interpretation. Although in Fig. 7.20 we concentrate attention on undrained tests, the interpretive technique is equally appropriate to very slow drained tests.

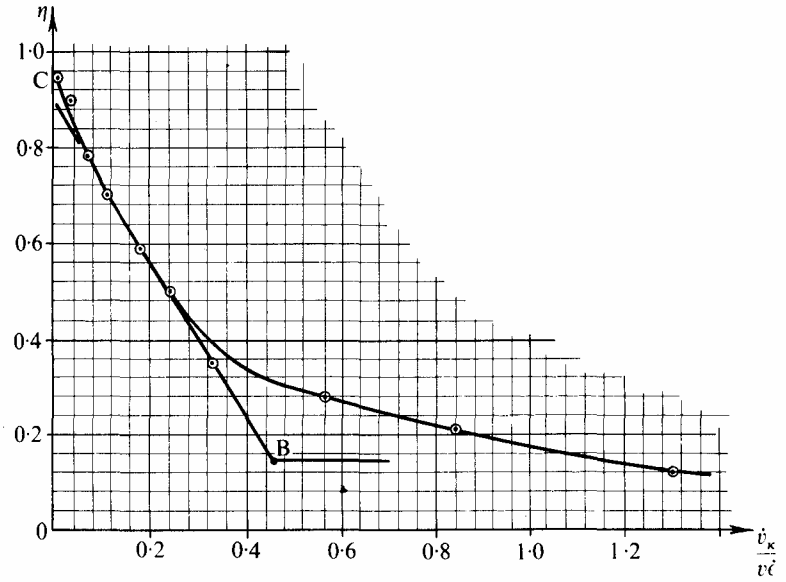

Fig. 7.19 Rate of Change of v during Undrained Axial Compression Test on Virgin Compressed Kaolin (After Loudon)

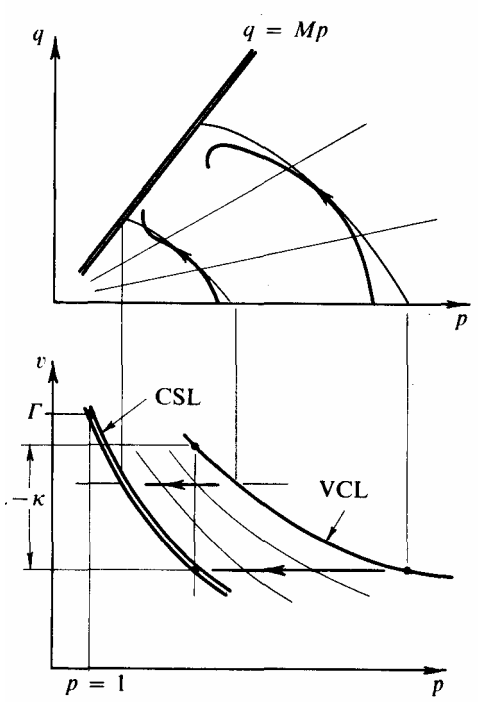

Fig. 7.20 Cam-clay Skeleton for Interpretation of Data

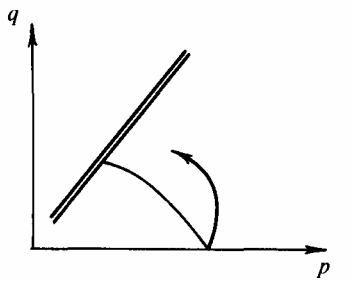

Fig. 7.21 Test Path for Test Carried out too quickly

7.9 Rendulic's Generalized Principle of Effective Stress

Experiments of the sort that we outlined in §7.1 were performed by Rendulic in Vienna and reported[10] by him in 1936. He presented his data in principal stress space, in the following manner. First he analysed the data of *drained* tests and plotted on the $(\sigma'_1, \sqrt{(2)}\sigma'_3)$ plane contours of constant water content; that is to say, if at $\sigma'_1 = 125$ lb/in^2 and $\sigma'_3 = 115$ lb/in^2 in one test that specimen has the same water content as another specimen at $\sigma'_1 = 128$ lb/in^2 and $\sigma'_3 = 108$ lb/in^2 in a different test then the points (125, 115) and (128, 108) would lie on one contour. Rendulic plotted the data of effective stress in *undrained* tests and found that these data lay along one or other of his previously determined contours. He thus made a major contribution to the subject by establishing the generalized principle of effective stress; for a given clay in equilibrium under given effective stresses at given initial specific volume, the specific volume after any principal stress increments was uniquely determined by those increments. This principle we embody in the concept of one stable-state boundary surface and many curved 'elastic' leaves as illustrated in Fig. 6.5: a small change $(\dot{p}, \dot{q})$ will carry the specimen through a well defined change $\dot{v}$ which may be partly or wholly recoverable. We could have mentioned the

contours of constant specific volume at an earlier stage but we have kept back our discussion of Rendulic's work until this late stage in order that no confusion can arise between our yield curves and his constant water content contours.

Rendulic[11] emphasized the importance of stress – strain theories rather than failure theories. He found that the early stages of tests gave contours that were symmetrical about the space diagonal, while states at failure lay unsymmetrically to either side. This led him to consider that *yielding* was governed by a modification of Mises' criterion with yield surfaces of revolution about the space diagonal, while *failure* might be governed by a different criterion.

In Henkel's slow strain-controlled axial tests on saturated remoulded clay that we have already quoted so extensively, the tests were timed so that there were virtually no pore-pressure gradients left at *failure.* Before failure, in the early stages of tests, these data do not define effective stress states with the same accuracy that lies behind Fig. 7.12. A precise comparison of Figs. 7.12 and 7.23 will quickly reveal differences between the two. However, the general concept and execution of these tests makes them worth close study. His interpretation[12] follows Rendulic's approach. In Fig. 7.22 he plots contours from drained tests and stress paths for undrained tests of a set of specimens all initially *virgin compressed.* In Fig. 7.23 he plots, in the same manner, data of a set of specimens all initially *overcompressed* to the same pressure 120 lb/in^2 and allowed to swell back to different pressures. These contours correspond respectively to our stable-state boundary surface (with some differences associated with early data of slow tests) and to the elastic wall that was discussed for Cam-clay. Cam-clay is only a conceptual model and clearly Figs. 7.22 and 7.23 show significant deviation for isotropic behaviour from the predictions of the simple model. The Figs. 7.22 and 7.23 also show data of failure which will be discussed in detail later.

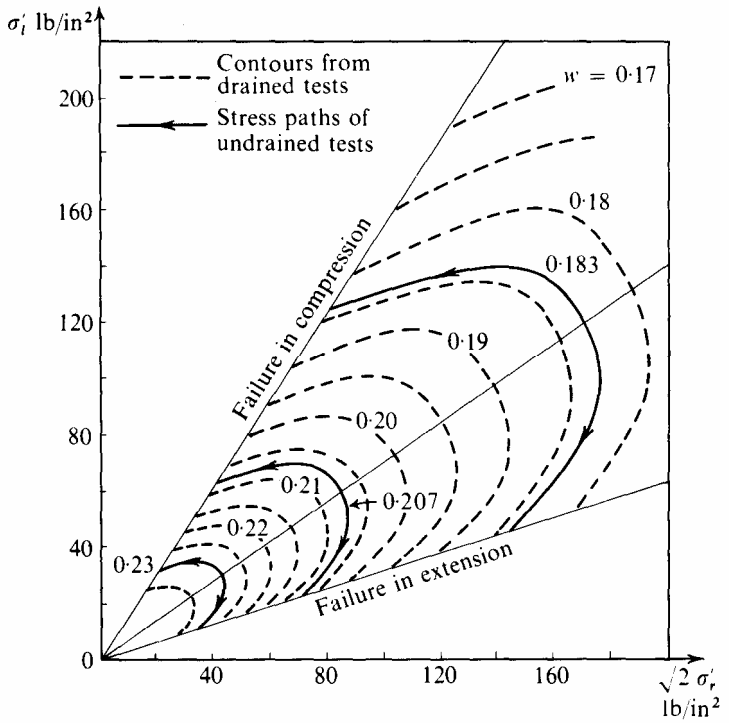

Fig. 7.22 Water Content Contours from Drained Tests and Stress Paths in Undrained Test for Virgin Compressed Specimens of Weald Clay (After Henkel)

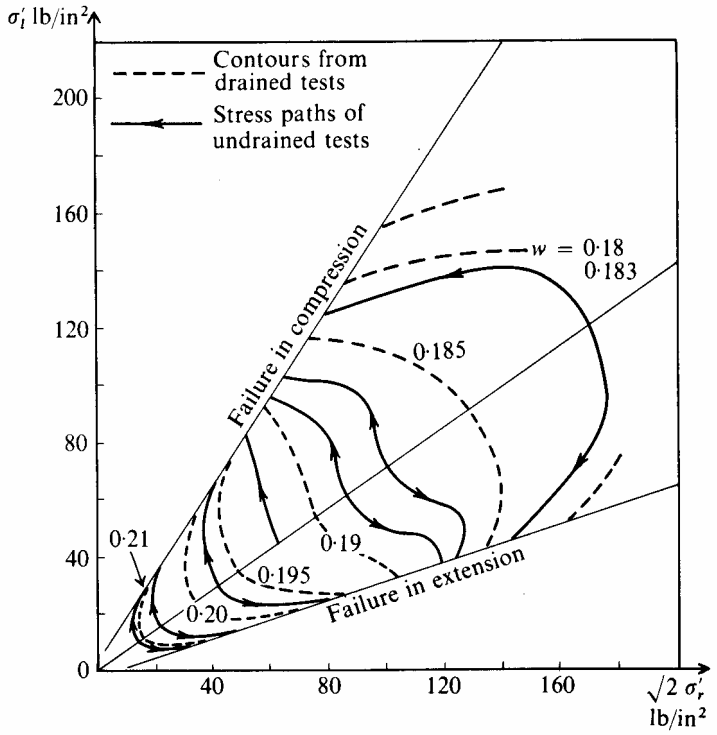

Fig. 7.23 Water Content Contours from Drained Tests and Undrained Stress Paths for Specimens of Weald Clay having a Common Consolidation Pressure of 120 lb/in^2 (After Henkel)

Rendulic clearly explained the manner in which pore-pressure is generated in saturated soil, and separated the part of the total stress that could be carried by the effective soil structure from the part of the total stress that had to be carried by pore-pressure. In the light of our development of the Cam-clay model, we can restate the generalized effective stress principle in an equivalent form: 'If a soil specimen of given initial specific volume, initial shape, and in equilibrium under initial principal effective stresses is subject to any principal strain-increments then these increments uniquely determine the principal effective stress-increments'.

The generalized principle of effective stress in one form or another makes possible an interpretation of the change of pore-pressure.

7.10 Interpretation of Pore-pressure Changes

Change of *effective* stress in soil depends on the deformation experienced by the effective soil structure. The pore-pressure changes in such a manner that the *total* stress continues to satisfy equilibrium.

Attempts have been made to relate such change of pore-pressure to change of total stress. Curves such as those in Fig. 7.13(c) have been observed in studies of axial tests on certain soft clays where the increase in major principal total stress was matched by the rise in pore-pressure. For example, if a virgin compressed specimen under initial total stresses

$$\sigma_r = 80 \text{ lb/in}^2 \qquad \sigma_l = 80 \text{ lb/in}^2 \qquad u_w = 50 \text{ lb/in}^2$$

was subjected to a total stress-increment $\dot{\sigma}_l = 10$ lb/in^2, it would come into a final equilibrium with

$$\sigma_r = 80 \text{ lb/in}^2 \qquad \sigma_l = 90 \text{ lb/in}^2 \qquad u_w = 60 \text{ lb/in}^2$$

The simple hypothesis which was first put forward was that the ratio of pore-pressure increment $\dot{u}_w$ to major principal total stress- increment $\dot{\sigma}_l$ was simply

$$\frac{\dot{u}_w}{\dot{\sigma}_l} = 1. \tag{7.11}$$

This relationship was modified by Skempton[13] who proposed the use of pore-pressure parameters A and B in a relationship

$$\dot{u}_w = B\{\dot{\sigma}_r + A|\dot{\sigma}_l - \dot{\sigma}_r|\}. \tag{7.12}$$

Here, B is a measure of the saturation of the specimen; for full saturation B=1. The parameter A multiplies the effect of q and relates the curves (*b*) and (*c*) of Fig. 7.13. An alternative coefficient introduced by Skempton for the case $\dot{\sigma}_l > \dot{\sigma}_r$ is

$$\frac{\dot{u}_w}{\dot{\sigma}_l} = \overline{B} = B\left\{1 - (1-A)\left(1 - \frac{\dot{\sigma}_r}{\dot{\sigma}_l}\right)\right\}. \tag{7.13}$$

In either form, if we introduce full saturation (B =1), and consider only the *compression* test ($\dot{\sigma}_r = 0$), both eqs. (7.12) and (7.13) reduce to

$$A = \frac{\dot{u}_w}{\dot{q}} \qquad \overline{B} = \frac{\dot{u}_w}{\dot{\sigma}_l} - \frac{\dot{u}_w}{\dot{q}}. \tag{7.14}$$

The simple hypothesis eq. (7.11) suggested that for virgin compressed clay a basis for prediction of pore-pressures would be $A = \overline{B} = 1$.

In Fig. 7.24(a) we show the predicted undrained test path for a virgin compressed Cam-clay specimen. The point V is an initial state, point W represents applied *total* stress and point X represents applied *effective* stress. For the simple case, when $\sigma_r = \text{const.}$ and $\dot{\sigma}_r = 0$ which we show in the figure,

$$\dot{u}_w + \dot{p} = \frac{\dot{q}}{3}.$$

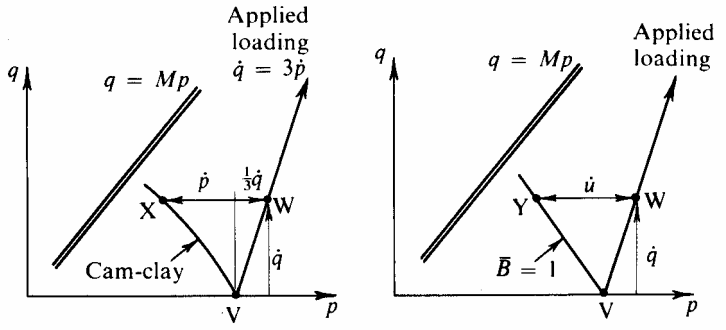

(a) $\mathrm{WX} = \dot{u} = \frac{1}{3}\dot{q} - \dot{p}$ (b) $\mathrm{WY} = \dot{u} = \dot{q}$

Fig. 7.24 Comparison of Cam-clay with $\overline{B} = 1$ Hypothesis

The yielding of Cam-clay in an undrained test was discussed in §6.7, where eq. (6.27) determines the changing *effective* stresses (q, p), and defined the Cam-clay path of Fig. 7.24(a) which is close to a straight line. In Fig. 7.24(b) we show the changing effective stresses that would be applicable to a material for which $\overline{B} = 1$. The $\overline{B} = 1$ hypothesis is only a little different from the prediction of Cam-clay, for which it can be shown that

$$\overline{B} = \frac{\dot{u}_w}{\dot{q}} = \frac{1}{3} - \frac{\dot{p}}{\dot{q}} = \frac{1}{3} + \frac{\Lambda}{M - \Lambda\eta} \tag{7.15}$$

for this type of test.

We will next consider what we have called ‘over compressed’ specimens, meaning specimens that have been virgin compressed under a high effective spherical pressure Np_0

and then permitted to swell back under a reduced effective spherical pressure p_0. In Fig. 7.25 on the graph v versus $\ln p$ we see the sequence of virgin compression to Np_0 at point J, followed by swelling to an effective pressure p_0 and a specific volume v_0 at point K. Points I and L are on the virgin compression and critical state lines at specific volume v_0. Swelling from J to K, with reduction of effective spherical pressure from Np_0 to p_0, results in increase of specific volume of $(\kappa \ln N)$. So we can calculate that the effective spherical pressures at I and L are

$$\left.\begin{aligned} &\ln p_e = \ln Np_0 - \frac{\kappa}{\lambda}\ln N, \\ &\ln p_u = \ln p_e - \Lambda \\ \therefore \text{for K,} \quad &\ln\left(\frac{p_0}{p_u}\right) = \Lambda(1 - \ln N), \end{aligned}\right\} \tag{7.16}$$

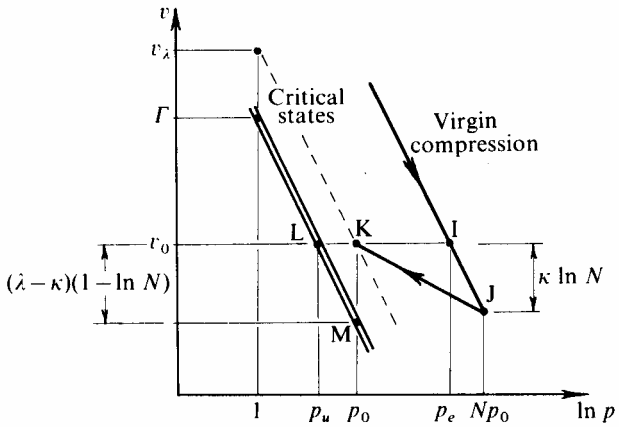

Fig. 7.25 Increase of Specific Volume during Isotropic Swelling in terms of Overcompression Ratio

and the separation of K from the critical state line is

$$\text{KM} = \lambda \ln\left(\frac{p_0}{p_u}\right) = (\lambda - \kappa)(1 - \ln N). \tag{7.17}$$

We have already defined the offset KM as $(v_\lambda - \Gamma)$, so that for any general point

$$v_\lambda - \Gamma = (\lambda - \kappa)(1 - \ln N) \tag{7.18}$$

from which we see at once that a family of specimens all having the same overcompression ratio N will have the same value of v_λ, i.e., lie on the same λ-line.

We can see in Fig. 7.26 the manner in which the pore-pressure u_w develops in an undrained compression test on an initially overcompressed specimen. The line KQ represents the applied total loading; and the curve KRL represents the behaviour of Cam-clay consisting of an initial elastic part KR and subsequent plastic part RL of the state path approaching the critical state at L. The ultimate pore-pressure u_u if the critical state $(p_u, q_u = Mp_u)$ were reached would be

$$u_u = p_0 - p_u + \tfrac{1}{3}Mp_u.$$

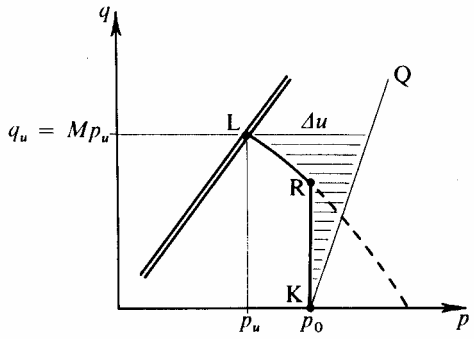

Fig. 7.26 Development of Pore-pressure during Undrained Compression Test on Overcompressed Specimen

Let us introduce a parameter A_u defined by

$$A_u = \frac{u_u}{q_u} = \frac{u_u}{Mp_u} \tag{7.19}$$

so that $$A_u = \frac{p_0 - p_u + \frac{1}{3}Mp_u}{Mp_u}.$$

But from eq. (7.17)

$$\frac{p_0}{p_u} = \exp\{\Lambda(1 - \ln N)\} = (\exp \Lambda)N^{-\Lambda}$$

$$\therefore \qquad MA_u = (\exp \Lambda)N^{-\Lambda} - 1 + \tfrac{1}{3}M \tag{7.20}$$

For the case of London clay with $\Lambda = 0.614$ and $M = 0.888$ this becomes

$$A_u \cong 2N^{-0.614} - 0.8. \tag{7.21}$$

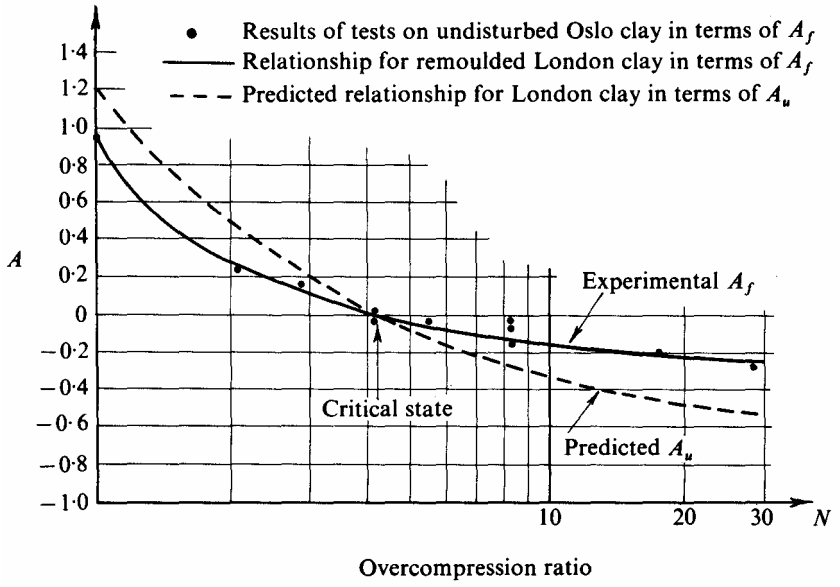

Fig. 7.27 Relationship between Pore-pressure Parameter *A* and Over-compression Ratio *N* (After Simons)

In Fig. 7.27 we show data of pore-pressure coefficient A_f observed at *failure* on sets of overcompressed specimens of undisturbed Oslo clay and remoulded London clay quoted

by Simons[14]. For comparison, the dotted line is the relationship predicted by eq. (7.21) for London clay for the pore-pressure coefficient A_u appropriate to the *critical state.*

From the work by Parry already quoted, we shall expect that on the wet (or loose) side of the critical state line $A_f < A_u$ and on the dry (or dense) side $A_f > A_u$. The cross-over of the experimental and predicted curves must occur when $A_f = A_u = 0$, which from eq. (7.21) will be when

$$N = 2.5^{1/0.614} = 4.45.$$

This pattern of behaviour is borne out in Fig. 7.27 and the fact that it is the same for the remoulded London clay specimens as for the undisturbed Oslo clay specimens suggests that the critical state concept has wide application.

However, we must emphasize that the pore-pressure parameter A is not itself a fundamental soil property. In Fig. 7.28(b) we illustrate the overcompression of two specimens X and Y and the virgin compression of a specimen W. In Fig. 7.28(a) we illustrate the changing effective stresses that would occur in undrained tests on these three specimens. At failure each has approached the near vicinity of the critical state C. *En route* to failure, the pore-pressure u_w is the horizontal offset between the faint lines WW', XX', YY' that represent total stress application and the firm lines WC, XC, YC that represent effective stress response. For specimen W the simple hypothesis $\overline{B} = 1$ has some meaning, but not for specimen Y where the pore-pressures show small initial positive values followed by subsequent negative pore-suction.

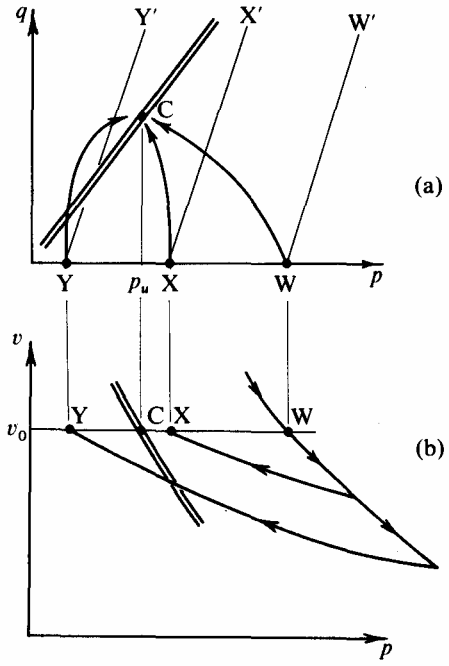

Fig. 7.28 Differing Pore-pressure Responses of Specimens with differing Amounts of Overcompression

There is nothing fundamentally significant about the applied loading lines. Other loading conditions would give different inclinations to these lines. The strains of the deforming effective soil structure, as it yields and approaches C from W or X or Y, do bear a fundamental relationship to the *effective* stresses. The pore-pressure simply carries whatever excess there may be of total pressure over and above effective spherical pressure.

We can take an example, other than the axial-test situation, and consider the advance of a pile tip in a layer of clay initially in a state of virgin plastic compression.

Figure 7.29(a) shows two positions I and II in the advance of that pile, and a small elemental specimen of clay being displaced. The geometry of displacement imposes on the specimen some increment of distortion $\dot{\varepsilon}$, see Fig. 7.29(b), and the rapid advance of the pile ensures that there is no drainage or volume change of the specimen. If the initial state (q, p) of the specimen is point I in Fig. 7.29(c), the subsequent state II is completely determined by the distortion $\dot{\varepsilon}$ at constant volume. As the pile tip advances, the deforming clay must experience a *fall* in effective pressure. The clay specimen moves relatively closer to the pile tip and total pressure must *rise* during the increment. There will be a marked rise in pore-pressure to ensure that total stresses continue to be in equilibrium round the pile tip. In general it seems that the analysis of such problems does not involve the pore-pressure parameters, but does require some fundamental statements of a relationship between change of effective stress and the deformation experienced by the effectively stressed soil.

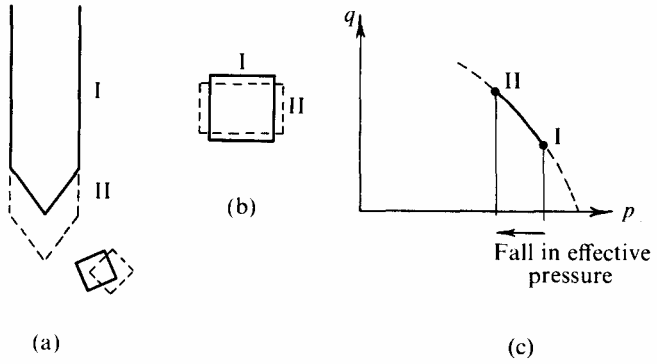

Fig. 7.29 Pressure Change caused by Advance of Tip of Pile

7.11 Summary

The close interpretation of data of very slow strain-controlled axial tests on saturated clay specimens has proved most rewarding. The position has been decribed in detail because it is hoped that it will prove to be of value to engineers who are involved in soil testing. In §7.8 we introduced new methods of plotting data which are illustrated in Figs. 7.18 and 7.19, and at the end of §7.8 it is concluded that the combination of Figs. 7.3 and 7.18 will give the best basis for interpretation of test data.

The last two sections, §7.9 and §7.10, have reviewed two notable alternative interpretations of the data of axial testing. The plotting of contours of constant water content by Rendulic produces an interesting display of data, and after our detailed development of the Cam-clay model we can appreciate the great contribution that was made by Rendulic's work. The introduction of pore-pressure parameters A, B, and $\overline{B}$ is particularly interesting in showing how $\overline{B} = 1$ corresponds well with the Cam-clay model. However, neither Rendulic's approach nor the use of pore-pressure parameters seem to offer us as complete an interpretation as can be obtained by introduction of the critical state and Cam-clay models.

When the new soil constants are obtained by interpretation of test data the question that immediately arises is of their *use* in design calculation. It is evident that the Coulomb failure criterion which we will approach in the next chapter is the main model with which design calculations are presently made. However, it will prove possible to use our new understanding of the yielding of soil to make a rational choice of Coulomb strength parameters for design calculations: in this sense the new constants may prove to be useful.

References to Chapter 7

1 Bishop, A. W. and Henkel, D. J. *The Measurement of Soil Properties in the Triaxial Test,* Arnold, 1957.

2 Andresen, A. and Simons, N. E. Norwegian Triaxial Equipment and Technique, *Proc. Res. Conf on Shear Strength of Cohesive Soils,* A.S.C.E., Boulder, pp. 695—709, 1960.

3 Schofield, A. N. and Mitchell, R. *3.* Correspondence on '"Ice Plug" Stops in Pore Water Leads', *Geotechnique* 17, 72 – 76, 1967.

4 Rowe, P. W. and Barden. L. Importance of Free Ends in Triaxial Testing, *Journ. Soil Mech. and Found. Div.,* A.S.C.E., 90, 1 – 27, 1964.

5 Loudon, P. A. *Some Deformation Characteristics of Kaolin,* Ph.D. Thesis, Cambridge University, 1967.

6 Henkel, D. J. The Effect of Overconsolidation on the Behaviour of Clays During Shear, *Géotechnique 6,* 139 – 150, 1956.

7 Parry, R. H. G. Correspondence on 'On the Yielding of Soils', *Géotechnique8,* 184 – 6, 1958.

8 Bishop, A. W., Webb, D. L. and Lewin, P. I. Undisturbed Samples of London Clay from the Ashford Common Shaft: Strength Effective Stress Relationships, *Géotechnique* 15, 1 – 31, 1965.

9 Thurairajah, A. *Some Shear Properties of Kaolin and of Sand,* Ph. D. Thesis, Cambridge University, 1961.

10 Rendulic, L. Pore-Index and Pore-water Pressure, *Bauingenieur* 17, 559, 1936.

11 Rendulic, L. A Consideration of the Question of Plastic Limiting States, *Bauingenieur* 19, 159 – 164, 1938.

12 Henkel, D. J. The Relationships between the Effective Stresses and Water Content in Saturated Clays, *Geotechnique* 10, 41 – 54, 1960.

13 Skempton, A. W. Correspondence on 'The Pore-pressure Coefficient in Saturated Soils', *Géotechnique* 10, 186 – 7, 1960.

14 Simons, N. E. The Effect of Overconsolidation on the Shear Strength Characteristics of an Undisturbed Oslo Clay, *Proc. Res. Conf on Shear Strength of Cohesive Soils,* A.S.C.E., Boulder, pp 747 – 763, 1960.

8
Coulomb's failure equation and the choice of strength parameters

8.1 Coulomb's Failure Equation

The past three chapters have developed stress – strain theories for soil: they have also recognized that in the general progress of deformation there will be a 'peak' stress at which a stress-controlled system can fail because of the state of an element of soil within the system. The question of the state of soil at peak stress was discussed in the first source of soil mechanics — the paper[1] by Coulomb in 1776.

Coulomb considered, Fig. 8.1(a), that soil was a rigid homogeneous material which could rupture into separate blocks. These blocks remained in contact but slid relative to each other along the contact surface. Coulomb observed such rupture surfaces in soil and rock. His experiments on solid rock specimens and on mechanisms with sliding contact suggested that both cohesion and friction must be overcome during slip along the rupture surface, Fig. 8.1(b). We follow Sokolovski and denote cohesion by ***k*** and angle of friction by $\boldsymbol{\rho}$ in order to ease the introduction to his text. (In general, symbols (c,ϕ) are used, but these have over the years become very confused by innumerable definitions and suffices.) If we call the effective stress component across the rupture surface σ', then the shearing stress τ that is available to resist motion along the rupture surface is written

$$|\tau| \le k + \sigma' \tan \boldsymbol{\rho}. \tag{8.1}$$

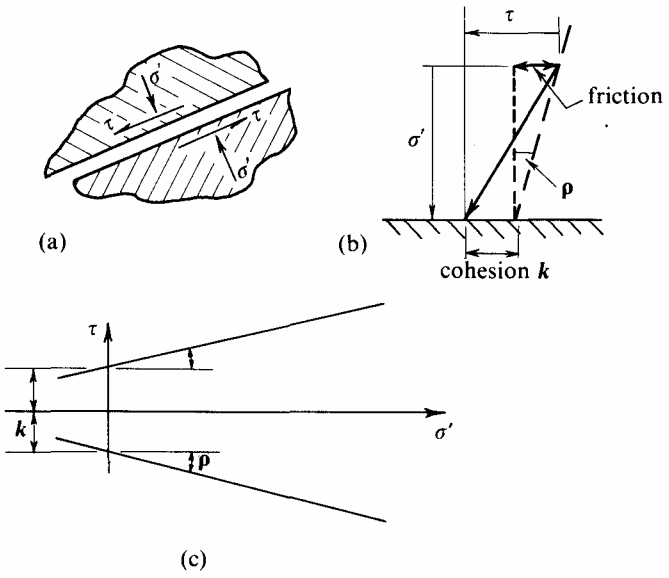

Fig. 8.1 Coulomb's Failure Criterion

This is the 'Coulomb equation': it is implicit in Coulomb's derivation of another eq. (9.5) to which we will come later, although it was not written explicitly in the 1776 paper.

For engineers 'classical' soil mechanics is the extensive set of design calculations and studies which is based on eq. (8.1). These studies reach their highest development in the recent text of Sokolovski on the limiting equilibrium of soil which are discussed with

other calculations of limiting equilibrium in chapter 9. Before we introduce these classical calculations we must decide what values of k and ρ to choose for each soil.

In this chapter we will meet two quite distinct sets of values of (k,ρ). The first set will be discussed in sections 8.2 to 8.4 where we are concerned with the experimental fact that data of *peak* strengths of soil specimens do fit a modified form of the Coulomb equation. However, in §8.5 we explain that it would be incorrect to use these 'peak' values (k,ρ) in design calculations, because strength falls from its peak to lower values after failure. The second set of values (k,ρ) that can be used rationally in design calculations are discussed in sections 8.6 to 8.8, which follows the rationale given by Bishop and Bjerrum[2] in 1960. It does seem that this choice of a second set of values (k,ρ) for design is consistent with our use of the critical state model and we will call these rationally chosen design values the *critical state* strengths.

8.2 Hvorslev's Experiments on the Strength of Clay at Failure

Studies of the strength of clay specimens in Terzaghi's laboratory in Vienna succeeded in fusing together the concept of effective stress and Coulomb's concept of failure. We have already explained how Rendulic correctly generalized the effective stress concept, and now we outline Hvorslev's work.

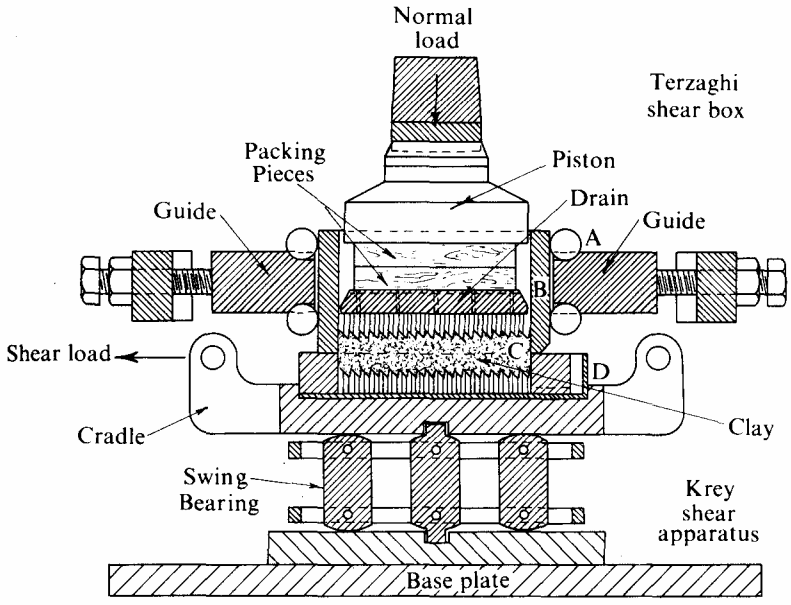

Fig. 8.2 Shear Apparatus used by Hvorslev

We know from the previous chapters 4, 5, and 6, that the specific volume of soil changes under changing effective stress, and we also know that yield strengths vary with specific volume. Equation (8.1), as it stands, takes no account of this change, and it was in elucidation of this point that the notable experiments of Hvorslev[3] made such a significant contribution.

Hvorslev used shear boxes of Terzaghi's design in a shear apparatus with a rocking cradle of Krey's design, as shown in Fig. 8.2. Clay specimens were consolidated from a slurry and brought into equilibrium under various normal loads. They were then subjected to successive increments of shear load: the experiments which we quote were very slow stress-controlled drained tests. Hvorslev defined 'failure' to be occurring under that shear

stress for which the very slow rates of shear displacement showed signs of continued acceleration.

Immediately after failure the shear boxes were quickly dismantled. A strip 3 mm thick and 2 cm wide was cut from the middle of the failure zone, as shown in Fig. 8.3; it was divided into five parts and the average water content for the zone of failure was determined. Observation of the rise or fall of the upper porous stone also indicated dilation or compression of the clay specimen during shear *before* failure.

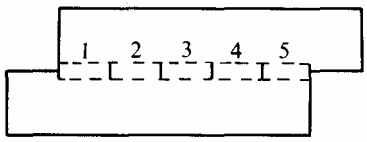

Fig. 8.3 Specimens for Determination of Final Water Content

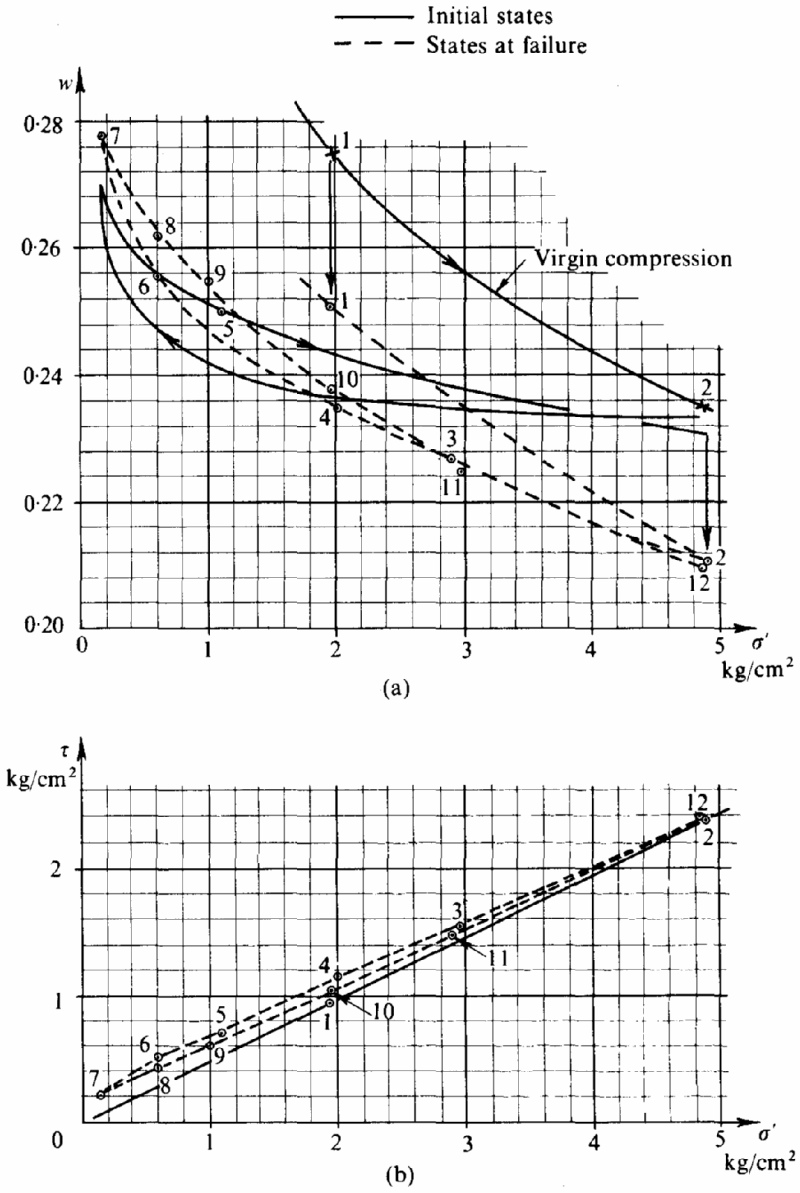

Fig. 8.4 Failure States of Specimens of Wiener Tegel V (After Hvorslev)

In Fig. 8.4(a) the solid line indicates a cycle of virgin compression, swelling, and recompression on a silty clay (Wiener Tegel V) said to resemble London clay. A dozen specimens were prepared each at a different stage in this cycle. Each specimen was then

sheared. Some exhibited a loss of water and others a gain during distortion. For all twelve specimens the circled dots indicate their state immediately after failure. A dashed line is drawn to link these points but this does not mean that a specimen changes; for instance, from the state at failure for 1 to the state at failure for 2. In Fig. 8.4(b) the set of failure strengths of these specimens is shown.

The data of Fig. 8.4 appear confusing, but Hvorslev introduced a major simplification. In Fig. 8.5 we re-plot the dashed curves of Fig. 8.4 together with the solid curve for virgin compression. For each water content on the dashed curve we read at the same water content on the solid curve a normal pressure which Hvorslev called the equivalent compressive pressure σ'_e; for clarity, only points 1, 4, and 7 are shown. Hvorslev found the equivalent pressures and replotted the data of Fig. 8.4(b) in the form of Fig. 8.6. All data lie on one straight line

$$\frac{\tau}{\sigma'_e} = k_0 + \frac{\sigma'}{\sigma'_e}\tan\rho_0 \qquad (8.2)$$

Introducing an equation for the virgin compression curve (in which l is an appropriate constant)

$$\left.\begin{aligned} & w - w_0 = -l\ln\sigma'_e \\ \text{or} \quad & \sigma'_e = \frac{\exp(w_0 - w)}{l} \end{aligned}\right\} \qquad (8.3)$$

we obtain an alternative form

$$\left.\begin{aligned} & \tau = k + \sigma'\tan\rho_0 \\ \text{where} \quad & k = k(w) = \frac{k_0 \exp w_0}{l}\exp(-w) \end{aligned}\right\} \qquad (8.4)$$

These equations (8.4) elucidate a major significance of the Coulomb equation: it is that the cohesion component ***k*** increases exponentially with decrease of water content.

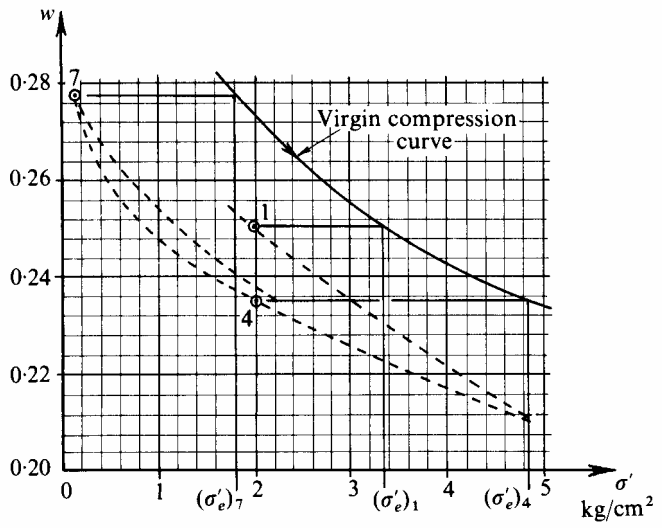

Fig. 8.5 Derivation of Equivalent Pressure (After Hvorslev)

This excellent set of accurate data was not subject to sufficiently close scrutiny by subsequent workers. It was not appreciated that the phenomenon that Hvorslev called failure was only observed in a limited range of states of soil: for Wiener Tegel V in Fig. 8.7 the range II is $0.05 < (\sigma'/\sigma'_e) < 0.6$ and it is most striking[4] that in range I for

$0.6 < (\sigma'/\sigma'_e)$ *no* failure was observed. There is an accumulation of points at the end C of the line on the boundary between regions I and II; in the light of the work of previous chapters we readily see that C indicates the near vicinity of the critical state. Specimens originally in region I, being wetter than critical, will have moved through that region in process of yielding without failure; not until they approach the critical states will failure have terminated the yielding process.

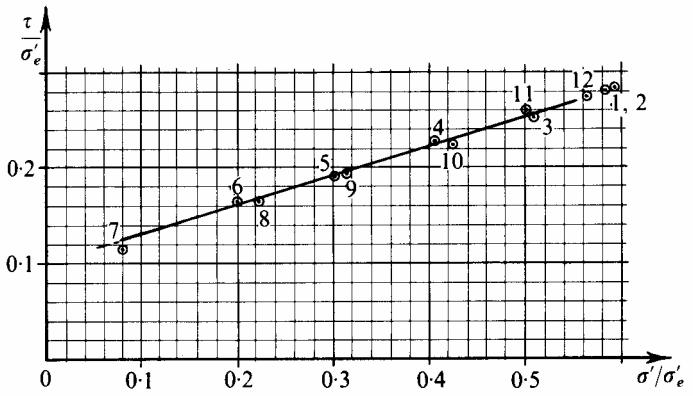

Fig. 8.6 Data of Failure (Wiener Tegel V) (After Hvorslev)

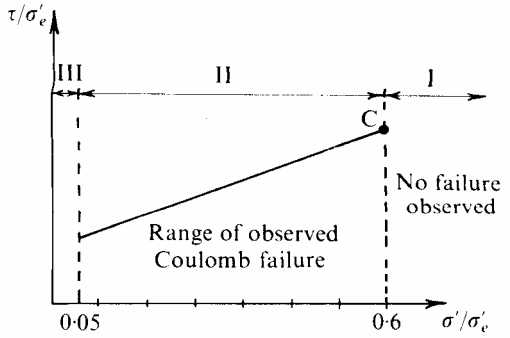

Fig. 8.7 Range of Observed Data of Failure

It is therefore clearly wrong to represent Hvorslev's results in the manner shown in Fig. 8.8(a), as some workers have done. It is wrong to consider the line OC to represent successive states of plastic compression in the presence of shear. In the near vicinity of the critical states plastic *distortion* increments are very large and no presently available test apparatus can hold a specimen in a condition close to the critical states sufficiently long for any controlled plastic *compression* to be imposed. It is also wrong to extend the lines of eq. (8.4) across the line OC into region I where Hvorslev did not obtain data of failure. A correct way to represent Hvorslev's equation is shown in Figs. 8.8(b) and (c) where we show what we call the *Hvorslev – Coulomb* surface in (σ', w, τ) space. This surface applies to a limited range of states *of failure* in the near vicinity (and rather to the dry side) of the critical states.

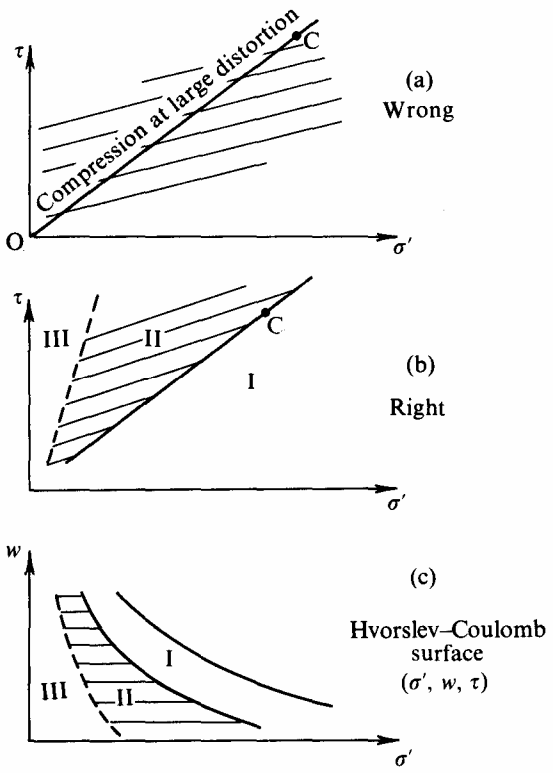

Fig. 8.8 Hvorslev – Coulomb Surface

Hvorslev himself went on from shear box tests to apply his criterion to analysis of some unconfined compression tests. He used q for the axial-deviator stress, and we have adhered to this usage. He suggested that Mises' function F of eq. (2.12) could be employed for soils. We can introduce a generalization of our parameters,

$$(\sigma'_2-\sigma'_3)^2+(\sigma'_3-\sigma'_1)^2+(\sigma'_1-\sigma'_2)^2=2q^{*2}$$

and

$$(\sigma'_1+\sigma'_2+\sigma'_3)=3p^*$$

and appendix C generalizes the Granta-gravel yield function in a form $F(p^*, v, q^*)=0$ that fulfils Hvorslev's suggestion. However, we also see that such yielding occurs in region I of Fig. 8.8 whereas we associate Coulomb's rupture with region II.

8.3 Principal Stress Ratio in Soil about to Fail

The Hvorslev – Coulomb surface specifies stress components only on the failure plane. From chapter 2 and appendix A we readily appreciate that this does not fully specify all the principal effective stress components in the soil continuum when it is yielding and about to fail. Let us assume that the rupture surface will be acted on by the maximum and minimum principal effective stresses σ'_{max} and σ'_{min}, so that the intermediate principal effective stress can have any magnitude in the range $\sigma'_{max} \rightarrow \sigma'_{min}$ without affecting the equilibrium or the inclination of the failure surface. We still need some additional assumption if we are to calculate the ratio of principal stresses $\sigma'_{max}/\sigma'_{min}$ in soil about to fail.

The first assumption to be considered is that of Rankine, who studied soil without cohesion ($k = 0$) or pore-pressure ($u_w = 0$). He asserted that in a continuous body of soil when the ratio of principal stresses reached its peak the obliquity of the stress vector on any plane could not exceed the angle of friction ρ. It followed, as we will see below, that Rankine could write

$$\frac{\sigma'_{\max}}{\sigma'_{\min}} \le \frac{1+\sin\rho}{1-\sin\rho} \tag{8.5}$$

A generalization became possible following the introduction of Mohr's circle of effective stress, see appendix A. For soil with cohesion k and friction ρ, introducing the notation

$$H = k\cot\rho \tag{8.6}$$

in Fig. 8.9, we see from the geometry of the figure that

$$\frac{\sigma'_{\max}+H}{\sigma'_{\min}+H} = \frac{\mathrm{JR}}{\mathrm{JP}} = \frac{\mathrm{RN}}{\mathrm{PL}} \quad (\Delta JPL \text{ similar to } \Delta JRN)$$

$$= \frac{\mathrm{RN}}{\mathrm{PL}} \quad (\text{tangents to circle from N and L})$$

$$= \frac{\mathrm{QM}\tan \mathrm{M\hat{Q}N}}{\mathrm{QM}\cot \mathrm{M\hat{L}Q}} \qquad (\text{tangents to circle from N and L})$$

but $\mathrm{M\hat{Q}N} = (\pi/4 + \rho/2) = \mathrm{M\hat{L}Q}$, so

$$\frac{\sigma'_{\max}+H}{\sigma'_{\min}+H} = \tan^2\left(\frac{\pi}{4}+\frac{\rho}{2}\right) = \left(\frac{1+\sin\rho}{1-\sin\rho}\right). \tag{8.7}$$

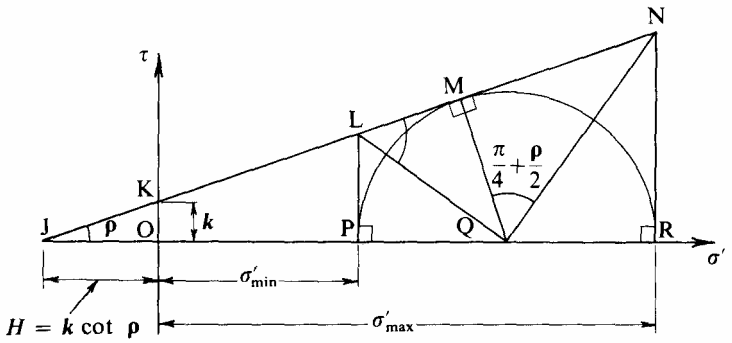

Fig. 8.9 Mohr–Rankine Criterion

Introducing $k = 0 = H$ we find Rankine's earlier expression to be included in eq. (8.7), which we now will call the *Mohr–Rankine* criterion for peak effective stress ratios in soil about to fail.

A distinction has now been made between the peak stress criterion in which the soil body is still considered to be a homogeneous continuum, and the Hvorslev–Coulomb equation for limiting equilibrium between two separate parts of an only just ruptured body. Further, we note that, at the Mohr–Rankine peak stress ratio, there are *two* directions through a soil body of planes on which the obliquities of stress vector are identical. The Mohr–Rankine criterion does not indicate in which of the two directions the Coulomb rupture is expected to be propagated.

A further uncertainty becomes apparent when we try to represent the Mohr–Rankine criterion in the (q, p) plane. At one extreme we have the extension test with the intermediate stress equal to the *major* principal stress, and at the other extreme the compression test where it is equal to the *minor* principal stress. Let us consider the simple case without cohesion, $k = 0$. The first possibility involves failure in extension with $\sigma'_r = \sigma'_{\max}$, $\sigma'_l = \sigma'_{\min}$, and

$$\sigma'_r = \left(\frac{1+\sin\rho}{1-\sin\rho}\right)\sigma'_l,$$

in which case

$$p = \frac{\sigma'_l + 2\sigma'_r}{3} = \left(\frac{3 + \sin\rho}{3 - 3\sin\rho}\right)\sigma'_l$$

$$-q = (\sigma'_r - \sigma'_l) = \left(\frac{2\sin\rho}{1 - \sin\rho}\right)\sigma'_l$$

so that $$\left(\frac{-q}{p}\right)_{\text{peak}} = \frac{6\sin\rho}{3 + \sin\rho} \quad (\sigma'_r > \sigma'_l). \tag{8.8}$$

The second possibility involves failure in compression with $\sigma'_l = \sigma'_{\max}$, $\sigma'_r = \sigma'_{\min}$, and

$$\sigma'_l = \left(\frac{1 + \sin\rho}{1 - \sin\rho}\right)\sigma'_r$$

which gives

$$\left(\frac{+q}{p}\right)_{peak} = \frac{6\sin\rho}{3 - \sin\rho} \quad (\sigma'_l > \sigma'_r). \tag{8.9}$$

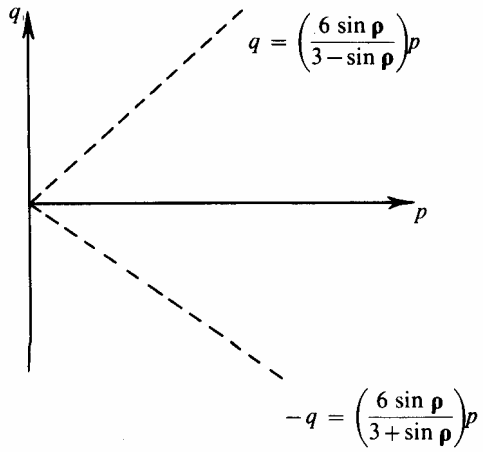

Fig. 8.10 Mohr–Rankine Limiting-stress Ratios

Thus there are two lines which are drawn dotted on the (q, p) plane, Fig. 8.10, and which indicate states when compression and extension tests respectively reach their peak Mohr–Rankine stress ratio.

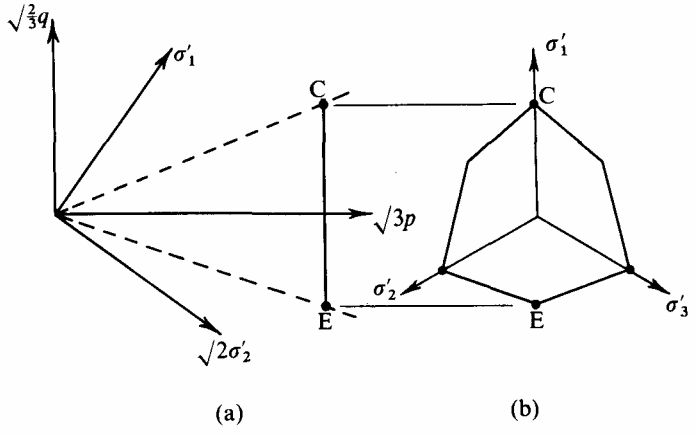

Fig. 8.11 Mohr–Rankine Criterion in Principal Stress Space

If we also want the principal stress space representation we simply convert scales by factors of $\sqrt{\frac{2}{3}}$ and $\sqrt{3}$, and obtain the dotted lines in Fig. 8.11(a). A section of principal stress space on the plane CE normal to the space diagonal is shown in Figs. 8.11(b) and 8.12. The peak stresses in Fig. 8.12 now lie on an irregular hexagonal cone of an almost triangular section in the plane perpendicular to the space diagonal. Principal points on the Mohr–Rankine peak stress locus are C and E, which refer to peak stress ratios in compression and extension.[5]

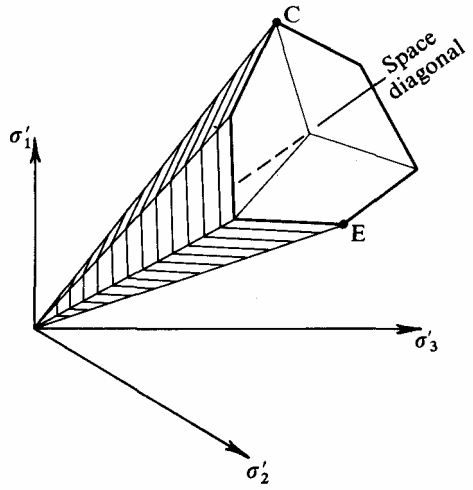

Fig. 8.12 Mohr–Rankine Limiting Surface for **k**=O

The yield surface of Fig. 5.1 is a surface of rotation about the space diagonal which, for states rather drier than critical, lies outside the irregular cone of Fig. 8.12. Thus, the Mohr – Rankine criterion predicts that for these states a limiting stress ratio occurs before the yield surface is reached. We now compare this prediction with some data of states of failure.

8.4 Data of States of Failure

We have already discussed the data of experiments which Henkel interpreted to give broad support to Rendulic's generalized effective stress principle. In Figs. 7.22 and 7.23 we see that state paths end with 'failure states' which lie on two lines rather similarly placed in their asymmetry about the space diagonal as the prediction of the Mohr – Rankine criterion. In detail neither a simple critical state curve, nor a simple Mohr – Rankine criterion with constant cohesion, will fit these data of *failure;* it is necessary to have cohesion varying with water content.

In Fig. 8.13 we present data of a comprehensive series of tests on Weald clay reported by Parry.[6] Each point shown is the failure condition (defined by maximum axial-deviator stress q) for one separate axial test quoted in Parry's tables. This series includes both compression and extension tests: and in each category three types of drained test ((a) σ'_r constant, (b) σ'_l constant, (c) p constant), and two types of undrained test ((a) σ_r constant (b) σ_l constant).

The results have been plotted in the same format as Hvorslev's presentation of Fig. 8.6, except that we have introduced a minor variation in our choice of parameters. Instead of dividing by Hvorslev's equivalent pressure σ'_e (or p_e) to make the parameters

dimensionless, we have divided by p_u which has exactly the same effect. The effective spherical pressure p_u can be plotted on the critical state line at the particular value of the water content w_f of each separate specimen at failure, whereas a point (p_e, w_f) could be plotted on the virgin compression line. The actual values adopted for p_u were taken from the similar plot to that of Fig. 7.5 for Weald clay. From chapter 6 we have already established that the ratio $p_e / p_u = \exp \Lambda$ and should be constant for any particular clay.

We see that although these data of failure are from a wide variety of tests (with significantly different stress paths) they are closely represented by a pair of lines of the Mohr – Rankine type of Fig. 8.10,

$$\frac{\sigma'_{\max} + H}{\sigma'_{\min} + H} = \frac{1 + \sin\rho}{1 - \sin\rho} = 1.95$$

where $H = 0.2 p_u = 0.107 p_e$ and $\rho = 18°47'$.

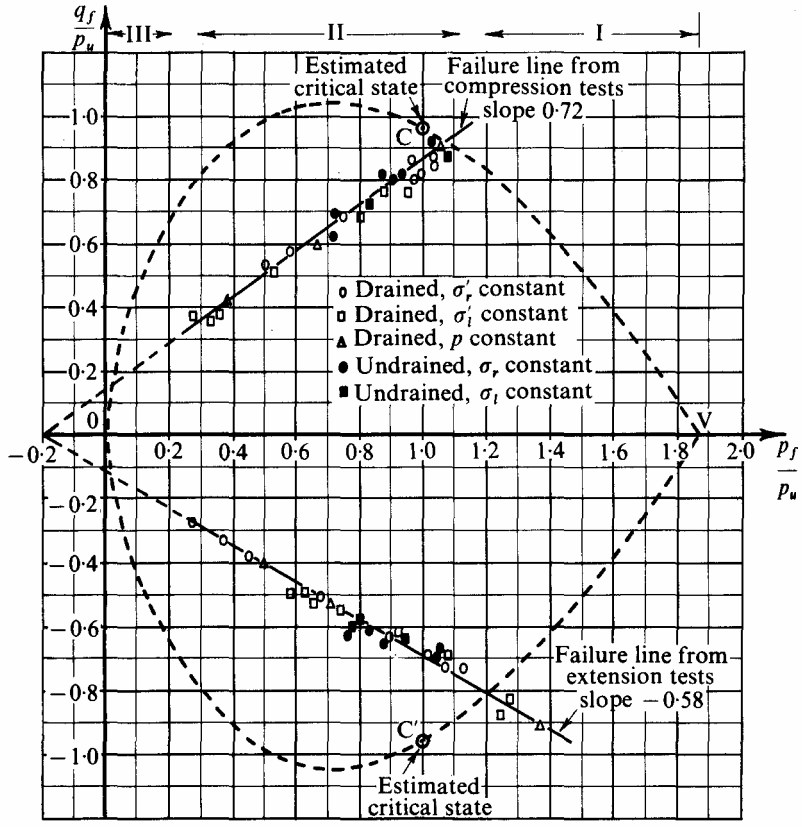

Fig. 8.13 Data of Failure from Tests on Weald Clay (After Parry)

The line for compression is from eq. (8.9)

$$\frac{+q_f}{p_f + 0.2 p_u} = \frac{6 \times 0.322}{3 - 0.322} = 0.72 \tag{8.10}$$

and the line for extension is from eq. (8.8)

$$\frac{-q_f}{p_f + 0.2 p_u} = \frac{6 \times 0.322}{3 + 0.322} = 0.58 \tag{8.11}$$

and the line for extension is from eq. (8.8)

$$\frac{-q_f}{p_f + 0.2 p_u} = \frac{6 \times 0.322}{3 + 0.322} = 0.58 \tag{8.11}$$

The closeness of the fitting suggests that we can extend Hvorslev's concept of cohesion as a function of specific volume (or water content), and introduce this concept also in the Mohr – Rankine peak stress ratio criterion.

As before, there is a range II of p_f / p_u to which the failure criterion is applicable, and to either side there are ranges I and III in which there are no data of *failure:* although the positions of the exact boundaries to range II are open to some doubt.

Also plotted is the section of the boundary surface appropriate to Weald clay which has an average $\kappa = 0.0346, \lambda = 0.093, \text{and } M = 0.95.$ This gives $\Lambda = 0.628$ and $p_e / p_u = \exp \Lambda = 1.875.$ With the exception of three results from extension tests this curve encloses all the data. (Extension tests are more susceptible to experimental error than conventional compression tests, particularly in regard to estimates of water content at failure w_f. Any error in w_f leads to a wrong choice of p_u which would move a plotted point directly towards or away from the origin of coordinates O.)

This use of the Coulomb equation to fit data of failure is close in essence to Hvorslev's use of the same equation with cohesion as a function of water content. We will not offer a theoretical explanation for the closeness of this fitting, but it is helpful to compare and contrast Figs. 8.13, 7.12, and 5.18. We began with a theoretical rigid/plastic model for which we predicted rigidity within a certain area of Fig. 5.18: we supposed that in a certain area of that figure stable yielding could progress towards an ultimate critical state. We learn from experiments that stable yielding does occur in the undrained axial test but in Fig. 7.12 we see failure intervene just before the specimen reaches a critical state. Now we find that lines such as those in Fig. 8.13 cut across the area of rigidity in Fig. 5.18, and these lines mark the *peak* stress ratios that can be attained.

Perhaps it is helpful here to draw an analogy with the simple theory of buckling of struts in which experiments on real struts terminate at peak loads less than the limiting loads predicted by simple elastic theory.

8.5 A Failure Mechanism and the Residual Strength on Sliding Surfaces

So far we have shown, for intact soil specimens, that the Mohr – Rankine or Hvorslev – Coulomb criteria do describe the limiting condition just before propagation of a failure surface. We now must consider what happens at and after such failure.

Consider in Fig. 8.14 the state path AB which Hvorslev's clay could have followed if it had been homogeneously remoulded at constant σ'. The portion AB represents deformation of the intact specimen before peak stress. The fact that when Hvorslev sampled water content he did not find all circled points in Fig. 8.4(a) lying close to the critical states, but rather found water contents such as B in Fig. 8.14(b), shows that the specimens stopped behaving uniformly at peak deviator stress. Photographs showed very thin slip zones or rupture surfaces in which most distortion became concentrated after failure. We show, in Fig. 8.15(a), the water content slice and, in Figs. 8.15(b), (c), a much magnified view of the 3 mm thick slice. Figure 8.15(b) shows homogeneous distortion and

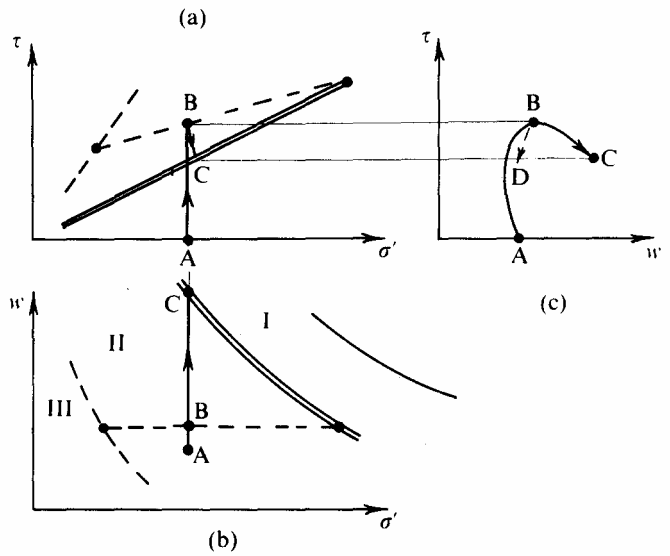

Fig. 8.14 Change in State at Failure in Drained Shear Test

uniform water content just *before* failure. Upon failure, soil in the thin slip zone experiences dilation (increase of water content) and *weakens* (decrease of shear strength τ) following path BC in Fig. 8.14(c). The gain in water content of the failure region is *temporarily* at the expense of the blocks to either side of the failure surface, which experience loss of water and increase of *stiffness* as the stress decreased following path BD in Fig. 8.14(c). Consequently, displacements are concentrated in the thin failure zone and Fig. 8.15(c) also shows water content change in the vicinity of the failure. Water is shown

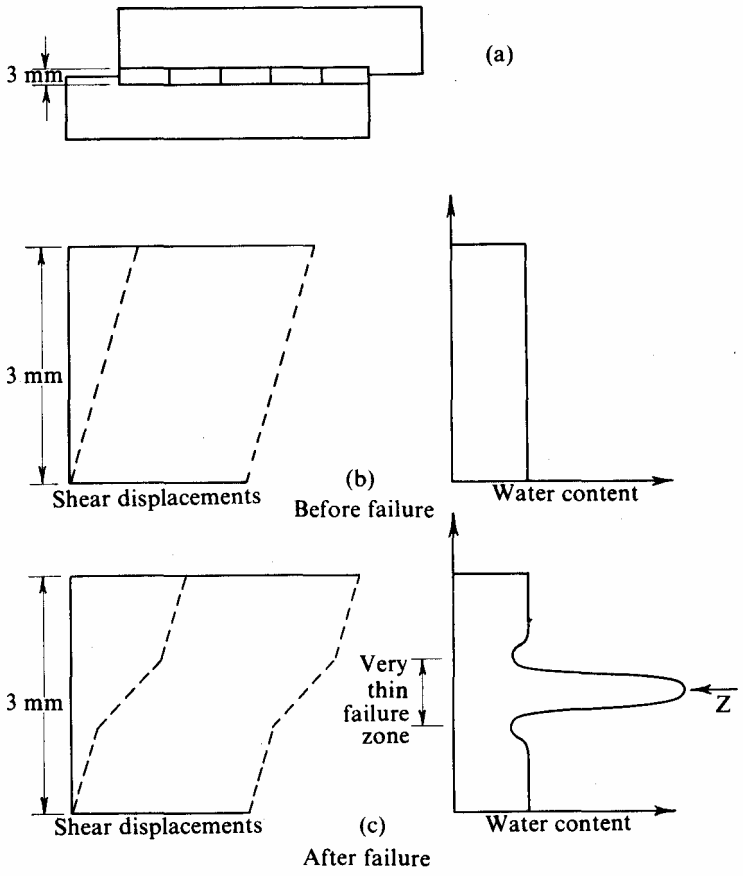

Fig. 8.15 Conditions in a Slip Zone

being sucked, with presumably a small value of pore- pressure, in towards the slip zone Z, but Hvorslev's rapid dismantling process ensured that the average water content that he measured represented the water content just before and at failure. By this interpretation the Hvorslev – Coulomb equation applies to peak stress ratios of an intact soil body.

The sucking in of water towards the thin slip zone, illustrated in Fig. 8.15(c), has been observed in the field. In an investigation of a retaining wall failure (which will be discussed at length in §8.8) Henkel reported the water content variation shown in Fig. 8.16,

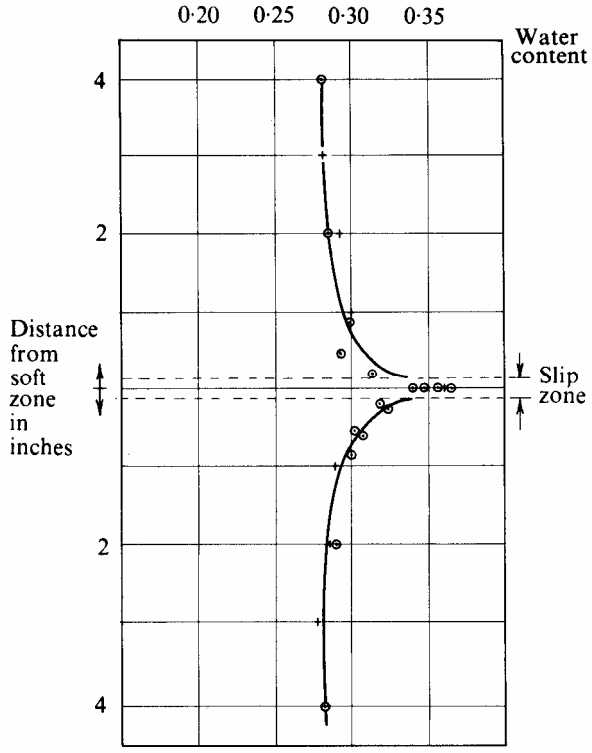

Fig. 8.16 Observations of Water Content of a Slip Zone (After Henkel)

and associated this with local dilation accompanying severe local shear strains. It is consistent with our critical state theories to link the changing water content with fall of stress from peak values (on the dry side) to critical state values.

As displacement on the rupture surface increases there appears to be some development of anisotropy: Hvorslev writes of a significant permanent change of structure in the vicinity of the rupture surface, which permitted one clay sample to be separated into two blocks along the rupture surface which was then seen to possess a dull shine.

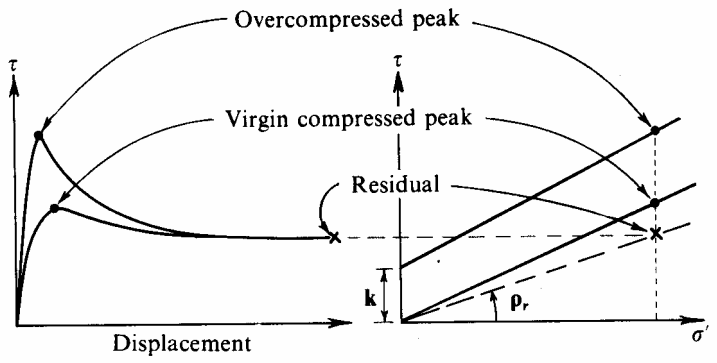

Fig. 8.17 Skempton's Definition of Residual Strength

Gould[7] studied landslides in coastal California and from their evident limiting equilibrium concluded that 'the strength actually mobilized in slides or mass creep is inversely proportional to the amount of displacement which has occurred previously in the shear zone'. He considered that 'the means by which large shear strain eliminates true cohesion is not clear', but writes of a 'pattern of irregular slick surfaces'. Wroth8 studied the strength of randomly packed 1 mm steel balls in simple shear, and found that after very large cumulative shear distortion the ultimate strength fell to two-thirds of the critical state strength, and this deterioration of strength was seen to correspond to a development of regularity of packing in the material. Hence, although it is consistent with our critical state concepts to predict a fall of strength from peak values (on the dry side) to critical state values, it is also clear that large displacements on sliding surfaces have to be associated with a further fall below the critical state values.

Skempton[9] (in the fourth Rankine lecture of the British Geotechnical Society in 1964) discusses the fall of strength, and a figure such as his Fig. 6 (our Fig. 8.17) shows the typical curves relating increasing displacement to fall of strength from peak values to what he identifies as a *residual strength* value. He also correlates fall of strength with passage of time after failure, but it is more consistent with our purely mechanical interpretation of the yielding of soil for us to follow Gould and associate fall of strength only with displacement on the rupture surface. Skempton shows (Fig. 8.17) a line of peak strengths of overcompressed soil which we reproduce in Fig. 8.18(a) as the line ABC, and a line of residual strengths which we reproduce as the line OEF. Between these lines Skempton interposes a line of peak strengths of virgin or lightly overcompressed soil. We see in Fig. 7.12 that the peak strength of axial compression tests of such soil occurs just before the critical state is reached. We wish to introduce in Fig. 8.18(a) a line ODC which corresponds to the critical state strengths.

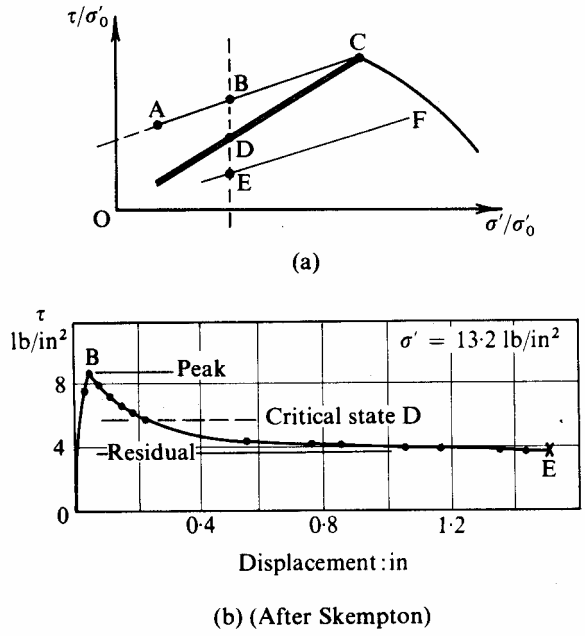

Fig. 8.18 Definition of Critical State Strength

The introduction of line ODC in Fig. 8.18(a) is based simply on our desire to approach this problem from a point of view that is consistent with our critical state theories. As soon as we attempt to define precisely the slope of the line ODC we find a deficiency in the existing development of our theories in that the symbols τ and σ' have

not appeared so far. To fit the Mohr-Rankine limiting surface of Fig. 8.12 to conditions in the rupture zone we must take $k = 0$ for soil in the critical state, so that $\tau = \sigma' \tan \rho$. We see that the peak of the undrained axial compression test of Fig. 7.12 occurs when $q/p \cong M$, so to fit ρ to the critical state we must, for example, use

$$\frac{q}{p} = M = 0.88 \qquad \text{for London clay,}$$

together with eq. (8.9)

$$\frac{6 \sin \rho}{3 - \sin \rho} = \left(\frac{q}{p} \right)_{\text{peak}} \cong M = 0.88$$

to give

$$\sin \rho = 0.383, \quad \rho = 22\tfrac{1}{2}^{\circ}, \qquad \text{for London clay}^{10}.$$

This gives $\tan \rho = 0.415$ and in Fig. 8.18(a) the line ODC has been drawn at the slope

$$\frac{\tau}{\sigma'} = 0.415$$

In Fig. 8.18(b) we show Skempton's curve for the fall of strength of weathered London clay at Hendon, with $\sigma' = 13.2\,\text{lb/in}^2$. For this we calculate

$$\tau = 0.415 \qquad \sigma' = 5.5\,\text{lb/in}^2$$

which is plotted in Fig. 8.18(b). It lies about half-way between Skempton's peak value and his residual value. Skempton himself introduces a residual factor R for interpolation between these extremes. It seems that our use of a critical state theory agrees well with the use of a residual factor that Skempton proposes in this case.

As the overcompression ratio increases, the line BDE in Fig. 8.18(a) will move nearer the origin with the consequence that the ratio (BD/BE) will increase. This suggests the use of a residual factor that increases with overcompression ratio N.

8.6 Design Calculations

In order to help us to stand back from the close detail of interpretation of data, and to take a rather more broad view of the general problems of design, let us review the well-known calculations that occur in structural engineering design. Design of a structure such as a welded steel portal frame, Fig. 8.19(a), can involve two stages of calculation. In one stage, Fig. 8.19(b), some simple calculations are made of the collapse of the frame under various extreme loadings, and the design consideration might be that when the expected working loads are increased by a load factor (for example this might be 2) the structure should not quite collapse. In another stage, Fig. 8.19(c), other calculations are made of the performance of the frame under various working conditions, and the design consideration might be that the deflections or perhaps the natural period of vibration of the structure should be within certain limits. At one stage of the design the steel is represented by a rigid/plastic model with a characteristic yield strength (fully plastic moment M_p in Fig. 8.19(e)). At another stage of the design the steel is represented by an elastic model with a characteristic elastic stiffness (EI in Fig. 8.19(f)). Experimental moment-curvature data for the steel, Fig. 8.19(d), are such that one model applies in one range of the data and another model applies in another range. Each design calculation illuminates one aspect of performance of the structure, and both are of importance to the designer.

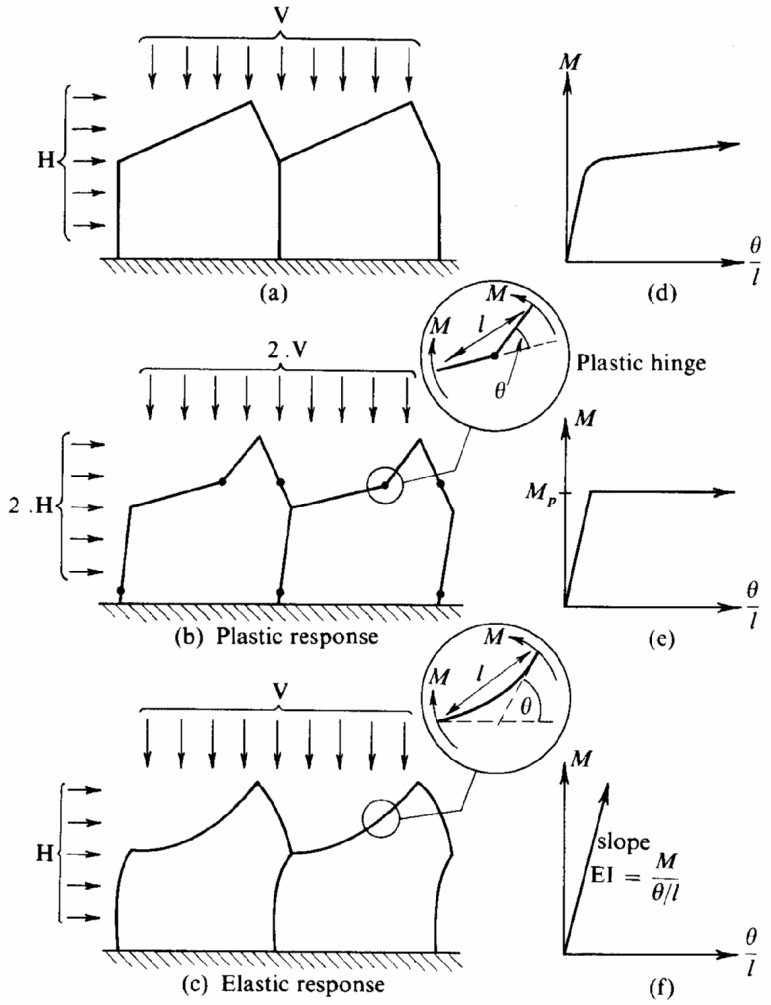

Fig. 8.19 Design of Steel Portal Frame

In soil mechanics we also have a variety of calculations that are appropriate to various aspects of design. Each calculation involves a well defined model such as those discussed in chapters 3 and 4, and the engineer must choose values for parameters such as permeability or compressibility that are appropriate to each specific soil. There is a well known and extensive set of classical calculations of limiting equilibrium based on Coulomb's equation, and Bishop and Bjerrum2 have discussed in a joint paper two different types of problem concerning the performance of loaded bodies of soil for which these classical calculations are appropriate, provided that the strength parameters (***k***, ρ) are chosen in a rational manner. It is usual to introduce a *factor of safety* to cover inadequacies in the design calculations. In a passage of his 1776 paper Coulomb expressed a wish that his retaining wall design should offer a resistance 'd'un quart en sus de celle qui seroit nécessaire pour l'équilibre' (a quarter above what is needed for equilibrium). Thus Coulomb used a load factor of 125, and today, in slope stability calculations, engineers adopt a similar value for a factor of safety applied to the chosen strength parameters. This is a low value which is clearly not appropriate to a peak strength such as is shown in Fig. 8.18, but which does appear to be appropriate to critical state strengths.

The two types of problem are:

I. The *immediate* problem of the equilibrium of soft 'wet' soil under rapidly applied loading. The whole soil mass yields as a perfectly plastic body with positive pore-pressure being generated throughout the interior (the significant lengths H of drainage path are of the same order as the overall dimensions of the body and the half- settlement times are long in comparison with typical loading times). Bishop and Bjerrum quote many cases for which the classical calculations with values (which are in effect critical state strengths)

$$k = c_u \quad \text{and} \quad \tan\rho = 0 \tag{8.12}$$

are clearly appropriate.

II. The *long-term* problem of the equilibrium of firm 'dry' soil. Under an increase of deviatoric stress without increase of effective spherical pressure, the whole soil body may rupture into a rubble of lubricated blocks (the significant lengths H of drainage paths are of the same order as the thickness of a slip zone). In typical cases the loading is sustained for a sufficient time for the conditions of the problem to become effectively 'drained' in the sense suggested in §4.6. Bishop and Bjerrum quote cases of long-term failure for which classical calculations *either* with values

$$k = 0 \quad \textit{and} \quad \frac{6\sin\rho}{3 - \sin\rho} = M \tag{8.13}$$

or with $k = 0$ and ρ at some suitable *residual* value would have been appropriate in design.

In identifying these two groups of problems, Bishop and Bjerrum drew on a wide experience of many case histories. We will not repeat their list of cases but will concentrate on two examples of failures which are well documented in the literature of the subject.

8.7 An Example of an Immediate Problem of Limiting Equilibrium

At a building site between Stirling and Glasgow in Scotland, during the construction of the roof of a single-storey building, the most heavily loaded footing failed and caused structural damage. Calculations subsequently showed[11] that this footing, at a depth of about 5 ft 6 in below ground level, had applied a net increase of pressure of about 2500 lb/ft^2 on an underlying layer of about 14 ft of soft clay. In the site investigation Skempton took small undisturbed cylindrical samples of the soft clay and tested them in rapid unconfined compression; the results, shown in Fig; 8.20, indicate that the soft clay had strength c_u of about 350 lb/ft^2. Skempton used alternative methods of calculation including

(a) limiting equilibrium with cohesion k alone on a slip circle (this type of calculation will be discussed in §9.4), and
(b) limiting equilibrium of a two-dimensional stress distribution in a purely cohesive soil (this type of calculation will be discussed in §9.6.1).

By these methods he estimated the bearing capacity of the clay layer to be about 2300 lb/ft^2. With various arguments which it is inappropriate to discuss in detail here, he demonstrated that this estimated bearing capacity correlated well with the increase of pressure that actually caused failure.

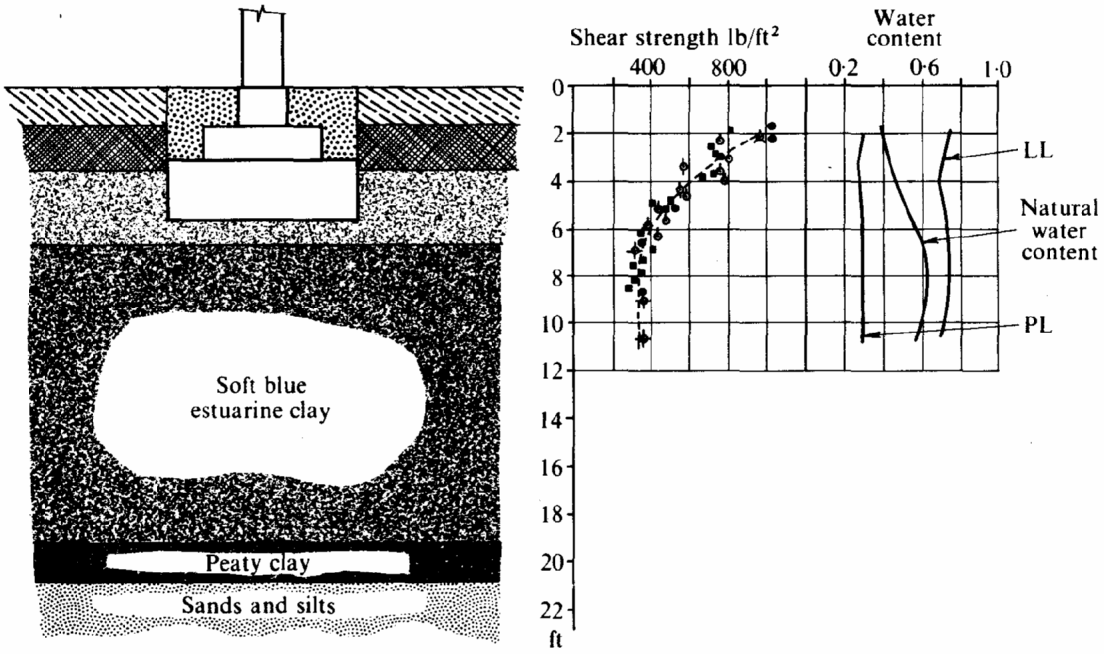

Fig. 8.20 An Example of an Immediate Failure of Bearing Capacity (After Skempton)

We need to review the reasons why, in this case, the immediate limiting equilibrium calculation using $k=c_u$, $\rho = 0$, was appropriate. In the first place the calculated amount of consolidation which took place in the few months of construction was negligible. The clay was compelled to deform at the same constant specific volume as it had initially, and whatever pore-pressures were generated would have had no time to dissipate. Second, although the clay might have been slightly overcompressed, the possible undrained test paths as shown in Fig. 7.28(a) all come to an end near the ultimate critical state point C. In the fully deformed state any history of overcompression would have been eradicated and the *effective* spherical pressure would have come close to the critical state value in Fig. 7.28(a). The *total* pressures could then be whatever values were applied, since any change in total pressure would simply cause variation of pore-pressure. (We know that *total* pressure cannot generate friction in an analogous situation when we accidentally tread on a bladder full of water, such as a rubber hot-water bottle. The weight on the foot generates water pressure but there is little pressure generated between the internal faces of the bladder so that there is little friction.) In Fig. 7.26 we see that $q_u = Mp_u$; the strength has a frictional character but it depends on the mean effective spherical pressure p_u in the deforming clay. The total pressure cannot alter the mean effective pressure unless there is some change in the specific volume, v_0 in Fig. 7.25. So the limiting equilibrium calculation proceeds on the basis of a constant (low) value of shear strength $k = c_u$, and no friction.

8.8 An Example of the Long-term Problem of Limiting Equilibrium

It is less easy to find good text-book examples of the drained than the undrained limiting equilibrium problem. Our choice of a retaining wall failure is dictated by the ease with which the original paper[12] can be found and the clarity with which the description and discussion[13] is developed.

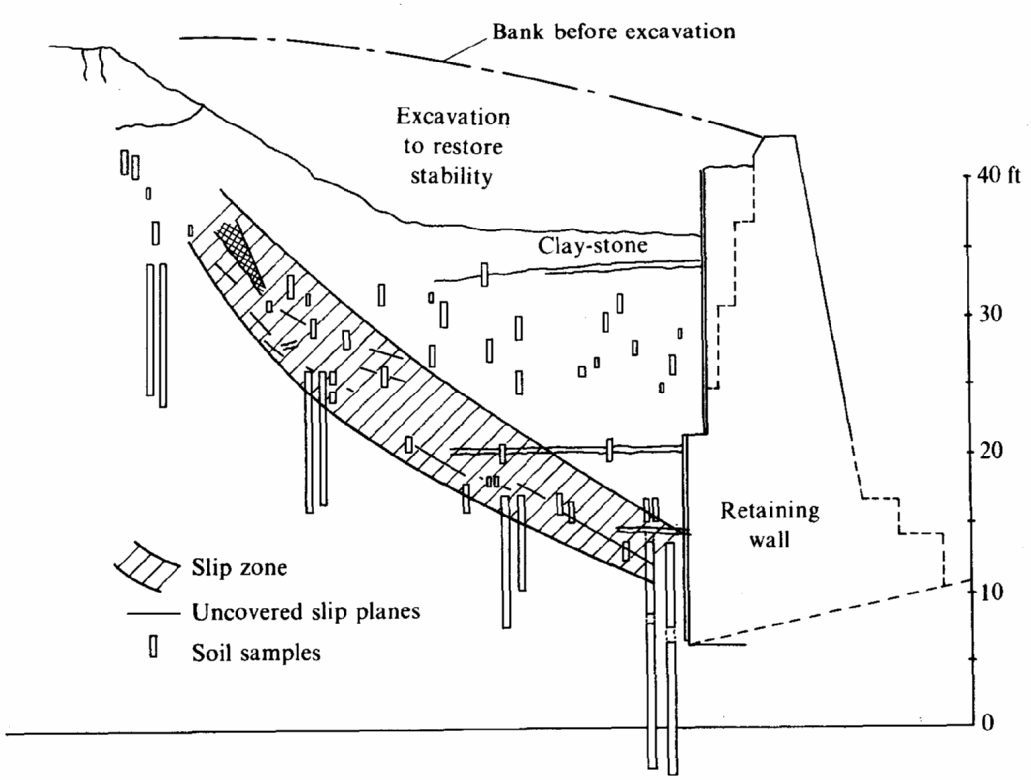

8.21 An Example of Long-term Failure of Retaining Wall (After Watson)

A railway cutting was made in 1912 through a gently sloping clay hill near Uxbridge, which is a suburb of London. Since then there has been a history of intermittent slips; and in 1937 when the railway was widened and a new retaining wall built, a serious slip occurred during its construction. The slope behind the wall cracked and was made good with hard-core rubble to support some houses at the top of the slope. In 1954 another serious slip broke the wall, and renewed cracks at the head of the slope made it necessary to demolish the houses. Forward movement of the toe of the wall menaced the railway tracks but promptly executed remedial works arrested movement and restored stability. The paper shows, Fig. 8.21, the findings of a site investigation by means of a trench cut into the slope. The stiff fissured London clay contained an inclined layer within which there were many thin slip zones which are seen to be *not* continuous. These thin slip zones were 'clearly exposed since large chunks of clay slipped away when digging near the surfaces, which appeared to consist of very thin moist slide-surfaces with marks of relative movement rather than softened zones'. Borings were put down in an endeavour to find these 'moist slide-surfaces', but examination of several samples known to be driven across slide-surfaces uncovered in the trench failed to locate the surfaces in the laboratory. Only in one sample did the moist zone attain sufficient thickness (about 50 mm) for increase of water content to show the results already indicated in Fig. 8.16. (Even at that thickness the remoulded softened clay paste in the slip zone remains 'drained' rather than 'undrained' in relation to the time of construction and loading.)

Henkel reported in the discussion the results of limiting equilibrium calculations which used straight slip surfaces in a manner outlined in the examples of §9.1 and §9.2. Henkel's choice of parameters was the value of $\rho = 20°$ that he found from an interpretation of data of peak-strengths of London clay specimens in the manner of §8.4, but he then found that the value of $\boldsymbol{k}$, which could have been contributing to stability of the ground which actually failed, was less than the peak value. In §8.6 from eq. (8.13) we suggest the comparable critical state parameters $\boldsymbol{k} = 0$ and $\rho = 22½°$ for London clay.

When such failure first takes place the body of clay disintegrates into a rubble of lubricated blocks, sliding on each other on very thin moist zones of soft, lubricating clay paste. Critical state theory explains the failure mechanism, and also gives us the key to the behaviour of this lubricating clay paste. The soft clay is being severely remoulded but it can only soften to the critical state that corresponds with its effective spherical pressure. This pressure, and the corresponding critical state strength, increase with depth in the rubble. The 'friction' concept involves a resistance to relative motion that depends on the effective stress between blocks. We can apply the well established friction calculations to the limiting equilibrium of a slipping rubble of clay blocks only because the strength with which the blocks adhere to each other is proportional to the pressure that has long been effective between them.

8.9 Summary

In chapter *5* we began asking what state of effective stress could be sustained in stable equilibrium by a block of our first model soil. We then developed a new group of critical state theories of yielding of soil but found that as yielding progressed there came a stage at which soil specimens in actual test systems 'failed' before they could be brought into a critical state. The data of peak strengths proved to be capable of very close description by the Coulomb equation, when properly modified to account for the effect of water content changes on cohesion. However, in classical calculations of limiting equilibrium for design purposes, it proves rational in general to use strength parameters ***(k,*** ρ) that are based on the critical state model rather than on the peak strengths. In chapter 9, the actual classical calculations of limiting equilibrium are given attention.

References to Chapter 8

1. Coulomb, C. A. Essai sur une application des règles de maximis et minimis a quelques problèmes de statique, relatifs a l'architecture, *Mémoires de Marhématique de l'Académie Royale des Sciences,* Paris, 7, 343 – 82, 1776.
2. Bishop, A. W. and Bjerrum, L. The Relevance of the Triaxial Test to the Solution of Stability Problems, *Res. Conf. on Shear Strength of Cohesive Soils, A.S.C.E.,* Boulder, pp. 437 – 501, 1960.
3. Hvorslev, M. J. *(Iber die Festigkeitseigenschaften Gestörter Bindiger Böden,* Køpenhavn, 1937.
4. Schofield, A. N. and Togrol, E. Critical States of Soil, *Bulletin of the Technical University of Istanbul,* 19, *39 – 56,* 1966.
5. Kirkpatrick, W. M. *The Behaviour of Sands under Three-dimensional Stress Systems,* Ph.D. Thesis, Glasgow University, 1954.
6. Parry, R. H. 0. Triaxial Compression and Extension Tests on Remoulded Saturated Clay, *Géotechnique,* 10, 166 – 80, 1960.
7. Gould, J. P. A Study of Shear Failure in Certain Tertiary Marine Sediments, *Res. Conf on Shear Strength of Cohesive Soils, A.S.C.E.,* Boulder, pp. 615 – 41, 1960.
8. Wroth, C. P. *Shear Behaviour of Soils,* Ph.D. Thesis, Cambridge University, 1958.
9. Skempton, A. W. Long-term Stability of Clay Slopes, *Géotechnique,* **14,** 77 – 101, 1964.
10. Burland, J. B. Reply to discussion in *Large Bored Piles,* Inst. Civ. Eng., London, p. 102, 1966.
11. Skempton, A. W. An Investigation of the Bearing Capacity of a soft Clay Soil, *J.I.C.E.,* 18, 307 – 21, 1942.

[12] Watson, J. D. Earth Movement affecting L.T.E. Railway in Deep Cutting East of Uxbridge, *Proc. Inst. Civ. Eng.,* Pt II, 5, 302 – 31, 1956.

[13] Henkel, D. J. Discussion on 'Earth Movement affecting L.T.E. Railway in Deep Cutting East of Uxbridge', *Proc. Inst. Civ. Eng.,* Pt II, *5,* 320 – 3, 1956.

9
Two-dimensional fields of limiting stress

9.1 Coulomb's Analysis of Active Pressure using a Plane Surface of Slip

In 1776, before the concept of stress was clear, Coulomb[1] published his notable first paper on the application of the differential calculus to problems of architectural statics. His basic assumption was that the effective stress components σ' normal and τ tangential to a rupture plane satisfied a relationship such as

$$|\tau| \leq k + \sigma' \tan\rho. \qquad (8.1 \text{ bis})$$

But the importance of Coulomb's work lies in the analysis that he developed rather than in this basic assumption.

Let us consider the simple case of a smooth vertical wall which retains a horizontal layer of uniform soil, illustrated by the section of Fig. 9.1(a). For convenience, the analysis will be applied to unit length of the wall (perpendicular to the section) and we shall examine the conditions of limiting equilibrium which apply to one possible (plane) surface of rupture XY.

The total forces acting on the wedge OXY are (a) the total force *R* acting across the rupture surface, (b) its weight $W = \frac{1}{2}\gamma a x$, and (c) the lateral force *L* supplied by the wall (which must be horizontal in this case). Suppose that this force *L* is applied through a hydraulic jack, and it is gradually reduced. We see directly from the triangle of forces in Fig. 9.1(a) that the force *R* must gradually be reduced, and more significantly that its inclination to the normal across the plane XY is increased.

At some stage during this process the distributed pressures across the plane XY could have resultants on three segments 1, 2, and 3 as shown in Fig. 9.1(b). We have no knowledge of the actual distribution of stress except for the facts that the polygon of forces in Fig. 9.1(b) must close, and that for each segment the local shear stress τ cannot exceed the limiting magnitude given by eq. (8.1).

However, if the jack force *L* can be reduced until on every segment of this particular rupture surface the limiting condition is reached then the local reactions can be divided into two parts of known magnitude. The force due to cohesion along the segment is proportional to the length of the segment; and in general with *curved* rupture surfaces the resultant of all cohesive reactions equals a cohesive force *C* parallel to the chord of the surface. The frictional reaction is inclined at the limiting angle ρ to the normal to the segment; and in general with curved rupture surfaces, the resultant *F* of all frictional reactions will depend on the distribution of normal pressure. If large normal pressures act at one end of the surface then the overall frictional reaction will be close to the normal to the curve at that end of the surface. However, in the special case of a *plane* surface of rupture the cohesion resultant *C* acts parallel with the plane and the overall frictional resultant *F* acts at an angle ρ to that plane.

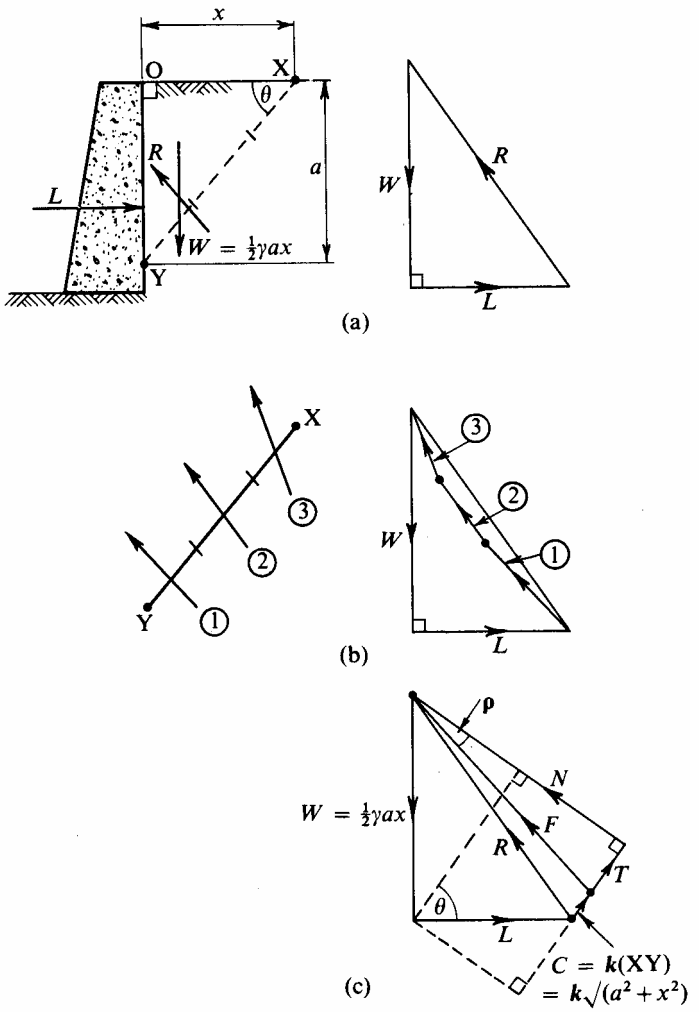

Fig. 9.1 Limiting Equilibrium of a Retaining Wall

So in the limiting case, the total sum of resolved components across each segment of the rupture surface must be as shown in Fig. 9.1(c), such that the total normal force

$$N = L\sin\theta + \tfrac{1}{2}\gamma ax\cos\theta$$

induces a total frictional resistance to sliding of

$$T = F\sin\rho = (L\sin\theta + \tfrac{1}{2}\gamma ax\cos\theta)\tan\rho$$

which together with the total cohesive force $C = k\sqrt{(a^2 + x^2)}$ must be in equilibrium with the resolved components of W and L

$$\tfrac{1}{2}\gamma ax\sin\theta - L\cos\theta.$$

Multiplying through by $\sqrt{(a^2 + x^2)}$ and eliminating θ we get

$$\left(\tfrac{1}{2}\gamma ax^2 + La\right)\tan\rho + k\left(a^2 + x^2\right) = \left(\tfrac{1}{2}\gamma a^2 x - Lx\right)$$

and collecting terms we obtain

$$L = \frac{\tfrac{1}{2}\gamma a^2 x - \tfrac{1}{2}\gamma ax^2\tan\rho - kx^2 - ka^2}{x + a\tan\rho} \tag{9.1}$$

for the *least* lateral force L that can successfully hold up the wedge OXY. If the total lateral force is allowed to fall below L then that particular wedge will actively slide down and increase the lateral force to the value L again.

If we plot L versus x we find the lower curve of Fig. 9.2(a) with a maximum value when

$$0 = \frac{dL}{dx} = \frac{\left(\frac{1}{2}\gamma a \tan\rho + k\right)\left(a^2 - 2ax\tan\rho - x^2\right)}{\left(x + a\tan\rho\right)^2} \tag{9.2}$$

which is satisfied by

$$x = a\tan\varepsilon, \qquad \text{where } \varepsilon = \left(\frac{\pi}{4} - \frac{\rho}{2}\right). \tag{9.3}$$

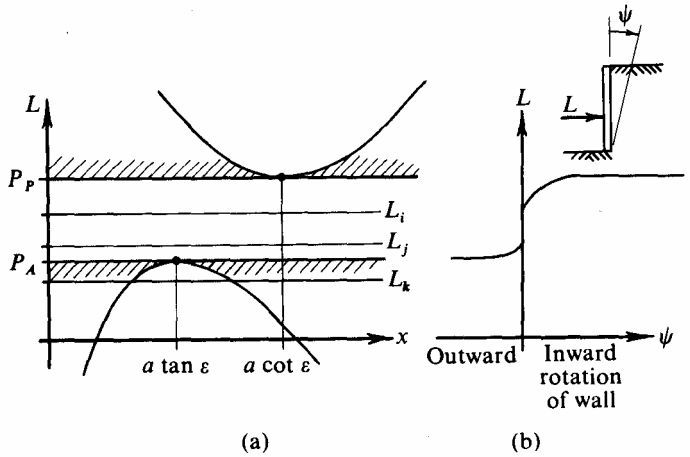

Fig. 9.2 Bounds of Possible Values for Lateral Force on Retaining Wall

The significance of this maximum is as follows. Suppose the lateral force on the jack is slowly reduced and let us represent this by a shift of the faint horizontal lines in Fig. 9.2(a) from value L_i to L_j. The first rupture plane that can become active is the one at $x = a\tan\varepsilon$, inclined to the wall at an angle $(\pi/4 - \rho/2)$. The lateral force cannot fall below this value. If the lateral force could be reduced to L_k there would be two possible rupture planes, but any attempt to reduce the total force will simply be matched by activity of the weakest slip wedge at $x = a\tan\varepsilon$. The magnitude of this active lateral force is found by substituting $x = a\tan\varepsilon$ in the expression for L to give

$$P_A = L = \tfrac{1}{2}\gamma a^2 \tan^2\varepsilon - 2ka\tan\varepsilon \tag{9.4}$$

Where P_A is Coulomb's active lateral pressure force. Coulomb himself published this expression in the form

$$P_A = ma^2 - lka \tag{9.5}$$

and it was the derivation of this equation that was probably Coulomb's major achievement in soil mechanics. He appreciated that for soil without cohesion (k = 0), P_A reduces to $\frac{1}{2}\gamma a^2 \tan^2\varepsilon$, and for soil without cohesion or friction $(k = \rho = 0)$ the active lateral force P_A is $\frac{1}{2}\gamma a^2$ and simply reduces to the fluid force. The presence of friction and cohesion together reduce the active lateral force needed to retain this soil, below that needed to retain a fluid of the same density.

9.2 Coulomb's Analysis of Passive Pressure

Coulomb's calculation was then developed by considering that the lateral force becomes so large that wedges of soil tend to slip upwards along plane surfaces of rupture.

In that case the variation of lateral force L corresponds to the upper curve in Fig. 9.2(a) given by an equation

$$L = \frac{\frac{1}{2}\gamma a^2 x - \frac{1}{2}\gamma a x^2 \tan\rho + kx^2 + ka^2}{x - a\tan\rho} \tag{9.6}$$

which can be obtained directly from the active case by changing the signs of k and ρ throughout. This curve has a minimum at $x = a\cot\varepsilon$ when

$$P_P = \tfrac{1}{2}\gamma a^2 \cot^2\varepsilon + 2ka\cot\varepsilon. \tag{9.7}$$

The significance of this minimum is that when the lateral force rises causing passive resistance of the soil, the first plane of rupture on which slip can occur is the plane inclined to the vertical wall at an angle $(\pi/4 + \rho/2)$. If slip occurs on this plane the soil can continue to resist passively but with lateral force of not more than P_P. This force is in excess of the fluid pressure $\frac{1}{2}\gamma a^2$ because of both friction and cohesion.

In the range of possible lateral force $P_A \le L \le P_P$ the soil is at rest. In the case of cohesionless soil with $\rho = 30^\circ, \tan^2\varepsilon = \frac{1}{3}$ and the ratio $P_P/P_A = 9$. This very wide range of possible values of L makes it necessary to introduce some additional consideration if a close estimate of a value of L is to be made. For example, in Coulomb's design free-standing walls withstand a lateral force 1.25 P_A without overturning. It is recognized that the lateral force L may well exceed this design value but if it does so, it is supposed that a little outward movement of the wall will relieve the lateral force, which will then fall to the design value. In several experiments on large model retaining walls Terzaghi[2] did establish this effect of Fig. 9.2(b); after a very small outward rotation (0.001 radian) of a retaining wall the lateral force fell to the active value, but much larger inward rotation (0.1 radian) was required before the lateral force approached the passive pressure. A phrase common in the literature is that the strains required to 'mobilize the strength' of the ground are large in the passive case and small in the active case.

However, we must not forget that Coulomb's calculation does not in itself contain any mention of the *magnitude* of strains or displacements. All that is specified is the *direction* of incipient movement on the slip plane as shown in Fig. 9.3.

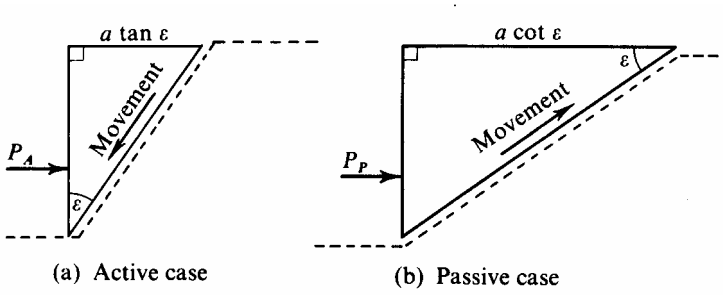

Fig. 9.3 Slip Planes for Active and Passive Failures

By putting $P_A = 0$ in the eq. (9.5) for the active force

$$0 = P_A = \frac{1}{2}\gamma a^2 \tan^2\varepsilon - 2ka\tan\varepsilon$$

Coulomb found the height to which a face could stand unsupported to be

$$a \le \frac{4k}{\gamma\tan\varepsilon}; \tag{9.8}$$

and a face of this height would certainly fail under its own self- weight. He went on to consider whether a larger active force (or a lower unsupported height of a vertical face)

would be found for some surface of sliding other than plane (Fig. 9.4) and introduced the important idea of using vertical slices to find the pressures on a curved rupture surface. Unfortunately, he was writing before the nature of stress in a continuum was well understood and he wrongly supposed that he needed to specify limiting stresses both on the rupture surface and on the vertical planes between slices; this error prevented Coulomb from making a successful development of the method of slices.

It is clearly possible to extend this simple method of analysis to obtain general solutions to problems where the retaining wall is battered, or rough, or the backfill is not horizontal or consists of several different strata.

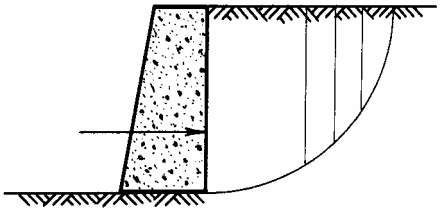

Fig. 9.4 Possible Curved Failure Surface Considered by Coulomb

9.3 Coulomb's Friction Circle and its Development in Gothenberg

In 1785 Coulomb wrote a prize paper[3] on problems of cordage and rigging of ships. This paper included the solution to the problem of slip of ropes round frictional bollards, and the solution to the problem of the torsion of round spars. The paper also introduced the friction circle construction for analysis of the slip of a shaft, Fig. 9.5, in a frictional plane bearing. The shaft turns and slips along a line contact such that the reaction is inclined to the radius R at the friction angle ρ. Conveniently a 'friction circle' of radius $R \sin \rho$ is drawn, and a graphical construction is made in which the limiting reaction is tangential to the friction circle. Coulomb's technique of 1785 was to be applied in 1916 to the problem of slip of soil on circular surfaces of rupture[4] by the engineers of the Swedish port of Gothenberg where there was a series of failures of the quay walls.

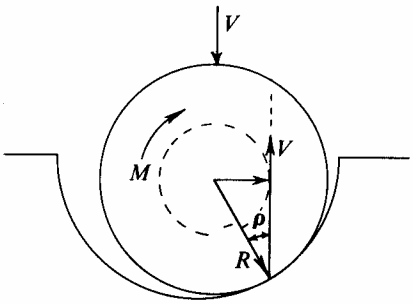

Fig. 9.5 Circular Shaft about to Slip

One successful design of quay wall, Fig. 9.6(a), was based on the consideration of straight planes of sliding. In Fig. 9.6(b) the active force A, due to pressure of retained soil and superposed traffic, is made small by placing highly frictional gravel behind the wall; and the passive force P, due to resistance of a wedge of soil in front of the toe of the quay, is made large by placing highly frictional gravel there also. The next quay wall, shown in Fig. 9.7, should have been by these considerations more stable than its forerunner; the clay below this new fill was considered to be stiffer than at the former site, and yet 'the quay wall slid slowly into the river in March 1916 just before it was completed and before any live load had been added to the quay area'. Borings and other observations showed that the

movement approximated to slip on a circular surface of sliding through the clay below the gravel fill. Yet another large quay wall was under construction for the Central Harbour and this failure made it imperative for the engineers concerned to revise their design principles.

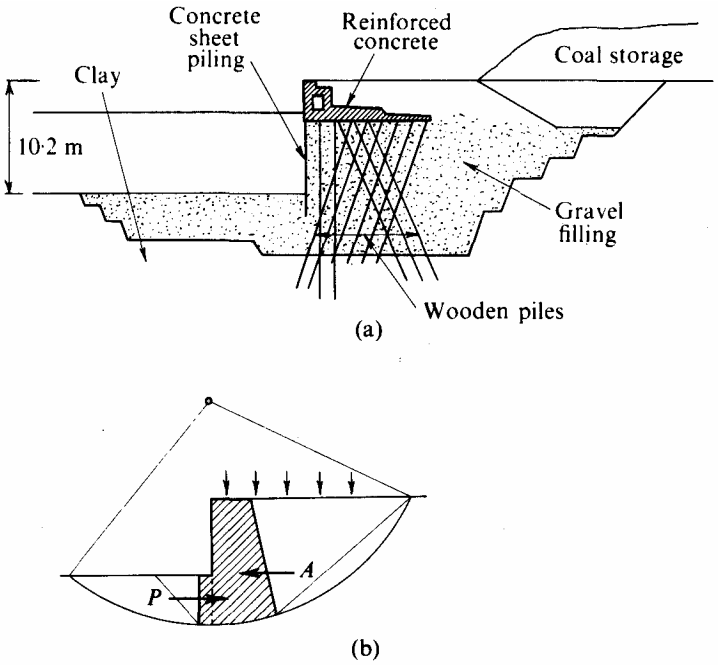

Fig. 9.6 Quay at the Sannegard Harbour 1914 (After Petterson)

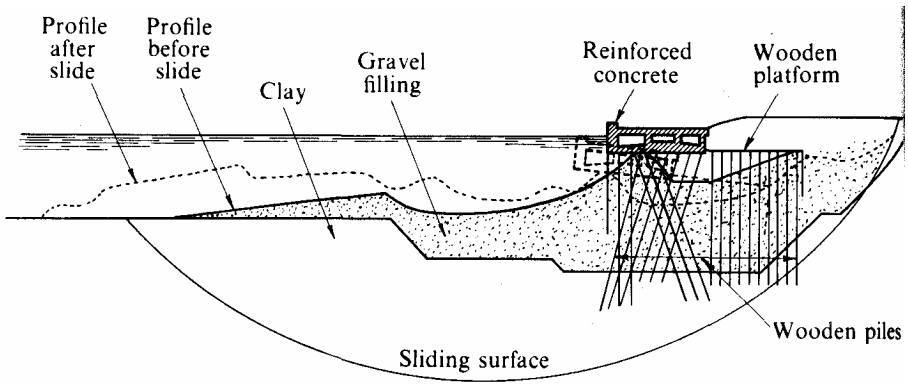

Fig. 9.7 The Stigberg Quay, Sliding Surface, 1 916 (After Petterson)

Their investigation was based on the general view held at that time, that friction governed the behaviour of all kinds of soil and that a graphical method of polygons of force was the most practical basis for the analysis. An existing gravel fill in the Central Harbour project was extended to form a test load: when this test was in the stage shown in Fig. 9.8 a crack was observed in the fill and the soil moved slowly about 17 cm outward and 25 cm downwards and did not come to rest for 9 days. Analysis of the failures of both the quay wall and test load was made in the manner shown in Fig. 9.8.

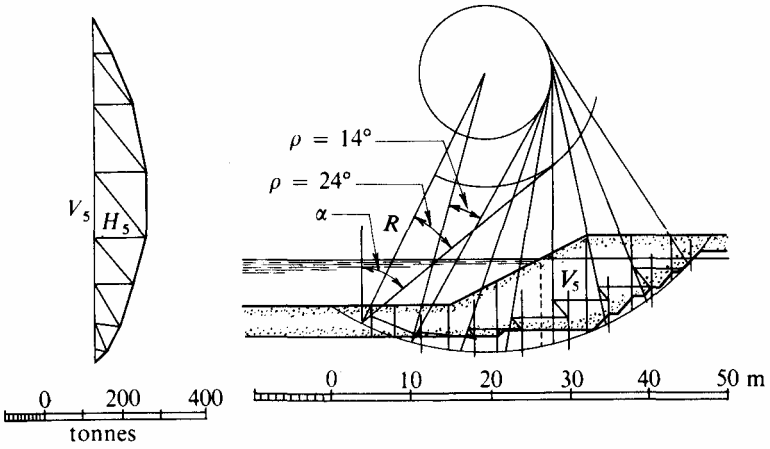

Fig. 9.8 Investigation of Stability under the Test Load in the Free Harbour, 1916 (After Petterson)

A possible circular sliding surface of radius R was drawn through the ground, the cross-section within the circle divided into vertical slices, and the vertical weight V and centre of gravity determined for each slice. A horizontal force H was assumed to act between slices at the lower third point of the interface. A tentative value was assumed for the friction angle effective along the circular arc and a friction circle of radius R sin ρ was drawn. For each slice number n the vertical weight V, was known, and the frictional reaction across the base of the slice had to be in a direction tangential to the friction circle inclined at an angle α_n to the vertical. Hence the difference between the horizontal forces to either side of this slice was

$$H_n - H_{n-1} = V_n \tan \alpha_n.$$

The force polygon of Fig. 9.8 was constructed starting from the first slice; when the last slice was reached the polygon should close with no horizontal reaction to the right. Trials with different values showed what frictional angle ρ was required just to maintain equilibrium of the sliding mass within that particular circular surface of sliding. Then many other possible sliding surfaces were thus analysed and it was considered that the surface which required the *largest* value of ρ was the most critical and failure would occur first along it. In the analysis of the Central Harbour failure of Fig. 9.8, a frictional angle ρ = 24° was assumed for the part of the sliding surface that passed through the gravel, and the largest value of ρ required for stability of the clay was found to be about 14°. For the quay wall failure of Fig. 9.7 the value of ρ required for stability was about 10°.

The analysis of these failures made it clear that quay walls with heavy gravel fills were unsuitable for that particular clay foundation. The design for the new quay wall in the Central Harbour was modified as shown in Fig. 9.9(a). The weight of gravel filling in front of the quay wall was unaltered but the weight below the quay was reduced; the quay became a loading platform resting on wooden piles that were driven down through a gravel slope into the underlying clay. The factor of safety of the new design was estimated as follows. The force polygon was started from both ends. A division was introduced at the vertical plane tangential to the friction circle. All slices to the right of this plane were considered to be actively causing an increase of horizontal force between slices, and the worst case included traffic loading on these slices; all slices to the left of this plane were considered to be passively resisting the horizontal force from the right and the worst case allowed no traffic loading on these slices. The polygons completed from each end up to this vertical plane gave a horizontal force H_A active from the right and a horizontal force

H_P available in passive resistance to the left. The ratio H_P/H_A was regarded as the factor of safety of the design: in the Central Harbour design this factor was about $1\frac{1}{2}$, and in another case a factor of $1\frac{1}{3}$ was considered satisfactory.

The method of slices was clearly capable of extension. Non circular surfaces could later be considered, and the division between 'active and passive slices' would then simply be found by drawing a tangent at slope ρ to the curve of sliding. Cohesion could also be considered and a suitable polygon of forces quite simply found. The effect of pore-pressure in producing variation of effective normal stress across the sliding surface was later introduced. Other later definitions of factor of safety included a ratio of moments taken about the centre of the circle of 'disturbing' active forces and 'restoring' passive forces.

An extensive literature[5–8] has been written on the analysis of equilibrium on rupture surfaces. When referring to these texts the reader should be careful to note what assumption each writer makes about distributions of pore-pressure and of total normal pressure along any assumed rupture surface, and what definition is used for factors of safety. In each of these respects a certain variation of practice exists.

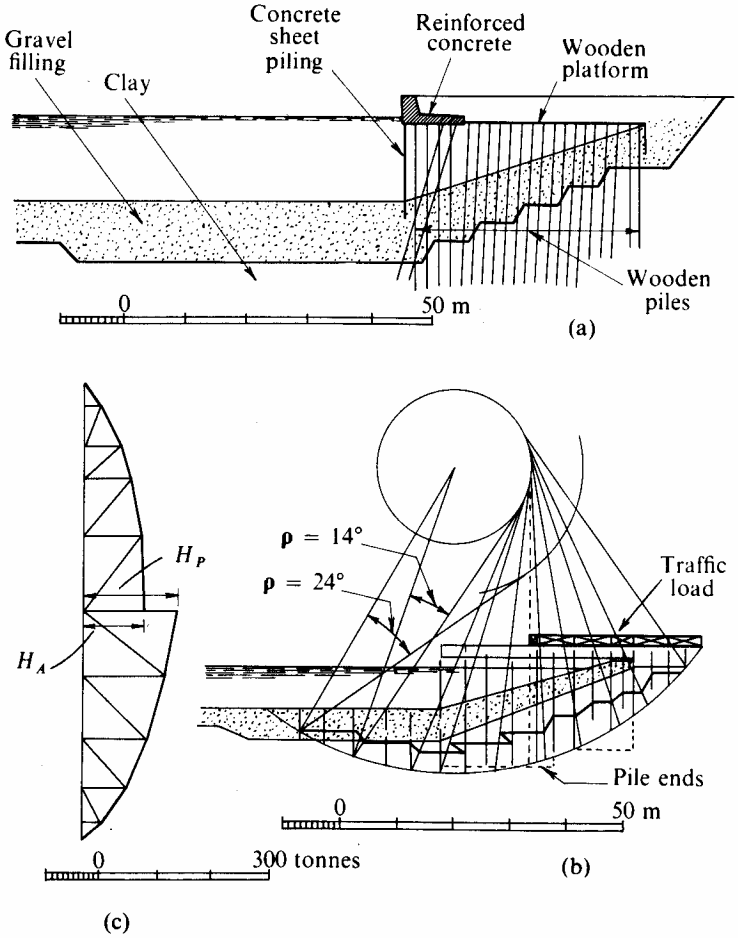

Fig. 9.9 Quay in the Free Harbour as built, and Evaluation of the Stability of the Quay in the Free Harbour, 191 6 (After Petterson)

9.4 Stability due to Cohesion Alone

Only a few years after the original analysis of the slips at Gothenberg alternative analyses were developed based on cohesion alone.

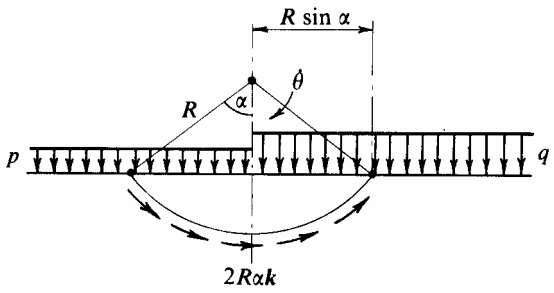

Fig. 9.10 Cylindrical Slip Surface in Clay

In Fig. 9.10 we show the section of a semi-infinite half-plane of homogeneous clay loaded to the right with a uniformly distributed load q and to the left with a uniformly distributed load p. Here we are again introducing nomenclature which will enable the reader to gain more ready access to Sokolovski's *Statics of Granular Media.*[9] No confusion need arise with the use of p and q in earlier chapters. The problem is analysed on the supposition that the clay ruptures and rotates clockwise on a cylindrical slip surface which will be assumed of unit length perpendicular to the section. All normal reactions on the slip surface pass through the centre of the slip-circle, and all tangential reactions are simply of magnitude k per unit length of arc. It is clear that the worst circles have centres over the edge which divides the loading, since any extension of q to the left or p to the right will reduce the loading power available for dissipation.

Let the family of circles with centres over the edge be determined by the parameter α, the half-angle shown in Fig. 9.10. During a small clockwise rotation of $\dot{\theta}$ it is assumed that the total power of the descending load less the power of the rising load must equal the power dissipated in overcoming cohesion on the cylindrical slip surface. The distance moved by the centre of gravity of both moving loads is $(\frac{1}{2}R\sin\alpha)\dot{\theta}$ so that

$$(q-p)R\sin\alpha(\tfrac{1}{2}R\sin\alpha)\dot{\theta} = k2R\alpha R\dot{\theta},$$

i.e.,
$$(q-p) = k\frac{4\alpha}{\sin^2\alpha}. \tag{9.9}$$

This expression for $(q-p)$ has a minimum when

$$0 = \frac{\mathrm{d}}{\mathrm{d}\alpha}\left(\frac{\alpha}{\sin^2\alpha}\right) = \operatorname{cosec}^2\alpha - 2\alpha\operatorname{cosec}^2\alpha\cot\alpha,$$

i.e., when
$$\tan\alpha = 2\alpha \tag{9.10}$$

which is satisfied by $\alpha = 1.1656 \text{ rad} = 66^\circ 47'$. On substitution in eq. (9.9) this gives, for the worst case, a maximum loading differential

$$(q-p)_{\max} = 5.53k. \tag{9.11}$$

Let us apply this result to the stability of river banks. In general a river bank may be most inclined to fail locally, as in Fig. 9.11, with a weight W of soil slipping round the circular arc AB. The resultant of the cohesion k round the arc AB is then equal to a force K parallel to the chord AB; the weight W simply depends on the geometry of the section and the unit weight γ of the soil. The triangle of forces shown in Fig. 9.11 indicates a value of $\boldsymbol{k}$ needed just to satisfy statical equilibrium. However, when slope protection works are put in hand and a well drained bank or an anchored sheet-pile wall or piled quay is built over purely cohesive ground, the possibility of deep-seated failure places an overall restriction on the difference of level or of loading that can be carried.

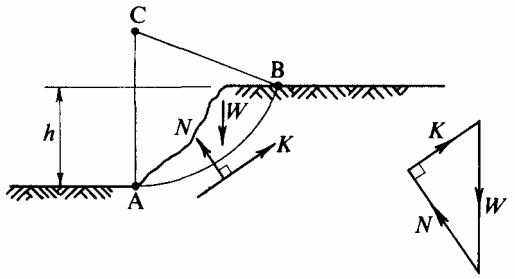

Fig. 9.11 Local Failure of River Bank

For example, imagine in Fig. 9.12 a wide river passing across land where there is a considerable depth of clay with cohesion k = 3 tonnes/m^2 and of saturated weight 16 tonnes/m^3. If the difference of level between the river banks and the river bed was h, then (ignoring the strength of the clay for the portion BD of the sliding surface,

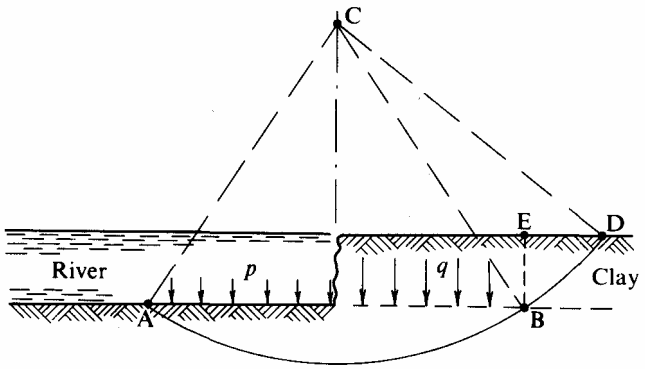

Fig. 9.12 Deep-seated Failure of River Bank

and the weight of the wedge BDE) for an approximate calculation we have $q = 1.6h$ and $p = \gamma_w h = 1.0h$ when the river bed was flooded or $p = 0$ when the river bed was dry giving in the worst case $(q - p) = 1.6h$. We also have from eq. (9.11)

$$(q - p)_{\max} = 5.53k = 16.6 \text{ tonnes/m}^2 \tag{9.12}$$

so that $$h \le \frac{16.6}{1.6} = 10\,\text{m, say}$$

which gives one estimate of the greatest expected height of the river banks. If the river were permanently flooded the depth of the river channel could on this basis be as great as

$$\frac{16.6}{0.6} \cong 27.6\,\text{m.} \tag{9.13}$$

An extensive literature has been written on the analysis of slip-circles where the soil is assumed to generate only cohesive resistance to displacement. We shall not attempt to reproduce the work here, but instead turn to the theory of plasticity which has provided an alternative approach to the solution of the bearing capacity of purely cohesive soils.

9.5 Discontinuity Conditions in a Limiting-stress Field

In this and the next section we have two purposes: the principal one is to develop an analysis for the bearing capacity problem, but we also wish to introduce Sokolovski's notation and provide access to the extensive range of solutions that are to be found in his *Statics of Granular Media.* In this section we concentrate on notation and develop simple conditions that govern discontinuities between bodies of soil, each at some Mohr—

Rankine limiting stress state: in the next section we will consider distribution of stress in a region near the edge of a load — a so-called 'field' of stresses that are everywhere limiting stresses.

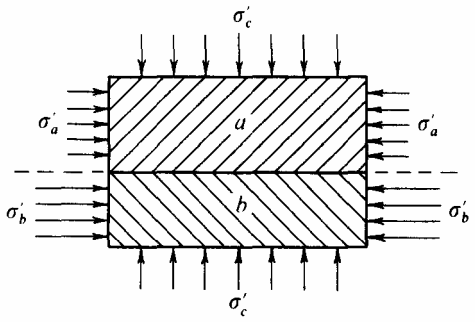

Fig. 9.13 Two Rectangular Blocks in Equilibrium with Discontinuity of Stress

In Fig. 9.13 we have a section through two separate rectangular blocks made of different perfectly *elastic* materials, *a* and *b,* where material *b* is stiffer than *a.* The blocks are subject to the boundary stresses shown, and if σ'_a and σ'_b are in direct proportion to the stiffnesses E_a and E_b then the blocks are in equilibrium with compatibility of strain everywhere. However, the interface between the blocks acts as a *plane of discontinuity* between two states of stress, such that the stress σ'_c across this plane must be continuous, but the stress parallel with the plane need not be.

In a similar way we can have a plane of discontinuity, *cc,* through a single perfectly *plastic* body such as that illustrated in Fig. 9.14(a). Just *above* the plane *cc* we have a typical small element *a* experiencing the stresses (σ'_a, τ_{ac}) and (σ'_c, τ_{ca}) which are represented in the Mohr's diagram of Fig. 9.14(b) by the points A and C respectively on the relevant circle *a*.

Just *below* the plane *cc* the small element *b* is experiencing the stresses (σ'_b, τ_{bc}) and (σ'_c, τ_{cb}) which are represented by the points B and C respectively on the relevant Mohr's circle *b.* In order to satisfy equilibrium we must have $\tau_{ac} \equiv \tau_{ca} \equiv \tau_{bc} \equiv \tau_{cb}$ but as before there is no need for σ'_a to be equal to σ'_b. Since the material is perfectly plastic there is no requirement for continuity or compatibility of strain across the plane *cc.*

We can readily obtain from the respective Mohr's circles the stresses acting on any plane through the separate elements a and *b;* and in Fig. 9.14(c) the principal stresses are illustrated. The key factor is that there is a marked jump in both the *direction* and *magnitude* of the major (and minor) principal stresses across the discontinuity — and this will be the essence of the plastic stress distributions developed in the remainder of this chapter. This will be emphasized in all the diagrams by showing the major principal stress in the form of a vector, and referring to it always as Σ'.

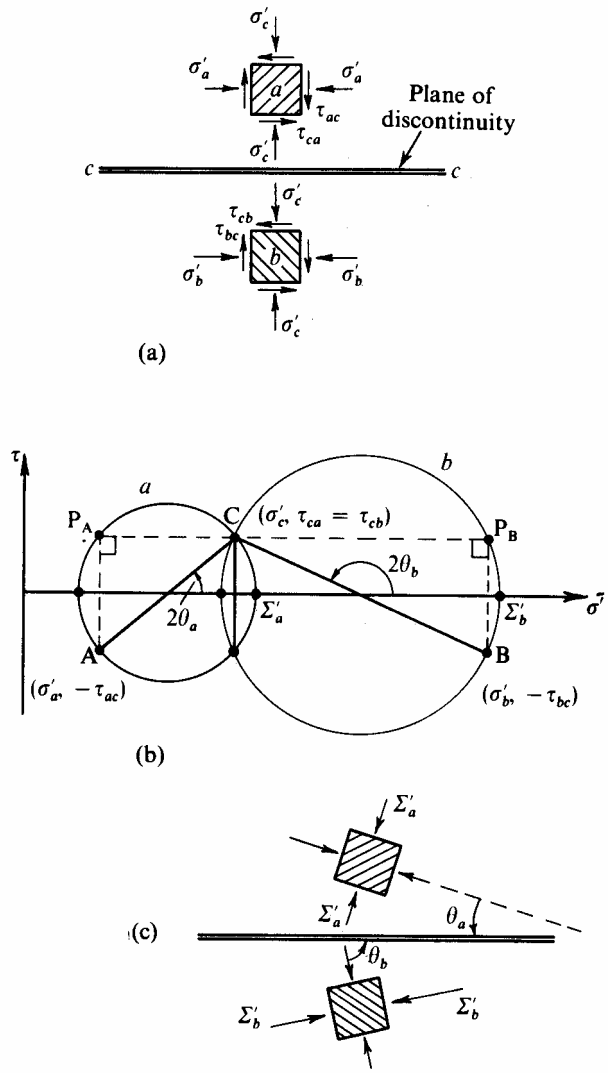

Fig. 9.14 Perfectly Plastic Body Containing Stress Discontinuity

In Fig. 9.15(a) we see a section through a plane body of soil across which there act stress components n normal and τ tangential to the section. These components define a point P in the stress plane of Fig. 9.15(b), in which we see also the Mohr—Rankine limiting lines

$$|\tau| = k + \sigma' \tan\rho,$$

intersecting the axis at O where OJ = k cot ρ = H. It proves convenient to transform all problems to equivalent problems of either perfectly frictional or perfectly cohesive soil. So in cases where $\rho \neq 0$ Sokolovski introduces an additional pressure H as well as the stress components n and t, and in Fig. 9.15(c) the *equivalent* stress (remembering that the symbols p and q are used by Sokolovski and in this chapter only for distributed loading on some planes) p' is such that $p'\sin\delta = t$ and $p'\cos\delta = (n + H)$.

In Fig. 9.16(a) there are seen to be two alternative circles of *limiting* stress through the point P. One circle has centre Q_+ and the other has centre Q_-. The line OP cuts these circles as shown in Fig. 9.16(a) and the angle Δ is such that

$$\sin\Delta = \frac{\sin\delta}{\sin\rho} \quad (\rho \neq 0). \tag{9.14}$$

We must be careful about the sign conventions associated with the definition of Δ. The angle of friction ρ is a material constant and is always positive (or zero), so that the sign of Δ is always the same as δ. All angles in Mohr's diagram are measured positive in an anticlockwise direction so that positive δ and Δ are associated with positive shear stress τ; in particular when P is below the σ'-axis, $\Delta<0$.

Use of this angle Δ was suggested by Caquot and was then brought in to the second edition of *Statics of Granular Media.*

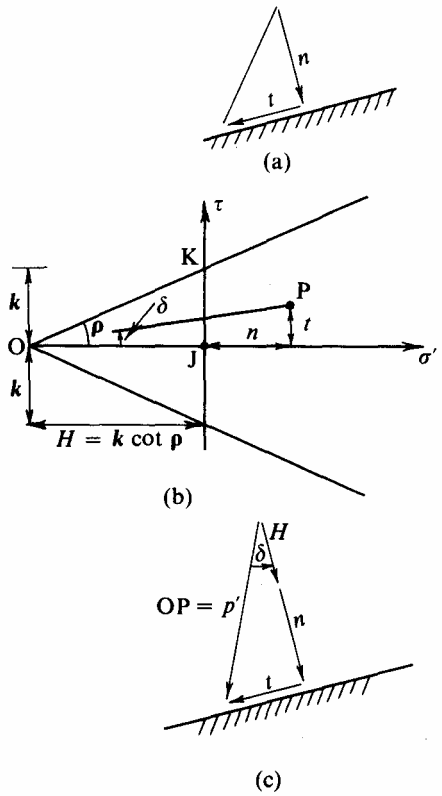

Fig. 9.15 Sokolovski's Equivalent Stress

Another symbol that figures extensively in the book is $\kappa = \pm 1,$ in such contexts as

$$\left.\begin{aligned} \sigma' &= p'\frac{\sin\Delta}{\sin(\Delta-\kappa\delta)} \\ \text{where}\quad \kappa=+1 \text{ gives } \sigma'_{+} &= \mathrm{OQ}_{+} = \mathrm{OP}\frac{\sin\Delta}{\sin(\Delta-\delta)} \\ \text{and}\quad \kappa=-1 \text{ gives } \sigma'_{-} &= \mathrm{OQ}_{-} = \mathrm{OP}\frac{\sin\Delta}{\sin(\Delta+\delta)}. \end{aligned}\right\} \tag{9.15}$$

This convenient notation permits Sokolovski to write general equations, and to distinguish between a *maximal* limiting-stress state when $\kappa=+1$ and a *minimal* limiting-stress state when $\kappa=-1$. These alternative states can exist cheek by jowl, facing each other across a discontinuity on which the stress components n and t act as in Fig. 9.16; this case represents the biggest allowable jump or change in stress across the discontinuity.

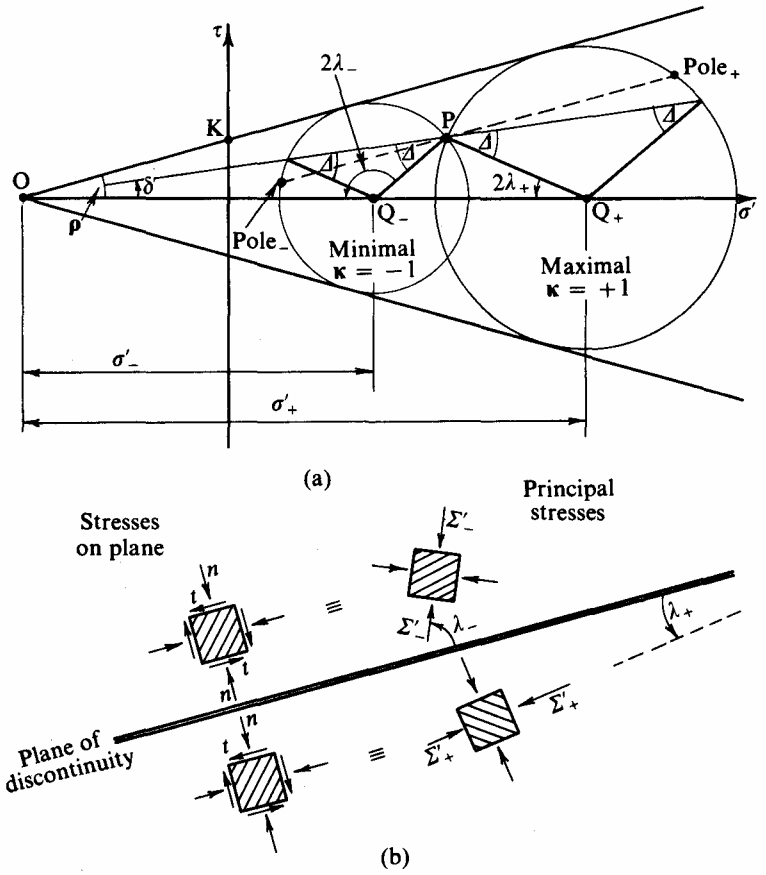

Fig. 9.16 Maximal and Minimal Limiting Stresses

The first condition that applies to these limiting stress states is that the shift in centre of the stress circles must satisfy the condition

$$\frac{\sigma'_+}{\sigma'_-} = \frac{\sin(\Delta+\delta)}{\sin(\Delta-\delta)} \qquad (9.16)\ \text{cf. Sokolovski (2.42)}$$

A second condition is that the change in inclination of the direction of the major principal stress Σ' also depends on Δ. In Fig. 9.16(b) we define the *anticlockwise* angles* *from* the direction of the discontinuity to the directions of Σ' on either side as λ_- and λ_+. The general condition is

$$2\lambda = (1-\kappa)\frac{\pi}{2} + \kappa\Delta - \delta + m\pi \qquad (9.17)\ \text{cf. Sokolovski (1.17)}$$

where m is an integer, chosen to agree with the sign convention for λ.

For $\kappa = +1$ we have $2\lambda_+ = \Delta - \delta$

$\kappa = -1$ we have $2\lambda_- = \pm\pi - \Delta - \delta$

where the + sign is associated with positive shear ($\delta > 0$) and the – sign is associated with negative shear ($\delta < 0$). The second condition applying to the discontinuity is therefore

$$\lambda_- - \lambda_+ = \pm\frac{\pi}{2} - \Delta \qquad (9.18)$$

* This is a minor departure from Sokolovski who measures the *clockwise* angle from Σ' *to* the discontinuity: it makes no difference to the mathematical expressions but means all angles have a consistent sign-convention.

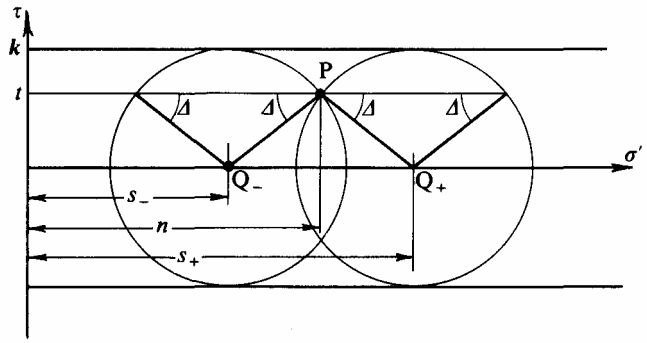

Fig. 9.17 Limiting-stress Circles for Purely Cohesive Material

If we consider instead the case of a perfectly cohesive soil (ρ=0) we have the situation of Fig. 9.17 for which this second condition remains valid. However, the first condition of eq. (9.16) must be expressed as

$$\frac{\sigma'_+}{\sigma'_-} = \frac{s_+ + H}{s_- + H} = \frac{\sin(\Delta + \delta)}{\sin(\Delta - \delta)}$$

so that as $\delta \to 0 (\text{and} \sigma'_+, \sigma'_-, p' \text{and} H \text{ each} \to \infty)$ it can be expanded to give

$$s_+ - s_- = 2k\cos\Delta. \qquad (9.19) \text{ cf. Sokolovski (4.32)}$$

We also have to redefine Δ in the form

$$\sin\Delta = \frac{t}{k} \quad (\rho = 0). \qquad (9.20)$$

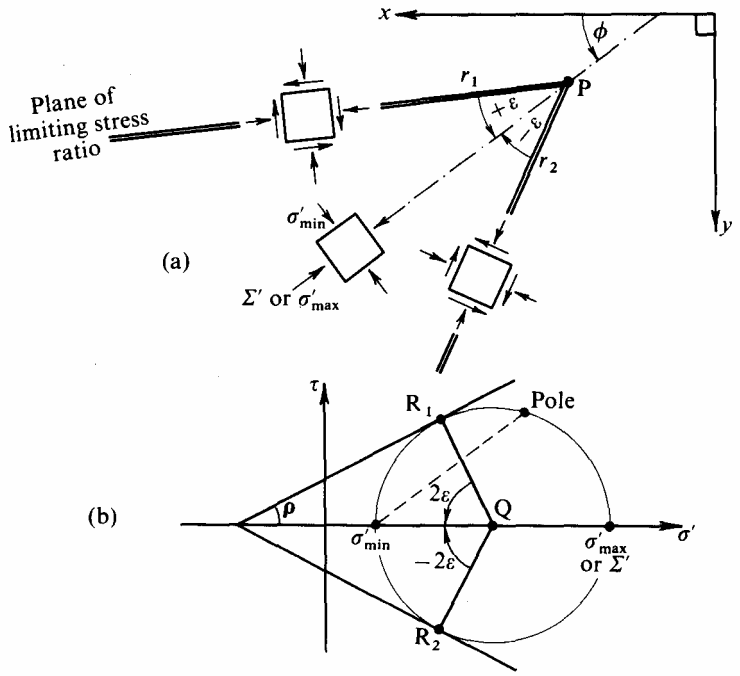

Fig. 9.18 Planes of Limiting-stress Ratio

We will be dealing with a number of discontinuities all at different inclinations, so it becomes important to have a pair of fixed reference axes. Sokolovski uses Cartesian coordinates x horizontal and positive to the left, and y vertical and positive downwards which is consistent with our sign convention for Mohr's circle (appendix A). The angle ϕ is defined to be the anticlockwise angle between the x-axis and the direction of major

principal stress Σ' in Fig. (9.18). This angle will play a large part in the remainder of this chapter, and should not be confused with its widespread use in the conventional definition for the angle of friction.

In Fig. 9.18(a) we have a point P in a perfectly plastic body in a state of limiting stress, with appropriate Mohr's circle in Fig. 9.18(b). From this we can establish the direction of the major principal stress Σ' and the directions r_1 and r_2 of the planes of limiting stress ratio. The angle between these is such that $\varepsilon = (\pi/4 - \rho/2)$ and this agrees with the definition in eq. (9.3) in §9.2 on Coulomb's analysis.

In order to define a limiting-stress state in soil of given properties **(*k*, ρ)** only two pieces of information are needed: one is the position of the centre of the stress circle, either σ' or *s,* and the other is the direction of major principal stress relative to the horizontal *x*-axis described by ϕ. Across a discontinuity the change of the values of these data is simply related to Δ, which is defined by eqs. (9.14) and (9.20).

9.6 Discontinuous Limiting-stress Field Solutions to the Bearing Capacity Problem

We can now turn to the bearing capacity problem. Previously, in §9.4 when we considered the possibility of circular rupture surfaces, we only attempted to specify the distribution of stress components across the sliding surface. In this section we will be examining the same problem on the supposition that there are discontinuities in the distribution of stress in the soil near a difference of surface loading, and we will fully specify limiting-stress states in the whole of the region of interest.

We shall simplify the problem by assuming the soil is weightless $(\gamma = 0)$, but we will see later that this is an unnecessary restriction and that the analysis can be extended to take account of self-weight. The cases of (a) purely frictional and (b) purely cohesive soils need to be considered separately, and the latter, which is easier, will be taken first.

9.6.1. *Purely cohesive soil* $(\rho = 0, \gamma = 0)$

Figures 9.19(a), 9.20(a), and 9.21(a) show a section of a semiinfinite layer of uniform soil supporting a known vertical stress *p* applied to the surface along the positive *x*-axis. The problem is to estimate the maximum vertical stress *q* that may be applied along the negative *x*-axis. In the limiting case the stress *p* must be a minor principal stress so that the associated major principal stress Σ' must be in a *horizontal* direction $(\phi = 0)$. In contrast, the stress *q* will be itself a major principal stress in the *vertical* direction $(\phi = \pi/2)$, so that somewhere in the vicinity of the *y*-axis we must insert one or more discontinuities across which the value of ϕ can change by π/2.

If we have *n* discontinuities it is simplest to have *n* equal changes of ϕ, i.e., $\delta\phi = +(\pi/2n)$ at each discontinuity. With the boundary conditions of Fig. 9.19 we shall be concerned with *negative* shear, i.e., $\Delta \le 0$, so that we select from eq. (9.18)

$$(\phi_- - \phi_+) = (\lambda_- - \lambda_+) = -\frac{\pi}{2} - \Delta$$

and for *each* discontinuity

$$\Delta = -\frac{\pi}{2} + \phi_+ - \phi_- = -\frac{\pi}{2} + \delta\phi = -\frac{\pi}{2} + \frac{\pi}{2n} = \frac{\pi}{2}\left(\frac{1}{n} - 1\right). \tag{9.21}$$

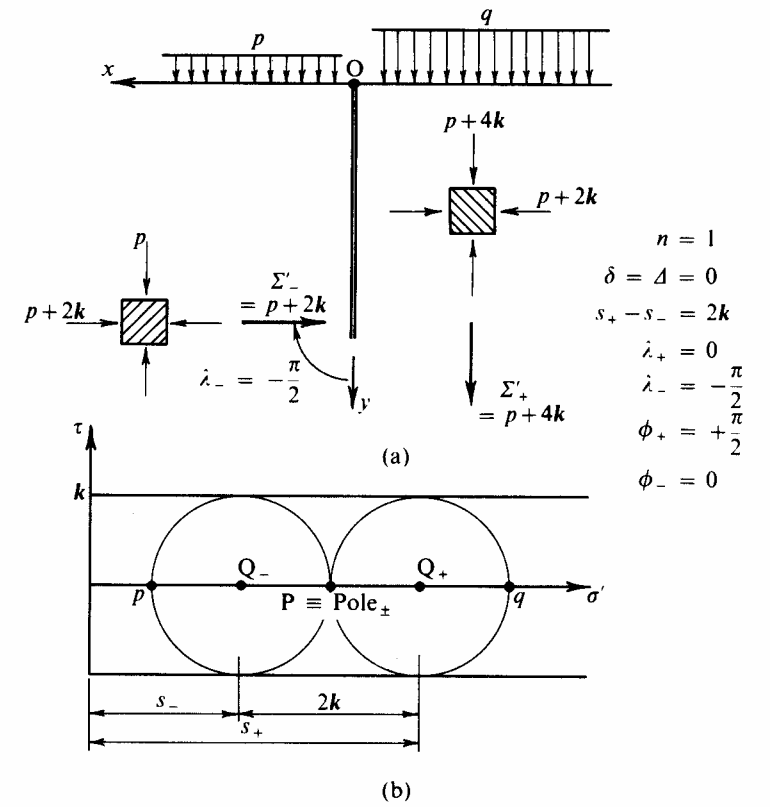

Fig. 9.19 Limiting-stress Field with One Discontinuity for Cohesive Soil

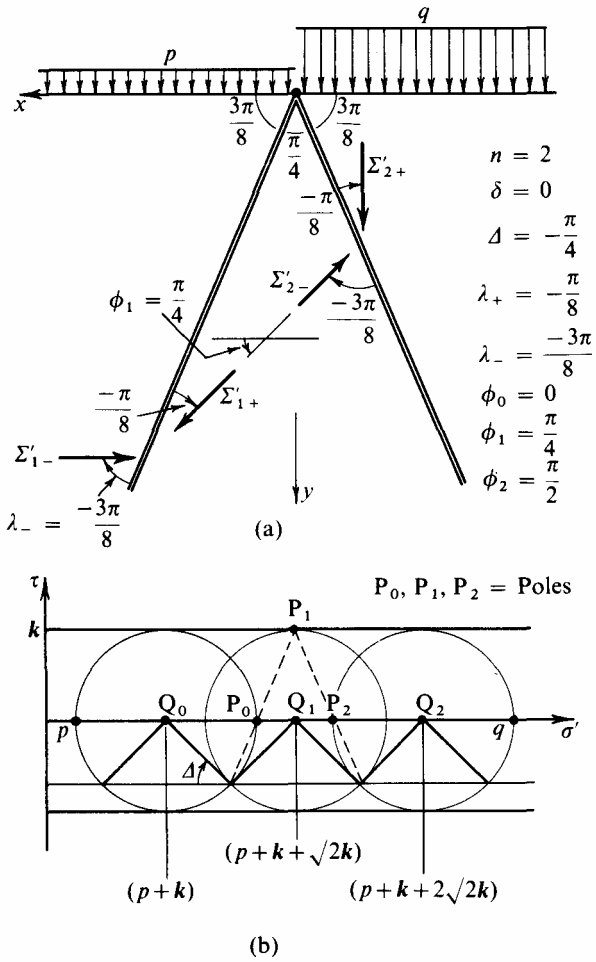

Fig. 9.20 Limiting-stress Field with Soil Discontinuities for Cohesive soil

Substituting in eq. (9.19) we have for the shift of Mohr's circles

$$(s_+ - s_-) = 2k\cos\Delta = 2k\cos\frac{\pi}{2}\left(\frac{1}{n}-1\right) = 2k\sin\frac{\pi}{2n} = 2k\sin\delta\phi. \tag{9.22}$$

The case of a *single* discontinuity $(n=1)$ is fully illustrated in Fig. 9.19, for which $\Delta = 0$ and the two stress circles have centres separated by a distance 2k. The corresponding value of q is $p + 4k$.

For the case of *two* discontinuities ($n = 2$) in Fig. 9.20, $\Delta = -\pi/4$ and the three stress circles have centres spaced $\sqrt{(2)}k$ apart giving $q_{\max} = p + 2k + 2\sqrt{(2)}k = p + 4.83k$.

When n becomes *large,* Fig. 9.21, it is convenient to adopt the differentials from eqs. (9.21) and (9.22)

$$\Delta = -\frac{\pi}{2} + \delta\phi$$

and

$$\delta s = s_+ - s_- = 2k\sin\delta\phi = 2k\ \delta\phi$$

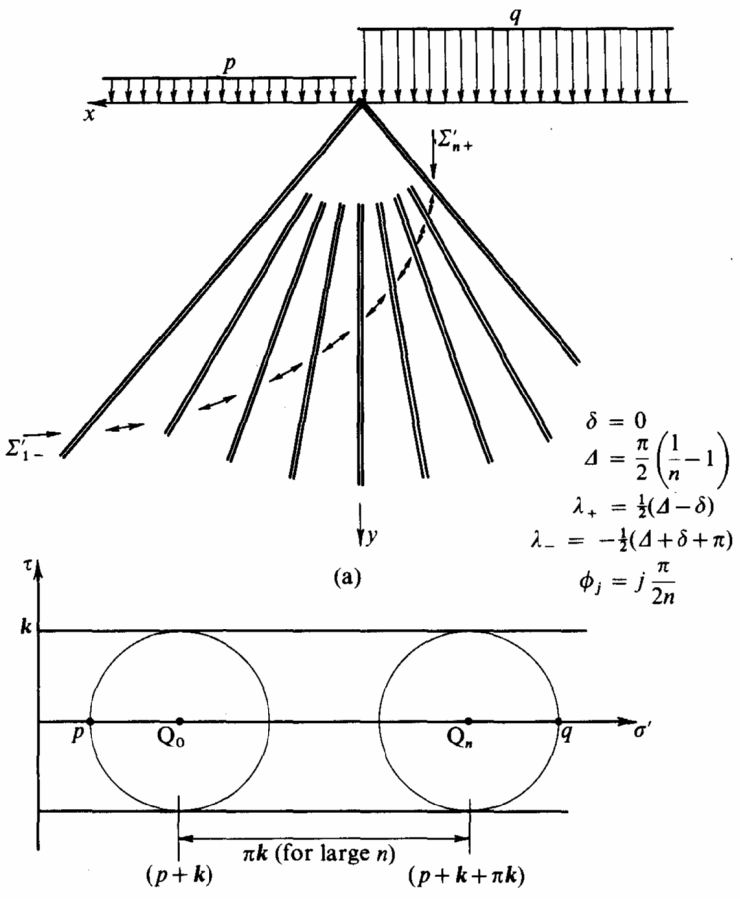

Fig. 9.21 Limiting-stress Field with *n* Discontinuities for Cohesive Soil

which are illustrated in Fig. 9.22(a). Integrating, we find that the total distance apart between the centres of the extreme stress circles becomes

$$\int \mathrm{d}s = \int_0^{\pi/2} 2k\,\mathrm{d}\phi = \pi k$$

leading to $q_{\max} = p + 2k + \pi k = p + 5.14k$.

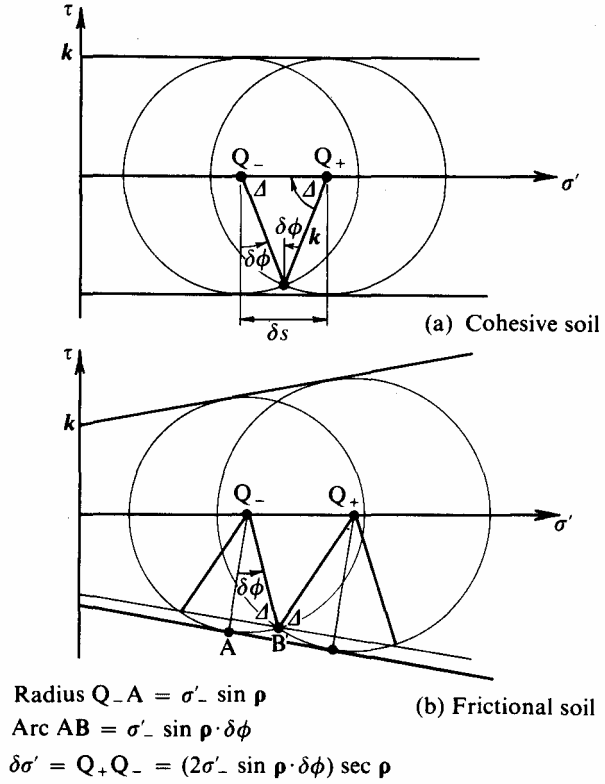

Fig. 9.22 Shift of Limiting Stress Circles for Small Change of ϕ

9.6.2 *Purely frictional soil* $(k = 0, \gamma = 0)$

Figures 9.23(a), 9.24(a), and 9.25(a) illustrate successive solutions to the same problem for n= 1, n=2, and large n except that the soil is now purely frictional. As before, we shall have a change of ϕ of $(\pi/2n)$ at each discontinuity, and negative shear $(\Delta \le 0)$ so that

$$\Delta = -\frac{\pi}{2} + \delta\phi = \frac{\pi}{2}\left(\frac{1}{n} - 1\right).$$

This must be substituted into the appropriate equation, (9.16), to give

$$\frac{\sigma'_+}{\sigma'_-} = \frac{\sin(\Delta + \delta)}{\sin(\Delta - \delta)} = \frac{\sin\Delta\cos\delta + \cos\Delta\sin\delta}{\sin\Delta\cos\delta - \cos\Delta\sin\delta}$$

and introducing $\sin\delta = \sin\Delta\sin\rho$ we obtain

$$\frac{\sigma'_+}{\sigma'_-} = \frac{\cos\delta + \cos\Delta\sin\rho}{\cos\delta - \cos\Delta\sin\rho} = \frac{\cos\delta + \sin\dfrac{\pi}{2n}\sin\rho}{\cos\delta - \sin\dfrac{\pi}{2n}\sin\rho} \tag{9.23}$$

For a *single* discontinuity when $n = 1, \delta = \Delta = 0$ and the two stress circles are spaced so that

$$\frac{\sigma'_+}{\sigma'_-} = \frac{1 + \sin\rho}{1 - \sin\rho};$$

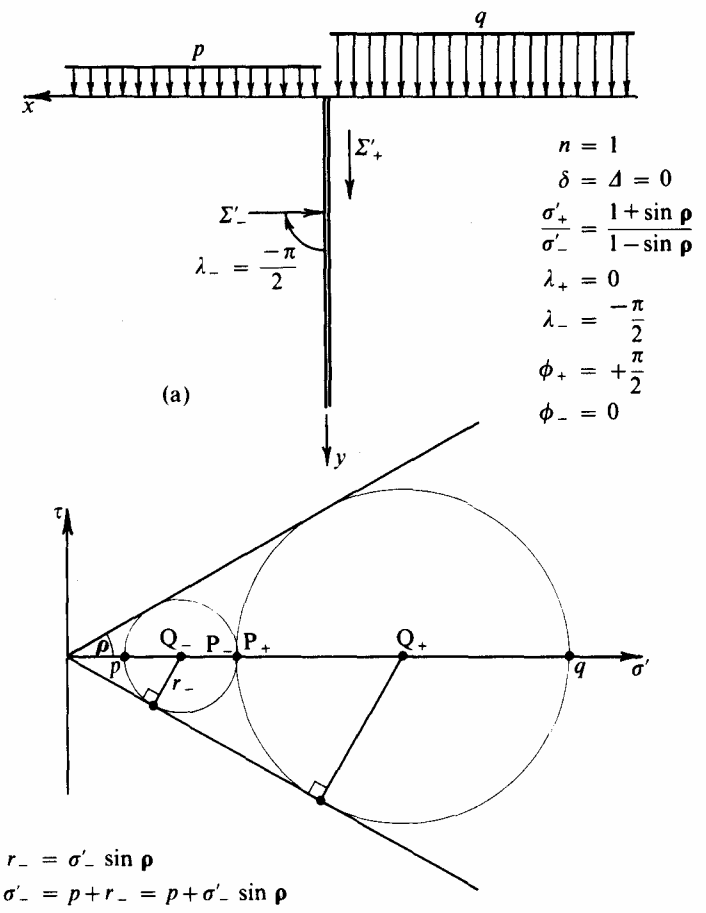

Fig. 9.23 Limiting-stress Field with One Discontinuity for Frictional Soil

in addition

$$p = \sigma'_{-}(1-\sin\rho)$$

$$q = \sigma'_{+}(1+\sin\rho)$$

which leads to

$$q_{\max} = p\left(\frac{1+\sin\rho}{1-\sin\rho}\right)^2.$$

To take a specific example, if ρ = 30° then $q_{\max} = 9p$.

For *two* discontinuities when

$$n = 2, \quad \Delta = -\pi/4, \qquad \sin\delta = -(1/\sqrt{2})\sin\rho$$

and on substitution in eq. (9.23) we can obtain

$$\frac{\sigma'_1}{\sigma'_0} = \frac{1+\sin\rho\sqrt{2-\sin^2\rho}}{1-\sin^2\rho} \qquad \frac{\sigma'_2}{\sigma'_0} = \left(\frac{1+\sin\rho\sqrt{2-\sin^2\rho}}{1-\sin^2\rho}\right)^2$$

and

$$q_{\max} = p\left(\frac{1+\sin\rho}{1-\sin\rho}\right)\left(\frac{1+\sin\rho\sqrt{2-\sin^2\rho}}{1-\sin^2\rho}\right)^2.$$

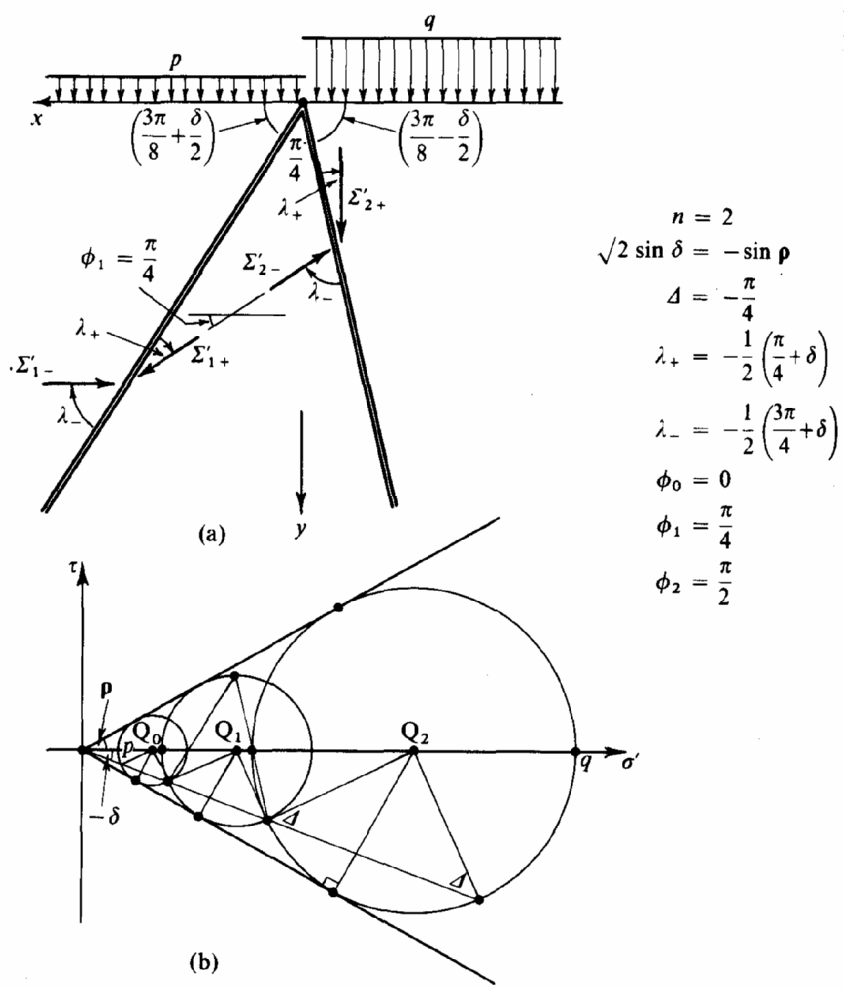

Fig. 9.24 Limiting-stress Field with Two Discontinuities for Frictional Soil

For $\rho = 30^\circ$ this gives $q_{\max} = 14.7p$.

When *n* is *large* we adopt the differential form as before. From eq. (9.16)

$$\sigma'_+ \sin(\Delta - \delta) = \sigma'_- \sin(\Delta + \delta)$$

$$\therefore \quad (\sigma'_+ - \sigma'_-)\sin\Delta\cos\delta = (\sigma'_+ + \sigma'_-)\cos\Delta\sin\delta$$

$$\therefore \quad \frac{(\sigma'_+ - \sigma'_-)}{(\sigma'_+ + \sigma'_-)} = \cot\Delta\tan\delta$$

and as $-\delta \to \rho$

$$\frac{\delta\sigma'}{2\sigma'} = -\cot\left(-\frac{\pi}{2}+\delta\phi\right)\tan\rho = \delta\phi\tan\rho.$$

Integrating, we find that the extreme stress circles are related by

$$\ln\left(\frac{\sigma'_n}{\sigma'_0}\right) = \int_{\sigma'_0}^{\sigma'_n}\frac{d\sigma'}{\sigma'} = \int_0^{\pi/2} 2\tan\rho\, d\phi = \pi\tan\rho$$

which leads to

$$q_{\max} = p\left(\frac{1+\sin\rho}{1-\sin\rho}\right)\exp(\pi\tan\rho).$$

For ρ=30° this gives $q_{\max} \cong 19p$.

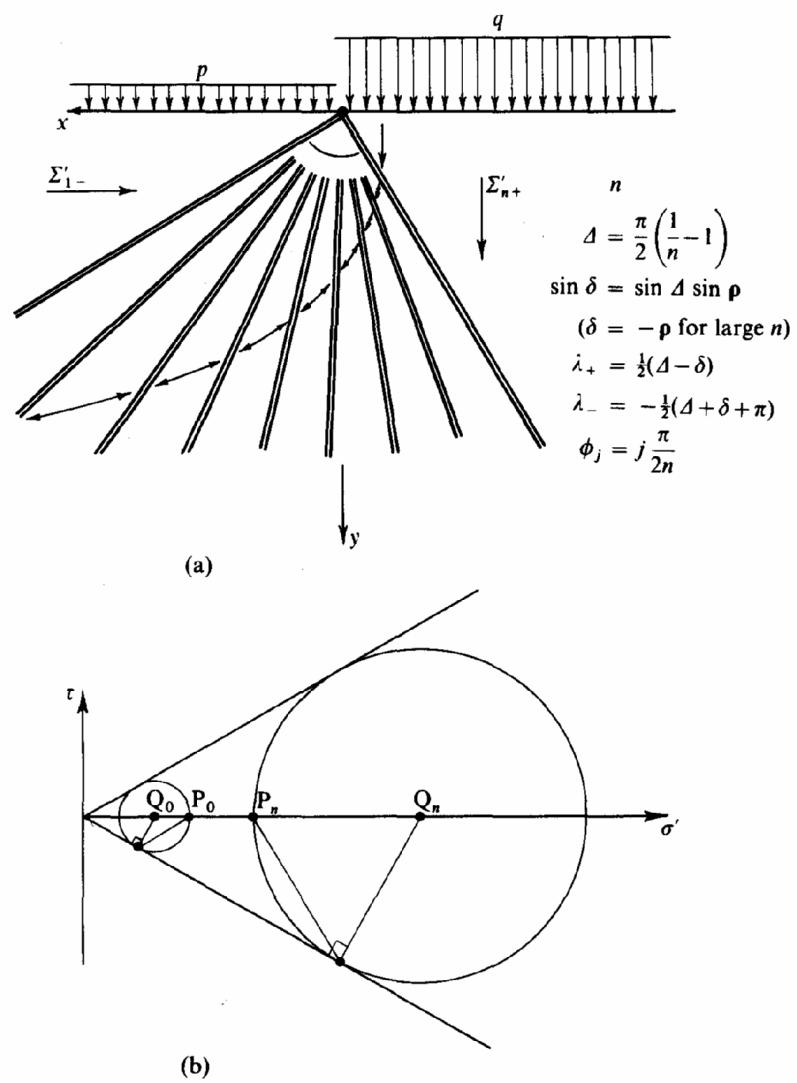

Fig. 9.25 Limiting-stress Field with *n* Discontinuities for Frictional Soil

In the six solutions presented above, each contains regions of *unform* stress separated by strong *discontinuities.* The change of pressure across each discontinuity is characterized by the change of the major principal stress Σ'. Essentially, in this analysis we have replaced the simple idea of one discontinuity of displacement around the surface of a slip circle, by a number of discontinuities of stress which allow successive rotations and changes in magnitude of the major principal stress.

9.7 Upper and Lower Bounds to a Plastic Collapse Load

We now have two strikingly different approximate solutions to the problem of bearing capacity of cohesive ground. In §9.4 our solutions are based on what can be called *kinematically admissible velocity fields*: the mechanism of sliding blocks is compatible with the imposed displacements and the power of the loads moving through the displacements equals the plastic power of dissipation in the cohesive ground. The general solution

$$(q - p) = k\frac{4\alpha}{\sin^2\alpha} \qquad (9.9 \text{ bis})$$

allows us to take for example in Fig. 9.10

$$\alpha = \frac{\pi}{2} \qquad (q - p) = 2\pi k = \underline{6.28k}$$

or equally to find a minimum at

$$\alpha = 66^\circ\,47' \qquad (q - p) = \underline{5.53k.}$$

In contrast in §9.6 we developed solutions based on what can be called *statically admissible stress fields*: the distributed stresses are in equilibrium with the applied loads and nowhere in the interior do they exceed the yield limit. The distribution with a *single* discontinuity Fig. 9.19 gave us

$$(q - p) = \underline{4k};$$

with *two* discontinuities Fig. 9.20 gave us

$$(q - p) = \underline{4.83k},$$

and a fan of *many* discontinuities Fig. 9.21 gave us

$$(q - p) = \underline{5.14k}.$$

These five estimates of the bearing capacity of cohesive ground can be brought into focus if we take advantage of certain theorems established by Prager and his co-workers.[10] Using some virtual work calculations and the normality condition for perfectly plastic associated flow, they showed that for perfectly plastic material solutions based on kinematically admissible velocity fields must be *upper bounds* to the actual collapse loads, whereas those based on statically admissible stress fields must be *lower bounds*. Hence we estimate that the *actual* bearing capacity $(q - p)_{\max}$ would lie in the range

$$6.28k > 5.53k \geq (q - p)_{\max} \geq 5.14k > 4.8k > 4k.$$

The calculations based on slip circles give us loads that are certainly powerful enough to cause failure in the assumed mechanism, and could well exceed the loads that we would calculate if we were able to think of another more subtle mechanism in which the surface could move down with less power being dissipated in the ground. The calculations based on stress distributions give us loads that the ground could certainly carry in the assumed manner, and these loads could well be exceeded if we were to think of a more subtle distribution by which we could pack a little more stress in the ground. To put the matter even more succinctly, the slip-circle calculations would be all right for demolition experts who wanted to be sure to order enough load to cause a failure; but civil engineers who want to be sure of not overloading the ground ought to think first of stress distributions.

Of course, to say this is to oversimplify the matter. The upper and lower bound theorems are established only for perfectly plastic materials: the present uncertainty about the flow rule and about the instability of soil that comes to fail on the ‘dry side’ of critical states makes it possible only to draw inferences. However, when we recall how slight are the factors of safety commonly used in slope design it is clearly wise to pay close attention to calculations that appear to offer us statically admissible stress distributions. The study of the solutions by the method of characteristics that are set out by Sokolovski becomes particularly attractive.

In the next section we briefly consider the simple effects of bodyweight in horizontal layers of soil of differing properties: in a later section we discuss Sokolovski’s general method for analysis of limiting-stress fields with body-weight acting throughout the field.

9.8 Lateral Pressure of Horizontal Strata with Self Weight ($\gamma > 0, \rho > 0$)

We illustrate the application of Sokolovski's method to the case of Fig. 9.26(a) in which two horizontal layers of frictional soil with different properties are shown to be retained by a smooth vertical wall. (We have chosen a simple problem in order to ease the introduction of further unfamiliar symbols and illustrate the nature of

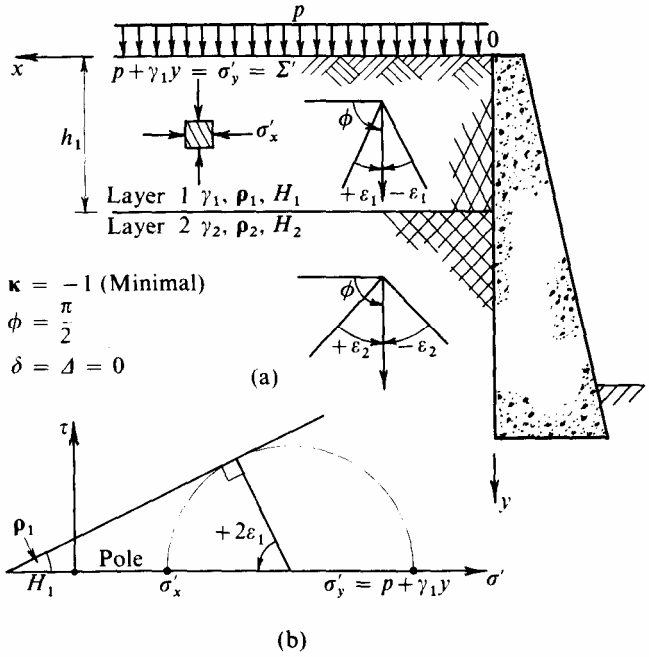

Fig. 9.26 Limiting Lateral Pressure on Retaining Wall: Active Case

Sokolovski's methods; the same solution could be obtained more directly by the conventional method due to Rankine.) The upper layer has thickness h_1 and material properties γ_1, ρ_1 and H_1, while the lower layer has properties γ_2, ρ_2 and H_2 and is of considerable thickness, extending below the base of the wall. A surcharge consisting of a vertical load $p \geq 0$ is assumed to act on the surface; so that Sokolovski's equivalent stress on the surface $(y = 0)$ is simply $p' = p + H_1$.

At a depth y below the surface the vertical stress will be:

$$\left.\begin{aligned} \sigma'_y &= p + \gamma_1 y \qquad (0 \leq y \leq h_1) \\ \sigma'_y &= p + \gamma_1 h_1 + \gamma_2 (y - h_1) \qquad (h_1 \leq y). \end{aligned}\right\} \tag{9.24}$$

In the *minimal* limiting stress state of *active* pressure on the wall the major principal stress Σ' will be vertical $\phi = (\pi/2)$, and the appropriate Mohr's circle for a point at depth y in the upper layer is shown in Fig. 9.26(b).

From the geometry of the figure, the minor principal stress σ'_x is related to σ'_y by the expression

$$\frac{\sigma'_x + H_1}{\sigma'_y + H_1} = \frac{1 - \sin\rho_1}{1 + \sin\rho_1} = \tan^2\left(\frac{\pi}{4} + \frac{\rho_1}{2}\right) = \tan^2 \varepsilon_1 \quad (\rho > 0). \tag{9.25}$$

We have an exactly similar situation for the lower layer, so that we can express the horizontal effective pressure experienced by the retaining wall in the active case as:

$$\left.\begin{aligned}\sigma'_x+H_1 &= (p+\gamma_1 y+H_1)\left(\frac{1-\sin\rho_1}{1+\sin\rho_1}\right) && 0\le y\le h_1\\ \sigma'_x+H_2 &= (p+\gamma_1 h_1+\gamma_2(y-h_1)+H_2)\left(\frac{1-\sin\rho_2}{1+\sin\rho_2}\right) && h_1\le y.\end{aligned}\right\} \tag{9.26}$$

The actual *total* pressure on the wall will include the pore-pressure; for fully saturated soil in the absence of any groundwater flow the pore-pressure $u_w=\gamma_w y$ will increase linearly with depth. The values of γ_1 and γ_2 for the soil must take into account any buoyancy effects.

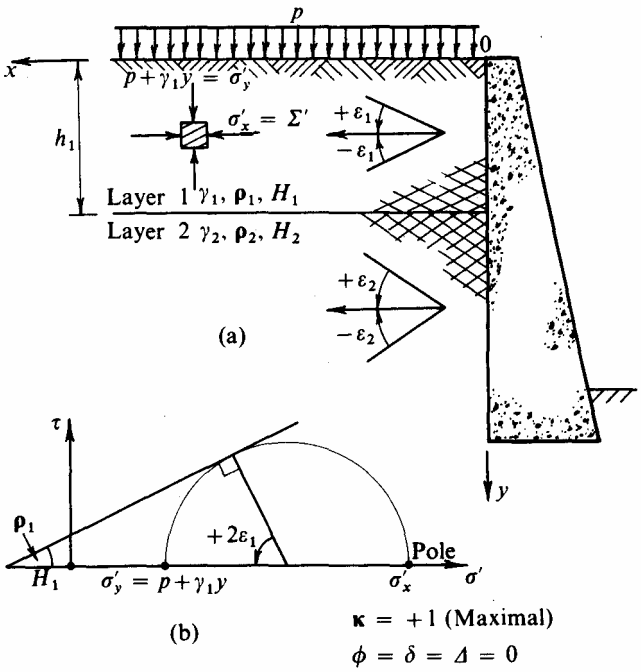

Fig. 9.27 Limiting Lateral Pressure on Retaining Wall: Passive Case

The *passive* case is illustrated in Fig. 9.27(a) where the limiting stress is now *maximal.* The major principal stress is horizontal (ϕ = 0); and in the related Mohr's diagram σ'_x and σ'_y have interchanged their positions from the active case. Equation (9.25) is directly replaced by

$$\frac{\sigma'_y+H_1}{\sigma'_x+H_1}=\frac{1-\sin\rho_1}{1+\sin\rho_1}=\tan^2\varepsilon_1 \tag{9.27}$$

so that for the *passive* case we have

$$\left.\begin{aligned}\sigma'_x+H_1 &= (p+\gamma_1 y+H_1)\left(\frac{1+\sin\rho_1}{1-\sin\rho_1}\right) && (0\le y\le h_1)\\ \sigma'_x+H_2 &= (p+\gamma_1 h_1+\gamma_2(y-h_1)+H_2)\left(\frac{1+\sin\rho_2}{1-\sin\rho_2}\right) && (h_1\le y).\end{aligned}\right\} \tag{9.28}$$

Using Sokolovski's elegant notation we can combine eqs. (9.26) and (9.28) and write

$$\left.\begin{aligned} \sigma'_x + H_1 &= (p + \gamma_1 y + H_1)(\tan\varepsilon_1)^{-2\kappa} && (0 \le y \le h_1) \\ \sigma'_x + H_2 &= (p + \gamma_1 h_1 + \gamma_2 (y - h_1) + H_2)(\tan\varepsilon_2)^{-2\kappa} && (h_1 \le y) \end{aligned}\right\} \tag{9.29}$$

where $\kappa = -1$ gives the active case
and $\kappa = +1$ gives the passive case.

In each layer the lateral pressure varies linearly with depth and the distributions are plotted in Fig. 9.28. The slopes

$$\frac{d\sigma'_x}{dy} = \gamma_1 (\tan\varepsilon_1)^{-2\kappa} \qquad (0 \le y \le h_1)$$

$$\frac{d\sigma'_x}{dy} = \gamma_2 (\tan\varepsilon_2)^{-2\kappa} \qquad (h_1 \le y)$$

depend only on the local value of γ and ρ. So change of cohesion $\boldsymbol{k}$ or surcharge p would only change the datum of the pressure-distribution line (as would a change in pore pressure u_w): it requires a change of density γ or friction ρ to rotate the line.

For the construction of Fig. 9.28 it has been assumed that the groundwater table is at the surface so that the soil is fully saturated, and the submerged bulk densities must be used for calculation of

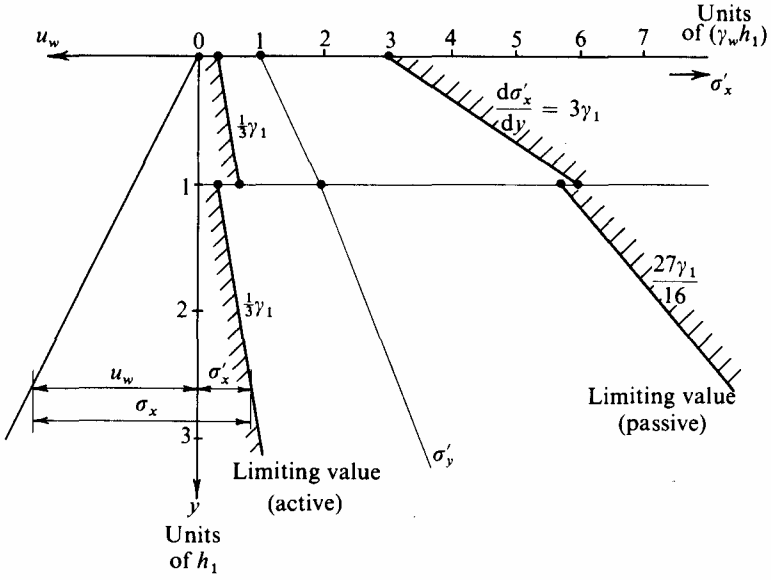

Fig. 9.28 Limiting Lateral Pressure Distribution

effective stresses. The following values have been adopted: $p = \gamma_w h_1$ and for the upper layer

$$\gamma'_1 = \gamma_w, \qquad H_1 = 0, \qquad \tan^2\varepsilon_1 = \tfrac{1}{3}, \qquad i.e., \rho_1 = \pi/6 = 30^\circ$$

and for the lower layer

$$\gamma'_2 = \tfrac{3}{4}\gamma_w, \qquad H_2 = \gamma_w h_1, \qquad \tan^2\varepsilon_2 = \tfrac{4}{9}, \qquad i.e., \rho_2 = 0.3945 = 22^\circ 36'.$$

Across the interface there is, of course, no sudden jump in the value of the vertical effective pressure σ'_y (although its derivative is not continuous); figuratively speaking, if an observer inserted the palm of his hand *horizontally* into the soil he could not detect where the interface was or whether the soil was in a maximal or minimal stress state.

However, just above the interface the lateral effective pressure would be

$$\sigma'_x = (\gamma_w h_1 + \gamma_w h_1 + 0)(3)^\kappa,$$

i.e., $\sigma'_x = 6\gamma_w h_1$ for $\kappa = +1$, or $\frac{2}{3}\gamma_w h_1$ for $\kappa = -1$

whereas just below

$$\sigma'_x + \gamma_w h_1 = (\gamma_w h_1 + \gamma_w h_1 + \gamma_w h_1)\left(\tfrac{9}{4}\right)^\kappa,$$

i.e., $\sigma'_x = 5\frac{3}{4}\gamma_w h_1$ for $\kappa = +1$, or $\frac{1}{3}\gamma_w h_1$ for $\kappa = -1$.

An observer who was able to insert the palm of his hand *vertically* could detect the presence of the interface and the state of the soil.

If a greater value of H_2, for example, $H_2 = 2\gamma_w h_1$, had been appropriate, we would have required $\sigma'_x = -\frac{2}{9}\gamma_w h_1$ to bring the soil just below the interface into a minimal limiting state. But since the *effective* stress between the soil and the wall cannot be tensile, Sokolovski introduces the restriction $\sigma'_x \geq 0$ that and concludes that where the mathematical expressions would lead to a negative value of σ'_x the soil cannot be in a limiting state.

In Fig. 9.28 the distribution of pore-pressure u_w has been drawn to the left of the vertical axis of y, with the result that the total lateral pressure at any depth is readily obtained.

Clearly this method can be extended to any number of strata, and can be adapted to take account of other groundwater conditions, or a particular layer that is considered to be purely cohesive.

9.9 The Basic Equations and their Characteristics for a Purely Cohesive Material

In this section we will be covering much of the material set out in Sokolovski's *Statics of Granular Media* §3 and §17, but in detail our treatment will be closer to that presented by Hildebrand.[11]

When we consider the two-dimensional field of stress acting on any material we have two differential equations of equilibrium. For the reference axes of Fig. 9.29 these are:

$$\left.\begin{aligned} \frac{\partial \sigma'_x}{\partial x} + \frac{\partial \tau_{xy}}{\partial y} &= 0 \\ \frac{\partial \tau_{xy}}{\partial x} + \frac{\partial \sigma'_y}{\partial y} &= \gamma \end{aligned}\right\} \tag{9.3}$$

which can be obtained directly by resolving the forces acting on the element, and using the identity of complementary shear stresses ($\tau_{xy} = \tau_{yx}$). We only require one further equation to make the three unknowns $\sigma'_x, \tau_{xy}, \sigma'_y$ determinate.

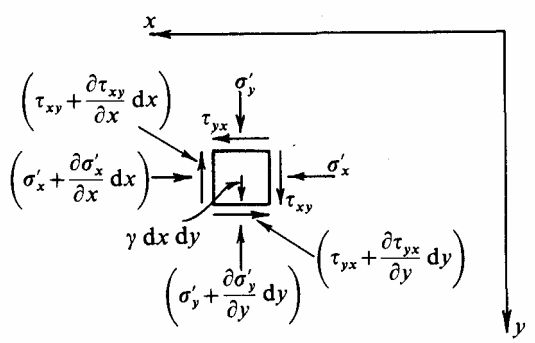

Fig. 9.29 Stresses Acting on Element of Soil

To take a simple example Fig. 9.30(a), consider the calculation of shear stress in a uniform horizontal cantilever of length *l,* of rectangular section with breadth *b* and depth *d,* and carrying a concentrated load *W* at its free end. If we assume the linear distribution of axial stress σ'_x across a vertical section (at a distance *x* from the

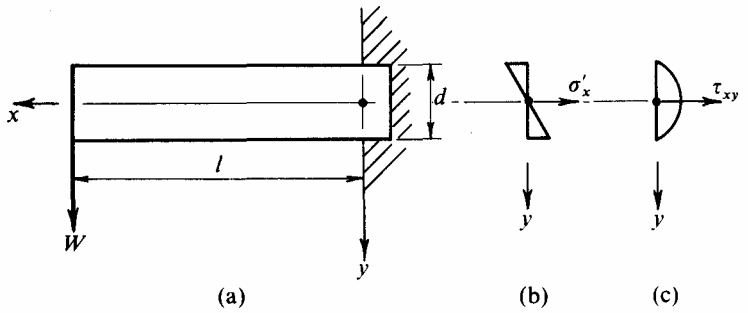

Fig. 9.30 Stress Distributions for Loaded Cantilever

root of the cantilever) in Fig. 9.30(b), then by taking moments we have

$$\frac{\sigma'_x}{y}.\frac{bd^3}{12} = W(l-x). \tag{9.31}$$

This equation is the third one necessary to make the problem completely determinate and we have no further freedom to make other specifications.

The first equilibrium equation (9.30a) gives

$$\frac{\partial \tau_{xy}}{\partial y} = -\frac{\partial \sigma'_x}{\partial x} = +\frac{12W}{bd^3}.y$$

and integrating with the boundary condition $\tau = 0$ at $y = \pm d/2$ we obtain the familiar parabolic distribution for shear stress

$$\tau_{xy} = \frac{6W}{bd^3}\left(y^2 - \frac{d^2}{4}\right) \tag{9.32}$$

which is illustrated in Fig. 9.30(c). (The second equilibrium equation leads to $\sigma'_y = \gamma y$; in normal circumstances this would be negligible compared with the values of σ'_x and τ_{xy})

It is significant that this result is independent of the actual material of the beam whether it is steel, concrete, wood, or plastic so long as the assumption of the linear distribution of σ'_x remains valid. The material properties will only influence the resulting elastic *strains* of the cantilever.

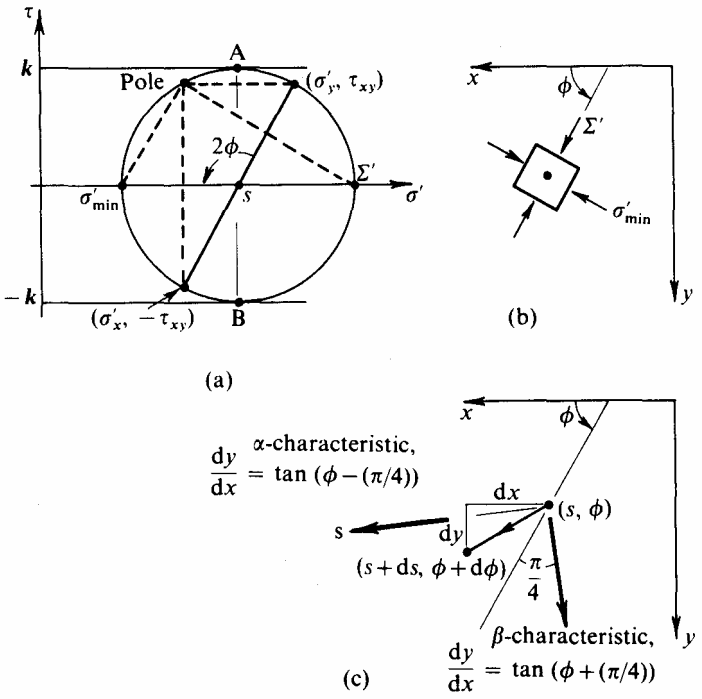

Fig. 9.31 Characteristic Directions for Cohesive Soil

In the same way, in the theory of two-dimensional limiting-stress fields as soon as we postulate that the stresses shall be limiting *everywhere* we have made the problem completely determinate. We now choose to concentrate on purely cohesive materials, so that the condition of limiting stress is given by

$$\tfrac{1}{4}(\sigma'_x - \sigma'_y)^2 + \tau_{xy}^2 = k^2 \tag{9.33}$$

which is the equation to the Mohr's circle of Fig. 9.31.

It is convenient to express this in an alternative form by the parameters s and ϕ (which respectively specify the centre of Mohr's circle and the direction of major principal stress) as follows:

$$\left.\begin{aligned} \sigma'_x &= s + k\cos 2\phi \\ \sigma'_y &= s - k\cos 2\phi \\ \tau_{xy} &= k\sin 2\phi. \end{aligned}\right\} \tag{9.34}$$

Substituting these into the equilibrium eqs. (9.30) we have

$$\left.\begin{aligned} &\frac{\partial s}{\partial x} - 2k\sin 2\phi\frac{\partial \phi}{\partial x} + 2k\cos 2\phi\frac{\partial \phi}{\partial y} = 0 \\ &\frac{\partial s}{\partial y} + 2k\cos 2\phi\frac{\partial \phi}{\partial x} + 2k\sin 2\phi\frac{\partial \phi}{\partial y} = \gamma \\ &\text{which together with the identities for total differentials} \\ &\frac{\partial s}{\partial x}\mathrm{d}x + \frac{\partial s}{\partial y}\mathrm{d}y = \mathrm{d}s \\ &\frac{\partial \phi}{\partial x}\mathrm{d}x + \frac{\partial \phi}{\partial y}\mathrm{d}y = \mathrm{d}\phi \end{aligned}\right\} \tag{9.35}$$

provide four equations for the four unknowns

$$\frac{\partial s}{\partial x}, \frac{\partial s}{\partial y}, \frac{\partial \phi}{\partial x}, \text{and } \frac{\partial \phi}{\partial y}.$$

The solution of the problem of limiting-stress distributions in purely cohesive materials lies in this set of four equations. Leaving aside the special case of finite discontinuity in values of s and ϕ we consider small regions or zones in which there is a continuous variation in values of these parameters. At a typical point (x, y) in Fig. 9.3 1(c) we have data of (s, ϕ) while at an adjacent point $(x + \mathrm{d}x, y + \mathrm{d}y)$ the data are $(s + \mathrm{d}s, \phi + \mathrm{d}\phi)$. If we know values of $\mathrm{d}x$, $\mathrm{d}y$, $\mathrm{d}s$, $\mathrm{d}\phi$ can we find values of $\partial s/\partial x, \partial s/\partial y, \partial \phi/\partial x, \partial \phi/\partial y$, and vice versa? If we can, then a reasonable approximation to the values of s and ϕ in a region surrounding the two points can be obtained by extrapolation. To decide whether this is possible we must examine the equations in detail.

In order to calculate the partial derivatives from given values of $\mathrm{d}x$, $\mathrm{d}y$, $\mathrm{d}s$, and $\mathrm{d}\phi$ we will need to invert the matrix of coefficients on the left-hand side of equations (9.35). This inversion will not be possible when the associated determinant is zero, i.e., when

$$0 = D = \begin{vmatrix} 1 & 0 & -\sin 2\phi & \cos 2\phi \\ 0 & 1 & \cos 2\phi & \sin 2\phi \\ \mathrm{d}x & \mathrm{d}y & 0 & 0 \\ 0 & 0 & \mathrm{d}x & \mathrm{d}y \end{vmatrix} = -(\mathrm{d}y)^2 \cos 2\phi + 2\mathrm{d}x\mathrm{d}y \sin 2\phi - (\mathrm{d}x)^2 \cos 2\phi$$

$$= -\left[\mathrm{d}y - \mathrm{d}x \tan\left(\phi + \frac{\pi}{4}\right)\right]\left[\mathrm{d}y - \mathrm{d}x \tan\left(\phi - \frac{\pi}{4}\right)\right]\cos 2\phi \qquad (9.36)$$

and

$$\tan\left(\phi + \frac{\pi}{4}\right)\tan\left(\phi - \frac{\pi}{4}\right) = 1.$$

Clearly for the directions given by $\mathrm{d}y/\mathrm{d}x = \tan\{\phi \pm (\pi/4)\}$ the determinant is zero; and we shall have no prospect of finding partial derivatives if the values of $\mathrm{d}s$ and $\mathrm{d}\phi$ that are adopted happen to come from adjacent points in one of these *characteristic* directions. It is necessary to study conditions *along* the characteristics.

Sokolovski multiplies the first equation of the set (9.35) by $\sin\{\phi \pm (\pi/4)\}$, the second equation by $-\cos\{\phi \pm (\pi/4)\}$ and adds the results to obtain (after some manipulation)

$$\left[\frac{\partial s}{\partial x} \mp 2k\frac{\partial \phi}{\partial x}\right]\cos\left(\phi \mp \frac{\pi}{4}\right) + \left[\frac{\partial s}{\partial y} \mp 2k\frac{\partial \phi}{\partial y} - \gamma\right]\sin\left(\phi \mp \frac{\pi}{4}\right) = 0. \qquad (9.37)$$

He then introduces two new parameters ξ and η where

$$\left.\begin{aligned} 2k\xi &= s - \gamma y + 2k\phi \\ 2k\eta &= s - \gamma y - 2k\phi. \end{aligned}\right\} \qquad (9.38)$$

Partial differentiation of these parameters and substitution into eq. (9.37) leads to

$$\left.\begin{aligned} \frac{\partial \xi}{\partial x}\cos\left(\phi + \frac{\pi}{4}\right) + \frac{\partial \xi}{\partial y}\sin\left(\phi + \frac{\pi}{4}\right) &= 0 \\ \frac{\partial \eta}{\partial x}\cos\left(\phi - \frac{\pi}{4}\right) + \frac{\partial \eta}{\partial y}\sin\left(\phi - \frac{\pi}{4}\right) &= 0. \end{aligned}\right\} \qquad (9.39)$$

Along the β-characteristic in Fig. 9.31(c),

$$\frac{\mathrm{d}y}{\mathrm{d}x} = \tan\left(\phi + \frac{\pi}{4}\right)$$

we can re-write the first equation as

$$0 = \frac{\partial \xi}{\partial x}\mathrm{d}x + \frac{\partial \xi}{\partial y}\mathrm{d}y = \mathrm{d}\xi \text{ (by definition)}$$

which leads to the important result that

$$\xi = \frac{s - \gamma y}{2k} + \phi = \text{constant} \qquad \left[\frac{\mathrm{d}y}{\mathrm{d}x} = \tan\left(\phi + \frac{\pi}{4}\right)\right]. \tag{9.40}$$

Similarly, *along* the α-characteristic

$$\frac{\mathrm{d}y}{\mathrm{d}x} = \tan\left(\phi - \frac{\pi}{4}\right)$$

the second equation leads to

$$0 = \frac{\partial \eta}{\partial x}\mathrm{d}x + \frac{\partial \eta}{\partial y}\mathrm{d}y = \mathrm{d}\eta,$$

$$\eta = \frac{s - \gamma y}{2k} - \phi = \text{constant} \qquad \left[\frac{\mathrm{d}y}{\mathrm{d}x} = \tan\left(\phi - \frac{\pi}{4}\right)\right]. \tag{9.41}$$

Although we cannot calculate the *partial* derivatives of s and ϕ we do know the *total* differentials of ξ and η along the characteristics. In the next sections we will show how this remarkable property of the characteristics may be used to solve problems of limiting-stress fields in a cohesive soil.

9.10 The General Numerical Solution

We will explain, in general terms, the development of the numerical solution for one simple example that involves a body of purely cohesive soil with self weight, in a *minimal* stress state, below a horizontal boundary Ox on which a vertical surcharge causes an unevenly distributed normal pressure. In Fig. 9.32(a) at points A_{00} and A_{11} on the boundary the normal pressures are p_0 and p_1, where

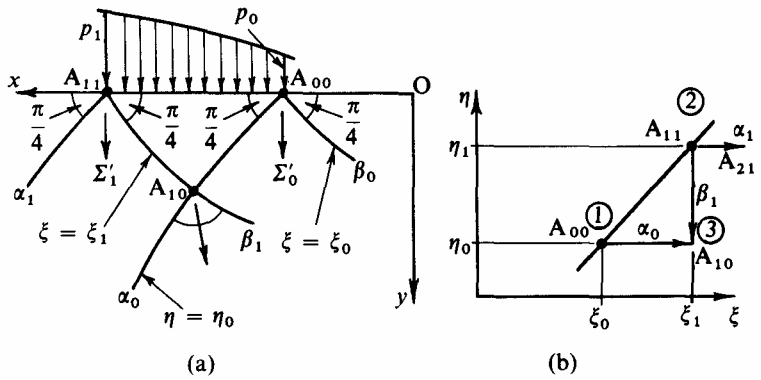

Fig. 9.32 Mapping of Characteristics for Numerical Solution

$p_0 < p_1$. Just below each of these points the states of stress in the soil are defined by

$$\left.\begin{aligned} s_0 &= p_0 - k \qquad \phi_0 = \frac{\pi}{2}, \\ s_1 &= p_1 - k \qquad \phi_1 = \frac{\pi}{2}. \end{aligned}\right\} \tag{9.42}$$

From these values we calculate

$$\xi_0 = \frac{p_0}{2k} - \frac{1}{2} + \frac{\pi}{2} \qquad \eta_0 = \frac{p_0}{2k} - \frac{1}{2} - \frac{\pi}{2}$$
$$\xi_1 = \frac{p_1}{2k} - \frac{1}{2} + \frac{\pi}{2} \qquad \eta_1 = \frac{p_1}{2k} - \frac{1}{2} - \frac{\pi}{2}$$

in Fig. 9.32(b) we display the plane of characteristics (ξ, η) on which we can plot points A_{00} and A_{11}.

Through A_{00} we draw the characteristic $\eta = \text{const.} = \eta_0$, through A_{11} we draw the characteristic $\xi = \text{const.} = \xi_1$, and these intersect in the point A_{10}. The point A_{10} is such that and therefore

$$\left.\begin{aligned} \xi &= \frac{s}{2k} + \phi - \frac{\gamma y}{2k} = \xi_1 = \frac{p_1}{2k} - \frac{1}{2} + \frac{\pi}{2} \\ \eta &= \frac{s}{2k} - \phi - \frac{\gamma y}{2k} = \eta_0 = \frac{p_0}{2k} - \frac{1}{2} - \frac{\pi}{2} \end{aligned}\right\} \tag{9.43}$$

and the stress parameters s and ϕ at the point A_{10} are clearly

$$\left.\begin{aligned} s &= \frac{p_1 + p_0}{2} - k + \gamma y \\ \phi &= \frac{p_1 - p_0}{4k} + \frac{\pi}{2}. \end{aligned}\right\} \tag{9.44}$$

So the consequence of the property of the characteristics (that total differentials are known along them) is that we now know exactly what the stresses are at this point A_{10} in the soil below the loaded surface. The remaining numerical problem is simply one of mapping; to find where the point A_{10} is on the (x, y) plane — that is to map the sheet $A_{11}A_{10}A_{00}$ from the (ξ, η) plane on to the (x, y) plane.

Sokolovski gives an approximate method that is quite effective for mapping out these points. A table is drawn up where each row and each column correspond to a characteristic. The table resembles the construction of lines on the (ξ,η) plane in Fig. 9.32(b). Diagonally across the table the values given to parameters (x, y, s,ϕ) are those for the appropriate positions on the boundary. At two points 1 and 2 within the table let the values (x_1, y_1, s_1,ϕ_1) and (x_2, y_2, s_2,ϕ_2) be known. To find the values at the next successive point 3, replace the differential equations by *recurrence formulae*

$$\left.\begin{aligned} &\left.\begin{aligned} (y_3 - y_1) &= (x_3 - x_1)\tan\left(\phi_1 - \frac{\pi}{4}\right) \\ s_3 - s_1 - 2k(\phi_3 - \phi_1) &= \gamma(y_3 - y_1) \end{aligned}\right\} \eta = \text{const.} \\ &\left.\begin{aligned} (y_3 - y_2) &= (x_3 - x_2)\tan\left(\phi_2 + \frac{\pi}{4}\right) \\ s_3 - s_2 - 2k(\phi_3 - \phi_2) &= \gamma(y_3 - y2) \end{aligned}\right\} \xi = \text{const.} \end{aligned}\right\} \tag{9.45}$$

and hence the values of (x_3, y_3, s_3,ϕ_3) may be determined. As this programme of calculation is followed so successive compartments of the table are filled. The numbers in each compartment fix the position of one node in the pattern of characteristics shown in Fig. 9.32(a) and the state of stress at that node.

It is clear that although the above paragraphs only cover one example, the same method will apply to soil with internal friction, with or without self weight: of course different recurrence formulae will be appropriate for different problems[12] and special

formulae will have to be developed to meet special difficulties at some boundaries, but for all such developments direct reference should be made to Sokolovski's texts.

9.11 Sokolovski's Shapes for Limiting Slope of a Cohesive Soil

We now consider Sokolovski's use of integrals of the equations of limiting equilibrium in regions throughout which either ξ or η has constant values. We consider only regions where ξ is constant, since those with η constant are the exact converse and the families of characteristics become interchanged. In the regions where ξ is constant everywhere and η varies then

$$\frac{s-\gamma y}{2k}+\phi=\xi=\xi_0=\text{constant} \tag{9.46}$$

and the one constant ξ_0 applies to *every* β-characteristic. The family of α-characteristics for which $\mathrm{d}y=\mathrm{d}x\tan(\phi-\pi/4)$ must become a set of straight lines since

$$\eta=\frac{s-\gamma y}{2k}-\phi=\xi-2\phi=\xi_0-2\phi \tag{9.47}$$

so that $\mathrm{d}\eta=-2\mathrm{d}\phi$ and ϕ will be constant along each α-characteristic. The equation of any α-characteristic becomes

$$\frac{y-y(\phi)}{x-x(\phi)}=\tan\left(\phi-\frac{\pi}{4}\right) \tag{9.48}$$

where $(x(\phi), y(\phi))$ are the coordinates of some fixed point on the characteristic.

For the special case when all α-characteristics pass through one point we can choose it as the origin of coordinates so that $x(\phi)\equiv y(\phi)\equiv 0;$ and the family of α-characteristics is simply a fan of radial straight lines. The curved β-characteristics having

$$\mathrm{d}y=\mathrm{d}x\tan\left(\phi+\frac{\pi}{4}\right)$$

are then segments of concentric circles orthogonal to these radii.

Solutions to specific problems can be constructed from patchwork patterns of such regions, as we see for the general case of the limiting stability of a slope of a cohesive soil shown in Fig. 9.34 (and as we saw for the case of high-speed fluid flow in Fig. 1.8). The essential feature of these solutions is that the values of one parameter (ξ in Fig. 9.34) which are imposed at one boundary (OA_0) remain unchanged and are propagated through the pattern and have *known* values at a boundary of interest ($0A_3$).

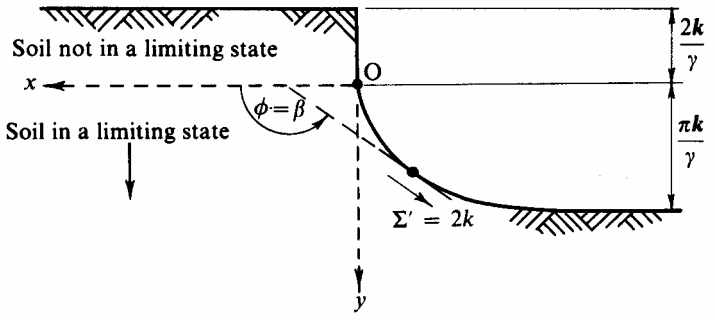

Fig. 9.33 Limiting Shape of Slope in Cohesive Soil

A limiting shape for a slope in cohesive soil is shown in Fig. 9.33 and we begin by making

a simple analysis of conditions along the slope, which forms the boundary of interest. Above O there is a vertical face of height $h = 2k/\gamma$ for which the soil (of self-weight γ and cohesion k) is *not* in a limiting state. At any point on the curved slope the major principal stress is at an angle ϕ equal to the angle β of the slope at that point, and of magnitude $2k$ so that the values of the parameters s and ϕ along the curve are

$$s = k \quad \text{and} \quad \phi = \beta \tag{9.49}$$

In Fig. 9.33 we have taken the slope at O to be vertical so that $\beta = \beta_0 = \pi/2$, but in Fig. 9.34 we show a generalized slope problem where the weight of soil above the line OA_0 is replaced by a uniformly distributed surcharge p, and $\beta_0 \neq \pi/2$. Below the line OA_0 in Fig. 9.34 is a region A_0OA_1 dependent on the conditions along the boundary OA_0. It is a region of a single state (ξ_0, η_0) with straight parallel characteristics in each direction and with

$$\left.\begin{aligned} s &= p + \gamma y - k \qquad \phi = \pi/2 \\ \xi &= \xi_0 = \frac{p-k}{2k} + \frac{\pi}{2} \\ \eta &= \eta_0 = \frac{p-k}{2k} - \frac{\pi}{2} \end{aligned}\right\} \tag{9.50}$$

The shape of the slope must be such that retains the value given in eq. (9.50), and that the conditions of eq. (9.49) are satisfied.

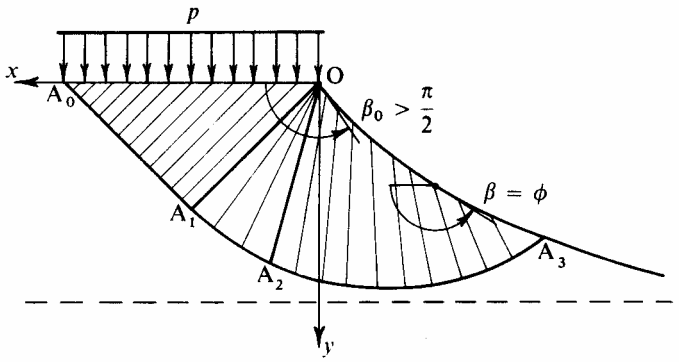

Fig. 9.34 General Limiting Shape of Slope in Cohesive Soil (After Sokolovski)

We have, therefore,

$$\xi = \frac{s - \gamma y}{2k} + \phi = \frac{k - \gamma y}{2k} + \beta \quad \text{and} \quad \xi = \xi_0 = \frac{p-k}{2k} + \frac{\pi}{2},$$
$$\text{so that} \qquad y = \frac{2k}{\gamma}(\beta - \beta_0) \qquad \text{where } \beta_0 = \left(\frac{p}{2k} + \frac{\pi}{2} - 1\right). \tag{9.51}$$

But at any point on the slope $\mathrm{d}y = \mathrm{d}x \tan\beta$ so that substituting for y from eq. (9.51) we find

$$\mathrm{d}x = \frac{2k}{\gamma}\cot\beta\,\mathrm{d}\beta$$

which can be integrated to give

$$\frac{\gamma x}{2k} = \ln\left(\frac{\sin\beta}{\sin\beta_0}\right). \tag{9.52}$$

The limiting slope must therefore have as its equation

$$\frac{\gamma x}{2k} = \ln \frac{\sin(\beta_0 + \gamma y/2k)}{\sin \beta_0} \tag{9.53}$$

and have a horizontal asymptote

$$\frac{\gamma y}{2k} = \pi - \beta_0 \tag{9.54}$$

Various slope profiles corresponding to different values of β_0 are shown in Fig. 9.35 which is taken from Fig. 178 of the earlier translation of Sokolovski's text.

In the particular case of Fig. 9.33 when $\beta_0 = \pi/2$ the slope equation becomes

$$\frac{\gamma x}{2k} = \ln \cos\left(\frac{\gamma y}{2k}\right) \tag{9.55}$$

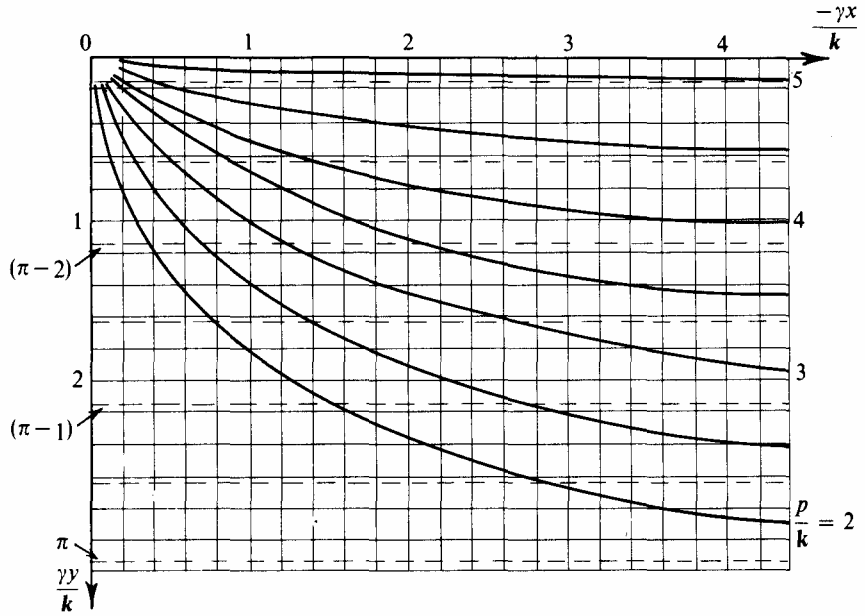

Fig. 9.35 Limiting Shapes of Slope in Cohesive Soil for Various Values of Surcharge (After Sokolovski)

having a horizontal asymptote $y = \pi k/\gamma$. Thus the maximum difference in height between the left and right hand levels of Fig. 9.33 is $(2 + \pi)k/\gamma$, which is the maximum difference predicted in §9.7.

9.12 Summary

At this stage of the book we are aware of the consequences of our original decision to set the new critical state concept among the classical calculations of soil mechanics. Our new models allow the prediction of *kinematics* of soil bodies, and yet here we have restricted our attention to the calculation of limiting equilibrium and have introduced Sokolovski's classical exposition of the *statics* of soil media. The reason for this decision is that it is this type of statical calculation that at present concerns practical engineers, and the capability of the new critical state concept to offer rational predictions of *strength* is of immediate practical importance. In this chapter we have reviewed the manner of working of the classical calculations in which the only property that is attributed to soil is strength. We hope that this will give many engineers an immediate incentive to make use of the new

critical state concept, and perhaps in due course become actively interested in the development of new calculations of *deformation* that the concept should make possible.

References to Chapter 9

1 Coulomb, C. A. Essai sur une application des règles de maximis et minimis a quelques problémes de statique, relatifs a l'architecture, *Mémoires de Mathématique de l'Académie Royale des Sciences,* Paris, 7, 343 – 82, 1776.

2 Terzaghi, K. Large Retaining Wall Tests, *Engineering News Record,* pp. 136, *259,* 316, 403, 503, 1934.

3 Coulomb, C. A. Théorie des machines simples, *Mémoires de Mathématique de l'Académie Royale des Sciences,* Paris, 10, 161 – 332, 1785.

4 Petterson, K. E. The Early History of Circular Sliding Surfaces, *Géotechnique,* 5, *275 –96,* 1955.

5 Fellenius, W. *Erdstatische Berechnungen,* Ernst, Berlin, 1948.

6 Taylor, D. W. *Fundamentals of Soil Mechanics,* Wiley, 1948.

7 Janbu, N. Earth Pressures and Bearing Capacity Calculations by Generalised Procedure of Slices, *Proc. 4th mt. Conf Soil Mech. and Found. Eng.,* London, vol 2, pp. 207 – 12, 1957.

8 Bishop, A. W. and Morgenstern, N. R. Stability Coefficients for Earth Slopes, *Géotechnique,* 10, 129 – 50, 1960.

9 Sokolovski, 'V. V. *Statics of Granular Media,* Pergamon, 1965.

10 Prager, W. *An Introduction to Plasticity,* Addison-Wesley, 1959.

11 Hildebrand, F. B. *Advanced Calculus for Application,* Prentice-Hall, 1963.

12 Mukhin, I. S. and Sragovich, A. I. Shape of the Contours of Uniformly Stable Slopes, *Inzhenernyi Sbornik,* 23, 121 – 31, 1956.

10
Conclusion

10.1 Scope

We have introduced the new critical state concept among older concepts of classical soil mechanics, but it would be wrong to leave any impression at the end of this book that the new concept merely rejuvenates the classical calculations. In this brief conclusion we concentrate only on the new concept of critical states and try to illustrate in a compact manner the new insight into the mechanical behaviour of soil under three headings:
§10.2 We acquire a new basis for engineering judgement of the state of ground and the consequences of proposed works.
§10.3 We can review existing tests and devise new ones.
§10.4 We can initiate new research into soil deformation and flow.

10.2 Granta-gravel Reviewed

Let us review the Granta-gravel model in Fig. 10.1(a), where we plot six curved λ-lines at equal spacings lettered VV, AA, BB, CC, DD, and EE on the (v, p) plane. The double line CC represents the *critical states* and the line VV represents *virgin isotropic compression* of Granta-gravel. Between VV and CC we have *wet states* of soil in which it consolidates in Terzaghi's manner, and AA and BB are typical curves of anisotropic compression. Under applied loading the *wet* soil flows and develops positive pore-pressures or drains and hardens; the whole soil body tends to deform plastically, and hence, the typical drainage paths are long and the *undrained* problem occurs resulting in *immediate* limiting equilibrium problems which involve calculations with $k = c_u$ and $\rho = 0$.

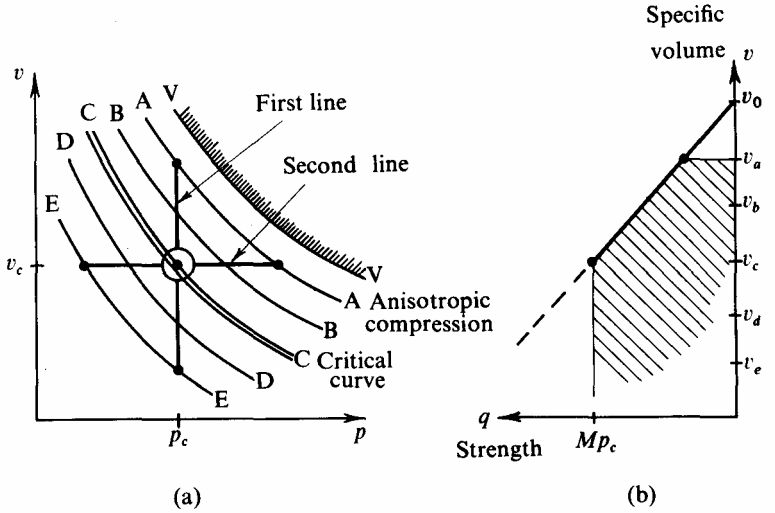

Fig. 10.1 Review of Granta-gravel

In contrast, the curves DD and EE are in the *dry states* of soil in which it ruptures and slips in Coulomb's manner as a rubble of blocks. Each thin slip zone has a short drainage path and the *drained* problem occurs resulting in *long-term* limiting equilibrium

problems which involve calculations with $k = 0$ and ρ at a value consistent with the critical states.

Across the Fig. 10.1(a) we draw two bold lines that correspond to two interesting engineering problems. The first line is at *constant effective spherical pressure* p_c and it intersects the λ-lines at specific volumes $v_a, v_b, v_c, v_d,$ and v_e. The second line is at *constant specific volume* v_c and it intersects the λ-lines at $p_a, p_b, p_c, p_d,$ and p_e. In Fig. 10.1(b) we plot the stable state boundary curve that corresponds to the first line; what does the figure imply?

We can think of $v_a, v_b, v_c, v_d,$ and v_e as being the alternative specific volumes to which a layer of saturated remoulded Granta-gravel can be compacted by alternative increasingly costly *compaction* operations. Suppose that the layer will eventually form part of an *embankment* in which it will be under some particular value of effective spherical pressure p_c. We consider what benefit is to be gained from increased compaction, and Fig. 10.1(b) shows that from v_a to v_b to v_c there is a steady increase in strength q, but from v_c to v_d to v_e further compaction is wasted. For, while individual blocks might have increasing strengths (near the dotted line in Fig. 10.1(b)), the engineering design of the embankment would have to proceed on the assumption that the blocks would be ruptured in the long-term problem and that the relevant strength parameter was Mp_c. There is no gain in *guaranteed* strength with increased compaction beyond the critical state.

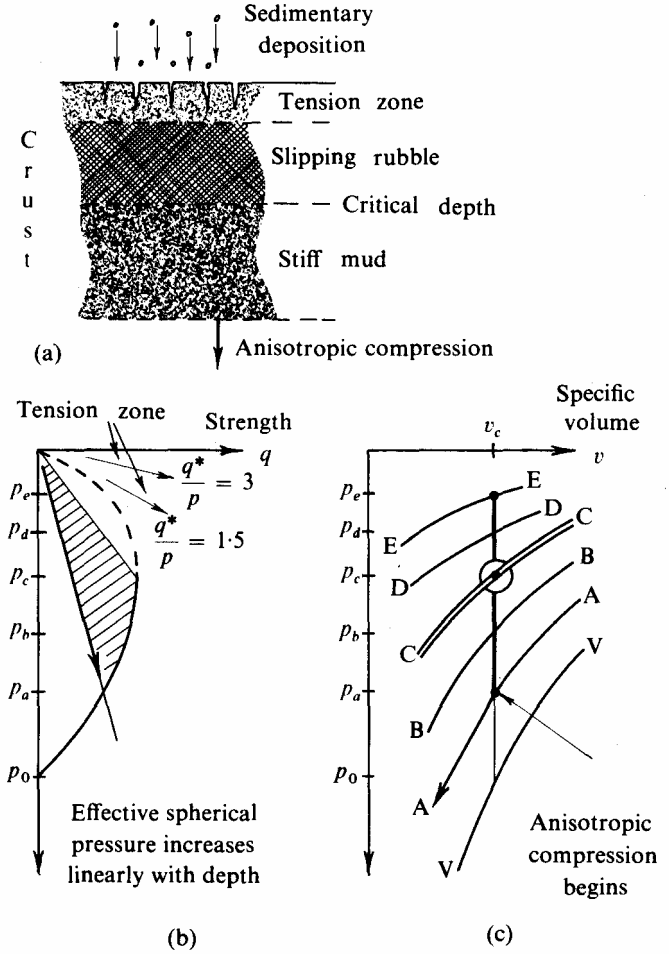

Fig. 10.2 The Crust of a Sedimentary Deposit

The second line in Fig. 10.1(a) at *constant specific volume* leads in Fig. 10.2 to three diagrams. Figure 10.2(c) is identical to part of Fig. 10.1(a) rotated through 90°, and 10.2(b) shows the stable state boundary curve that corresponds to the second line; what do these figures imply?

Figure 10.2(a) shows a *sedimentary deposit* of saturated remoulded (isotropic and homogeneous) Granta-gravel with particles falling on to the surface and forming a deposit of *constant* specific volume v_c. As the deposit builds up so the effective spherical pressure on any layer of material steadily increases; we plot the axis of p increasing downwards with depth in the deposit. In Fig. 10.2(c) the deposit of Granta-gravel remains rigid at specific volume of v_c to a depth at which anisotropic compression (under K_0 conditions) occurs under effective spherical pressure p_a. The sediment above that depth forms a sort of *crust:* we can ask what would be the response of material at various depths to any disturbance. During any deformation the Granta-gravel will require a sufficient supply of power to satisfy the basic equation, (5.19),

$$\frac{p\dot{v}}{v} + q\dot{\varepsilon} = Mp|\dot{\varepsilon}|.$$

At a depth where the effective spherical pressure is p_a, there is enough power available from plastic collapse of volume to satisfy eq. (5.19) without any need for a large additional deviatoric stress to cause the disturbance. At a smaller depth, where the effective spherical pressure is only p_b, there is less power available from plastic collapse of volume and more deviatoric stress would be needed to cause the disturbance: that is to say, the material gains strength *higher* in the crust. At a critical depth where the effective spherical pressure is p_c, there is no plastic collapse of volume, and the crust has its greatest strength. Above the critical depth we expect the material to deform as a rubble of slipping blocks in Coulomb's manner.

A small digression is appropriate about the possible tension zones in Fig. 10.2(b). Introducing $\sigma'_1 > \sigma'_2 = \sigma'_3 = 0$ into the generalized stress parameters briefly suggested in §8.2

$$p^* = \frac{\sigma'_1+\sigma'_2+\sigma'_3}{3}, \qquad q^* = \left| \left(\frac{(\sigma'_2-\sigma'_3)^2 + (\sigma'_3-\sigma'_1)^2 + (\sigma'_1-\sigma'_2)^2}{2} \right)^{\frac{1}{2}} \right|$$

we find $p^* = \sigma'_1/3, q^* = \sigma'_1,$ and $q^*/p^* = 3,$ which gives one radial line shown in Fig. 10.2(b). Another radial line with $q^*/p^* = 1.5$ corresponds with $\sigma'_1 = \sigma'_2 > \sigma'_3 = 0$ where we find $p^* = (2\sigma'_1/3)$ and $q^* = \sigma'_1.$ These two lines indicate the range of values $1.5 < (q^*/p^*) < 3$ in which one or more of the principal effective stress components $(\sigma'_1, \sigma'_2, \sigma'_3)$ becomes zero. In that zone we can have stressed soil bodies with one stress-free face, which implies that slight tension cracks or local pitting of the surface of the sedimentary deposit could occur.

Finally, moving down through the deposit in Fig. 10.2(a) we have first a shallow zone of possible tension cracks above a zone of slipping rubble; below a critical depth (which is a function of v_c) the material would behave as a stiff mud, readily expelling water under small deviatoric stress, and finally all material below the depth associated with p_a is in some state of anisotropic compression at a specific volume less than v_c. A Granta-gravel sediment would not experience this anisotropic compression until it was overlain by a thickness of crust formed by subsequent sediment.

In Fig. 10.1(b) we have considered the value of compaction to alternative specific volumes, and in Fig. 10.2 the state of a sedimentary deposit. Clearly with the critical state concept we have acquired a new basis for engineering judgement of the state of ground and the consequences of proposed works.

10.3 Test Equipment

We have seen (6.9) that the plasticity index corresponds to a critical state property that could be measured with more precision by other tests, such as indentation by a falling cone. Our discussion of the refined axial-test apparatus of §7.1 shows that an apparatus which attains this high standard can give data of altogether greater value than the conventional slow strain-controlled axial-test apparatus in current use. The new critical state concept gives an edge to our decisions on the value of various pieces of existing test equipment.

All that we have written in this book has been concerned with saturated remoulded soil. Of course engineers need to test unsaturated soil, to test natural anisotropic or sensitive soil, and to test soil *in situ.* The new critical state concept enables us to separate effects that can be associated with isotropic behaviour from these special effects that are not predicted by the critical state models. The critical state concept gives a rational basis for design of new tests that explore aspects of behaviour about which little is known at present.

10.4 Soil Deformation and Flow

The limiting equilibrium calculations that we have introduced in chapters 8 and 9 correspond to problems of the 'strength' of a soil body experiencing imposed *total* stress changes indicated by the arrows from B and D in Fig. 10.3(a). The arrow from B corresponds to a problem of *immediate* limiting equilibrium (such as that discussed in §8.7), and the arrow from D corresponds to a problem of *long-term* limiting equilibrium (such as that discussed in §8.8).

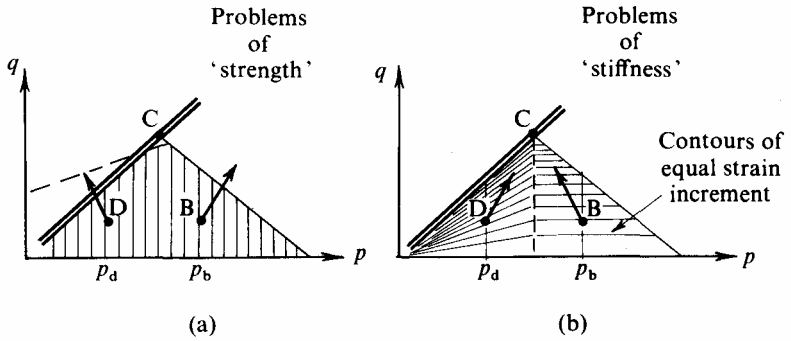

Fig. 10.3 Engineering Design Properties

However, we have not considered in this book a wide class of civil engineering design problems concerned with the 'stiffness' of a soil body. For example, in Fig. 10.3(b) the arrow of *effective* stress change from D might correspond to the distortion of firm ground beneath the base of a deep-bored cylinder foundation, and the arrow of *effective* stress change from B might correspond to the distortion of soft ground around a sheet-piled excavation. This type of design problem must become increasingly important in civil engineering practice, and it is clear that a better understanding of the stiffness of soil and its strain characteristics is required.

The critical state models that we have discussed in this book provide the basis for calculation of deformation in the rather special case of yielding of 'wet' soil. These models as they stand will not allow prediction of distortion for the loading of Fig. 10.3 because they are rigid for such loading, but research experiments and theoretical modifications to the models (for example, to allow recoverable distortion) do suggest the existence of 'contours' of equal distortion increments such as those shown in Fig. 10.3(b).

In addition to research experiments on axial-test specimens, a wide variety of other experiments on models and on other shapes of specimen is being conducted by us and our colleagues and by research workers in our own and in other laboratories. In reading reports of such research it is helpful to recall the differences between Figs. 10.3(a) and (b). Engineering design calculations at present concentrate on *strength:* as increasing skill is shown by designers so *stiffness* becomes a problem of increasing importance. Present research which explores the stiffness of apparently rigid soil bodies should prove to be of increasing importance to engineering designers as their skill in design increases.

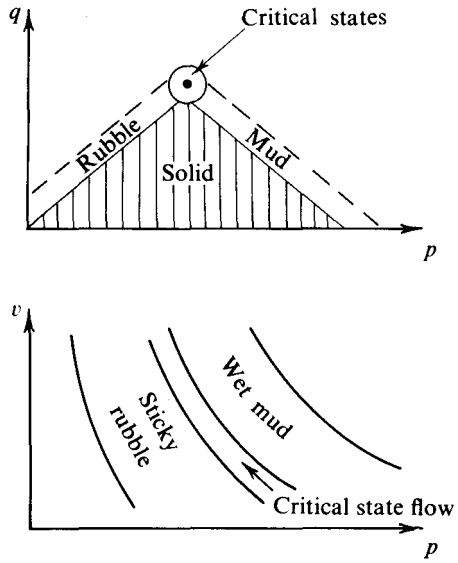

Fig. 10.4 Material Handling Properties

Throughout this book we have taken the civil engineer's viewpoint that it is, in general, undesirable for soil-material to move. We could equally well have taken the viewpoint of a material-handling engineer who wants powders and rubble to move freely. In Fig. 10.4 we repeat the (q, p) and (v, p) diagrams and indicate in a very crude manner the difference between states (p, v, q) in which the material (a) oozes as wet mud, (b) slips as a rubble of blocks (that stick to each other with an adhesion that depends on the pressure between the blocks), and (c) flows in the critical states. Clearly there are others as well as the civil engineer who may profit from the concept of §1.8 that 'granular materials, if continuously distorted until they flow as a frictional fluid, will come into a well-defined critical state'.

APPENDIX A

Mohr's circle for two-dimensional stress

Compressive stresses have been taken as *positive* because we shall almost exclusively be dealing with them (as opposed to tensile stresses) and because this agrees with the universal practice in soil mechanics. Once this sign convention has been adopted we are left with no choice for the associated conventions for the signs of shear stresses and use of Mohr's circles.

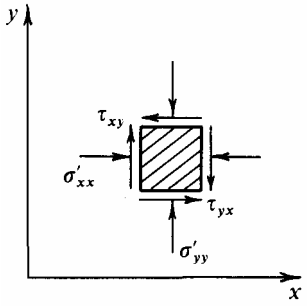

Fig. A.1 Stresses on Element of Soil

The positive directions of stresses should be considered in relation to the Cartesian reference axes in Fig. Al, in which it is seen that when *acting* on the pair of faces of an element *nearer* the origin they are in the *positive* direction of the parallel axis. The plane on which the stress acts is denoted by the first subscript, while the direction in which it acts is denoted by the second subscript. Normal stresses are often denoted by a single subscript, for example, σ'_x instead of σ'_{xx}.

For *Mohr's circle* of stress (Fig. A.2) we must take *counterclockwise* shear as *positive,* and use this convention *only* for the geometrical interpretation of the circle itself and revert to the mathematical convention for all equilibrium equations. Hence

X has coordinates $(\sigma'_{xx}, -\tau_{xy})$

and Y has coordinates $(\sigma'_{yy}, +\tau_{yx})$

But from equilibrium we require that $\tau_{xy} = \tau_{yx}$.

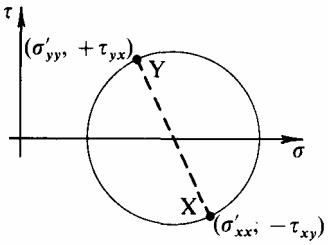

Fig. A.2 Mohr's Circle of Stress

Suppose we wish to relate this stress condition to another pair of Cartesian axes (*a*, *b*) in Fig. A.3 which are such that the counterclockwise angle between the *a*- and *x*-axes is $+\theta$.

Then we have to consider the equilibrium of wedge-shaped elements which have *mathematically* the stresses in the directions indicated.

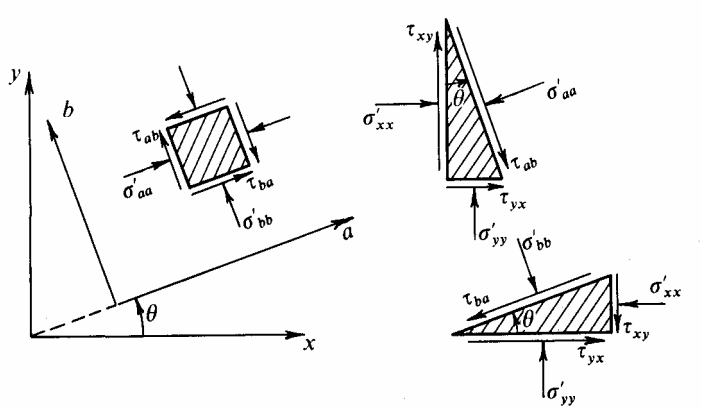

Fig. A.3 Stresses on Rotated Element of Soil

Resolving forces we get:

$$\left.\begin{aligned}
\sigma'_{aa} &= \frac{\sigma'_{xx}+\sigma'_{yy}}{2} + \frac{\sigma'_{xx}-\sigma'_{yy}}{2}\cos 2\theta + \tau_{xy}\sin 2\theta \\
\tau_{ab} &= \frac{-(\sigma'_{xx}-\sigma'_{yy})}{2}\sin 2\theta + \tau_{xy}\cos 2\theta \\
\sigma'_{bb} &= \frac{\sigma'_{xx}+\sigma'_{yy}}{2} - \frac{\sigma'_{xx}-\sigma'_{yy}}{2}\cos 2\theta - \tau_{xy}\sin 2\theta \\
\tau_{ba} &= -\frac{(\sigma'_{xx}-\sigma'_{yy})}{2}\sin 2\theta + \tau_{xy}\cos 2\theta = \tau_{ab}.
\end{aligned}\right\} \qquad \text{(A.1)}$$

In Mohr's circle of stress

A has coordinates $(\sigma'_{aa}, -\tau_{ab})$

and B has coordinates $(\sigma'_{bb}, +\tau_{ba})$.

A very powerful geometric tool for interpretation of Mohr's circle is the construction of the *pole,* point P in Fig. A.4. Through

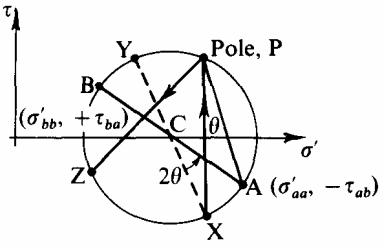

Fig. A.4 Definition of Pole for Mohr's Circle

any point on the circle a line is drawn parallel to the plane on which the corresponding stresses act, and the pole is the point where this line cuts the circle. In the diagram XP has been drawn parallel to the *y*-axis, i.e., the plane *on* which σ'_{xx} and τ_{xy} act.

This construction applies for *any* point on the circle giving the pole as a unique point. Having established the pole we can then reverse the process, and if we wish to know the stresses acting on some plane through the element of soil we merely draw a line through P parallel to the plane, such as PZ, and the point Z gives us the desired stresses at once.

This result holds because the angle XCA is $+2\theta$ (measured in the counterclockwise direction) as can be seen from eqs. (A.1) and by simple geometry the angle XPA is half this, i.e., $+\theta$ which is the angle between the two planes in question, Ox and Oa.

APPENDIX B

Typical input data of undrained triaxial test for processing by computer

```
DATA
PAL 556/OBSERVATIONS/2

T
T

TNORMALLY CONSOLIDATED SPESTONE III KAOLIN TO 60·8 P.S.I.
UNDRAINED TEST

TSTRAIN RATE ·0019 IN./MIN. DATE 6/8/65

1.25        Number of test
55·3155     Water content of initial slurry: (a) Wt of bottle and wet sample: gm
49·6691                                      (b) Wt of bottle and dry sample: gm
46·1257                                      (c) Wt of bottle: gm
3·851       Initial diameter of specimen: cm
3·848
3·846
3·853
3·842
3·848
·01         Thickness of membrane: in
3·3626      Initial length of specimen: in
60·1067     Water content after preconsolidation. (Bottle weights as above)
51·2065
38·2157
14·62       Volume of water expelled during consolidation: cm³
0           ,,  ,,  ,,  ,,  ,,  test: cm³
−8·265      ,,  ,,  ,,  ,,  ,,  final unloading: cm³
111·6228    Water contents of four samples from specimen (Bottle weights
99·1068       at end of test after unloading              as above)
78·6222
119·8637
105·0578
80·627
118·4883
104·2674
81·0522
119·423
105·7703
83·9292     Wt of final scraps of specimen on sheath, etc.
62·5111
62·3748
2·64        Specific gravity of soil particles
1720        Calibration factor of load measuring device: lb/in
·26         Value of λ
1·8         Zero value of pore-pressure transducer: lb/in²
60·8        Maximum consolidation pressure: lb/in²
```

0 Volume of water expelled during overconsolidation 'rebound' : cm^3
2·5 Membrane strength factor : lb/in
·05 Value of κ
3·46 $(\Delta V/V_0)/(\Delta l/l_0)$ during consolidation
60·8 Final pressure during consolidation : lb/in^2

1 Program instruction

81 Cell pressure during test : lb/in^2

1·474	500	21·8	First column — Vertical dial gauge readings : in
1·475	554	24·9	
1·476	577	26·5	Second column — Dial gauge readings of axial load measuring device : 10^{-4} in
1·477	591	27·1	
1·478	602	28·9	Third column — Pore-pressure readings : lb/in^2
1·479	611	30	
1·480	618	30·9	
1·481	624	32	
1·482	630	32·5	
1·484	640	33·6	
1·486	647	34·8	
1·488	654	35·6	
1·490	659·5	36·4	
1·492	665	37·2	
1·494	670	38	
1·496	675	38·9	
1·498	680	39·5	
1·500	685	40	
1·505	694	41·5	
1·510	702	43	
1·515	708·5	44·3	
1·520	714·5	45·1	
1·525	720	46·2	
1·531	725·7	47	
1·535	730	48	
1·540	733·8	48·5	
1·545	737·2	49·1	
1·550	740·5	49·8	
1·555	743·6	50·3	
1·560	746	51	
1·565	749	52	
1·570	751·2	52	
1·575	753·5	52·4	
1·580	755·5	53	
1·590	759	53·1	
1·600	762·2	54·5	
1·610	765	55	
1·621	768	55·6	
1·640	771	56·5	
1·660	777	57·1	
1·680	780·8	58	
1·700	784·8	58·5	
1·720	786·8	59·1	
1·740	788·1	59·8	
1·760	789	60·1	
1·777	791·5	60·5	
1·800	793	61	
1·821	794	61·2	
1·841	798·3	61·9	
1·860	799·3	62	
1·881	801	62·4	
1·900	803	62·4	
1·920	804·8	62·7	
1·940	806·5	63	
1·960	807	63	
1·980	807·8	63·1	
2·000	808	63·1	
2·020	808·1	63·1	
2·047	808	63·5	
2·051	806·6	63·5	
2·104	791·5	64	

Typical output data of undrained triaxial test processed by computer

JOB TITLE — (PAL 556/TRIAXIAL/1) . . . 23 5 66
STREAM NO. 1

NORMALLY CONSOLIDATED SPESTONE III KAOLIN TO 60·8 P.S.I. UNDRAINED TEST
STRAIN RATE ·0019 IN./MIN. DATE 6/8/65

TRIAXIAL TEST NO. 1.25

MC AFTER MIX			1·593	
INITIAL VOLUME CUB IN AND CC			5·902	96·722
MC AFTER TEST	TOP QUARTER		0·611	
	TOP HALF		0·606	
	BOTTOM HALF		0·613	
	BOTTOM QUARTER		0·625	
INITIAL MC AND VR		A	0·684	1·806
		B	0·695	1·834
		C	0·685	1·809

WHERE A FROM FINAL MC
B FROM INITIAL VOLUME
C FROM INITIAL MC

INITIAL VOLUME OF WATER CC 61·634
WEIGHT OF SOLIDS GRAM 90·108

AXIAL STRAIN	VOL STRAIN	SHEAR STRAIN	VOIDS RATIO	PORE PRESS	DEV STRESS	VP STRESS	Q P	Q PE	P PE
0·00000	0·00000	0·00000	1·377	0·00	0·00	61·00	0·000	0·000	1·000
0·00031	0·00000	0·00031	1·377	3·10	5·96	59·89	0·099	0·098	0·982
0·00062	0·00000	0·00062	1·377	4·70	8·49	59·13	0·144	0·139	0·969
0·00093	0·00000	0·00093	1·377	5·30	10·03	59·04	0·170	0·164	0·968
0·00124	0·00000	0·00124	1·377	7·10	11·24	57·65	0·195	0·184	0·945
0·00156	0·00000	0·00156	1·377	8·20	12·22	56·87	0·215	0·200	0·932
0·00187	0·00000	0·00187	1·377	9·10	12·99	56·23	0·231	0·213	0·922
0·00218	0·00000	0·00218	1·377	10·20	13·64	55·35	0·247	0·224	0·907
0·00249	0·00000	0·00249	1·377	10·70	14·30	55·07	0·260	0·234	0·903
0·00311	0·00000	0·00311	1·377	11·80	15·39	54·33	0·283	0·252	0·891

0·00374	0·00000	0·00374	1·377	13·00	16·14	53·38	0·302	0·265	0·875
0·00436	0·00000	0·00436	1·377	13·80	16·90	52·83	0·320	0·277	0·866
0·00499	0·00000	0·00499	1·377	14·60	17·49	52·23	0·335	0·287	0·856
0·00561	0·00000	0·00561	1·377	15·40	18·07	51·62	0·350	0·296	0·846
0·00624	0·00000	0·00624	1·377	16·20	18·61	51·00	0·365	0·305	0·836
0·00686	0·00000	0·00686	1·377	17·10	19·14	50·28	0·381	0·314	0·824
0·00749	0·00000	0·00749	1·377	17·70	19·67	49·86	0·395	0·322	0·817
0·00812	0·00000	0·00812	1·377	18·20	20·20	49·53	0·408	0·331	0·812
0·00968	0·00000	0·00968	1·377	19·70	21·14	48·35	0·437	0·347	0·793
0·01125	0·00000	0·01125	1·377	21·20	21·97	47·12	0·466	0·360	0·773
0·01283	0·00000	0·01283	1·377	22·50	22·63	46·04	0·492	0·371	0·755
0·01440	0·00000	0·01440	1·377	23·30	23·24	45·45	0·511	0·381	0·745
0·01598	0·00000	0·01598	1·377	24·40	23·79	44·53	0·534	0·390	0·730
0·01787	0·00000	0·01787	1·377	25·20	24·35	43·92	0·554	0·399	0·720
0·01914	0·00000	0·01914	1·377	26·20	24·78	43·06	0·575	0·406	0·706
0·02073	0·00000	0·02073	1·377	26·70	25·14	42·68	0·589	0·412	0·700
0·02231	0·00000	0·02231	1·377	27·30	25·45	42·18	0·603	0·417	0·692
0·02390	0·00000	0·02390	1·377	28·00	25·76	41·59	0·619	0·422	0·682
0·02550	0·00000	0·02550	1·377	28·50	26·04	41·18	0·632	0·427	0·675
0·02709	0·00000	0·02709	1·377	29·20	26·24	40·55	0·647	0·430	0·665
0·02869	0·00000	0·02869	1·377	30·20	26·51	39·64	0·669	0·435	0·650
0·03029	0·00000	0·03029	1·377	30·20	26·69	39·70	0·672	0·438	0·651
0·03189	0·00000	0·03189	1·377	30·60	26·89	39·36	0·683	0·441	0·645
0·03350	0·00000	0·03350	1·377	31·20	27·05	38·82	0·697	0·443	0·636
0·03671	0·00000	0·03671	1·377	31·30	27·31	38·80	0·704	0·448	0·636
0·03994	0·00000	0·03994	1·377	32·70	27·54	37·48	0·735	0·451	0·614
0·04317	0·00000	0·04317	1·377	33·20	27·72	37·04	0·748	0·454	0·607
0·04675	0·00000	0·04675	1·377	33·80	27·92	36·51	0·765	0·458	0·598
0·05294	0·00000	0·05294	1·377	34·70	28·02	35·64	0·786	0·459	0·584
0·05950	0·00000	0·05950	1·377	35·30	28·41	35·17	0·808	0·466	0·577
0·06610	0·00000	0·06610	1·377	36·20	28·57	34·32	0·832	0·468	0·563
0·07274	0·00000	0·07274	1·377	36·70	28·75	33·88	0·849	0·471	0·555
0·07943	0·00000	0·07943	1·377	37·30	28·72	33·27	0·863	0·471	0·545
0·08617	0·00000	0·08617	1·377	38·00	28·61	32·54	0·879	0·469	0·533
0·09295	0·00000	0·09295	1·377	38·30	28·47	32·19	0·884	0·467	0·528
0·09875	0·00000	0·09875	1·377	38·70	28·51	31·80	0·897	0·467	0·521
0·10665	0·00000	0·10665	1·377	39·20	28·39	31·26	0·908	0·465	0·512
0·11391	0·00000	0·11391	1·377	39·40	28·23	31·01	0·910	0·463	0·508
0·12089	0·00000	0·12089	1·377	40·10	28·41	30·37	0·936	0·466	0·498
0·12756	0·00000	0·12756	1·377	40·20	28·28	30·23	0·936	0·464	0·496

AXIAL STRAIN	VOL STRAIN	SHEAR STRAIN	VOIDS RATIO	PORE PRESS	DEV STRESS	VP STRESS	Q P	Q PE	P PE
0·13498	0·00000	0·13498	1·377	40·60	28·19	29·80	0·946	0·462	0·488
0·14174	0·00000	0·14174	1·377	40·60	28·15	29·78	0·945	0·461	0·488
0·14891	0·00000	0·14891	1·377	40·90	28·07	29·46	0·953	0·460	0·483
0·15613	0·00000	0·15613	1·377	41·20	27·99	29·13	0·961	0·459	0·478
0·16340	0·00000	0·16340	1·377	41·20	27·78	29·06	0·956	0·455	0·476
0·17073	0·00000	0·17073	1·377	41·30	27·61	28·90	0·955	0·453	0·474
0·17811	0·00000	0·17811	1·377	41·30	27·38	28·83	0·950	0·449	0·473
0·18555	0·00000	0·18555	1·377	41·30	27·14	28·75	0·944	0·445	0·471
0·19566	0·00000	0·19566	1·377	41·70	26·80	28·23	0·949	0·439	0·463
0·19718	0·00000	0·19718	1·377	41·70	26·63	28·18	0·945	0·436	0·462
0·21726	0·00000	0·21726	1·377	42·20	24·64	27·01	0·912	0·404	0·443

AXIAL STRAIN	VL	VK	DVK VDE	DQ PEDE	DP PEDE	Q PE	Q P	DVP DET
0·00016	3·444	2·583	−1·247	314·047	−58·738	0·049	0·050	1·247
0·00047	3·440	2·582	−0·858	133·513	−39·816	0·118	0·122	0·858
0·00078	3·438	2·581	−0·099	81·093	−4·579	0·152	0·157	0·099
0·00109	3·435	2·581	−1·618	63·596	−73·602	0·174	0·182	1·618
0·00140	3·430	2·580	−0·910	51·930	−40·606	0·192	0·205	0·910
0·00171	3·427	2·579	−0·770	40·282	−33·944	0·207	0·223	0·770
0·00202	3·423	2·579	−1·067	34·448	−46·397	0·218	0·239	1·067
0·00233	3·420	2·578	−0·345	34·415	−14·829	0·229	0·253	0·345
0·00280	3·418	2·578	−0·455	28·585	−19·393	0·243	0·271	0·455
0·00343	3·414	2·577	−0·593	19·861	−24·911	0·258	0·293	0·593
0·00405	3·410	2·576	−0·348	19·824	−14·400	0·271	0·311	0·348
0·00467	3·407	2·575	−0·387	15·462	−15·841	0·282	0·327	0·387
0·00530	3·404	2·575	−0·391	15·433	−15·837	0·291	0·342	0·391
0·00592	3·401	2·574	−0·408	13·966	−16·313	0·301	0·357	0·408
0·00655	3·398	2·574	−0·480	13·939	−18·928	0·309	0·373	0·480
0·00718	3·395	2·573	−0·284	13·912	−11·069	0·318	0·388	0·284
0·00780	3·393	2·573	−0·218	13·886	−8·452	0·327	0·401	0·218
0·00890	3·389	2·572	−0·325	9·844	−12·406	0·339	0·423	0·325
0·01047	3·382	2·571	−0·343	8·657	−12·777	0·353	0·452	0·343
0·01204	3·376	2·569	−0·310	6·910	−11·249	0·366	0·479	0·310
0·01361	3·371	2·569	−0·175	6·310	−6·224	0·376	0·501	0·175
0·01519	3·367	2·568	−0·272	5·714	−9·527	0·385	0·523	0·272
0·01693	3·363	2·567	−0·154	4·840	−5·304	0·395	0·544	0·154
0·01851	3·358	2·566	−0·328	5·515	−11·107	0·403	0·565	0·328
0·01993	3·355	2·565	−0·118	3·730	−3·928	0·409	0·582	0·118
0·02152	3·352	2·565	−0·154	3·265	−5·108	0·415	0·596	0·154
0·02311	3·349	2·564	−0·189	3·136	−6·172	0·420	0·611	0·189
0·02470	3·345	2·564	−0·130	2·898	−4·181	0·425	0·626	0·130
0·02629	3·342	2·563	−0·204	2·110	−6·491	0·429	0·640	0·204
0·02789	3·337	2·562	−0·299	2·759	−9·342	0·432	0·658	0·299

AXIAL STRAIN	VL	VK	DVK VDE	DQ PEDE	DP PEDE	Q PE	Q P	DVP DET
0·02949	3·334	2·561	0·020	1·866	0·622	0·436	0·671	−0·020
0·03109	3·333	2·561	−0·112	1·965	−3·436	0·439	0·678	0·112
0·03269	3·331	2·561	−0·183	1·627	−5·585	0·442	0·690	0·183
0·03510	3·329	2·560	−0·002	1·343	−0·062	0·446	0·700	0·002
0·03833	3·324	2·559	−0·226	1·165	−6·726	0·450	0·719	0·226
0·04156	3·318	2·558	−0·076	0·937	−2·220	0·453	0·742	0·076
0·04496	3·315	2·558	−0·086	0·885	−2·459	0·456	0·757	0·086
0·04984	3·310	2·557	−0·082	0·264	−2·295	0·458	0·775	0·082
0·05622	3·305	2·556	−0·042	0·991	−1·170	0·463	0·797	0·042
0·06280	3·300	2·555	−0·078	0·400	−2·102	0·467	0·820	0·078
0·06942	3·295	2·554	−0·041	0·436	−1·088	0·470	0·840	0·041
0·07609	3·291	2·553	−0·057	−0·079	−1·497	0·471	0·856	0·057
0·08280	3·286	2·552	−0·070	−0·257	−1·790	0·470	0·871	0·070
0·08956	3·281	2·551	−0·033	−0·356	−0·844	0·468	0·882	0·033
0·09585	3·278	2·551	−0·044	0·134	−1·085	0·467	0·890	0·044
0·10270	3·275	2·550	−0·046	−0·263	−1·126	0·466	0·902	0·046
0·11028	3·271	2·549	−0·023	−0·347	−0·567	0·464	0·909	0·023
0·11740	3·268	2·549	−0·063	0·423	−1·505	0·464	0·923	0·063
0·12422	3·264	2·548	−0·015	−0·329	−0·356	0·465	0·936	0·015
0·13127	3·262	2·548	−0·041	−0·203	−0·951	0·463	0·941	0·041
0·13836	3·260	2·547	−0·001	−0·099	−0·033	0·462	0·946	0·001
0·14533	3·258	2·547	−0·032	−0·170	−0·743	0·461	0·949	0·032
0·15252	3·256	2·546	−0·033	−0·195	−0·746	0·459	0·957	0·033
0·15977	3·254	2·546	−0·007	−0·452	−0·151	0·457	0·958	0·007
0·16707	3·253	2·546	−0·016	−0·387	−0·353	0·454	0·956	0·016
0·17442	3·252	2·546	−0·008	−0·509	−0·170	0·451	0·953	0·008
0·18183	3·251	2·545	−0·008	−0·525	−0·175	0·447	0·947	0·008
0·19061	3·248	2·545	−0·038	−0·555	−0·833	0·442	0·947	0·038
0·19642	3·246	2·544	−0·029	−0·908	−0·636	0·438	0·947	0·029
0·20722	3·240	2·543	−0·044	−1·624	−0·949	0·420	0·929	0·044

APPENDIX C

A yield function and plastic potential for soil under general principal stresses

The yield function, $F(p, q)$, for Granta-gravel, from eq. (5.27), is

$$F = q + Mp\left(\ln\frac{p}{p_u} - 1\right) = 0 \tag{C.1}$$

where

$$p = \frac{\sigma'_l + 2\sigma'_r}{3},\ q = \sigma'_l - \sigma'_r,\quad \text{and} \qquad p_u = \exp\left(\frac{\Gamma - v}{\lambda}\right).$$

We can treat the function F^* as a plastic potential in the manner of §2.10, provided we know what plastic strain-increments correspond to the stress parameters p and q. In §5.5 we found that $\dot{\upsilon}/\upsilon$ corresponded to p, and $\dot{\varepsilon}$ corresponded to q. Therefore, from eq. (2.13), we can first calculate

$$\frac{\partial F}{\partial q} = v\dot{\varepsilon} = 1,$$

so that the scalar factor v is

$$v = \frac{1}{\dot{\varepsilon}}, \tag{C.2}$$

and then we can calculate

$$\frac{\partial F}{\partial p} = v\frac{\dot{\upsilon}}{\upsilon} = \frac{1}{\dot{\varepsilon}}\frac{\dot{\upsilon}}{\upsilon} = M\ln\frac{p}{p_u} = \left(M - \frac{q}{p}\right).$$

This restates eq. (5.21) and thus provides a check of this type of calculation.

We wish to generalize the Granta-gravel model in terms of the three principal stresses and obtain a yield function $F^*(\sigma'_1, \sigma'_2, \sigma'_3, p_u)$ where p_u remains as specified above. Let us retain the same function as before, eq. (C.1), but introduce the generalized parameters of §8.2,

$$p^* = \left(\frac{\sigma'_1 + \sigma'_2 + \sigma'_3}{3}\right)$$

and

$$q^* = \frac{1}{\sqrt{2}}\left\{(\sigma'_2 - \sigma'_3)^2 + (\sigma'_3 - \sigma'_1)^2 + (\sigma'_1 - \sigma'_2)^2\right\}^{\frac{1}{2}}.$$

The function F^* then has equation

$$F^* = \frac{1}{\sqrt{2}}\left\{(\sigma'_2 - \sigma'_3)^2 + (\sigma'_3 - \sigma'_1)^2 + (\sigma'_1 - \sigma'_2)^2\right\}^{\frac{1}{2}} + M\left(\frac{\sigma'_1 + \sigma'_2 + \sigma'_3}{3}\right)\left\{\ln\left(\frac{\sigma'_1 + \sigma'_2 + \sigma'_3}{3p_u}\right) - 1\right\} = 0 \tag{C.3}$$

This function F^* generates a surface of revolution about the diagonal of principal stress space as shown in Fig. 5.1. Variation of p_u generates successive surfaces as indicated in Fig. 5.2.

Let us treat F^* as a plastic potential. Clearly, the stress parameters $(\sigma'_1, \sigma'_2, \sigma'_3)$ are associated with plastic strain-increments $(\dot{\varepsilon}_1, \dot{\varepsilon}_2, \dot{\varepsilon}_3)$ since the loading power is

$$\sigma'_1 \dot{\varepsilon}_1 + \sigma'_2 \dot{\varepsilon}_2 + \sigma'_3 \dot{\varepsilon}_3 = \frac{\dot{E}}{\upsilon}. \tag{C.4}$$

Therefore, from eq. (2.13) we calculate

$$\begin{aligned}
\frac{\partial F^*}{\partial \sigma'_1} &= v^* \dot{\varepsilon}_1 = \frac{3\{\sigma'_1 - [(\sigma'_1+\sigma'_2+\sigma'_3)/3]\}}{2\left\{\left[(\sigma'_2-\sigma'_3)^2 + (\sigma'_3-\sigma'_1)^2 + (\sigma'_1-\sigma'_2)^2\right]/2\right\}^{\frac{1}{2}}} + \frac{M}{3}\ln\left(\frac{\sigma'_1+\sigma'_2+\sigma'_3}{3p_u}\right) \\
\frac{\partial F^*}{\partial \sigma'_2} &= v^* \dot{\varepsilon}_2 = \frac{3\{\sigma'_2 - [(\sigma'_1+\sigma'_2+\sigma'_3)/3]\}}{2\left\{\left[(\sigma'_2-\sigma'_3)^2 + (\sigma'_3-\sigma'_1)^2 + (\sigma'_1-\sigma'_2)^2\right]/2\right\}^{\frac{1}{2}}} + \frac{M}{3}\ln\left(\frac{\sigma'_1+\sigma'_2+\sigma'_3}{3p_u}\right) \\
\frac{\partial F^*}{\partial \sigma'_3} &= v^* \dot{\varepsilon}_3 = \frac{3\{\sigma'_3 - [(\sigma'_1+\sigma'_2+\sigma'_3)/3]\}}{2\left\{\left[(\sigma'_2-\sigma'_3)^2 + (\sigma'_3-\sigma'_1)^2 + (\sigma'_1-\sigma'_2)^2\right]/2\right\}^{\frac{1}{2}}} + \frac{M}{3}\ln\left(\frac{\sigma'_1+\sigma'_2+\sigma'_3}{3p_u}\right)
\end{aligned} \tag{C.5}$$

If we introduce $\dot{\varepsilon}^*$, *a scalar* measure of distortion increment that generalizes eq. (5.6) and eq. (5.9), in the form

$$\dot{\varepsilon}^* = \frac{\sqrt{2}}{3}\left\{(\dot{\varepsilon}_2 - \dot{\varepsilon}_3)^2 + (\dot{\varepsilon}_3 - \dot{\varepsilon}_1)^2 + (\dot{\varepsilon}_1 - \dot{\varepsilon}_2)^2\right\}^{\frac{1}{2}} \tag{C.6}$$

then, as in eq. (C.3), we find from eq. (C.5) that

$$v^* = \frac{1}{\dot{\varepsilon}^*} \tag{C.7}$$

It is now convenient and simple to separate (C.5) into two parts:

$$\frac{\dot{\varepsilon}_1 + \dot{\varepsilon}_2 + \dot{\varepsilon}_3}{\dot{\varepsilon}^*} = M - \frac{q^*}{p^*}, \tag{C.8}$$

and

$$\begin{aligned}
\frac{\dot{\varepsilon}_2 - \dot{\varepsilon}_3}{\dot{\varepsilon}^*} &= \frac{3}{2}\frac{\sigma'_2 - \sigma'_3}{q^*} \\
\frac{\dot{\varepsilon}_3 - \dot{\varepsilon}_1}{\dot{\varepsilon}^*} &= \frac{3}{2}\frac{\sigma'_3 - \sigma'_1}{q^*} \\
\frac{\dot{\varepsilon}_1 - \dot{\varepsilon}_2}{\dot{\varepsilon}^*} &= \frac{3}{2}\frac{\sigma'_1 - \sigma'_2}{q^*}
\end{aligned} \tag{C.9}$$

The first part, eq. (C.8), is a scalar equation relating the first invariant of the plastic strain-increment tensor to other scalar invariants. The second part, eqs. (C.9), is a group of equations relating each component of a plastic strain-increment deviator tensor to a component of a stress deviator tensor. We will now show that these equations can be conveniently employed in two calculations.

First, we consider the corner of the yield surface. When $q^* = 0$ and $\sigma'_1 = \sigma'_2 = \sigma'_3 = p^*$, we find that eqs. (C.9) become indeterminate, but eq. (C.8) gives

$$\dot{\varepsilon}^* = \left(\frac{\dot{\varepsilon}_1 + \dot{\varepsilon}_2 + \dot{\varepsilon}_3}{M}\right) \tag{C.10}$$

Here, as in §6.6, we find that a plastic compression increment under isotropic stress is associated with a certain measure of distortion.

Next, we consider what will occur if we can make the generalized Granta-gravel sustain distortion in plane strain at the critical state where $(\dot{\varepsilon}_1 + \dot{\varepsilon}_2 + \dot{\varepsilon}_3) = 0.$ In plane strain $\dot{\varepsilon}_2 = 0,$ so at the critical state, $\dot{\varepsilon}_1 + \dot{\varepsilon}_3 = 0.$ With eqs. (C.9) these give

$$\frac{3}{2}\frac{\sigma'_2 - \sigma'_3}{q^*} = -\frac{\dot{\varepsilon}_3}{\dot{\varepsilon}^*} = +\frac{\dot{\varepsilon}_1}{\dot{\varepsilon}^*} = \frac{3}{2}\frac{\sigma'_1 - \sigma'_2}{q^*}$$

from which

$$\sigma'_2 = \frac{\sigma'_1 + \sigma'_3}{2}. \tag{C.11}$$

We satisfy this equation if we introduce the simple shear parameters (*s, t*) where $\sigma'_1 = s + t, \sigma'_2 = s, \sigma'_3 = s - t.$ In terms of these parameters, the values of p* and q* are

$$p^* = s \quad \text{and} \qquad q^* = \frac{1}{\sqrt{2}}\left\{t^2 + 4t^2 + t^2\right\}^{\frac{1}{2}} = \left(\sqrt{3}\right)t$$

The yield function *F** at the critical state reduces to

$$q^* - Mp^* = 0,$$

so that

$$t = \frac{M}{\sqrt{3}}s. \tag{C.12}$$

This result was also obtained by J. B. Burland[1] and compared with data of simple shear tests. In fact the shear tests terminated at the appropriate Mohr-Rankine limiting stress ratio before the critical state stress ratio of eqn. (C. 12) was reached.

[1] Burland, J. B. *Deformation of Soft Clay,* Ph.D. Thesis, Cambridge University, 1967.